NEW POSSIBILITIES FOR
MOLECULAR IMAGING AND
INTERVENTION IN BREAST CANCER
AND OTHER FEMALE MALIGNANCIES

Angela Collarino

NEW POSSIBILITIES FOR MOLECULAR IMAGING AND INTERVENTION IN BREAST CANCER AND OTHER FEMALE MALIGNANCIES

Angela Collarino

Cover illustration

Artist impression using the city maps of Leiden and Rome to represent the lymphatic drainage of primary tumours to the lymph nodes in female cancers.

Cover design and layout Elizabeth J. de Koster

ISBN 978-90-365-4437-5

Printed by Gildeprint, Enschede, Netherlands

NEW POSSIBILITIES FOR MOLECULAR IMAGING AND INTERVENTION IN BREAST CANCER AND OTHER FEMALE MALIGNANCIES

DISSERTATION

to obtain

the degree of doctor at the University of Twente,

on the authority of the rector magnificus,

prof.dr. T.T.M. Palstra,

on account of the decision of the graduation committee,

to be publicly defended

on Thursday the 21st of December 2017 at 12.45 PM

by

Angela Collarino

born on the 11th of May 1984

in Lagonegro, Potenza, Italy

This dissertation has been approved by

Supervisor

Prof. dr. L.F. de Geus-Oei

Co-supervisors

Dr. L.M. Pereira Arias-Bouda

Dr. R.A. Valdés Olmos

to Antonio

TABLE OF CONTENTS

GENERAL INTRODUCTION AND OUTLINE OF THIS THESIS

CHAPTER 1

GENERAL INTRODUCTION

Female cancers include common malignancies like breast, uterus, cervix and ovarian cancer as well as rare tumours affecting vulva and vagina. The latter account for approximately 2% of all malignancies in women in The Netherlands (**Figure 1**). [1]

Parallel to the growing use of positron emission tomography with low-dose CT (PET/CT) using ^{18}F-fluorodeoxyglucose (^{18}F-FDG) for breast cancer, the interest for nuclear medicine in breast imaging has increased due to the development of dedicated breast devices with relatively low radiation dose and high sensitivity for small breast tumours. [2, 3] Moreover, recent technological developments have led to the possibility to biopsy breast lesions-guided by radiotracers. [4-6] Furthermore, the introduction of quantitative single photon emission computed tomography (SPECT)/CT enables the use of this device for monitoring of therapy response in women with locally advanced breast cancer. [7]

Additionally, continuous advances of hybrid SPECT/CT and PET/CT devices may prove of additional value in the diagnostic workup of women with vulvar cancer. [7, 8] In particular, the incorporation of SPECT/CT could improve the detection of sentinel lymph node(s) (SLNs) and aid surgical management strategies. Besides, the adjunct delayed PET/CT acquisition could enable better identification of lymph node metastases.

Hence, the rationale behind this thesis is to validate novel molecular imaging possibilities in breast and vulvar cancer and to simultaneously encompass all current and future applications of nuclear medicine in a specific field concerning female cancers.
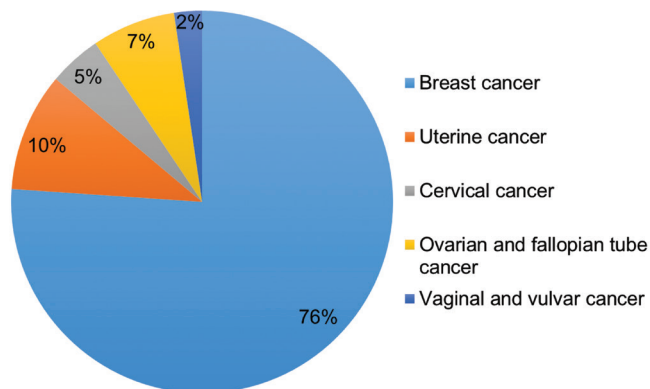
Figure 1. Distribution of female cancers according to incidence in The Netherlands in 2016.[1]

OUTLINE OF THIS THESIS

Part I of this thesis introduces the concept of molecular imaging by using ^{99m}Tc-sestamibi in breast cancer. **Chapter 2** provides an overview of the current use and shortcomings of ^{99m}Tc-sestamibi imaging in the prediction of pathological nonresponse to neoadjuvant chemotherapy in breast cancer. In **chapter 3**, the experimental validation of SPECT/CT quantification for response monitoring in breast cancer is presented. In **chapter 4**, the clinical impact of molecular breast imaging (MBI) using ^{99m}Tc-sestamibi is evaluated in 287 women with proven invasive breast cancer scheduled for breast-conserving surgery.

Part II of this thesis focuses on ^{99m}Tc-sestamibi-guided biopsy in breast cancer. In **chapter 5**, the methodological aspects of dedicated ^{99m}Tc-sestamibi-guided biopsy are described and compared to the available radiology-guided biopsy tools (mammography-, ultrasound- and magnetic resonance imaging-guided biopsy). In **chapter 6**, the first clinical experience using stereotactic biopsy guided by ^{99m}Tc-sestamibi is evaluated in 38 women.

Part III of this thesis is on radioguided intervention in other female cancers. **Chapter 7** describes the state-of-the-art SLN mapping in gynaecological malignancies including cervical cancer, endometrial cancer and vulvar cancer. In **chapter 8**, we investigated SPECT/CT for anatomical mapping of lymphatic drainage and the possible implications for the extent of the inguinal lymph node dissection in patients with vulvar cancer. In **chapter 9**, we evaluated the value of dual-time-point ^{18}F-FDG PET/CT in the prediction of lymph node status in patients with invasive vulvar cancer scheduled for inguinofemoral lymph node dissection.

In **part IV** of this thesis, **chapter 10** discusses the novel frontiers of dedicated molecular imaging in breast cancer diagnosis. Finally, **chapter 11** highlights future perspectives for nuclear medicine in vulvar cancer and other gynaecological malignancies.

ADDITIONAL INFORMATION ABOUT THE DEVICES INVOLVED IN THIS THESIS

MBI has been recently developed for breast cancer detection. [9] This tool is based on the use of single-photon emitting radiotracers like ^{99m}Tc-sestamibi. [10] MBI uses a compact gamma-camera with a single or dual-head detector, with a small field-of-view (20 x 15 cm) and high spatial resolution (≈ 3 mm).[11, 12] Patients are scanned in sitting position with mild breast compression. MBI image projections are comparable to those of mammography.[13] In this thesis, the used MBI device was a single detector known as breast-specific gamma-imaging (BSGI, Dilon 6800, Dilon Technologies, Newport News, Virginia, US) (**Figure 2**). This device was employed for detecting additional breast tumours and extension of the index lesion in 287 women with invasive breast cancer.

Figure 2. BSGI system is equipped with a single detector head and a compression paddle to immobilise the breast during image acquisition.

MBI-guided biopsy is a new tool for breast biopsy based on the use of ^{99m}Tc-sestamibi as radiotracer. For the biopsies included in this thesis, the device was based on the previously described BSGI system and was adjusted with: **a)** a grid compression paddle in which an embedded source of Cerium-139 is used as reference to determine the height of the paddle during the stereotactic imaging; **b)** a single-head detector with sliding slant-hole collimator for 20 degree angle views used for stereotactic localisation of ^{99m}Tc-sestamibi-avid lesions and **c)** dedicated software for calculating the x, y, z coordinates of the breast lesion (**Figure 3**). [4, 14] The first clinical experience with this biopsy tool concerning 38 patients is reported in this thesis.
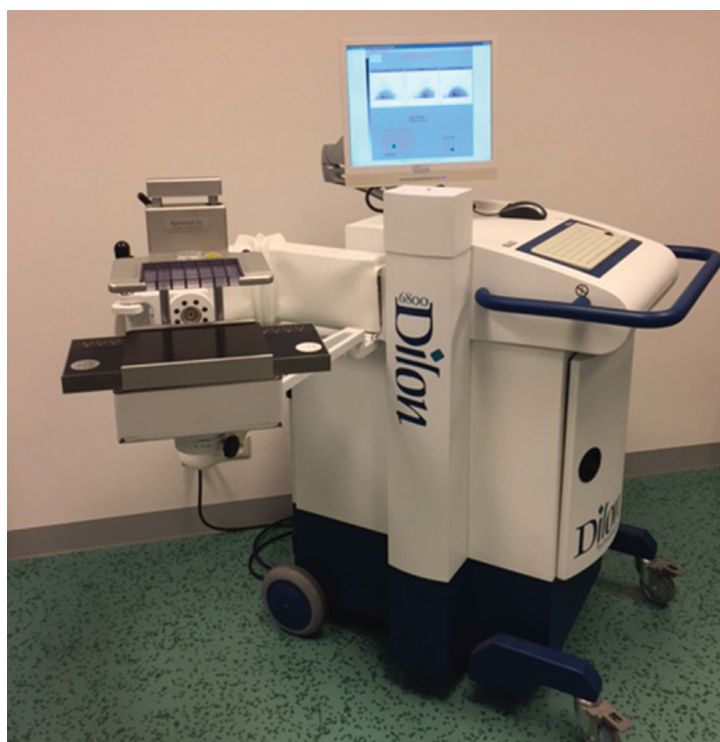
Figure 3. MBI-guided biopsy device based on the BSGI camera is equipped with a grid paddle for breast immobilisation and vacuum-assisted biopsy. Due to a slant-hole collimator placed oppositely to the biopsy device two stereotactic images may be acquired to calculate the depth of the primary lesion in the breast.

SPECT/CT is a hybrid device that combines functional and anatomic information and is based on the use of single-photon emitting radiotracers. [7] This tool is equipped with two detectors with a large field-of-view (39 x 51 cm) that rotate 360 degrees, obtaining images for 3-dimensional reconstruction. Patients are scanned in lying position. For the evaluation performed in chapter 3 of this thesis the applied SPECT/CT system (Discovery NM/CT 670 Pro, GE Healthcare, Milwaukee, US) (**Figure 4**) was a last generation device with the possibility to quantify radiotracer uptake in the lesion. [7] The experimental validation of SPECT/CT quantification for response monitoring in breast cancer is presented in this thesis.

Nowadays, SPECT/CT is increasingly used for detection and anatomical localisation of sentinel lymph nodes (SLN). [15] Indeed, preoperative SPECT/CT provides a roadmap for surgeons, allowing to choose the best surgical approach to identify SLNs in the operating room. For SLN localisation as described in chapter 8 of this thesis, SPECT/CT studies for SLN mapping in 83 patients with vulvar cancer were performed.

Figure 4. Discovery NM/CT 670 Pro SPECT/CT with two heads for SPECT acquisition in the foreground and a full ring for CT acquisition in the posterior part of the device.

PET/CT is based on the use of positron-emitting radiotracers like the glucose analogue ^{18}F-FDG. This device combines a full-ring PET detector with a CT scanner. Patients are scanned in lying position. Recently, ^{18}F-FDG PET/CT has been incorporated into the National Comprehensive Cancer Network (NCCN) guidelines in the United States for vulvar cancer. [16] Based on the rationale that malignant cells have increased ^{18}F-FDG-uptake as compared to benign cells, [17] in chapter 9 this thesis evaluates the value of dual-time-point ^{18}F-FDG PET/CT for the lymph node assessment in 33 patients with vulvar cancer scheduled for inguinofemoral lymph node dissection (**Figure 5**).

Figure 5. Gemini GXL PET/CT (Philips, Cleveland OH, US).

REFERENCES

1. Netherlands Cancer Registry. http://www.cijfersoverkanker.nl
2. Berg WA. Nuclear breast imaging: clinical results and future directions. J Nucl Med. 2016;57(1):46S-52S.
3. Hsu DF, Freese DL, Levin CS. Breast-dedicated radionuclide imaging systems. J Nucl Med. 2016;57(1):40S-5S.
4. Kieper DA, Welch BL, Fairchild LH, inventors; Dilon Technologies, Inc., assignee. Gamma guided stereotactic localization system. US Patent US8249693. August 21, 2012.
5. Raylman RR, Majewski S, Weisenberger AG, Popov V, Wojcik R, Kross B, *et al*. Positron emission mammography-guided breast biopsy. J Nucl Med. 2001;42(6):960-6.
6. Hellingman D, Teixeira SC, Donswijk ML, Rijkhorst EJ, Moliner L, Alamo J, *et al*. A novel semi-robotized device for high-precision (18)F-FDG-guided breast cancer biopsy. Rev Esp Med Nucl Imagen Mol. 2017;36(3):158-65.
7. Ritt P, Sanders J, Kuwert T. SPECT/CT technology. Clin Transl Imaging. 2014;2(6):445-57.
8. van der Vos CS, Koopman D, Rijnsdorp S, Arends AJ, Boellaard R, van Dalen JA, *et al*. Quantification, improvement, and harmonization of small lesion detection with state-of-the-art PET. Eur J Nucl Med Mol Imaging. 2017;44(1):4-16.
9. Sun Y, Wei W, Yang HW, Liu JL. Clinical usefulness of breast-specific gamma imaging as an adjunct modality to mammography for diagnosis of breast cancer: a systemic review and meta-analysis. Eur J Nucl Med Mol Imaging. 2013;40(3):450-63.
10. Fowler AM. A molecular approach to breast imaging. J Nucl Med. 2014;55(2):177-80.
11. Prekeges J. Breast imaging devices for nuclear medicine. J Nucl Med Technol. 2012;40(2):71-8.
12. Hruska CB, O'Connor MK. Nuclear imaging of the breast: translating achievements in instrumentation into clinical use. Med Phys. 2013;40(5):050901.
13. Goldsmith SJ, Parsons W, Guiberteau MJ, Stern LH, Lanzkowsky L, Weigert J, *et al*. SNM practice guideline for breast scintigraphy with breast-specific gamma-cameras 1.0. J Nucl Med Technol. 2010;38(4):219-24.
14. Collarino A, Valdés Olmos RA, van der Hoeven AF, Pereira Arias-Bouda LM. Methodological aspects of (99m)Tc-sestamibi guided biopsy in breast cancer. Clin Transl Imaging. 2016;4(5):367-76.
15. Valdés Olmos RA, Rietbergen DD, Vidal-Sicart S, Manca G, Giammarile F, Mariani G. Contribution of SPECT/CT imaging to radioguided sentinel lymph node biopsy in breast cancer, melanoma, and other solid cancers: from "open and see" to "see and open". Q J Nucl Med Mol Imaging. 2014;58(2):127-39.
16. Koh WJ, Greer BE, Abu-Rustum NR, Campos SM, Cho KR, Chon HS, *et al*. Vulvar Cancer, Version 1.2017, NCCN Clinical Practice Guidelines in Oncology. J Natl Compr Canc Netw. 2017;15(1):92-120.
17. Cheng G, Torigian DA, Zhuang H, Alavi A. When should we recommend use of dual time-point and delayed time-point imaging techniques in FDG PET? Eur J Nucl Med Mol Imaging. 2013;40(5):779-87.

PART I

MOLECULAR IMAGING USING 99MTC-SESTAMIBI IN BREAST CANCER

IS ^{99M}TC-SESTAMIBI
IMAGING ABLE TO
PREDICT PATHOLOGICAL
NONRESPONSE TO
NEOADJUVANT
CHEMOTHERAPY
IN BREAST CANCER?

A META-ANALYSIS
EVALUATING
CURRENT USE
AND SHORTCOMINGS

A Collarino
EJ de Koster
RA Valdés Olmos
LF de Geus-Oei
LM Pereira Arias-Bouda

CHAPTER 2

ABSTRACT

PURPOSE Interest in technetium-99m (^{99m}Tc)-sestamibi imaging for neoadjuvant chemotherapy (NAC) response monitoring in locally advanced breast cancer (LABC) is increasing but remains matter of discussion. The present study conducted a meta-analysis of the diagnostic performance of ^{99m}Tc-sestamibi to predict pathologic nonresponse to NAC in primary LABC.

METHODS A systematic data search was performed. Studies with a minimum of 10 LABC patients that had evaluated ^{99m}Tc-sestamibi imaging for NAC nonresponse using conventional planar scintimammography, breast-specific gamma-imaging and/or single photon emission computed tomography (SPECT)/computed tomography (CT) were included. The histopathological findings were the reference standard. The meta-analysis was performed using a mixed logistic regression model.

RESULTS The search revealed 14 eligible studies with 529 patients. Of the 14 studies, 11 had evaluated scintimammography and 3 breast-specific gamma-imaging. No studies examining SPECT or SPECT/CT were found. The overall estimated pooled sensitivity, specificity, positive and negative likelihood ratios of ^{99m}Tc-sestamibi imaging to predict nonresponsiveness to NAC were 70.3% (95% confidence interval [CI], 56.5%-81.3%), 90.1% (95% CI, 77.5%-96.0%), 7.13 (95% CI, 3.08-16.53) and 0.33 (95% CI, 0.22-0.49), respectively. Only 3 studies (107 patients) evaluated ^{99m}Tc-sestamibi imaging during NAC, reported an estimated pooled sensitivity of 87% (95% CI, 72%-100%) and specificity of 93% (95% CI, 85%-100%).

CONCLUSION Only planar ^{99m}Tc-sestamibi imaging has been investigated for NAC nonresponse in LABC but showed low sensitivity to predict pathologic nonresponse. However, most studies focused on the prediction of pathologic complete response after NAC. Although experience is limited, ^{99m}Tc-sestamibi uptake during NAC seems highly sensitivity for the prediction of nonresponsiveness. Features such as SPECT/CT imaging, standardised quantification, relation to tumour subtypes, and proper timing have been insufficiently evaluated and require further investigation.

INTRODUCTION

Breast cancer (BC) is the most frequent malignancy in women worldwide. In the Unites States, 246,660 new cases and 40,450 deaths were estimated to have occurred in 2016. [1] Locally advanced BC (LABC) encompasses stage IIb-III invasive BC and presents with $\geq$ 1 of the following features: a primary tumour > 5 cm (T3), a tumour of any size with direct skin or chest wall invasion (T4), lymph node metastases (N2-N3), or inflammatory BC. [2] Neoadjuvant chemotherapy (NAC), also known as preoperative chemotherapy, is the first-line treatment for LABC. NAC enables breast-conserving surgery by reducing the tumour size. It also eradicates micrometastatic disease and allows for assessment of tumour chemosensitivity in vivo. [3, 4] Tumour resistance to chemotherapy is the major cause of therapy failure in LABC. The early prediction of the response to NAC might allow for a timely switch to alternative drugs in those without a response, avoiding ineffective chemotherapy, and offering more personalised therapy. In recent years, ^{18}F-fluorodeoxyglucose (^{18}F-FDG) positron emission tomography (PET) with or without computed tomography (CT) has been evaluated for the early prediction of the NAC response after the first or second cycle of therapy, showing a pooled sensitivity of 88% (95% confidence interval [CI], 80%-94%) and specificity of 70% (95% CI, 63%-77%). [5] Therefore, the role of early ^{18}F-FDG PET/CT to monitor the metabolic response remains unclear, most probably owing to the low number of included studies (7 studies). [5] Moreover, ^{18}F-FDG uptake is strongly influenced by the breast tumour subtype (e.g., estrogen receptor-negative tumours, triple negative tumours, and tumours with high expression of proliferation marker Ki-67 have high tumour ^{18}F-FDG uptake). [6] To date, technetium-99m (99mTc)-methoxyisobutylisonitrile (^{99m}Tc-sestamibi) is the most widely used non-PET radiotracer in oncology. Although originally introduced as a perfusion agent for nuclear cardiology studies, [7] it has been applied as a tumour-seeking agent since 1994 for breast malignancies.[8, 9] ^{99m}Tc-sestamibi accumulates principally within the mitochondria, and its diagnostic value is based on the increased vascularity and greater cytoplasmic mitochondrial density in breast cancer cells. [10, 11] However, cellular accumulation of ^{99m}Tc-sestamibi is reduced in cases of overexpression of multidrug resistance-associated plasma membrane proteins such as P-glycoprotein (Pgp) and multidrug resistance associated protein, and the anti-apoptotic Bcl-2 protein on the outer mitochondrial membrane. [12] ^{99m}Tc-sestamibi was originally validated as a transport substrate for Pgp, [13] which is encoded by the multidrug resistance (MDR) gene and functions as an energy dependent efflux pump for many drugs.[14, 15]

At present, [99mTc]-sestamibi allows for in vivo assessment of tumour chemoresistance and could potentially identify nonresponding patients early during NAC. For breast functional imaging using [99mTc]-sestamibi, several modalities, such as scintimammography (SMG), breast-specific gamma-imaging (BSGI), and single photon emission computed tomography (SPECT)/computed tomography (CT) have been validated. However, only a few of the studies reported on LABC and the chemotherapy response. Therefore, the aim of the present meta-analysis was to evaluate the diagnostic value of [99mTc]-sestamibi imaging to predict pathologic nonresponse to NAC in primary LABC and to establish which modalities were involved.

MATERIALS AND METHODS

SEARCH STRATEGY

We performed a systematic data search of the PubMed/MEDLINE and Embase databases using the Preferred Reporting Items for Systematic Reviews and Meta-analysis (PRISMA) guidelines. [16] The following keywords were used: "sestamibi" AND "breast cancer" AND "neoadjuvant chemotherapy." Multiple synonyms were included, such as "MIBI," "mamma," and "preoperative". No start date limit was applied, and the search was continued until September 5, 2016. The language was restricted to English. The references of the retrieved reports were screened to identify additional studies.

STUDY SELECTION

Two of us (A.C., L.M.P.A.-B.) independently screened the title and abstracts of the retrieved studies. Original articles investigating the value of [99mTc]-sestamibi imaging to predict a pathologic nonresponse to NAC in primary LABC patients were eligible for inclusion. Review articles, letters to the editor, editorials, and case reports were excluded. Also excluded were articles that had included < 10 patients, had overlapping patient data, or that had been written in a language other than English. Two of us (A.C., L.M.P.A.-B.) then independently reviewed the full-text version of the remaining reports to confirm their eligibility for inclusion.

QUALITY ASSESSMENT

Subsequently, 2 of us (A.C., E.J.d.K.) independently evaluated the methodological quality of the included studies using the Quality Assessment of Diagnostic Accuracy Studies tool, version 2

(QUADAS-2). [17] The QUADAS-2 tool grades the risk of bias and applicability on 4 key domains (i.e., patient selection, index test, reference standard, and flow and timing), supported by a limited number of signaling questions. The results of the quality appraisals from both authors were compared, and any disagreements were resolved by consensus after re-evaluation and discussion of the respective references. The QUADAS-2 scores for all included studies were tabulated, and a summary report was constructed.

DATA EXTRACTION

For each approved study, information was extracted concerning the study data (authors, year of publication, country of origin), study design (prospective or retrospective), number of evaluated patients with LABC, and method (type of imaging, time of acquisition, type of analysis, definition of response on ^{99m}Tc-sestamibi imaging, and method of pathologic assessment). Individual study data were extracted to retrieve the number of true-positive (TP), true-negative (TN), false-positive, and false-negative ^{99m}Tc-sestamibi scans. The TP scan results were defined as showing no response to NAC on ^{99m}Tc-sestamibi imaging with confirmed tumour presence at pathologic examination. The TN scan results were those showing a response to NAC on ^{99m}Tc-sestamibi imaging with subsequent confirmed significant tumour reduction or complete tumour absence at pathologic examination. The extracted data were ordered into 2 x 2 contingency tables, from which estimations for the pooled diagnostic performance parameters could be calculated using the classic equations.

STATISTICAL ANALYSIS

Statistical analyses were performed using Stata/MP, version 14.2 (StataCorp LP, College Station, TX). [18] The pooled sensitivity, specificity, and positive and negative likelihood ratios (LRs) and their corresponding 95% CIs were estimated using the metandi and midas commands in Stata/MP. [19, 20] The metandi command applies a 2-level mixed logistic regression model with independent binomial distributions for the TP and TN results dependent on the sensitivity and specificity in each study, and a bivariate normal model for the logic transforms of between study sensitivity and specificity. [20] The user-written midas command uses a bivariate mixed-effects binary regression model to estimate pooled test performance parameters. [19] Pooled results are presented in forest plots and summary receiver operating characteristic (ROC) plots, including the area under the summary ROC curve (AUC). Heterogeneity between studies was assessed by visual inspection of the forest plots and estimated using the inconsistency index I^2. Because sensitivity and specificity

are often inversely related, the threshold effect was assessed. The metandi and midas commands can only be applied to data from a minimum of 4 studies. For meta-analysis of fewer studies, we used the Stata/MP metaprop command and random effects modelling to estimate the pooled sensitivity, specificity, and positive and negative LRs.

RESULTS

DATA SEARCH AND STUDY SELECTION

The systematic study selection is shown in a flowchart in **Figure 1**. The initial data search identified 167 citations, including 48 citations from PubMed/MEDLINE and 119 from Embase. Forty-four duplicate studies were excluded. Screening of titles and abstracts excluded 109 articles according to the inclusion and exclusion criteria previously described. Specifically, the excluded articles were 64 off-topic studies, 18 conference abstracts, 15 review articles, 4 case reports, 6 articles written in a language other than English, and 2 studies with < 10 patients. The full text of the 14 remaining articles was retrieved. These articles had no data overlap. No additional studies were found by screening the references of the selected articles. Finally, the 14 eligible articles (529 patients) were included in the present meta-analysis (**Figure 1**). [21-34]

QUALITY APPRAISAL

The results of the QUADAS-2 assessment are shown in **Figure 2**. The risk of bias was mostly scored as low. However, the risk of bias for the domain "patient selection" often remained unclear owing to absent reports on patient inclusion criteria and consecutiveness of inclusion. No real concerns on the applicability of the studies for this meta-analysis were present. All the studies were deemed of sufficient methodological quality, and no articles were excluded from further analysis.

STUDY CHARACTERISTICS

The results for 529 patients from 14 studies were included in the present meta-analysis. The characteristics of the selected studies are outlined in **Table 1**. Most of the included reports concerned prospective trials. The sample size of the included studies varied from 17 to 122 patients, SMG was used as the imaging modality in 11 studies [21-27, 31-34] and BSGI in 3 studies. [28-30] No studies using SPECT or SPECT/CT were found. Only 3 studies evaluated the role of [99mTc]-sestamibi to predict nonresponsiveness during NAC. [23, 29, 34]

Figure 1. Flow chart showing search strategy.
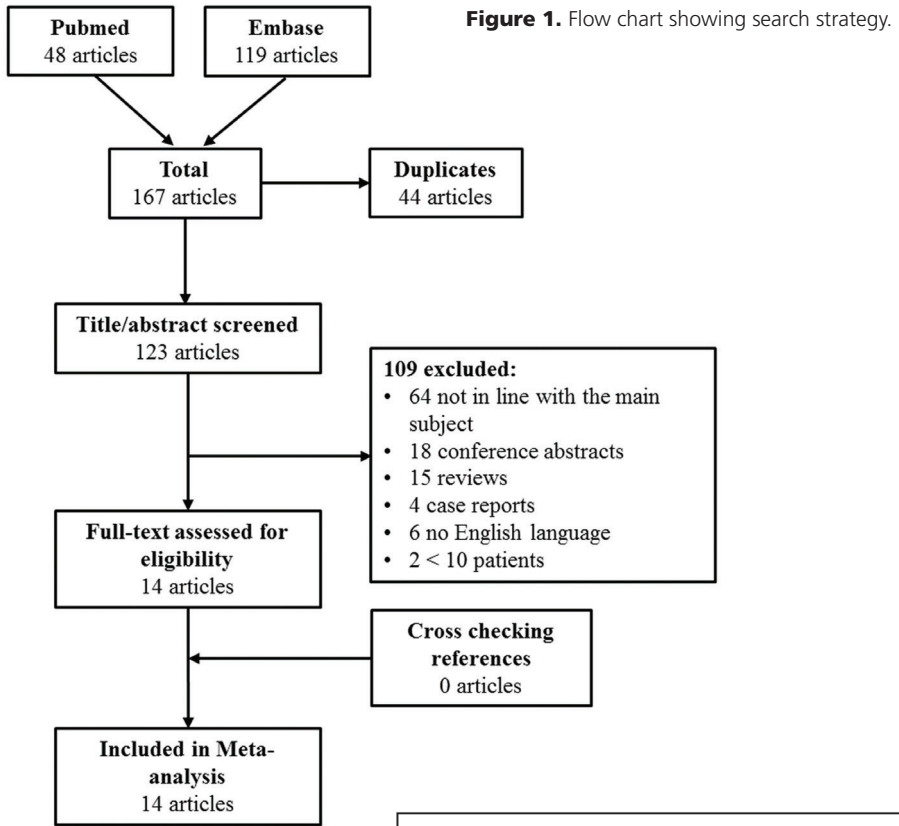
Figure 2.

Summary of methodological quality scored according to Quality Assessment of Diagnostic Accuracy Studies tool, version 2 (QUADAS-2).
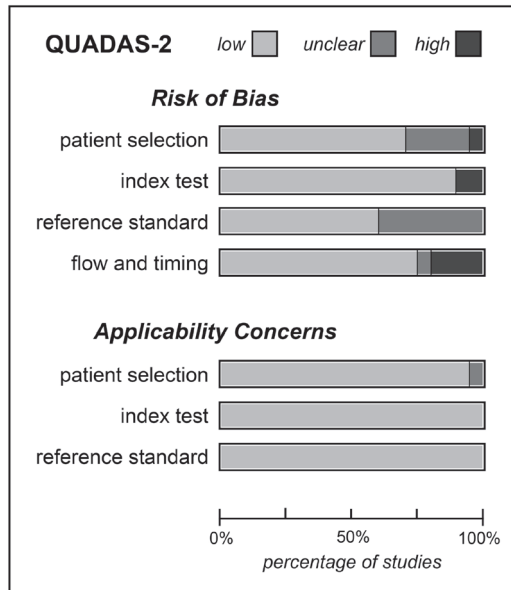
Table 1. Characteristics of included studies

Investigator	Year	Country	Study type	Patients (lesions)	Imaging in relation to NAC	Imaging modality
Maini et al [21]	1997	Italy	-	29	After	SMG
Ciarmiello et al [22]	1998	Italy	Prospective	39	Before	SMG
Mankoff et al [23]	1999	USA	-	29	During	SMG
Cayre et al [24]	2002	France	Prospective	45	Before	SMG
Sciuto et al [25]	2002	Italy	Prospective	30	Before	SMG
Mezi et al [26]	2003	Italy	Prospective	24	After	SMG
Marshall et al [27]	2005	UK	Prospective	26	After	SMG
Roedler et al [28]	2012	US	Prospective	17[a] (18)	After	BSGI
Mitchell et al [29]	2013	US	Prospective	19	During	BSGI
Lee et al [30]	2014	Korea	Retrospective	122	After	BSGI
Trehan et al [31]	2014	India	Prospective	20	Before	SMG
Evangelista et al [32]	2014	Italy	Prospective	18	After	SMG
Evangelista et al [33]	2014	Italy	-	51	Before	SMG
Novikov et al [34]	2015	Russia	Prospective	59	During	SMG

Acquisition point and analysis type	Definition of response on MIBI Imaging	Response definition	Pathologic criteria for response	Pathologic criteria for nonresponse
Early (10 min); delayed (90 min); visual analysis	No uptake	pCR	Fibrosis or isolated tumour cells	Invasive carcinoma >25%
Dynamic planar, 5 min, 1 h; 2 h and 4 h; $T_{(1/2)}$ (cut-off, 204 min)	T(1/2) >204 min	pCR	No tumour cells or scattered tumour cells	Macroscopic residual tumour
Early (10 min); visual analysis	Decreased uptake	pR	Tumour size reduced >50% or complete eradication	Tumour size reduced <50% or increased
Early (10 min); visual analysis	Medium or high uptake	pCR	Sataloff criteria	Sataloff criteria
Early (10 min); delayed (4 h) WOR (cut-off, 45%)	WOR ≤45%	pR	Tumour size reduced >75%	Tumour size reduced <75% or increased
Early (10 min); delayed (4 h); WOR (cut-off, 56%)	WOR ≤56%	pCR	No tumour cells found	Tumour cells found
Early (10 min); T/B	T/B ratio,1.0	pCR	N/A	N/A
Early (5 min); T/B	T/B ratio, ≤1.0	pCR	Complete eradication	No complete eradication
Early (5 min); T/B	T/B ratio reduction, ≥50%	pCR	No invasive disease and DCIS	Invasive disease and DCIS
Early (10 min); visual analysis	No uptake	pCR	No invasive disease and DCIS	Invasive disease and DCIS
Early (10 min); delayed (2 h); WOR (cut-off, 45%)	WOR ≤45%	pR	Tumour size reduced >50% or complete	Tumour size reduced <50% or increased
Early (5min); delayed (3 h); WOR (cut-off, 45%)	WOR ≤45%	pCR	N/A	N/A
Early (5 min); delayed (3 h); WOR (cut-off, 45%)	WOR ≤45%	pCR	Sataloff criteria	Sataloff criteria
Early (10 min); T/B	T/B ratio reduction, >70%	pCR	No tumour cells found	Tumour cells found

BSGI breast-specific gamma-imaging, DCIS ductal carcinoma in situ, MIBI 99mTc-sestamibi, pCR pathologic complete response, pR pathologic response, SMG scintimammography, $T_{(1/2)}$ time to half clearance, T/B tumour to background, WOR washout rate, [a] one of 17 patients underwent neoadjuvant hormonal therapy.

META-ANALYSIS RESULTS

The results of the meta-analysis are outlined in **Table 2**, and forest plots of the accuracy parameters of the 14 included studies are presented in **Figure 3**. The estimated pooled sensitivity, specificity, positive LR, and negative LR of ^{99m}Tc-sestamibi imaging to predict a nonresponse to NAC (presence of residual tumour) was 70.3% (95% CI, 56.5%-81.3%), 90.1% (95% CI, 77.5%-96.0%), 7.13 (95% CI, 3.08-16.53), and 0.33 (95% CI, 0.22-0.49), respectively. The ROC curve showed an AUC of 0.88 (95% CI, 0.85-0.91; **Figure 4**). Significant heterogeneity was found among the studies. The I^2 was 79.1% for sensitivity and 79.6% for specificity. The proportion of heterogeneity that was likely due to by the threshold effect was 0.30.

Of the 14 studies, 11 used a strict criterion for the TN definition based on a pathologic complete response (pCR; complete tumour absence). This resulted in an estimated pooled sensitivity, specificity, positive LR, and negative LR of ^{99m}Tc-sestamibi imaging to predict a nonresponse to NAC (presence of microscopic residual tumour) was 69% (95% CI, 54%-80.3%), 91% (95% CI, 72%-97.3%), 7.41 (95% CI, 2.3-24), and 0.35 (95% CI, 0.23-0.52), respectively. The ROC curve showed an AUC of 0.86 (95% CI, 0.83-0.89). Significant heterogeneity was seen among the studies, with an I^2 of 81% for both sensitivity and specificity. In contrast, using significant tumour reduction (pR) for the definition of TN as applied in 3 studies, the estimated pooled sensitivity and specificity of ^{99m}Tc-sestamibi imaging for predicting a nonresponse to NAC were 74% (95% CI, 39%-100%) and 92% (95% CI, 85%-100%). The I^2 was 82.5% for sensitivity and 0% for specificity.

A subgroup analysis of ^{99m}Tc-sestamibi imaging used during NAC treatment was performed on 3 eligible studies with 107 patients. The diagnostic performance of ^{99m}Tc-sestamibi imaging during NAC in the 3 included studies is listed in **Table 3**. The estimated pooled sensitivity and specificity of ^{99m}Tc-sestamibi to predict a nonresponse during NAC were 87% (95% CI, 72%-100%) and 93% (95% CI, 85%-100%), respectively. The I^2 was 67% for sensitivity and 0% for specificity.
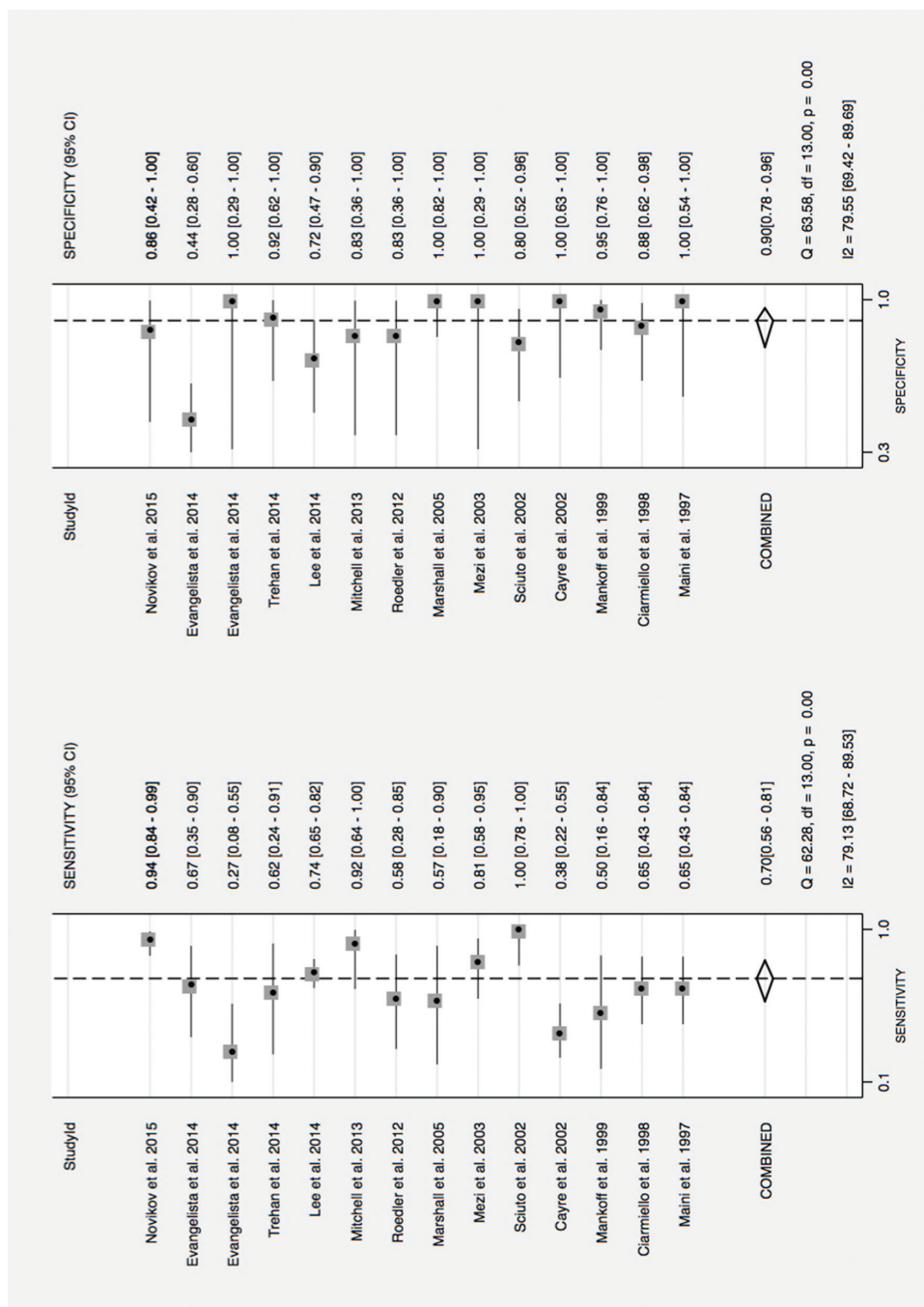
Figure 3. Forest plots of overall sensitivity and specificity for the prediction of neoadjuvant chemotherapy nonresponse in locally advanced breast cancer using technetium-99m sestamibi imaging.
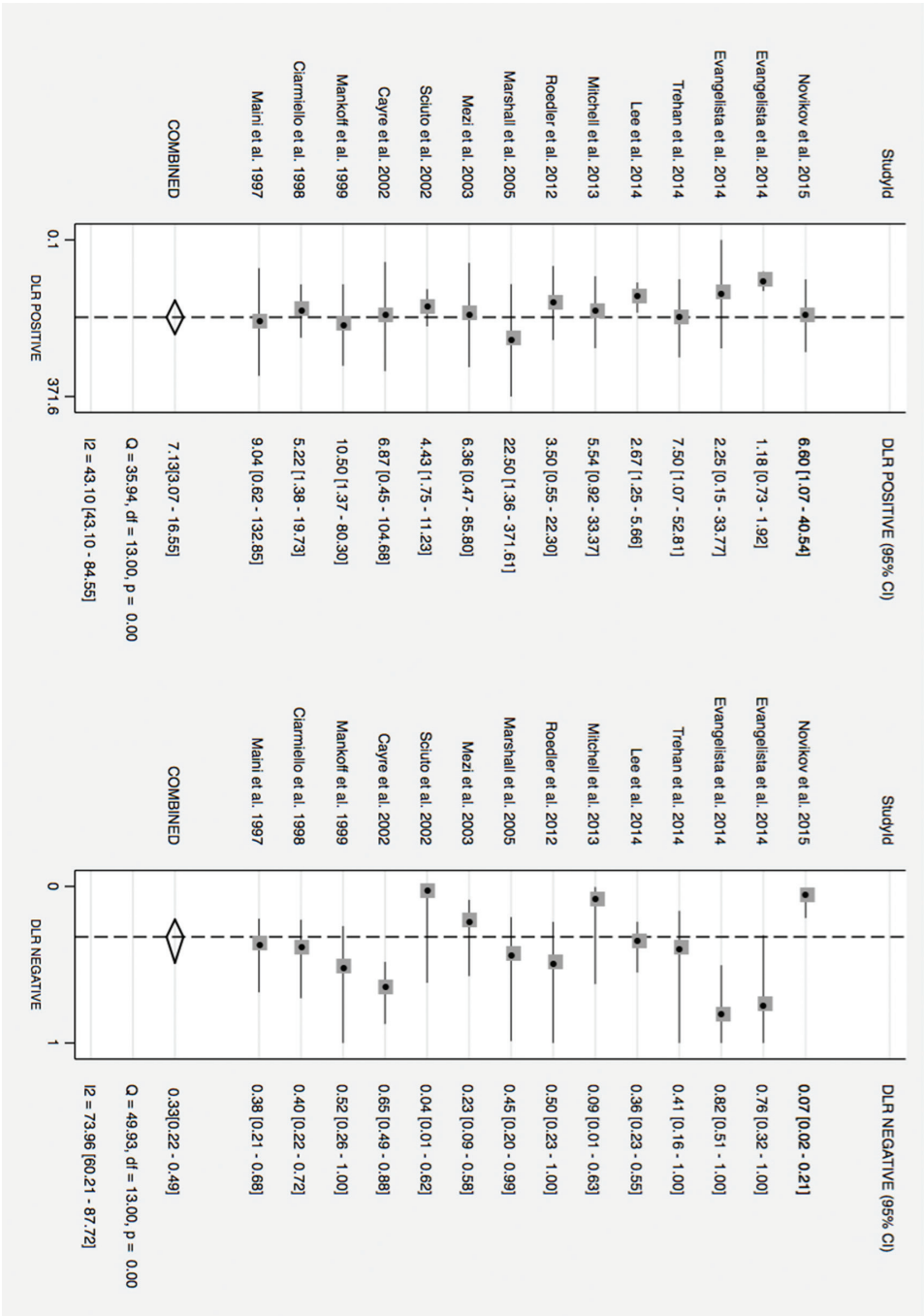
Figure 3 (*continued*). Forest plots of overall positive and negative likelihood ratios for the prediction of neoadjuvant chemotherapy nonresponse in locally advanced breast cancer using technetium-99m sestamibi imaging.
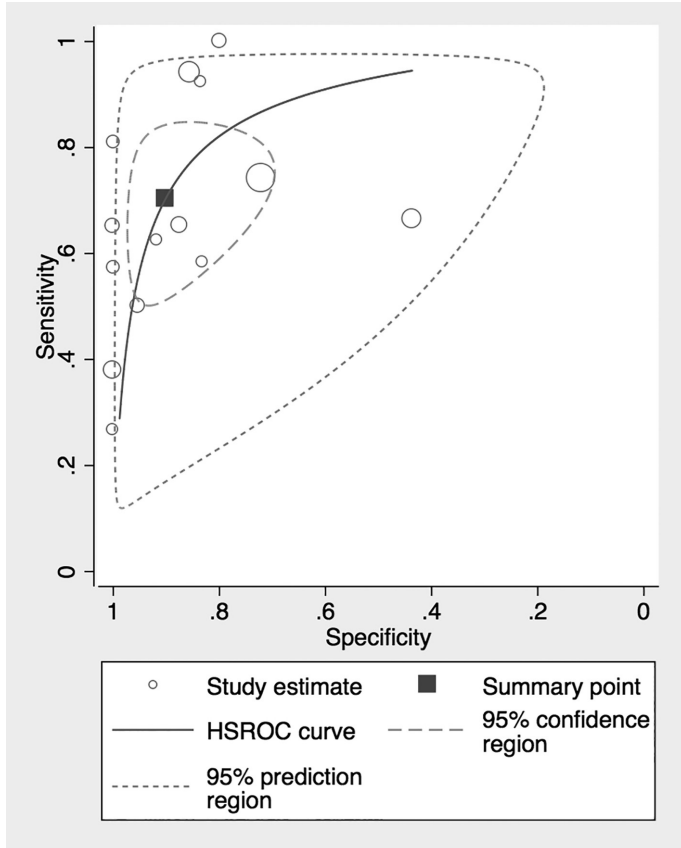
Figure 4. Hierarchical summary receiver operating characteristic curve (HSROC) for prediction of neoadjuvant chemotherapy nonresponse in locally advanced breast cancer using technetium-99m sestamibi imaging.

Table 2. Pooled diagnostic performance estimates for prediction of
NAC nonresponse using technetium-99m sestamibi imaging

Investigator	Patients (n)	TP	FP	FN	TN	NAC response (%)
Maini et al [21]	29	15	0	8	6	21%
Ciarmiello et al [22]	39	15	2	8	14	41%
Mankoff et al [23]	29	4	1	4	20	72%
Cayre et al [24]	45	14	0	23	8	18%
Sciuto et al [25]	30	15	3	0	12	50%
Mezi et al [26]	24	17	0	4	3	13%
Marshall et al [27]	26	4	0	3	19	73%
Roedler et al [28]	18	7	1	5	5	33%
Mitchell et al [29]	19	12	1	1	5	32%
Lee et al [30]	122	77	5	27	13	15%
Trehan et al [31]	20	5	1	3	11	60%
Evangelista et al [32]	18	4	0	11	3	17%
Evangelista et al [33]	51	8	22	4	17	76%
Novikov et al [34]	59	49	1	3	6	12%
POOLED RESULTS	529	246	37	104	142	33.8%

Sensitivity (%)	Specificity (%)	Positive LR	Negative LR
65 (43-84)	100 (54-100)	9.04 (0.62-132.85)	0.38 (0.21-0.68)
65 (43-84)	88 (62-98)	5.22 (1.38-19.73)	0.40 (0.22-0.72)
50 (16-85)	95 (76-100)	10.50 (1.37-80.30)	0.52 (0.26-1.06)
38 (22-55)	100 (63-100)	6.87 (0.45-104.68)	0.65 (0.49-0.88)
100 (78-100)	80 (52-96)	4.43 (1.75-11.23)	0.04 (0.00-0.62)
81 (58-95)	100 (29-100)	6.36 (0.47-85.80)	0.23 (0.09-0.58)
57 (18-90)	100 (82-100)	22.50 (1.36-371.61)	0.45 (0.20-0.99)
58 (28-85)	83 (36-100)	3.50 (0.55-22.30)	0.50 (0.23-1.07)
92 (64-100)	83 (36-100)	5.54 (0.92-33.37)	0.09 (0.01-0.63)
74 (65-82)	72 (47-90)	2.67 (1.25-5.66)	0.36 (0.23-0.55)
63 (24-91)	92 (62-100)	7.50 (1.07-52.81)	0.41 (0.16-1.02)
27 (8-55)	100 (29-100)	2.25 (0.15-33.77)	0.82 (0.51-1.33)
67 (35-90)	44 (28-60)	1.18 (0.73-1.92)	0.76 (0.32-1.84)
94 (84-99)	86 (42-100)	6.60 (1.07-40.54)	0.07 (0.02-0.21)
70.3 (56.5-81.3)	**90.1 (77.5-96.0)**	**7.13 (3.08-16.53)**	**0.33 (0.22-0.49)**

Data in parentheses are 95% confidence intervals. **FP** false positive, **FN** false negative, **LR** likelihood ratio, **NAC** neoadjuvant chemotherapy, **TN** true negative, **TP** true positive.

Table 3. Pooled diagnostic performance estimates for prediction of NAC nonresponse using ^{99m}Tc-sestamibi imaging performed during NAC

Investigator	Patients (n)	TP	FP	FN	TN	NAC response (%)	Sensitivity (%)	Specificity (%)
Mankoff *et al* [23]	29	4	1	4	20	72%	50 (16-85)	95 (76-100)
Mitchell *et al* [29]	19	12	1	1	5	32%	92 (64-100)	83 (36-100)
Novikov *et al* [34]	59	49	1	3	6	12%	94 (84-99)	86 (42-100)
POOLED RESULTS	107	65	3	8	31	31.8%	87 (72-100)	93 (85-100)

Data in parentheses are 95% confidence intervals. **FN** false negative, **FP** false positive, **NAC** neoadjuvant chemotherapy, **TN** true negative, **TP** true positive.

DISCUSSION

Although consensus exists about ^{18}F-FDG PET/CT as a useful tool for the staging of LABC, [35] its role in therapy monitoring remains a matter of discussion. The use of ^{18}F-FDG PET/CT for this purpose likely depends on the breast cancer subtype and combined application of magnetic resonance imaging (MRI). [6, 36] As an alternative to ^{18}F-FDG PET/CT, ^{99m}Tc-sestamibi allows the in vivo assessment of tumour chemoresistance and could potentially identify nonresponding patients early during NAC. The results from our meta-analysis of 14 studies showed that ^{99m}Tc-sestamibi imaging based on planar imaging has a relatively low sensitivity (70.3%) and high specificity (90.1%) to correctly predict nonresponse in LABC patients undergoing NAC.

However, the number of available studies using ^{99m}Tc-sestamibi was rather limited, and an adequate comparison of the results was quite difficult owing to the substantial heterogeneity among the studies. Because of the findings from the present meta-analysis, we would like to discuss the heterogeneity among the studies from a clinical viewpoint and make suggestions for improvement of the technique and future research.

The most remarkable heterogeneity was that the studies focused on different tasks for ^{99m}Tc-sestamibi imaging. The studies included in our meta-analysis used different definitions to describe NAC response and nonresponse. Most studies used a strict definition of TN (response), defined

as the absence of tumour cells in the surgical specimen after NAC (pCR). Using this definition, we found that ^{99m}Tc-sestamibi imaging had a relatively low sensitivity (69%) and high specificity (91%) for the prediction of microscopic residual disease after NAC. This suggests that ^{99m}Tc-sestamibi imaging is not clinically useful to rule out the presence of residual tumour. However, these results are comparable to the performance of ^{18}F-FDG PET/CT for this indication. Recent meta-analyses have shown that MRI and ^{18}F-FDG PET/CT might play a complementary role for this purpose, [37, 38] albeit it is unlikely that any imaging modality will be able to rule out microscopic foci of viable tumour cells.

A more attainable goal for ^{99m}Tc-sestamibi imaging in this respect would to identify treatment failure at an early stage during NAC, which would enable clinicians to adjust the chemotherapy plan. However, only a few of the investigated studies focused on this task. Only 3 studies investigated the ability of ^{99m}Tc-sestamibi to predict nonresponsiveness before or early during NAC, showing a moderate sensitivity (74%) and a high specificity (92%). However, because of the limited number of studies and their methodological heterogeneity, conclusions could not be drawn. Further studies are needed to assess the role of ^{99m}Tc-sestamibi in predicting nonresponsiveness to NAC at an early stage.

Another source of heterogeneity was the diversity in imaging modalities used in the studies. Most of the included studies used conventional SMG. Compared with dedicated breast devices such as BSGI and molecular breast imaging (MBI), traditional SMG has the following drawbacks: **1)** limited intrinsic resolution for breast lesions < 1 cm; **2)** a greater effect of scatter radiation from the heart and liver owing to the large field-of-view; **3)** an inability to apply light breast compression for motion reduction and minimise breast tissue attenuation, and **4)** limited possibilities for breast positioning, thus the impossibility of multiple projections comparable to that with mammography. [39] These limitations result in low resolution and contrast of breast lesions and might, in particular, limit the detection of small residual tumours using conventional SMG. In contrast, modern BSGI and dual-head MBI systems achieve a resolution of 2 to 5 mm and provide a lower scatter fraction. [40, 41] Furthermore, the solid-state, cadmium-zinc-telluride, dual-head technology of new MBI devices allows for a reduction of the administered dose of ^{99m}Tc-sestamibi to 150 to 300 MBq. [42]

None of the ^{99m}Tc-sestamibi studies assessing the response to NAC used SPECT or SPECT/CT. SPECT is a tomographic technique with better contrast resolution compared with conventional planar imaging and, [43] combined with CT in a SPECT/CT device, provides fused functional and

anatomic images. The new generation of SPECT/CT systems includes, not only a more sensitive SPECT, but also an improved CT component able to display an anatomic environment with specific landmarks to evaluate the functional SPECT findings. Although the spatial resolution of SPECT/CT is lower than that of MBI systems, modern SPECT/CT systems provide the possibility of absolute quantification, enabling measurement of quantitative tumour parameters such as the SPECT standardised uptake value and functional tumour volume. This in vivo absolute tumour quantification might improve the performance of ^{99m}Tc-sestamibi imaging as a therapy monitoring tool in LABC. Moreover, recent improvements in SPECT/CT technology have resulted in the development of a dedicated breast SPECT/CT system with high intrinsic resolution comparable to that of modern MBI devices. However, although this dedicated SPECT/CT camera, which combines the advantage of high resolution and eligibility for in vivo quantification, has high clinical potential, [44] it requires validation in larger series of patients.

In addition to the variability in imaging techniques, the methods and criteria used for image interpretation were diverse in the currently available data. Some studies used the washout rate (WOR) of the tracer as an evaluation parameter, [25, 26, 31-33] and others evaluated the tumour-to-background uptake ratios. [27-29, 34] We believe that the ^{99m}Tc-sestamibi WOR is the best parameter for predicting tumour nonresponse to NAC because it reflects tumour cell chemoresistance. In particular, the rapid washout of ^{99m}Tc-sestamibi (WOR ≤45%) was associated with tumour chemoresistance due to the overexpression of Pgp and MDR1. [12] In contrast to the PET/CT approach, which applies standardised PET Response Criteria in Solid Tumours to assess ^{18}F-FDG tumour uptake, [45] response evaluation criteria for functional ^{99m}Tc-sestamibi imaging have not yet been established.

Finally, most studies used different timing for ^{99m}Tc-sestamibi monitoring in relation to NAC (before, during, or after treatment). The combined interpretation of the results hints that the timing of ^{99m}Tc-sestamibi imaging is a possible key to accurately delineating a model of prediction for the NAC response. The studies that used ^{99m}Tc-sestamibi imaging during NAC for response evaluation showed relatively high performance for predicting nonresponsiveness (pooled sensitivity and specificity rates of 87% and 93%, respectively). Again, conclusions should not yet be drawn because of the limited number of studies and because different definitions of the pathologic response were applied (pCR vs. significant tumour reduction). The early prediction of response and nonresponse during NAC might allow switching to alternative chemotherapy schedules for those with no response, thereby tailoring their personal treatment and reducing unnecessary side

effects. As previously mentioned, we found that ^{99m}Tc-sestamibi imaging before or during the course of NAC had a moderate pooled sensitivity (74%) and high specificity (92%) to correctly predict treatment failure, although the number of studies investigating this task of ^{99m}Tc-sestamibi imaging was limited. In contrast, PET/CT and MRI assessments during NAC could potentially demonstrate a similar accuracy if the 2 modalities are used together, but the evidence is limited. [36] The correlation between ^{99m}Tc-sestamibi uptake and tumour subtype (luminal, human epidermal growth factor receptor, triple negative) was evaluated in only 3 studies. [21, 30, 33] Although few data were included, no strong correlation was found between ^{99m}Tc-sestamibi uptake and tumour subtype. This appears to contrast with the results from PET/CT studies showing ^{18}F-FDG uptake is strongly influenced by breast tumour subtype. [6]

Recently, Guo *et al* [46] published a meta-analysis of 14 studies that used ^{99m}Tc-sestamibi to predict the NAC response in breast cancer. Of the 14 studies evaluated in their analysis, 13 were also included in our study. Although the method and analysis of Guo *et al* [46] were well described, some individual patient data were incorrectly cited and concerns exist with respect to their data extraction. Meta-regression was performed but did not include the necessary study level parameters to determine the factors related to heterogeneity. We deemed the number of available studies too small to perform a strong and accurate meta-regression analysis; therefore, we opted for a qualitative discussion. Finally, Guo *et al* [46] did not relate their results to the clinical setting nor suggest possible future investigations in this field. In the future, it will be necessary to determine whether standardisation of ^{99m}Tc-sestamibi imaging and quantification might improve the results. Also, a focus on early response monitoring, the incorporation of variables such as tumour subtype, SPECT/CT, and/or MBI, the application of appropriate imaging criteria for determining the response, and the determination of the appropriate timing are needed. In analogy to the PET/CT approach, a semiautomatic segmentation tool allowing measurement of regional concentrations of tumour uptake in MBq/mL should be validated further in future ^{99m}Tc-sestamibi studies that include dedicated SPECT/CT for early NAC response monitoring.

Furthermore, the incorporation of new tracers as possible markers of early tumour response might become relevant when using SPECT/CT for monitoring. In particular, tracers such as ^{99m}Tc-avß3, with high affinity for the avß3 integrin in endothelial cells undergoing angiogenesis, [47, 48] ^{99m}Tc-annexin V assessing apoptosis, [49] ^{99m}Tc-DMSA, [50] and ^{99m}Tc-bombesin [51, 52] might provide new insights.

Finally, it is necessary to highlight some limitations in our meta-analysis. First, the assessed heterogeneity among the studies was not completely eliminated by the subgroup analysis.

Second, the research was limited to the English language, which introduced an additional possible selection bias. Third, a limited number of studies were included in the subgroup analysis, highlighting the need for larger series and more multicentre studies.

CONCLUSION

Only conventional planar ^{99m}Tc-sestamibi SMG and, to a limited extent, dedicated breast planar imaging have been investigated to monitor the NAC nonresponse in LABC patients. Low sensitivity and high specificity were found to predict pathologic nonresponsiveness, albeit most studies focused on the prediction of pCR after NAC and not on the early prediction of treatment failure. ^{99m}Tc-sestamibi imaging during NAC seems highly sensitive for the prediction of nonresponsiveness; however, the experience is limited to a few small and heterogenic studies. Future research should focus on the early prediction of treatment failure using quantitative SPECT/CT and MBI, standardisation of the definition of the ^{99m}Tc-sestamibi response and timing, and the possible associations with tumour subtypes.

REFERENCES

1. Siegel RL, Miller KD, Jemal A. Cancer statistics, 2016. CA Cancer J Clin. 2016;66(1):7-30.
2. Edge SB, Byrd DR, Compton CC, *et al.* AJCC cancer staging manual. 7th ed. New York, NY: Springer; 2010.
3. Kaufmann M, von Minckwitz G, Mamounas EP, Cameron D, Carey LA, Cristofanilli M, *et al.* Recommendations from an international consensus conference on the current status and future of neoadjuvant systemic therapy in primary breast cancer. Ann Surg Oncol. 2012;19(5):1508-16.
4. Dialani V, Chadashvili T, Slanetz PJ. Role of imaging in neoadjuvant therapy for breast cancer. Ann Surg Oncol. 2015;22(5):1416-24.
5. Wang Y, Zhang C, Liu J, Huang G. Is 18F-FDG PET accurate to predict neoadjuvant therapy response in breast cancer? A meta-analysis. Breast Cancer Res Treat. 2012;131(2):357-69.
6. Keam B, Im SA, Koh Y, Han SW, Oh DY, Cho N, *et al.* Early metabolic response using FDG PET/CT and molecular phenotypes of breast cancer treated with neoadjuvant chemotherapy. BMC Cancer. 2011;11:452.
7. Wackers FJ, Berman DS, Maddahi J, Watson DD, Beller GA, Strauss HW, *et al.* Technetium-99m hexakis 2-methoxyisobutyl isonitrile: human biodistribution, dosimetry, safety, and preliminary comparison to thallium-201 for myocardial perfusion imaging. J Nucl Med. 1989;30(3):301-11.
8. Kao CH, Wang SJ, Liu TJ. The use of technetium-99m methoxyisobutylisonitrile breast scintigraphy to evaluate palpable breast masses. Eur J Nucl Med. 1994;21(5):432-6.
9. Burak Z, Argon M, Memi A, Erdem S, Balkan Z, Duman Y, *et al.* Evaluation of palpable breast masses with 99Tcm-MIBI: a comparative study with mammography and ultrasonography. Nucl Med Commun. 1994;15(8):604-12.
10. Maublant JC, Zhang Z, Rapp M, Ollier M, Michelot J, Veyre A. In vitro uptake of technetium-99m-teboroxime in carcinoma cell lines and normal cells: comparison with technetium-99m-sestamibi and thallium-201. J Nucl Med. 1993;34(11):1949-52.
11. Scopinaro F, Schillaci O, Scarpini M, Mingazzini PL, Di Macio L, Banci M, *et al.* Technetium-99m sestamibi: an indicator of breast cancer invasiveness. Eur J Nucl Med. 1994;21(9):984-7.
12. Moretti JL, Hauet N, Caglar M, Rebillard O, Burak Z. To use MIBI or not to use MIBI? That is the question when assessing tumour cells. Eur J Nucl Med Mol Imaging. 2005;32(7):836-42.
13. Piwnica-Worms D, Chiu ML, Budding M, Kronauge JF, Kramer RA, Croop JM. Functional imaging of multidrug-resistant P-glycoprotein with an organotechnetium complex. Cancer Res. 1993;53(5):977-84.
14. Gottesman MM, Fojo T, Bates SE. Multidrug resistance in cancer: role of ATP-dependent transporters. Nat Rev Cancer. 2002;2(1):48-58.
15. de Geus-Oei LF, van Eerd-Vismale J, Molthoff C, Corstens F, Oyen W, Boerman O. Tracers to monitor the response to chemotherapy: in vitro screening of four radiopharmaceuticals. Cancer Biother Radiopharm. 2004;19(4):457-65.
16. Moher D, Liberati A, Tetzlaff J, Altman DG; PRISMA Group. Preferred reporting items for systematic reviews and meta-analyses: the PRISMA statement. Ann Intern Med. 2009;151(4):264-9.
17. Whiting PF, Rutjes AW, Westwood ME, Mallett S, Deeks JJ, Reitsma JB, *et al.* QUADAS-2: a revised tool for the quality assessment of diagnostic accuracy studies. Ann Intern Med. 2011;155(8):529-36.
18. Stata Statistical Software: Release 14 [computer program]. 2015 College Station, TX: StataCorp LP.
19. Dwamena B. MIDAS: Stata module for meta-analytical integration of diagnostic test accuracy studies. Statistical Software Components S456880, Boston College Department of Economics 2007; revised 05 Feb 2009.
20. Harbord RM. metandi: Meta-analysis of diagnostic accuracy using hierarchical logistic regression. The Stata Journal 2009; 9:211-29.
21. Maini CL, Tofani A, Sciuto R, Semprebene A, Cavaliere R, Mottolese M, *et al.* Technetium-99m-MIBI scintigraphy in the assessment of neoadjuvant chemotherapy in breast carcinoma. J Nucl Med. 1997;38(10):1546-51.
22. Ciarmiello A, Del Vecchio S, Silvestro P, Potena MI, Carriero MV, Thomas R, *et al.* Tumor clearance of technetium 99m-sestamibi as a predictor of response to neoadjuvant chemotherapy for locally advanced breast cancer. J Clin Oncol. 1998;16(5):1677-83.

23. Mankoff DA, Dunnwald LK, Gralow JR, Ellis GK, Drucker MJ, Livingston RB. Monitoring the response of patients with locally advanced breast carcinoma to neoadjuvant chemotherapy using [technetium 99m]-sestamibi scintimammography. Cancer. 1999;85(11):2410-23.

24. Cayre A, Cachin F, Maublant J, Mestas D, Feillel V, Ferrière JP, et al. Single static view 99mTc-sestamibi scintimammography predicts response to neoadjuvant chemotherapy and is related to MDR expression. Int J Oncol. 2002;20(5):1049-55.

25. Sciuto R, Pasqualoni R, Bergomi S, Petrilli G, Vici P, Belli F, et al. Prognostic value of (99m)Tc-sestamibi washout in predicting response of locally advanced breast cancer to neoadjuvant chemotherapy. J Nucl Med. 2002;43(6):745-51.

26. Mezi S, Primi F, Capoccetti F, Scopinaro F, Modesti M, Schillaci O. In vivo detection of resistance to anthracycline based neoadjuvant chemotherapy in locally advanced and inflammatory breast cancer with technetium-99m sestamibi scintimammography. Int J Oncol. 2003;22(6):1233-40.

27. Marshall C, Eremin J, El-Sheemy M, Eremin O, Griffiths PA. Monitoring the response of large (>3 cm) and locally advanced (T3-4, N0-2) breast cancer to neoadjuvant chemotherapy using (99m)Tc-Sestamibi uptake. Nucl Med Commun. 2005;26(1):9-15.

28. Wahner-Roedler DL, Boughey JC, Hruska CB, Chen B, Rhodes DJ, Tortorelli CL, et al. The use of molecular breast imaging to assess response in women undergoing neoadjuvant therapy for breast cancer: a pilot study. Clin Nucl Med. 2012;37(4):344-50.

29. Mitchell D, Hruska CB, Boughey JC, Wahner-Roedler DL, Jones KN, Tortorelli C, et al. 99mTc-sestamibi using a direct conversion molecular breast imaging system to assess tumor response to neoadjuvant chemotherapy in women with locally advanced breast cancer. Clin Nucl Med. 2013;38(12):949-56.

30. Lee HS, Ko BS, Ahn SH, Son BH, Lee JW, Kim HJ, et al. Diagnostic performance of breast-specific gamma imaging in the assessment of residual tumor after neoadjuvant chemotherapy in breast cancer patients. Breast Cancer Res Treat. 2014;145(1):91-100.

31. Trehan R, Seam RK, Gupta MK, Sood A, Dimri K, Mahajan R. Role of scintimammography in assessing the response of neoadjuvant chemotherapy in locally advanced breast cancer. World J Nucl Med. 2014;13(3):163-9.

32. Evangelista L, Cervino AR, Sanco R, Bignotto M, Saibene T, Michieletto S, et al. Use of a portable gamma camera for guiding surgical treatment in locally advanced breast cancer in a post-neoadjuvant therapy setting. Breast Cancer Res Treat. 2014;146(2):331-40.

33. Evangelista L, Cervino AR, Michieletto S, Saibene T, Orvieto E, Bozza F, et al. Staging of locally advanced breast cancer and the prediction of response to neoadjuvant chemotherapy: complementary role of scintimammography and 18F-FDG PET/CT. Q J Nucl Med Mol Imaging. 2017;61(2):205-15.

34. Novikov SN, Kanaev SV, Petr KV, Tatyana SY, Elena TA, Ludmila JA, et al. Technetium-99m methoxyisobutylisonitrile scintimammography for monitoring and early prediction of breast cancer response to neoadjuvant chemotherapy. Nucl Med Commun. 2015;36(8):795-801.

35. Senkus E, Kyriakides S, Ohno S, Penault-Llorca F, Poortmans P, Rutgers E, et al. Primary breast cancer: ESMO Clinical Practice Guidelines for diagnosis, treatment and follow-up. Ann Oncol. 2015;26(5):v8-30.

36. Pengel KE, Koolen BB, Loo CE, Vogel WV, Wesseling J, Lips EH, et al. Combined use of [18]F -FDG PET/CT and MRI for response monitoring of breast cancer during neoadjuvant chemotherapy. Eur J Nucl Med Mol Imaging. 2014;41(8):1515-24.

37. Gu YL, Pan SM, Ren J, Yang ZX, Jiang GQ. Role of Magnetic Resonance Imaging in Detection of Pathologic Complete Remission in Breast Cancer Patients Treated With Neoadjuvant Chemotherapy: A Meta-analysis. Clin Breast Cancer. 2017;17(4):245-55.

38. Liu Q, Wang C, Li P, Liu J, Huang G, Song S. The Role of (18)F-FDG PET/CT and MRI in Assessing Pathological Complete Response to Neoadjuvant Chemotherapy in Patients with Breast Cancer: A Systematic Review and Meta-Analysis. Biomed Res Int. 2016;2016:3746232.

39. Brem RF, Schoonjans JM, Kieper DA, Majewski S, Goodman S, Civelek C. High-resolution scintimammography: a pilot study. J Nucl Med. 2002;43(7):909-15.

40. Brem RF, Floerke AC, Rapelyea JA, Teal C, Kelly T, Mathur V. Breast-specific gamma imaging as an adjunct imaging modality for the diagnosis of breast cancer. Radiology. 2008;247(3):651-7.

41. Hruska CB, Phillips SW, Whaley DH, Rhodes DJ, O'Connor MK. Molecular breast imaging: use of a dual-head dedicated gamma camera to detect small breast tumors. AJR Am J Roentgenol. 2008;191(6):1805-15.

42. Long Z, Conners AL, Hunt KN, Hruska CB, O'Connor MK. Performance characteristics of dedicated molecular breast imaging systems at low doses. Med Phys. 2016;43(6):3062-70.

43. Spanu A, Farris A, Chessa F, Sanna D, Pittalis M, Manca A, *et al.* Planar scintimammography and SPECT in neoadjuvant chemo or hormonotherapy response evaluation in locally advanced primary breast cancer. Int J Oncol. 2008;32(6):1275-83.

44. Mann SD, Perez KL, McCracken EK, Shah JP, Wong TZ, Tornai MP. Initial In Vivo Quantification of Tc-99m Sestamibi Uptake as a Function of Tissue Type in Healthy Breasts Using Dedicated Breast SPECT-CT. J Oncol. 2012;2012:146943.

45. Wahl RL, Jacene H, Kasamon Y, Lodge MA. From RECIST to PERCIST: Evolving Considerations for PET response criteria in solid tumors. J Nucl Med. 2009;50(1):122S-50S.

46. Guo C, Zhang C, Liu J, Tong L, Huang G. Is Tc-99m sestamibi scintimammography useful in the prediction of neoadjuvant chemotherapy responses in breast cancer? A systematic review and meta-analysis. Nucl Med Commun. 2016;37(7):675-88.

47. Bach-Gansmo T, Bogsrud TV, Skretting A. Integrin scintimammography using a dedicated breast imaging, solid-state gamma-camera and (99m)Tc-labelled NC100692.Clin Physiol Funct Imaging. 2008;28(4):235-9.

48. O'Connor MK, Morrow MMB, Hunt KN, Boughey JC, Wahner-Roedler DL, Conners AL, *et al.* Comparison of Tc-99m maraciclatide and Tc-99m sestamibi molecular breast imaging in patients with suspected breast cancer. EJNMMI Res. 2017;7(1):5.

49. Symmans WF, Volm MD, Shapiro RL, Perkins AB, Kim AY, Demaria S, *et al.* Paclitaxel-induced apoptosis and mitotic arrest assessed by serial fine-needle aspiration: implications for early prediction of breast cancer response to neoadjuvant treatment. Clin Cancer Res. 2000;6(12):4610-7.

50. van Leeuwen FW, Buckle T, Batteau L, Pool B, Sinaasappel M, Jonkers J, *et al.* Potential value of color-coded dynamic breast-specific gamma-imaging; comparing (99m)Tc-(V)-DMSA, (99m)Tc-MIBI, and (99m)Tc-HDP in a mouse mammary tumor model. Appl Radiat Isot. 2010;68(12):2117-24.

51. Scopinaro F, Varvarigou A, Ussof W, De Vincentis G, Archimandritis S, Evangelatos G, *et al.* Breast cancer takes up 99mTc bombesin. A preliminary report. Tumori. 2002;88(3):S25-8.

52. Scopinaro F, De Vincentis G, Varvarigou AD. Use of radiolabeled bombesin in humans. J Clin Oncol. 2005;23(13):3170-1.

EXPERIMENTAL VALIDATION OF ABSOLUTE SPECT/CT QUANTIFICATION FOR RESPONSE MONITORING IN BREAST CANCER

A Collarino
LM Pereira Arias-Bouda
RA Valdés Olmos
P van der Tol
P Dibbets-Schneider
LF de Geus-Oei
FHP van Velden

CHAPTER 3

ABSTRACT

PURPOSE Recent developments in iterative image reconstruction enable absolute (semi) quantification of SPECT/CT studies by incorporating compensation for collimator-detector response, attenuation and scatter as well as resolution recovery into the reconstruction process (Evolution; Q.Metrix package; GE Healthcare). The aim of this experimental study is to assess its quantitative accuracy for potential clinical ^{99m}Tc-sestamibi (MIBI)-related SPECT/CT application in neoadjuvant chemotherapy response studies in breast cancer.

METHODS Two phantoms were filled with MIBI and acquired on a SPECT/CT gamma-camera (Discovery 670 Pro; GE Healthcare), i.e. a Jaszczak phantom and a NEMA IEC body phantom containing six spheres that were filled with an activity concentration reflecting clinical MIBI uptake. Subsequently, volumes-of-interest (VOI) of each sphere were drawn (semi)automatically on SPECT using various isocontour methods or manually on CT. Finally, prone MIBI SPECT/CT scans were acquired 5 and 90 min p.i. in a locally advanced breast cancer patient.

RESULTS Activity concentration in the four largest spheres converged after 9 iterations of Evolution. Depending on the count statistics, the accuracy of the reconstructed activity concentration varied between -4.7 to -0.16% (VOI covering the entire phantom) and from 6.9 to 10% (8.8 cm ø cylinder VOI placed in the centre of the phantom). Recovery coefficients of SUV_{max} were 1.59, 1.78, 1.85 and 1.68 for spheres with 37, 28, 22 and 17 mm ø, respectively. Recovery coefficients of SUV_{mean} were 0.96, 1.07, 1.11 and 0.95 (42% isocontour), 0.96, 1.06, 1.08 and 0.93 (36% isocontour with local background correction) and 0.96, 1.09, 1.03 and 1.03 (CT). Patient study results were concordant with the phantom validation.

CONCLUSION Absolute SPECT/CT (semi)quantification of breast studies using MIBI seems feasible (<12% deviation) when a 42% isocontour is used for delineation for tumours of at least 17 mm diameter. However, with tumour shrinkage, response evaluation should be handled with caution, especially when using SUV_{max}.

INTRODUCTION

Neoadjuvant chemotherapy is currently considered standard care for locally advanced breast cancer (LABC). [1] It improves long-term outcome and increases breast-conserving surgery rates due to down-staging and reduction of tumour size. [2, 3] Hence, monitoring tumour response early during neoadjuvant chemotherapy may guide to switch to other drugs in case of nonresponse, avoiding futile delay of effective treatment, unnecessary side effects, avoiding unnecessary costs and enabling a more personalised approach. In recent years, ^{99m}Tc-sestamibi (MIBI) has been increasingly used in molecular breast imaging (MBI) as radiotracer for detecting breast cancer. [4] MIBI uptake reflects increased vascularity and higher cytoplasmic mitochondrial density in breast tumour cells. [5, 6] Additionally, the rapid washout of MIBI from tumour cells indicates the over-expression of P-glycoprotein, an energy-dependent efflux-pump for many drugs, as well as the over-expression of Bcl-2, an anti-apoptotic protein. [7, 8] Therefore, MIBI allows in vivo evaluation of tumour chemoresistance and potentially identify nonresponding patients who would benefit from modified therapy schedules earlier in the treatment process. Until now, only three studies have evaluated the usefulness of MIBI imaging to predict nonresponsiveness early in the neoadjuvant chemotherapy in LABC. [9] Because of this limited experience and the methodological heterogeneity of the studies, the role of MIBI imaging in response monitoring during neoadjuvant chemotherapy in LABC remains a matter of discussion. Moreover, there are no studies evaluating the usefulness of single photon emission computed tomography with integrated low-dose X-ray computed tomography (SPECT/CT) for this goal. Published studies have been based on scintimammography acquired with a conventional gamma-camera or on MBI using compact single- or dual-head cadmium zinc telluride gamma detectors. Compared to MBI, SPECT/CT has the advantage of providing three-dimensional (3D) whole-body imaging, fused functional and anatomical images as well as correction for tissue attenuation and scattering with the low-dose CT. SPECT/CT also allows the prone acquisition of breast without compression, using a dedicated coil device in a similar manner as magnetic resonance imaging (MRI). Although modern MBI systems appear to have a higher spatial resolution than SPECT/CT, [10] there is a possible role for SPECT/CT in the early detection of nonresponsiveness to neoadjuvant chemotherapy in patients with large tumours as frequently observed in LABC. Furthermore, in analogy to positron emission tomography (PET), recent developments in iterative image reconstruction enable absolute (semi) quantification of SPECT/CT studies by incorporating compensation for collimator-detector response, photon attenuation and photon scatter as well as resolution recovery into the reconstruction process (Evolution; Q.Metrix package; GE Healthcare, Milwaukee, US). [11-13]

Hence, SPECT/CT offers a (semi)-quantitative analysis of tumour uptake in terms of standardised uptake values (SUV) for serial assessment of breast cancer response to neoadjuvant chemotherapy. The aim of this experimental study is to assess quantitative accuracy of Evolution, making use of phantom studies, for potential application of MIBI-related SPECT/CT in breast cancer patients receiving neoadjuvant chemotherapy. As part of a proof-of-concept in vivo evaluation, a patient study was acquired and evaluated using Evolution.

MATERIALS AND METHODS

PHANTOM STUDIES

As recommended by the vendor, the camera sensitivity of the SPECT/CT gamma-camera (Discovery NM/CT 670 Pro; GE Healthcare) was measured using a Petri dish that was filled evenly (2-3 mm deep) with a MIBI-surrogate solution consisting of ^{99m}Tc-pertechnetate (90 MBq) and water. This Petri dish was placed on a foam holder, which was positioned on the first detector. The second detector was located at an equal distance from the Petri dish as the first detector. The acquisition was started with a matrix of 256 x 256, without a zoom factor, and was stopped when at least 4 million counts were measured on both detectors. The camera sensitivity was calculated as specified by the vendor. [11]

All phantoms were filled with the MIBI-surrogate and acquired using a low-energy, high-resolution collimator, non-circular orbit, step-and-shoot mode and 120 views. A low-dose CT scan was acquired for attenuation correction purposes. All SPECT data were reconstructed using Evolution with a matrix of 128 x 128 without zoom.

Firstly, three phantom experiments were acquired using the National Electrical Manufacturers Association (NEMA) International Electrotechnical Commission (IEC) body phantom containing six spheres with various diameters (i.e. 10, 13, 17, 22, 28 and 37 mm) with volumes ranging from 0.53 to 26.52 mL. In the first two experiments the background compartment was filled with an activity concentration of ~3.7 kBq/mL, which reflects clinical MIBI uptake in normal breast tissue, [14] with four sphere-to-background ratios (i.e. ~9.7:1, 6.6:1, 5.0:1 and 3.4:1), simulating various tumour-to-background ratios. A third experiment was performed with a higher activity concentration in the background compartment of 8.3 kBq/mL and a sphere-to-background ratio of 9.4:1. All phantom measurements were acquired using 20 sec per view and reconstructed using 10 subsets and up to 20 iterations. All three measurements were used to assess the

recovery coefficients (calculated by the ratio between the reconstructed activity and the true activity as measured with the dose calibrator). The first measurement was used to assess **(1)** the convergence of Evolution and **(2)** the interobserver variability for manual delineation on CT. The first and the second measurement were used to assess the effects of various tumour-to-background ratios on the performance of Evolution.

Secondly, a Jaszczak phantom was filled with an activity concentration of 38 kBq/mL and acquired with 1 to 24 sec per view in order to assess the performance of Evolution under different count statistics, ranging from 0.7 to 21.4 million counts, mimicking an activity concentration of 1.4 to 43 kBq/mL when the acquisition parameters were set to 20 sec per view and 120 views.

PATIENT STUDY

Following informed consent, a 66-year-old woman (BMI of 22.06 kg/m^2) with proven invasive ductal carcinoma in the right breast with a maximum diameter of 3 cm, received a single IV injection of 586 MBq MIBI. Five min after injection a first SPECT/CT in hanging breast mode (early) was acquired followed by a second hanging breast SPECT/CT (delayed) at 90 min p.i. For both studies SPECT data were acquired using a low-energy, high-resolution collimator, non-circular orbit, step-and-shoot mode, 20 sec per view, 120 views, with a matrix of 128 x 128 without zoom. Consecutively, a low-dose CT was acquired with the patient breathing normally using a voltage of 100 kV and auto tube current modulation of 100 mA (30-150 mA) and with dose reduction using adaptive statistical iterative reconstruction (ASIR). SPECT images were reconstructed using Evolution with the settings that were recommended by the phantom studies. This patient study is part of an ongoing prospective clinical trial, approved by the Medical Ethics Review Committee of the Leiden University Medical Centre (trial code: NL60403.058.17). Written informed consent is received from all individual participants. Inclusion criteria for the clinical trial are age $\geq$ 18 years, proven LABC with at least one index breast lesion of $\geq$ 2 cm and the patient is scheduled for neoadjuvant chemotherapy or other systematic treatment. Exclusion criteria are pregnancy, prior breast surgery, chemotherapy or radiation therapy, clinical or radiological evidence of metastatic lymph nodes or distant metastases.

DATA ANALYSIS

Evolution was said to converge when the relative difference in activity concentration for a certain volume-of-interest (VOI) was less than 0.5% between the previous and current number of iterations. Convergence was assessed for the background compartment, the lung insert and the

four largest spheres of the NEMA IEC body phantom.

For the NEMA IEC body phantom, four cylindrical VOIs with a volume of 260 mL and one cylindrical VOI with a volume of 103 mL were delineated on the low-dose CT images to assess the reconstructed activity concentrations of the background compartment and the lung insert, respectively. For the six spheres, VOIs were delineated on the low-dose CT images by three experienced nuclear medicine physicians. In addition, VOIs were drawn (semi)automatically on the SPECT images by using various isocontour methods that apply a threshold of either 36, 42, 50 or 70% of the maximum voxel intensity inside a target, either with (denoted with an A, e.g. A36%) or without (no denotation, e.g. 36%) local background correction. [15-17]

For each VOI the following parameters were calculated: the maximum voxel (to simulate the effects on SUV_{max}), mean activity concentration (to simulate the effects on SUV_{mean}), and coefficient of variation (COV, to illustrate the noise level, calculated by the standard deviation of the activity concentration divided by the mean activity concentration times 100%). Further, recovery coefficients were calculated by dividing the max and mean values by the true activity concentration.

For the Jaszczak phantom, one cylindrical VOI was drawn over the entire phantom and 5 cylindrical VOIs, placed in the centre of the phantom, were drawn for a length of 14 cm with a 1.1, 2.2, 4.4, 6.6 and 8.8 cm. For each VOI, mean activity concentration and COV were obtained.

For the patient study, VOIs were drawn (semi)automatically on the primary breast tumour (using the threshold methods as recommended from the phantom study) and manually on healthy breast tissue (>30 mL) for both the early and delayed SPECT/CT scans. For each VOI, mean and max activity concentration, mean and max SUV (SUV_{mean} and SUV_{max}; body-weighted), and functional tumour volume were calculated.

RESULTS

CAMERA SENSITIVITY, CONVERGENCE AND NOISE LEVEL

The camera sensitivity was 75.0 cps/s/MBq. For the background compartment, the four largest spheres and the lung insert, Evolution converged after 4, 9 and 16 iterations, respectively (**Figure 1A**), corresponding to a noise level as measured in the background compartment of 31, 50 and 70%, respectively (**Figure 1B**).
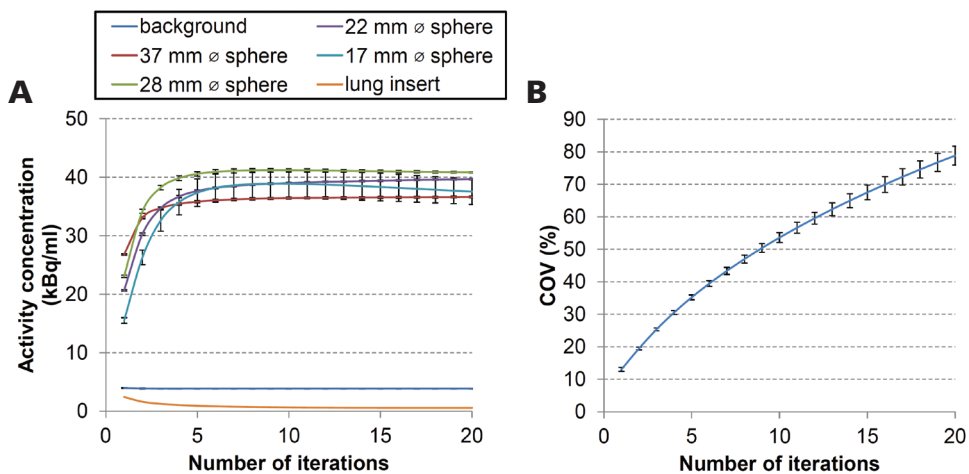
Figure 1. Effects of increasing the number of iterations of Evolution (with 10 subsets). Effects on the mean activity concentration derived from manually delineated VOI of the 17, 22, 28 and 37 mm ø spheres and the background compartment (A), and COV measured in the background compartment (B). Mean activity concentrations of the spheres were obtained by averaging the activity concentration from CT-derived VOI of three observers. COV was obtained by averaging the COV of four VOIs of the background compartment. Error bars indicate the SD.

COUNT STATISTICS

When lowering the total number of measured counts from 21.4 million to 0.7 million, the deviation of the reconstructed activity from the true activity of the 8.8 cm ø cylinder ranged from 6.9 to 10% when 9 iterations of Evolution were applied, while this deviation for the 1.1 cm ø cylinder ranged from -3.7 to 31% (**Figure 2A**). Only when the entire phantom was delineated, this deviation for the 8.8 cm ø cylinder lowered to a range of -4.7 to -0.16%. Similar trends (but with lower or higher amplitude) were observed for data obtained with 4 and 16 iterations of Evolution, respectively. When lowering the total number of measured counts from 21.4 million to 0.7 million, COV increased from 8.6 to 42%, from 14 to 69% and from 19 to 95% for 4, 9 and 16 iterations, respectively (**Figure 2B**). These data suggest that the measured activity concentration should be corrected by applying a multiplication factor of 0.94.
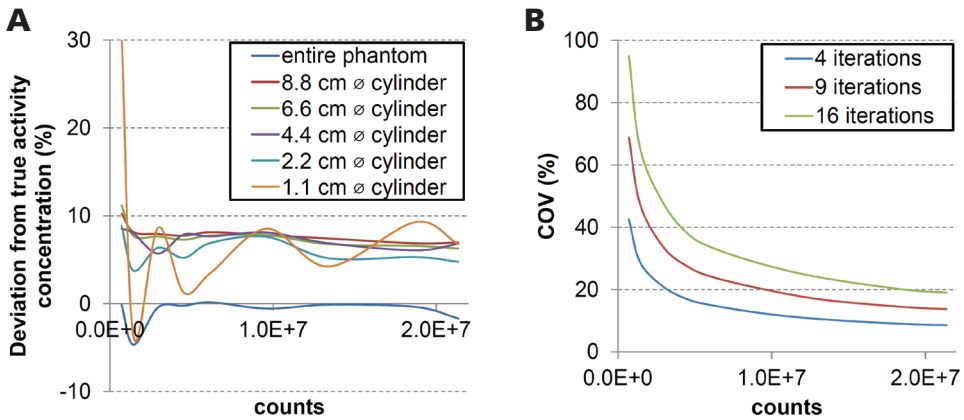
Figure 2. Performance of Evolution under various count statistics: Deviation of the reconstructed activity concentration (9 iterations, 10 subsets), derived from cylindrical VOI with various diameters, from the true activity concentration (A), and COV for 4, 9 and 16 iterations as measured in the 8.8 cm ø cylinder (B).

CT-BASED DELINEATION

Figure 3 shows axial images obtained from the NEMA IEC body experiments. After several iterations, the largest sphere starts to resemble a structure with heterogeneous tracer uptake. In addition, more iterations also impact the round shape of the spheres. Only the five largest spheres can be seen.

When the multiplication factor is applied, recovery coefficients for the mean activity concentration are well within 10% for spheres of 17 mm ø and larger (**Figure 4B**). By correcting for motion, the recovery coefficients do not improve considerably (**Figure 4C**), and therefore, no motion correction was applied in the remainder of this study.

The 13 mm ø sphere showed a recovery coefficient between 0.29 and 0.36, and 0.32 and 0.40 for the mean and maximum activity concentration, respectively. As a result, thresholding cannot result in a recovery coefficient around 1.0 for the 13 mm ø sphere. Therefore, data from the 13 mm ø sphere are not presented in the remainder of this study.
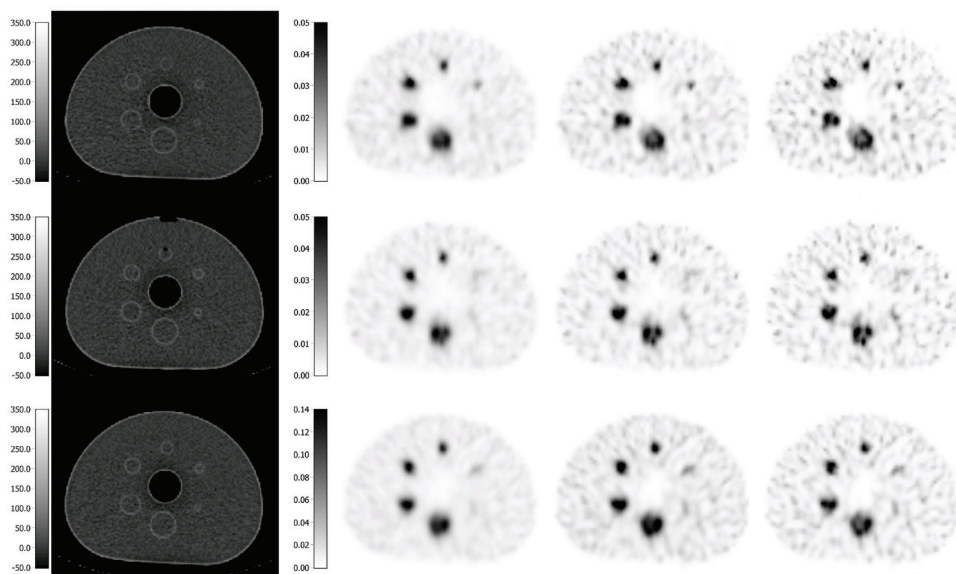
Figure 3. Axial slices of the three measurements of the NEMA IEC body phantom. From top to bottom: Two experiments with 3.6 kBq/mL and one experiment with 8.3 kBq/mL in the background compartment. Sphere-to-background ratio was ~10:1. From left to right: CT images (colour bars are expressed in Hounsfield units), and three SPECT images reconstructed with 4, 9 and 12 iterations of Evolution (colour bars are expressed in MBq/mL).
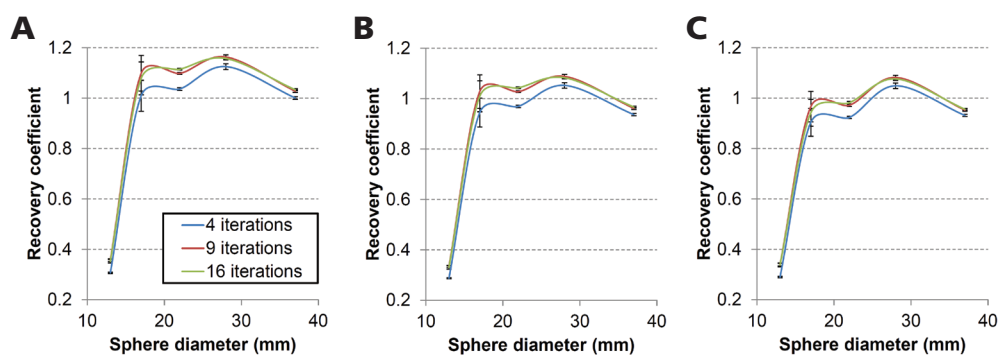
Figure 4. Recovery coefficients obtained using CT-based delineation. Recovery coefficient of Evolution with (C) and without (A, B) motion correction, and with (B, C) and without (A) the multiplication factor. Recovery coefficients were obtained by using the average of the mean activity concentration obtained from CT-derived VOI of three observers. Error bars indicate the SD.

THRESHOLD-BASED DELINEATION WITHOUT CORRECTING FOR LOCAL BACKGROUND

For low count statistics images typically observed in MIBI SPECT/CT breast cancer studies, recovery coefficients of SUV_{max} ranged between 1.59 – 1.85 and 1.50 – 2.37 for the two measurements (**Figures 5D and 5E**, respectively), when 9 iterations of Evolution were applied. By increasing the count statistics, this range narrowed to 1.49 – 1.67 (**Figure 5F**). By increasing the number of iterations to 16, the overestimation of the recovery coefficients of SUV_{max} for the low count statistics images increased to 1.91 – 2.09 and 1.53 – 3.20 (**Figures 5G and 5H**, respectively), and for the increased count statistics image to 1.63 – 1.78 (**Figure 5I**).

For first measurement of low count statistics images and 9 iterations of Evolution, most isocontour methods overestimated the recovery coefficients of SUV_{mean} (>12%), except for the 36% and 42% isocontour methods (0.89 – 1.02 and 0.95 – 1.11, respectively). This was, however, not true for the second measurement of low count statistics images (**Figure 5E**). For the third measurement with increased count statistics, only the 42% and 50% isocontour methods showed recovery coefficients of SUV_{mean} that were smaller or equal to 12% (0.88 – 1.00 and 0.99 – 1.10, respectively).

VARIOUS SPHERE-TO-BACKGROUND RATIOS AND CORRECTION FOR LOCAL BACKGROUND

When 9 iterations of Evolution were applied, local background correction provided only small changes in recovery coefficients of SUV_{mean} (<6%; **Figure 6**), whereas a change in tumour-to-background ratio could result in a large change in recovery coefficients (<22%, <98%, <70% and <88% for the 37, 28, 22 and 17 mm ø spheres, respectively).

PATIENT STUDY

When 9 iterations of Evolution were applied, the mean activity concentration of healthy breast tissue was 4.7 and 3.7 kBq/mL for the early and delayed acquisition, respectively, resulting in a SUV_{mean} of 0.5 g/mL. Similar results were obtained for SUV_{max} and SUV_{mean} for both the 42% and the A36% isocontour methods (**Table 1**), except for the functional volume (i.e. 19-24% larger for delayed compared to early acquisition). The tumour-to-background ratios (calculated by dividing SUV_{max} of the tumour by the SUV_{mean} of healthy tissue) were 11:1 and 7:1 for the early and delayed acquisition, respectively, also demonstrated visually in **Figure 7**. Compared to 9 iterations, SUV_{max} increased by 9% for the early acquisition when 16 iterations were applied, while SUV_{mean} increased by only 4%.
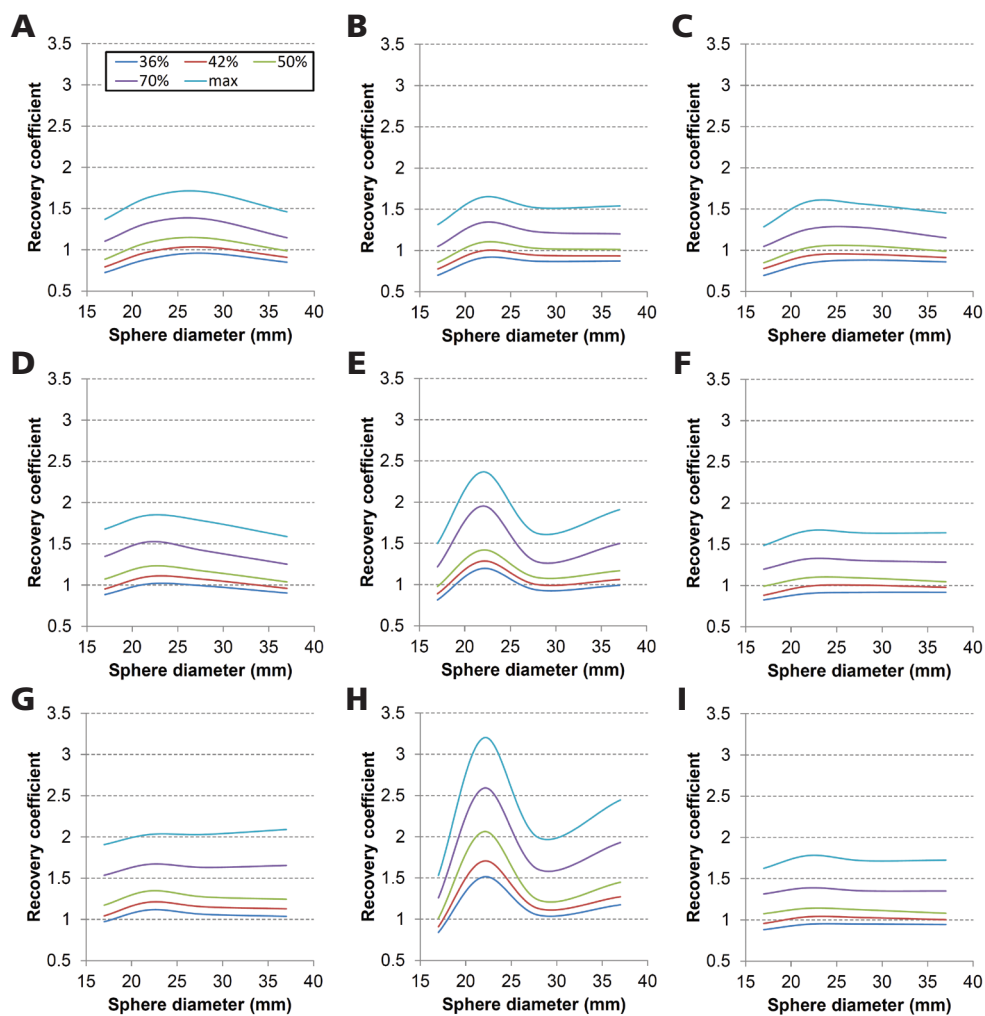
Figure 5. Recovery coefficients obtained using SPECT threshold-based delineation. Recovery coefficients of Evolution with 4 (A, B, C), 9 (D, E, F) and 16 (G, H, I) iterations, obtained using 36, 42, 50, 70% isocontour methods and the maximum voxel; (A, D, G and B, E, H) two experiments with 3.6 kBq/mL and (C, F, I) one experiment with 8.3 kBq/mL in the background compartment. Sphere-to-background ratio was ~10:1. For all data the multiplication factor was applied.
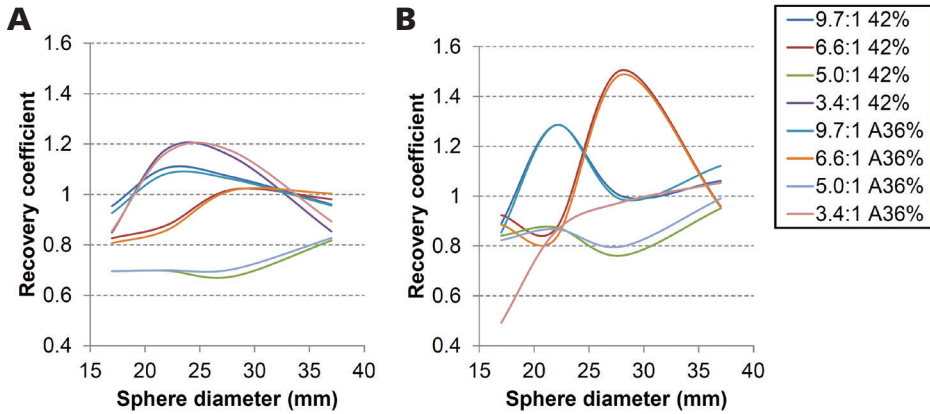
Figure 6. Recovery coefficients of mean activity concentration obtained using Evolution (9 iterations and 10 subsets) followed by a 42% isocontour method without local background correction or a 36% isocontour method with local background correction (A36%). Two experiments with 3.6 kBq/mL are shown with various sphere-to-background ratios (A and B). For all data the multiplication factor was applied.
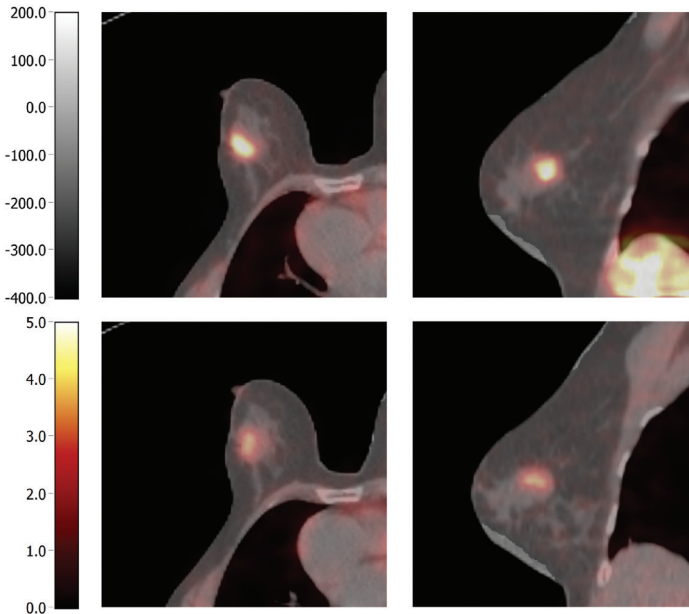
Figure 7. Transversal (left) and sagittal (right) fused SPECT/CT images show focal MIBI uptake corresponding to a primary invasive ductal carcinoma located in the upper outer quadrant of the right breast. Top row: early acquisition after 5 min p.i. Bottom row: delayed acquisition after 90 min p.i. SPECT images were reconstructed with 9 iterations of Evolution. Colour bars are expressed in Hounsfield units (CT) and SUV (g/mL, SPECT).

Table 1. Quantitative results from the MIBI breast cancer patient

VOI	Isocontour method	Number of iterations	Mean activity concentration (kBq/mL)		Maximum activity concentration (kBq/mL)		SUV_{mean} (g/mL)		SUV_{max} (g/mL)		Volume (mL)	
			Early	Late	Early	Late	Early	Late	Early	Late	Early	Late
Tumour	42%	4	31	17	52	28	3.4	2.2	5.7	3.6	4.9	6.1
		9	31	17	51	28	3.4	2.2	5.6	3.6	5.5	6.8
		16	33	17	56	28	3.6	2.2	6.1	3.7	5.0	7.2
	A36%	4	31	17	52	28	3.4	2.2	5.7	3.6	4.9	5.8
		9	31	17	51	28	3.4	2.2	5.6	3.6	5.6	6.7
		16	33	17	56	28	3.6	2.2	6.1	3.7	5.2	7.1
Healthy breast tissue	-	4	4.6	3.5	9.3	6.6	0.5	0.5	1.0	0.9	-	-
		9	4.7	3.7	12	8.4	0.5	0.5	1.4	1.1	-	-
		16	4.7	3.7	15	9.8	0.5	0.5	1.7	1.3	-	-

DISCUSSION

Due to its well-known mechanisms for uptake and washout, MIBI appears to be an attractive radiotracer for in vivo evaluation of tumour chemoresistance and potential identification of nonresponding patients receiving neoadjuvant chemotherapy. The increasing use of neoadjuvant chemotherapy for LABC demands for accurate monitoring of tumour response in order to enable clinicians to consider other drugs in cases without response. To differentiate responders from nonresponders in an accurate way, quantification of tracer accumulation is needed. Recent developments in iterative image reconstruction enable (semi)-quantitative SPECT/CT evaluation by incorporating compensation for collimator-detector response, photon attenuation and scatter as well as resolution recovery into the reconstruction process. [12, 13] In the experimental part of the present study we evaluated the accuracy of this technique to calculate reconstructed activity concentrations and SUV utilising various phantom measurements. It was shown that the activity concentrations in the spheres converged when at least 9 iterations of Evolution are applied (with 10 subsets). Therefore, 9 iterations (10 subsets) seem to be optimal for MIBI SPECT/CT breast cancer studies. Although more iterations (i.e. 16) result in convergence of areas with very low to no tracer uptake, these number of iterations also lead to noise amplification, resulting in a large overestimation and/or fluctuation (over the sphere size) of the maximum activity concentration (and thus SUV_{max}) and thereby in inaccurate and/or instable measurements of mean activity concentrations (and thus in SUV_{mean}). Therefore, the use of 16 iterations of Evolution is not recommended for these type of studies, but could still be of interest for studies where quantification of regions with low to no uptake is essential.

Even for 9 iterations of Evolution, recovery coefficients of SUV_{max} are largely overestimated (ranging between 1.49 and 2.37) for MIBI SPECT/CT studies. These recovery coefficients are much higher compared to those obtained using PET/CT, even when resolution modelling for PET/CT is applied. [18] This might be explained by the high noise level observed in MIBI SPECT/CT studies (50% measured in the NEMA IEC body phantom), while the noise level of a typical FDG-PET/CT study should ideally be less than 15%. [19] The background activity concentration (~3.7 kBq/mL) and sphere-to-background ratios applied in the phantom studies were chosen as such since they resemble the in vivo situation. [14] Hypothetically, the noise level could be lowered by administering more activity to the patient or by increasing the time per view. However, both solutions are not desirable, as the former will increases (increased) the radiation exposure (i.e. does not fulfil the as-low-as-reasonably-achievable, ALARA, principle) and the latter will increase the acquisition duration,

causing more patient discomfort (i.e. it is our experience that patients are not able to stay in prone position for longer than 20 to 25 min per scan).

Ideally, lesions should be delineated on the CT image to obtain the most accurate recovery coefficients (**Figure 3**). However, CT is not a suitable technique to delineate tumour tissue from healthy breast tissue. Therefore, delineation of the lesions can only be performed on the SPECT image in case of clinical MIBI SPECT/CT breast cancer studies. A 42% threshold of SUV_{max} and an A36% threshold of SUV_{max} (i.e. corrected for local background of surrounding tissue) resulted, in general, in SUV_{mean} values that closely resembled the true activity (within 12%) for tumours of 17 mm diameter or larger (**Figure 5**). However, since these isocontour methods are based on the maximum intensity voxel (i.e. SUV_{max}) and the accuracy of SUV_{max} has shown to be hampered by the high noise levels in these images, this high noise level could also influence the accuracy of SUV_{mean} when derived using the isocontour methods. Therefore, SUV_{mean} values should be evaluated with care, especially in therapy response monitoring, where the tumour-to-background ratio might change (**Figure 6**) or tumour shrinkage might occur (**Figure 5**). Ideally, other delineation methods that have recently been explored for SPECT/CT and PET/CT should be evaluated for their accuracy of obtaining $SUV_{mean.}$ [20-22] Unfortunately, these delineation methods are currently not available in the Q.Metrix software package. Therefore, these methods should be investigated in future SPECT/CT breast cancer studies.

It is worth remembering that even though both the 42% isocontour and A36% isocontour methods most accurately resemble the true activity for MIBI SPECT/CT studies, these methods may not always result in useful tumour delineation. [15, 23]

Higher thresholds may be desirable to prevent delineation of neighbouring tissue with high tracer uptake or in case of heterogeneous tracer uptake in the tumour. [16] Background correction did not result in an apparent benefit in the current study. Nevertheless, the applicability of local background correction could be further investigated in future clinical studies.

Figure 3 clearly showed the previously described "evaporation" effect, wherein counts in low-activity regions gravitate towards high-activity regions, [24] becoming more apparent when the number of iterations increases. This resulted in the more heterogeneous tracer uptake in the larger spheres observed when the number of iterations increased.

Finally, camera sensitivity was measured as recommended by the vendor. However, this resulted in overestimation of the activity concentrations in both the background compartment and the

spheres. Ideally, it should be measured on a homogeneously filled phantom as done in PET to obtain a closer correspondence between reconstructed activity concentrations and true activity concentrations (as obtained from the dose calibrator).

Our study has limitations. First, no dedicated breast phantom was used in the experimental studies fitting the prone support device used in patient studies. Second, we were not able to compare the performance of the Q.Metrix software (that uses the Evolution reconstruction algorithm) to other commercially available quantitative SPECT/CT tools. In spite of these limitations, this study has several strengths. To our knowledge, this is the first experimental validation of (semi)-quantitative SPECT/CT applied for response monitoring. To date, only a few phantom studies have assessed the accuracy of quantitative SPECT/CT for ^{99m}Tc-radiotracers. [25, 26] On the basis of our results, the Q.Metrix quantification tool may be applicable in breast tumours with a diameter larger than 17 mm. Thus, (semi)-quantitative SPECT/CT is potentially helpful for early monitoring response (after 1 or 2 cycles of therapy) in locally advanced breast tumours. Moreover, the use of (semi)-quantitative SPECT/CT in oncological practice may be extended to locally advanced tumours in other organs and is potentially of application in other clinical indications. [13]

The proof-of-concept clinical examination included in the present study was performed according to our phantom setting. Additionally, in analogy with PET/CT and MRI, we used prone position of the patient with hanging breasts in order to provide a better visualisation and delineation of the primary tumour. [27, 28] Both acquisitions (at 5 min and at 90 min p.i.) in hanging breast mode were feasible and relatively well tolerated by the patient. This approach is now investigated in our ongoing clinical trial. Interestingly, the measured activity in the normal breast tissue in the included patient corresponded well with the average MIBI uptake values as measured in normal breast tissue by Mann *et al.* using a dedicated breast SPECT/CT device. [14]

In conclusion, absolute (semi)quantification of SPECT/CT breast studies using MIBI seems feasible (<12% deviation) when 9 iterations (10 subsets) of Evolution are used and tumours (at least 17 mm ⌀) are delineated using a 42% isocontour method. However, in case of tumour shrinkage or a change in tumour viability, response evaluation should be handled with caution especially when using SUV_{max}. Future experimental studies should focus on optimisation of SPECT-based delineation methods. In a further clinical study, currently in progress, we aim to establish the reproducibility and clinical relevance of the SPECT/CT quantification tool evaluated in this experimental setting.

REFERENCES

1. Cardoso F, Costa A, Senkus E, Aapro M, André F, Barrios CH, *et al.* 3rd ESO-ESMO International Consensus Guidelines for Advanced Breast Cancer (ABC 3). Ann Oncol. 2017;28(1):16-33.

2. Killelea BK, Yang VQ, Mougalian S, Horowitz NR, Pusztai L, Chagpar AB, *et al.* Neoadjuvant chemotherapy for breast cancer increases the rate of breast conservation: results from the National Cancer Database. J Am Coll Surg. 2015;220(6):1063-9.

3. Cance WG, Carey LA, Calvo BF, Sartor C, Sawyer L, Moore DT, *et al.* Long-term outcome of neoadjuvant therapy for locally advanced breast carcinoma: effective clinical downstaging allows breast preservation and predicts outstanding local control and survival. Ann Surg. 2002;236(3):295-302.

4. Sun Y, Wei W, Yang HW, Liu JL. Clinical usefulness of breast-specific gamma imaging as an adjunct modality to mammography for diagnosis of breast cancer: a systemic review and meta-analysis. Eur J Nucl Med Mol Imaging. 2013;40(3):450-63.

5. Maublant JC, Zhang Z, Rapp M, Ollier M, Michelot J, Veyre A. In vitro uptake of technetium-99m-teboroxime in carcinoma cell lines and normal cells: comparison with technetium-99m-sestamibi and thallium-201. J Nucl Med. 1993;34(11):1949-52.

6. Scopinaro F, Schillaci O, Scarpini M, Mingazzini PL, Di Macio L, Banci M, *et al.* Technetium-99m sestamibi: an indicator of breast cancer invasiveness. Eur J Nucl Med. 1994;21(9):984-7.

7. Piwnica-Worms D, Chiu ML, Budding M, Kronauge JF, Kramer RA, Croop JM. Functional imaging of multidrug-resistant P-glycoprotein with an organotechnetium complex. Cancer Res. 1993;53(5):977-84.

8. Korsmeyer SJ. BCL-2 gene family and the regulation of programmed cell death. Cancer Res. 1999;59(7):1693s-1700s.

9. Collarino A, de Koster EJ, Valdés Olmos RA, de Geus-Oei LF, Pereira Arias-Bouda LM. Is technetium-99m sestamibi imaging able to predict pathologic monresponse to neoadjuvant chemotherapy in breast ancer? A meta-analysis evaluating current use and shortcomings. Clin Breast Cancer. 2017; In press.

10. Hruska CB, Weinmann AL, Tello Skjerseth CM, Wagenaar EM, Conners AL, Tortorelli CL, *et al.* Proof of concept for low-dose molecular breast imaging with a dual-head CZT gamma camera. Part II. Evaluation in patients. Med Phys. 2012;39(6):3476-83.

11. GE Healthcare. NM Quantification - Q.Metrix for SPECT/CT package (white paper); 2017.

12. Bailey DL, Willowson KP. Quantitative SPECT/CT: SPECT joins PET as a quantitative imaging modality. Eur J Nucl Med Mol Imaging. 2014;41(1):S17-25.

13. Bailey DL, Willowson KP. An evidence-based review of quantitative SPECT imaging and potential clinical applications. J Nucl Med. 2013;54(1):83-9.

14. Mann SD, Perez KL, McCracken EK, Shah JP, Wong TZ, Tornai MP. Initial in vivo quantification of Tc-99m sestamibi uptake as a function of tissue type in healthy breasts using dedicated breast SPECT-CT. J Oncol. 2012;2012:146943.

15. Cheebsumon P, van Velden FH, Yaqub M, Frings V, de Langen AJ, Hoekstra OS, *et al.* Effects of image characteristics on performance of tumor delineation methods: a test-retest assessment. J Nucl Med. 2011;52(10):1550-8.

16. Frings V, van Velden FH, Velasquez LM, Hayes W, van de Ven PM, Hoekstra OS, *et al.* Repeatability of metabolically active tumor volume measurements with FDG PET/CT in advanced gastrointestinal malignancies: a multicenter study. Radiology. 2014;273(2):539-48.

17. Erdi YE, Wessels BW, Loew MH, Erdi AK. Threshold estimation in single photon emission computed tomography and planar imaging for clinical radioimmunotherapy. Cancer Res. 1995;55(23):5823s-5826s.

18. Quak E, Le Roux PY, Hofman MS, Robin P, Bourhis D, Callahan J, *et al.* Harmonizing FDG PET quantification while maintaining optimal lesion detection: prospective multicentre validation in 517 oncology patients. Eur J Nucl Med Mol Imaging. 2015;42(13):2072-82.

19. Boellaard R, Willemsen AT, Arends B, Visser EP. EARL procedure for assessing PET/CT system specific patient FDG activity preparations for quantitative FDG PET/CT studies. http://earl.eanm.org/html/img/pool/EARL-procedure-for-optimizing-FDG-activity-for-quantitative-FDGPET-studies_version_1_1.pdf.

20. Hatt M, Cheze le Rest C, Turzo A, Roux C, Visvikis D. A fuzzy locally adaptive Bayesian segmentation approach for volume determination in PET. IEEE Trans MedImaging. 2009;28(6):881-93.

21. Geets X, Lee JA, Bol A, Lonneux M, Grégoire V. A gradient-based method for segmenting FDG-PET images: methodology and validation. Eur J Nucl Med Mol Imaging. 2007;34(9):1427-38.

22. Pacilio M, Basile C, Shcherbinin S, Caselli F, Ventroni G, Aragno D, *et al*. An innovative iterative thresholding algorithm for tumour segmentation and volumetric quantification on SPECT images: Monte Carlo-based methodology and validation. Med Phys. 2011;38(6):3050-61.

23. Cheebsumon P, Boellaard R, de Ruysscher D, van Elmpt W, van Baardwijk A, Yaqub M, *et al*. Assessment of tumour size in PET/CT lung cancer studies: PET- and CT-based methods compared to pathology. EJNMMI Res. 2012;2(1):56.

24. Grootjans W, Meeuwis AP, Slump CH, de Geus-Oei LF, Gotthardt M, Visser EP. Performance of 3DOSEM and MAP algorithms for reconstructing low count SPECT acquisitions. Z Med Phys. 2016;26(4):311-22.

25. Gnesin S, Leite Ferreira P, Malterre J, Laub P, Prior JO, Verdun FR. Phantom validation of Tc-99m absolute quantification in a SPECT/CT commercial device. Comput Math Methods Med. 2016;2016:4360371.

26. Armstrong IS, Hoffmann SA. Activity concentration measurements using a conjugate gradient (Siemens xSPECT) reconstruction algorithm in SPECT/CT. Nucl Med Commun. 2016;37(11):1212-7.

27. Teixeira SC, Koolen BB, Vogel WV, Wesseling J, Stokkel MP, Vrancken Peeters MJ, *et al*. Additional prone 18F-FDG PET/CT acquisition to improve the visualization of the primary tumor and regional lymph node metastases in stage II/III Breast Cancer. Clin Nucl Med. 2016;41(4):e181-6.

28. Teixeira SC, Rebolleda JF, Koolen BB, Wesseling J, Jurado RS, Stokkel MP, *et al*. Evaluation of a hanging-breast PET system for primary tumor visualization in patients with stage I-III breast cancer: comparison with standard PET/CT. AJR Am J Roentgenol. 2016;206(6):1307-14.

THE CLINICAL IMPACT OF MOLECULAR BREAST IMAGING IN WOMEN WITH PROVEN INVASIVE BREAST CANCER SCHEDULED FOR BREAST-CONSERVING SURGERY

CHAPTER 4

A Collarino
RA Valdés Olmos
L van Berkel
PA Neijenhuis
L Wijers
F Smit
LF de Geus-Oei
LM Pereira Arias-Bouda

ABSTRACT

PURPOSE To investigate the clinical utility of molecular breast imaging (MBI) in patients with proven invasive breast cancer scheduled for breast-conserving surgery (BCS).

METHODS Following approval by the Institutional Review Board and written informed consent, records of patients with newly diagnosed breast cancer scheduled for BCS who had undergone MBI for local staging in the period from March 2012 to December 2014 were retrospectively reviewed.

RESULTS A total of 287 women (aged 30–88 y) were evaluated. MBI showed T stage migration in 26 patients (9%), with frequent detection of in situ carcinoma around the tumour. Surgical management was adjusted in 14 of these patients (54%). In 17 of 287 patients (6%), MBI revealed 21 proven additional lesions in the ipsilateral, contralateral breast or both. In 18 of these additional foci (86%), detected in 15 patients, malignancy was found. Thirteen of these 15 patients had ipsilateral cancer and 2 patients bilateral malignancy. In total, MBI revealed a larger tumour extent, additional tumour foci or both in 40 patients (14%), leading to treatment adjustment in 25 patients (9%).

CONCLUSION MBI seems to be a useful imaging modality with a high predictive value in revealing ipsilateral and bilateral disease not visualised by mammography and ultrasound. It may play an important role in delineating the extent of the index lesion during preoperative planning. Incorporation of MBI in the clinical workup as an adjunct modality to mammography and ultrasound may lead to better selection of patients who could benefit from BCS.

INTRODUCTION

Invasive breast cancer is the most common cancer among women, with an incidence of 14,608 new cases in 2016 in The Netherlands.[1] In the last decades breast-conserving surgery (BCS), also called lumpectomy, has gained importance due to the possibility to remove the tumour preserving the natural shape of the breast.[2] Breast-conserving surgery with adjuvant radiotherapy (breast-conserving therapy; BCT) is the preferred locoregional treatment in early-stage breast cancer (BC).[3] BCT is contraindicated in small breasts with large primary tumours and when two or more foci of cancer are located in different quadrants of the breast (multicentric tumours).[2, 4] Therefore, accurate definition of the extent of the primary tumour and exclusion of additional foci of cancer (multifocal, multicentric and contralateral BC) is important in order to conduct the appropriate surgical treatment. Currently, magnetic resonance imaging (MRI) and molecular breast imaging (MBI) have been indicated to assess tumour extent and multifocal, multicentric and contralateral disease in adjunction to mammography (MG) and ultrasonography (US).[3, 5] MBI is a functional imaging technique consisting of a dedicated breast gamma-camera equipped with a small field-of-view (FOV) single- or dual-head detector, producing high-resolution images corresponding to the standard projections used in MG.[6-10] In MBI tumour-seeking radiopharmaceuticals like ^{99m}Tc-sestamibi are used. Uptake of this tracer into tumour cells is based on increased vascularity and high mitochondrial density.[11-13] Compared to MRI, MBI is easy to interpret, is associated with low costs and is not contraindicated in patients with claustrophobia, overweight, implanted devices and renal insufficiency.

The purpose of this study was to investigate the clinical utility of MBI in adjunction to MG and US for delineation of the extent of the index lesion and to rule out additional tumour foci in patients with invasive BC scheduled for BCS.

MATERIALS AND METHODS

PATIENTS

The Institutional Review Board approved this retrospective study and informed consent was obtained from all patients. Patients were included if they fulfilled the following criteria: **a)** presence of histopathologically proven invasive BC; **b)** after conventional clinical workup (including MG and US) the patient was scheduled for BCS; **c)** the patient had undergone pre-treatment MBI for assessment of tumour extent and presence of multifocal or multicentric disease; **d)** complete individual data were available concerning clinical workup, imaging, surgery and histopathology.

MBI ACQUISITION

MBI imaging was performed using a dedicated device equipped with a single detector system also known as breast-specific gamma-imaging (BSGI; Dilon 6800, Dilon Technologies, Newport News, Virginia, US). Images were acquired with the patient in seated position and with the breast in light compression. Each patient received an injection of approximately 600 MBq of ^{99m}Tc-sestamibi into an antecubital vein contralateral to the breast lesion. Approximately 5-10 min after the injection, craniocaudal (CC) and mediolateral oblique (MLO) planar images were obtained for each breast, comparable with those of MG. The acquisition time for each image was 8 min, giving a total acquisition time of approximately 40 min per study. If relevant, additional planar images (lateromedial or mediolateral view, anteroposterior view (axilla) or axillary craniocaudal view) were acquired from the ipsilateral breast.

MBI IMAGE ANALYSIS

All MBI images were evaluated by two nuclear medicine physicians of our Institute and were directly compared with the most recent MG following the functional Breast Imaging Reporting and Data System (BI-RADS) classification. [5, 14]

The size of the index lesion was calculated by measuring the maximum diameter (mm) of the pathological uptake on the MBI images ($_{MBI}$T stage). In case of more than one lesion, the maximum diameter of the largest tumour was used. Index lesion size detected on MBI was compared with the lesion size obtained with MG and US ($_{MORPHOLOGICAL}$ T stage).

MBI-detected abnormalities were considered to be additional tumour lesions when they were suspicious on MBI (BI-RADS 4 or 5) and occult on MG and US. The additional breast lesions were classified as follows: **1)** multifocal lesions when located in the same quadrant of the breast as the index tumour; **2)** multicentric lesions when located in a different quadrant of the breast compared to the index tumour and **3)** contralateral lesions when located in the contralateral breast. The size of each additional lesion was measured on MBI corresponding to the maximum diameter (mm) of the pathological uptake. Histopathology was obtained from all additional MBI lesions after incisional needle-biopsy or surgical excision. The biopsy was performed using US-guided biopsy when the lesion was visible at second-look US, or using MBI-guided biopsy if the lesion remained occult on second-look US.

STATISTICAL ANALYSIS

Statistical analysis was performed using Microsoft Excel 2010. Based on T stage migration (upstaging) after MBI, the percentage of patients in who surgical management was adjusted based on the MBI

results was calculated. Based on the biopsy- or excision-acquired pathological findings, all additional lesions with malignant histopathology (invasive tumour and ductal carcinoma in situ (DCIS) were considered true positive, while all additional lesions with benign histopathology were defined false positive. On the basis of the detected additional lesions on MBI the lesion-based Positive Predictive Value (PPV) was calculated using the formula True Positive/True Positive + False Positive x 100.

RESULTS

Records of 304 women with proven invasive BC scheduled for BCS who underwent MBI between March 2012 and December 2014 were reviewed. Seventeen of these women, who had additional MBI-detected lesions without histopathological diagnosis, were excluded from the analysis. The remaining 287 patients who fulfilled the inclusion criteria were enrolled in this retrospective study. The characteristics of the patients are reported in **Table 1**.

The mean age of the patients was 60 y (range, 30–88 y). The mean morphological maximum tumour diameter, obtained with MG and US, was 18 mm (range, 3–55 mm). In 246 patients (86%) the index lesion concerned invasive ductal carcinoma (IDC), in 24 patients (8%) invasive lobular carcinoma (ILC) and in 1 patient (0.3%) mixed IDC and ILC. The remaining 16 patients (5.7%) had other tumour types including 6 mucinous carcinomas, 3 papillary carcinomas, 3 apocrine carcinomas, 2 medullary carcinomas, and 2 tubular carcinomas.

Concerning the diameter of the index lesion, concordance between MBI and radiologic imaging was found in 261 patients (91%). In 26 out of 287 patients (9%), MBI showed T stage migration with adjustment of the surgical management in 14 of these 26 patients (54%) (**Table 2**).

Five patients underwent unilateral mastectomy, 1 patient bilateral mastectomy, another 5 patients were treated with large lumpectomy, 2 patients received NAC before BCS and 1 patient underwent quadrantectomy. In 10 of these 14 patients, the larger tumour extent on MBI was related to histopathologically proven DCIS around the invasive lesion (**Figure 1**).

In 17 of 287 patients (6%), MBI revealed 21 proven additional lesions in the ipsilateral breast, contralateral breast or both breasts (**Table 3**). The median size of these lesions on MBI was 10 mm (range, 7-35 mm). Histopathologic features were obtained by needle-biopsy from 16 out of 21 lesions in 12 patients and by surgical excision from the other 5 lesions concerning another 5 patients. Breast needle-biopsies were performed under guidance of US in 10 of 12 patients and under MBI guidance in 2 of 12 patients.

Table 1. Patient characteristics

No. of patients	287
Mean age (y)	60 (range, 30-88)
Menopausal status	
Pre-/perimenopausal	79
Postmenopausal	208
Breast tissue composition *	
a	35
b	107
c	127
d	18
Mean tumour size (mm)	18 (range, 3-55)
Multifocal/multicentric	18
T Stage prior to surgery	
T1a	6
T1b	63
T1c	128
T2	89
Unknown	1
Tumour type	
IDC	246
ILC	24
Mixed IDC/ ILC	1
Other	16
Tumour subtype	
HER2-positive	40
ER-positive/HER2-negative	199
Triple negative	38
Scarff-Bloom Richardson Grade	
1	43
2	112
3	124
Unknown	8

***a** almost entirely fat, **b** scattered fibroglandular density, **c** heterogeneously dense, **d** extremely dense, **IDC** invasive ductal carcinoma, **ILC** invasive lobular carcinoma, **DCIS** ductal carcinoma in situ, **ER** estrogen receptor, **HER2** human epidermal growth factor receptor 2.

Table 2. T stage migration and treatment adjustment following MBI

No. of patients	Morphological size (mm)	MBI size (mm)	T stage migration	Treatment plan before MBI	Treatment plan after MBI
1	20	24	T1 >T2	BCS	BCS
2	20	24	T1 >T2	BCS	BCS
3	16	35	T1 >T2	BCS	Large BCS
4	17	30	T1 >T2	BCS	BCS
5	11	35	T1 >T2	BCS	Large BCS
6	50	55	T2 >T3	NAC and BCS	NAC and BCS
7	40	63	T2 >T3	NAC and BCS	NAC and BCS
8	19	40	T1 >T2	BCS	Large BCS
9	20	27	T1 >T2	BCS	Mastectomy
10	19	30	T1 >T2	BCS	Large BCS
11	17	30	T1 >T2	BCS	Large BCS
12	20	42	T1 >T2	BCS	NAC and BCS
13	10	85	T1 >T3	BCS	Mastectomy
14	23	26	T1 >T2	Left BCS	Mastectomy
	13	80	T1 >T3	Right BCS	Mastectomy
15	15	21	T1 >T2	BCS	BCS
16	20	32	T1 >T2	BCS	BCS
17	20	24	T1 >T2	BCS	BCS
18	10	26	T1 >T2	BCS	BCS
19	7	30	T1 >T2	BCS	Mastectomy
20	20	25	T1 >T2	BCS	BCS
21	40	120	T2 >T3	BCS	NAC and BCS
22	40	90	T2 >T3	BCS	Quadrantectomy
23	40	90	T2 >T3	BCS	Mastectomy
24	19	23	T1 >T2	BCS	BCS
25	16	23	T1 >T2	BCS	BCS
26	16	90	T1 >T3	BCS	Mastectomy

MBI molecular breast imaging, BCS breast-conserving surgery, NAC neoadjuvant chemotherapy.

In 15 out of these 17 patients (88%) the 18 additional lesions turned out to be malignant. In 13 of these 15 patients, the malignant lesions concerned ipsilateral tumours (15/18 lesions) and in 2 patients bilateral tumours (3/18 lesions) (**Figure 2**).

The surgical management was adjusted in 12 out of these 15 patients (80%). In more detail, 3 patients were converted to NAC and mastectomy, while 7 patients underwent ipsilateral mastectomy instead of BCS, 1 patient was treated with bilateral mastectomy and 1 patient with bilateral BCS. From the 18 additional proven malignant lesions (true positives) on MBI, 6 lesions were smaller than 10 mm (range, 6-8 mm). The pathologic findings of the 18 tumours included 10 IDC, 3 ILC and 5 DCIS. The remaining 3 additionally detected lesions on MBI were benign lesions (false positives) revealing mastopathy in one, one with fibroadenoma and one with a mixed pattern of mastopathy and adenosis. The MBI lesion-related PPV was 86%.

Overall, MBI showed an unexpected larger tumour extent, additional tumour foci or both in 40 of 287 included patients (14%). In one of these 40 patients, MBI revealed both a larger index tumour as well as multicentricity (patient n°19 in **Table 2** and n°10 in **Table 3**). In 4 of these 40 patients (10%) the index lesion concerned ILC. Twenty patients (50%) had non-dense breast tissue with breast composition a in 4 and breast composition b in 16 patients. Owing to the use of MBI the overall treatment was adjusted in 25 patients (9%) (**Figure 3**).
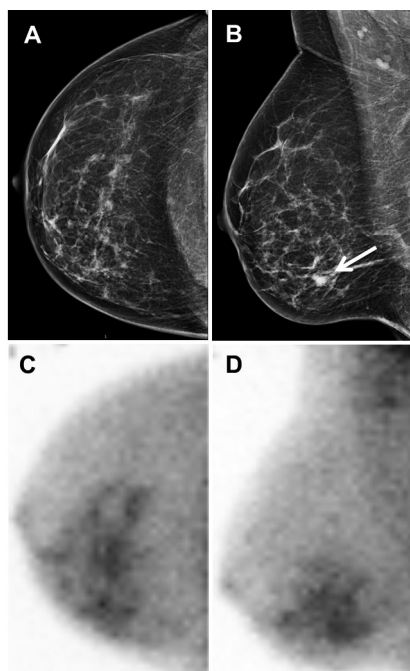
Figure 1. A 52-year-old woman (patient 13, Table 2) with invasive breast cancer. Right craniocaudal mammographic image (A) and right mediolateral oblique mammographic image (B) showing a breast mass of 10 mm with new calcifications in the lower inner quadrant of the right breast, best visible on the mediolateral oblique view (white arrow). Right craniocaudal (C) and right mediolateral oblique MBI (D) images showing a large and heterogeneous area of pathological uptake (85 mm) in the lower inner quadrant of the right breast. The treatment changed from lumpectomy to mastectomy. Pathological findings revealed intracystic papillary adenocarcinoma and extralesional ductal carcinoma in situ with extension towards the nipple.

Table 3. Additional suspicious lesions detected on MBI and occult on MG and US

No. of patients	No. of additional lesions	Size (mm)	Multi-focal lesions	Multi-centric lesions	Contra-lateral lesions	Biopsy/ surgical excision	Malignant lesions	Benign lesions	Treatment plan before MBI	Treatment plan after MBI
1	2	8 R; 7 L		1 R	1 L	US-guided	IDC/DCIS		BCS	Bilateral mastectomy
2	1	35		1		MBI-guided		Mastopathy and adenosis	BCS	BCS
3	1	8	1			US-guided	IDC		BCS	BCS
4	1	7	1			US-guided		Mastopathy	BCS	BCS
5	2	12; 11		2		US-guided	2 ILC		NAC and BCS	NAC and mastectomy
6	1	8	1			Excision	DCIS		BCS	BCS
7	1	7	1			Excision	DCIS		BCS	BCS
8	1	10		1		Excision	DCIS		BCS	Mastectomy
9	1	11		1		US-guided	IDC		BCS	Mastectomy
10	1	6		1		Excision	DCIS		BCS	Mastectomy
11	1	11		1		US-guided	IDC		BCS	Mastectomy
12	1	26	1			MBI-guided	IDC		NAC and BCS	NAC and mastectomy
13	1	14	1			Excision	IDC		BCS or mastectomy	Mastectomy
14	2	10; 30	1	1		US-guided	2 IDC		NAC and BCS	NAC and mastectomy
15	2	12; 12			2 L	US-guided	IDC	Fibroadenoma	BCS	Bilateral BCS
16	1	10		1		US-guided	IDC		BCS	Mastectomy
17	1	10	1			US-guided	ILC		BCS	Mastectomy

MBI molecular breast imaging, R right, L left, IDC invasive ductal carcinoma, ILC invasive lobular carcinoma, DCIS ductal carcinoma in situ, BCS breast-conserving surgery, NAC neoadjuvant chemotherapy.
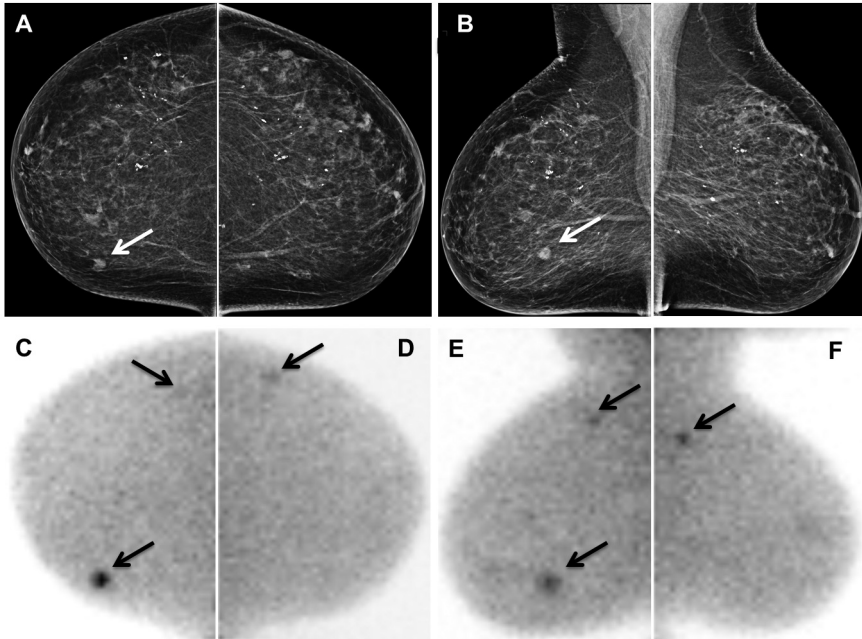
Figure 2. A 71-year-old woman (patient 1, Table 3) with invasive ductal carcinoma of the right breast and two additional tumour foci (1 in ipsilateral breast and 1 in contralateral breast). Right craniocaudal (A) and right mediolateral oblique mammographic (B) images showing a mass of 9 mm in the lower inner quadrant of the breast (white arrows). Right craniocaudal MBI image (C) showing two foci with pathological ^{99m}Tc-sestambi uptake (arrows), one intense accumulation medially corresponding to the mass seen on mammography and a mild accumulation laterally corresponding to the new 8 mm lesion located in the upper outer quadrant (multicentric lesion). Left craniocaudal MBI image (D) shows a new mild focal accumulation in the upper outer quadrant (arrow). Right mediolateral oblique MBI image (E) shows two intense foci (arrows): a caudal accumulation corresponding to the mass seen on mammography and a cranial accumulation (8 mm) corresponding to the new lesion located in the upper outer quadrant (multicentric lesion). Left mediolateral oblique MBI image (F) showing a focal intense accumulation of 7 mm in the upper outer quadrant (contralateral lesion). For both additional lesions the patient underwent US-guided biopsy after second-look US, which revealed invasive ductal carcinoma in the additional lesion in the right breast and ductal carcinoma in situ in the additional lesion in the left breast. The treatment changed from local excision (right breast) to bilateral mastectomy.
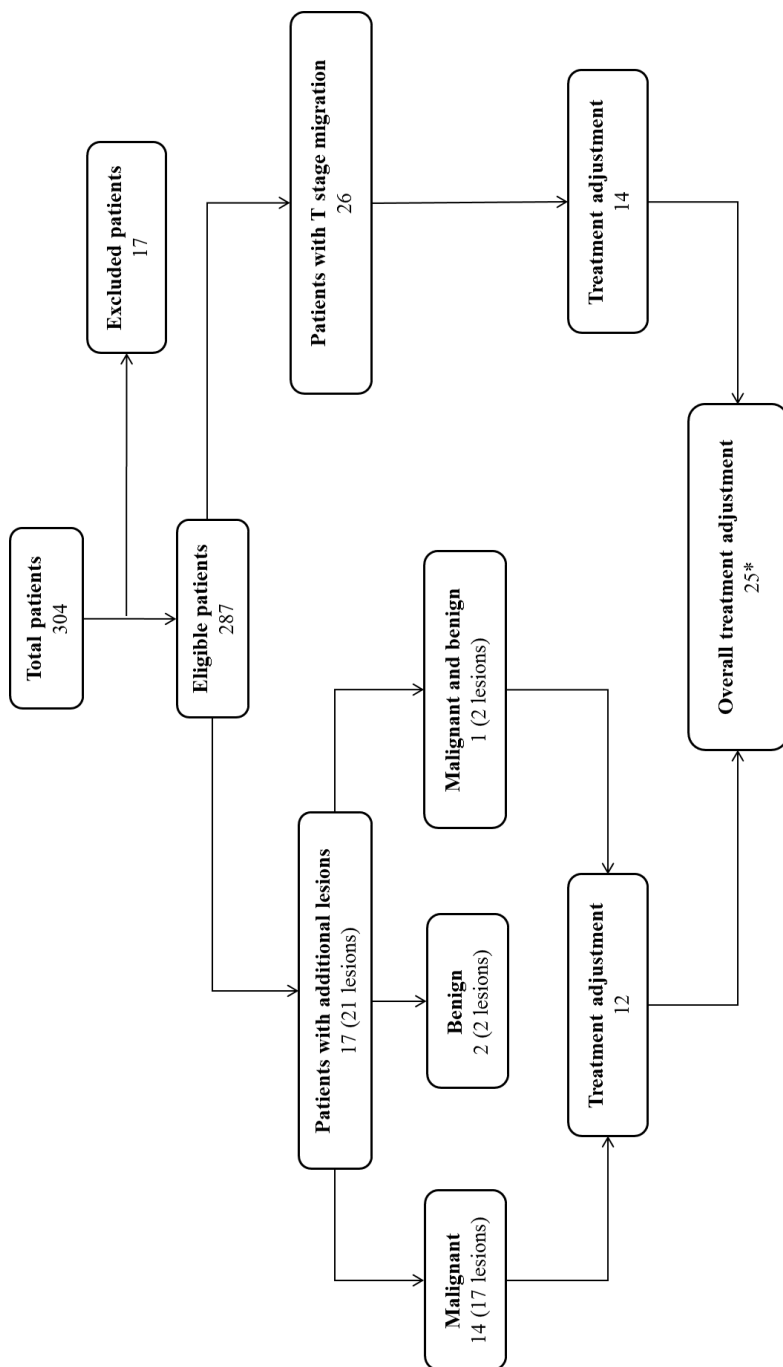
Figure 3. Flowchart showing the impact of preoperative MBI in the study population

* One patient had both T stage migration as well as an additional malignant lesion on MBI.

DISCUSSION

In the present study we evaluated the clinical impact of ^{99m}Tc-sestamibi MBI, incorporated in the diagnostic workup of patients with newly diagnosed BC scheduled for BCS, as an adjunct modality to MG and US. Based on our data, the preoperative use of MBI in this specific patient population resulted in the detection of a significantly larger disease extent, additional tumour foci or both in 14% of patients, albeit 50% of these patients had non-dense breast tissue on MG and only 10% had lobular type of carcinoma. The unexpected MBI findings led to treatment adjustment in 9% of all patients.

Evaluation of the extent of the index lesion using MBI showed a change of the local stage in 26 patients (9%) and local excision was abandoned in 14 of these patients. In our series, a larger disease extent as detected on MBI was mainly due to the visualisation of DCIS located around the invasive tumour, which is in concordance with the findings of Spanu *et al.* [15] Interestingly, in the majority of these patients no calcifications were found in the DCIS area on MG. Although it is not possible to distinguish carcinoma in situ from invasive tumour based on the ^{99m}Tc-sestamibi uptake pattern, the total area of pathological ^{99m}Tc-sestamibi uptake guided our surgeons during the surgical procedure, increasing the rate of complete surgical treatment and avoiding additional surgeries. Therefore we postulate that MBI offers the possibility to plan resection of the index lesion more accurately based on the extension of ^{99m}Tc-sestamibi uptake.

Additional lesions were visualised on MBI in 17 women (6%). Two of these patients underwent MBI-guided biopsy since the additional lesions remained occult even after second-look US. MBI-guided biopsy is a biopsy modality approved by the U.S. Food and Drug Administration (FDA) in 2009. This tool is based on stereotactic localisation of the ^{99m}Tc-sestamibi avid lesion [16, 17] and is currently used in our clinical workup. [18] In our series, MBI-detected lesions corresponded to additional proven tumours in 15 women (5% overall detection rate). This is in line with the results reported in previous studies in the literature. [15, 19-24] Lesion-related analysis demonstrated that 18 out of 21 additional lesions visualised on MBI resulted in true cancer. The high PPV of 86% suggests that a positive MBI scan is highly predictive for occult tumour. This is in concordance with the relative high specificity of this technique as described in the literature. [25] A possible explanation is the highly specific uptake of ^{99m}Tc-sestamibi by tumour cells as compared to the surrounding breast tissue. [11-13] This also suggests that a significant number of the 17 patients with histopathologically unproven suspicious lesions on MBI, who therefore were excluded from our study, may indeed have had multifocal tumours, multicentric tumours or both. Moreover, MBI detected 6 subcentimetre additional cancers in our series. This agrees with prior studies

[15, 22, 23] reporting the ability of MBI to identify occult tumours smaller than 1 cm. Recently, new MBI systems based on dual-head cadmium-zinc-telluride detectors have been introduced offering improved sensitivity for detection of small tumours. [10] In our series the detection of additional tumours on MBI has led to the abandonment of lumpectomy in 11 women. Combining the contribution of MBI in relation to investigating disease extent and presence of multifocal and multicentric disease, the overall management was adjusted in 9% of all patients with newly diagnosed BC scheduled for lumpectomy. Additionally, MBI showed a low false-positive rate, thus avoiding unnecessary biopsies, complementary imaging and patient anxiety.

In the light of our results, MBI could be a valid adjunct modality to MG and US for detecting both the extent of index lesions and additional tumour foci. Presently, MRI is widely used in the clinical workup of newly diagnosed breast cancer in women. Although MRI shows high sensitivity, its low specificity and high costs limit a wide application of this modality. Additionally, MRI is not applicable in patients with claustrophobia, overweight, implanted devices and renal insufficiency. [26] MBI has the potential to overcome these limitations becoming a useful tool for almost all newly diagnosed breast cancer patients. Additionally, MBI is easy to perform and is associated with low costs. On the other hand, MBI requires the IV injection of a radiotracer, like ^{99m}Tc-sestamibi, which means radiation exposure for the patient. However, recent technological advances in MBI allow a significant reduction of the injected dose of the radiopharmaceutical. [10]

Finally, it is necessary to address the principal limitation of the present study: it concerns a retrospective study based on data collected in a single institution. On the other hand, this study represents the first series evaluating the additional clinical value of MBI in a large population of patients with proven invasive breast cancer scheduled for breast-conserving surgery.

CONCLUSION

The results of the present study imply that MBI is a useful imaging modality, which reveals a high rate of multifocal or multicentric lesions and bilateral disease not visualised by mammography and ultrasound. Additionally, MBI may play an important role in accurate delineation of the tumour extent during preoperative planning. Therefore, the incorporation of this modality to the clinical workup may lead to better selection of patients who might benefit of BCS. However, larger and prospective studies are needed to confirm these findings.

REFERENCES

1. Netherlands Cancer Registry. http://www.cijfersoverkanker.nl

2. Clough KB, Kaufman GJ, Nos C, Buccimazza I, Sarfati IM. Improving breast cancer surgery: a classification and quadrant per quadrant atlas for oncoplastic surgery. Ann Surg Oncol. 2010;17(5):1375-91.

3. Gradishar WJ, Anderson BO, Balassanian R *et al*. Breast cancer version 2.2016, NCCN Clinical Practice Guidelines in Oncology. http://www.nccn.org/professionals/physician_gls/pdf/breast.pdf

4. Winchester DP, Cox JD. Standards for breast-conservation treatment. CA Cancer J Clin. 1992;42(3):134-62.

5. Goldsmith SJ, Parsons W, Guiberteau MJ, Stern LH, Lanzkowsky L, Weigert J, *et al*. SNM practice guideline for breast scintigraphy with breast-specific gamma-cameras 1.0. J Nucl Med Technol. 2010;38(4):219-24.

6. Brem RF, Schoonjans JM, Kieper DA, Majewski S, Goodman S, Civelek C. High-resolution scintimammography: a pilot study. J Nucl Med. 2002;43(7):909-15.

7. Rhodes DJ, O'Connor MK, Phillips SW, Smith RL, Collins DA. Molecular breast imaging: a new technique using technetium Tc 99m scintimammography to detect small tumors of the breast. Mayo Clin Proc. 2005;80(1):24-30.

8. Jones EA, Phan TD, Blanchard DA, Miley A. Breast-specific gamma-imaging: molecular imaging of the breast using 99mTc-sestamibi and a small-field-of-view gamma-camera. J Nucl Med Technol. 2009;37(4):201-5.

9. Weinmann AL, Hruska CB, O'Connor MK. Design of optimal collimation for dedicated molecular breast imaging systems. Med Phys. 2009;36(3):845-56.

10. Hruska CB, Weinmann AL, Tello Skjerseth CM, Wagenaar EM, Conners AL, Tortorelli CL, *et al*. Proof of concept for low-dose molecular breast imaging with a dual-head CZT gamma camera. Part II. Evaluation in patients. Med Phys. 2012;39(6):3476-83.

11. Mankoff DA, Dunnwald LK, Gralow JR, Ellis GK, Schubert EK, Charlop AW, *et al*. [Tc-99m]-sestamibi uptake and washout in locally advanced breast cancer are correlated with tumor blood flow. Nucl Med Biol. 2002;29(7):719-27.

12. Scopinaro F, Schillaci O, Scarpini M, Mingazzini PL, Di Macio L, Banci M, *et al*. Technetium-99m sestamibi: an indicator of breast cancer invasiveness. Eur J Nucl Med. 1994;21(9):984-7.

13. Delmon-Moingeon LI, Piwnica-Worms D, Van den Abbeele AD, Holman BL, Davison A, Jones AG. Uptake of the cation hexakis(2-methoxyisobutylisonitrile)-technetium-99m by human carcinoma cell lines in vitro. Cancer Res. 1990;50(7):2198-202.

14. Conners AL, Hruska CB, Tortorelli CL, Maxwell RW, Rhodes DJ, Boughey JC, *et al*. Lexicon for standardized interpretation of gamma camera molecular breast imaging: observer agreement and diagnostic accuracy. Eur J Nucl Med Mol Imaging. 2012;39(6):971-82.

15. Spanu A, Sanna D, Chessa F, Manca A, Cottu P, Fancellu A, *et al*. The clinical impact of breast scintigraphy acquired with a breast specific -camera (BSGC) in the diagnosis of breast cancer: incremental value versus mammography. Int J Oncol. 2012;41(2):483-9.

16. Kieper DA, Welch BL, Fairchild LH, inventors; Dilon Technologies, Inc., assignee. Gamma guided stereotactic localization system. US Patent US8249693. August 21, 2012.

17. Collarino A, Valdés Olmos RA, van der Hoeven AF, Pereira Arias-Bouda LM. Methodological aspects of (99m)Tc-sestamibi guided biopsy in breast cancer. Clin Transl Imaging. 2016;4(5):367-76.

18. Collarino A, Valdés Olmos RA, Neijenhuis PA, den Hartog WC, Smit F, de Geus-Oei. First clinical experience using stereotactic breast biopsy guided by 99mTc-sestamibi. AJR Am J Roentgenol. 2017. In press.

19. Lee A, Chang J, Lim W, Kim BS, Lee JE, Cha ES, *et al*. Effectiveness of breast-specific gamma imaging (BSGI) for breast cancer in Korea: a comparative study. Breast J. 2012;18(5):453-8.

20. Killelea BK, Gillego A, Kirstein LJ, Asad J, Shpilko M, Shah A, *et al*. George Peters Award: How does breast-specific gamma imaging affect the management of patients with newly diagnosed breast cancer? Am J Surg. 2009;198(4):470-4.

21. Zhou M, Johnson N, Gruner S, Ecklund GW, Meunier P, Bryn S, *et al*. Clinical utility of breast-specific gamma imaging for evaluating disease extent in the newly diagnosed breast cancer patient. Am J Surg. 2009;197(2):159-63.

22. Brem RF, Floerke AC, Rapelyea JA, Teal C, Kelly T, Mathur V. Breast-specific gamma imaging as an adjunct imaging modality for the diagnosis of breast cancer. Radiology. 2008;247(3):651-7.
23. Brem RF, Shahan C, Rapleyea JA, Donnelly CA, Rechtman LR, Kidwell AB, *et al.* Detection of occult foci of breast cancer using breast-specific gamma imaging in women with one mammographic or clinically suspicious breast lesion. Acad Radiol. 2010;17(6):735-43.
24. Zhou M, Johnson N, Blanchard D, Bryn S, Nelson J. Real-world application of breast-specific gamma imaging, initial experience at a community breast center and its potential impact on clinical care. Am J Surg. 2008;195(5):631-5.
25. Sun Y, Wei W, Yang HW, Liu JL. Clinical usefulness of breast-specific gamma imaging as an adjunct modality to mammography for diagnosis of breast cancer: a systemic review and meta-analysis. Eur J Nucl Med Mol Imaging. 2013;40(3):450-63.
26. Berg WA, Blume JD, Adams AM, Jong RA, Barr RG, Lehrer DE, *et al.* Reasons women at elevated risk of breast cancer refuse breast MR imaging screening: ACRIN 6666. Radiology. 2010;254(1):79-87.

PART II

99MTC-SESTAMIBI-GUIDED BIOPSY
IN BREAST CANCER

METHODOLOGICAL ASPECTS OF 99MTC-SESTAMIBI-GUIDED BIOPSY IN BREAST CANCER

adapted from:

A Collarino
RA Valdés Olmos
AF van der Hoeven
LM Pereira Arias-Bouda

CHAPTER 5

ABSTRACT

PURPOSE This review aims to discuss the methodological aspects of dedicated molecular breast imaging (MBI) using ^{99m}Tc-sestamibi as radiotracer to guide biopsy of occult or unclear breast lesions on mammography (MG) and ultrasound (US) that are suspicious on MBI (BI-RADS criteria 4 and 5), including its advantages, limitations and future clinical applications.

METHODS Literature search was performed using the PubMed/MEDLINE database and "^{99m}Tc-sestamibi", "biopsy" and "breast cancer" as keywords. The search was restricted to English language.

RESULTS There are few studies on ^{99m}Tc-sestamibi guided biopsy methods; to our knowledge, no full studies have yet been reported on clinical validation of this new biopsy procedure. This review describes technical aspects of ^{99m}Tc-sestamibi-guided biopsy and discusses the advantages and limitations of this procedure in comparison with MG, US and magnetic resonance imaging (MRI)-guided biopsy.

CONCLUSIONS MBI-guided biopsy appears to be a complementary modality and is principally indicated in the case of occult or unclear breast lesions on MG/US that are suspicious on MBI. The future indication is in targeted biopsies in patients with large heterogeneous tumours. Further studies are needed to define the accuracy of this biopsy procedure.

INTRODUCTION

Breast cancer (BC) is the most common cancer type in women with an estimated 246,660 new cases and 40,450 deaths in the United States, in 2016. [1] Mammography (MG) is the imaging modality of reference in screening and diagnosis of BC. [2] However, MG has an overall sensitivity of 78%, decreasing to 48%–64% in women with dense breasts. [3] Ultrasonography (US) is the most common adjunct imaging modality, improving the sensitivity to 78% when used together with MG in women with dense breasts. [4] However, breast US is associated with a higher call-back rate and false-positive biopsy rate. [5] Due to the limitations of both modalities, magnetic resonance imaging (MRI) may be used as an adjunct modality. MRI is, for example, recommended as an adjuvant screening modality in high-risk women, [6] increasing the detection rate to 9.5 per 1000 women-years at risk [7] with a sensitivity of 71%–92% and a specificity of 79%–86%. [8, 9] However, breast MRI is costly and limited in women with claustrophobia, obese patients and patients with renal failure. [10] In addition, in the clinical setting MRI shows a relatively low specificity and positive predictive value [11] leading to a high rate of unnecessary biopsies. In the last few years, molecular breast imaging (MBI), also called breast-specific gamma-imaging (BSGI), has been introduced as an adjunct modality in BC detection. MBI is a functional tool based on the use of ^{99m}Tc-sestamibi as tumour tracer. [12] Recently, a ^{99m}Tc-sestamibi MBI-guided biopsy system has been developed, applicable in patients with suspicious breast lesions on MBI (BI-RADS criteria 4–5), which are occult or unclear on MG/US. [13] We performed a search of the literature in PubMed/MEDLINE database using "[99m]Tc-sestamibi" AND "biopsy" AND "breast cancer" as keywords. The search was restricted to English language. The references of the retrieved articles were examined to identify additional articles.

The aim of this review is to discuss the methodological aspects of this novel radioguided-biopsy method, including its advantages, limitations and future clinical applications.

[99m]TC – SESTAMIBI MBI TECHNIQUE AND INTERPRETATION

Increased uptake of ^{99m}Tc-sestamibi in BC cells is based on increased vascularity and cytoplasmic mitochondrial density and activity. [14, 15] However, overexpression of multidrug resistance membrane proteins (Pgp and MRP1) and anti-apoptotic Bcl-2 protein of the outer mitochondrial membrane can limit retention of ^{99m}Tc-sestamibi in tumour cells. [16] In 2002, the first study described the performance of this functional breast-dedicated modality in patients with breast tumours. [17] Since

then, MBI has been validated in several studies. [18] In screening studies in women with dense breasts and increased BC risk, the addition of MBI to MG significantly increased sensitivity to 91% with a detection rate of 11–12 per 1000 screened women. [19, 20] A recent meta-analysis, including 19 studies, showed that MBI has a sensitivity of 95% and specificity of 80% in detecting BC. Additionally, the authors reported that MBI detected MG-occult breast lesions in 4% and additional lesions in 6% of patients with suspicious MG or proven breast lesions. [18] ^{99m}Tc-sestamibi-MBI refers to functional imaging of the breast using a breast-dedicated high-resolution, small field-of-view (FOV) gamma-camera; the images, based on the detection of increased uptake of ^{99m}Tc-sestamibi in the tumour in comparison to normal tissue, are independent of breast density. The original MBI system still employs a single detector with a 20 x 15 cm FOV, containing an array of sodium iodide (NaI) crystals (3 x 3 mm pixel size) coupled to position sensitive photomultiplier tubes (PSPMTs). Most literature reports have been based on the use of a single-head system (Dilon 6800, Dilon Technologies, Newport News, Virginia). In recent years, dual-head detection became available following the introduction of the MBI devices Discovery NM750b (GE Healthcare, Milwaukee, Wisconsin) and LumaGem 3200s (Gamma Medica, Inc., Northridge, California) which employ two opposite cadmium-zinc-telluride (CZT) detectors with small FOV (24 x 16 resp. 20 x 16 cm) and 2.5 resp. 1.6 mm pixel size; these devices are aimed to provide better energy resolution. [21] A summary of the commercially available MBI devices is shown in **Table 1**.

In both single-head and dual-head MBI devices, the patient is seated during the entire study and the breast is positioned directly on the detector(s) with light compression to limit patient motion. Patients receive an IV injection of the radiotracer (600–800 MBq ^{99m}Tc-sestamibi for single-head MBI or 300 MBq for dual-head MBI-systems) in an antecubital vein contralateral to the breast lesion. Approximately 5–10 min after the injection of the radiotracer, standard planar images are performed for each breast in the craniocaudal (CC) and mediolateral oblique (MLO) projections. The acquisition time for each image is 8–10 min with a total acquisition time of approximately 40 min per study. If needed, additional images may be acquired (lateromedial or mediolateral view, anteroposterior view (axilla) or axillary craniocaudal view). These projections correspond to the standard projections used in MG (**Figure 1**).

For interpretation of the images a viewing system should be available which enables the adjustment of the image contrast and simultaneous display of the mammographic and scintigraphic images. The scintigraphic images are interpreted according to a functional BI-RADS classification, based on the guidelines of the Society of Nuclear Medicine (SNM) as shown in **Table 2** and **Figure 2**. [12] Recently, a lexicon for the description of MBI images has been developed, [22] based on familiar

Table 1. Summary of characteristics of commercially available devices for molecular breast imaging

Device	Single/dual-head	Detector	FOV (cm)	Pixel size (mm)	Light detection	Biopsy-guidance	Additional information
Dilon 6800 (Dilon Technologies)	Single-head	NaI	20 x 15	3 x 3	PSPMTs	FDA-approved	www.dilon.com
Dilon 6800 Acella (Dilon Technologies)	Single-head	CsI	25 x 20	3.2 x 3.2	PSPMTs	FDA-approved	www.dilon.com
GE Discovery NM750b MBI (GE Healthcare)	Single/Dual-head	CZT	24 x 16	2.5 x 2.5	Semiconductor	In development	www3.gehealthcare.com
LumaGEM 3200s (Gamma Medica)	Dual-head	CZT	20 x 16	1.6 x 1.6	Semiconductor	In development	www.gammamedica.com

CsI cesium iodide, CZT cadmium zinc telluride, FDA The Food and Drug Administration, FOV field-of-view, NaI sodium iodide, PSPMTs position sensitive photomultiplier tubes.
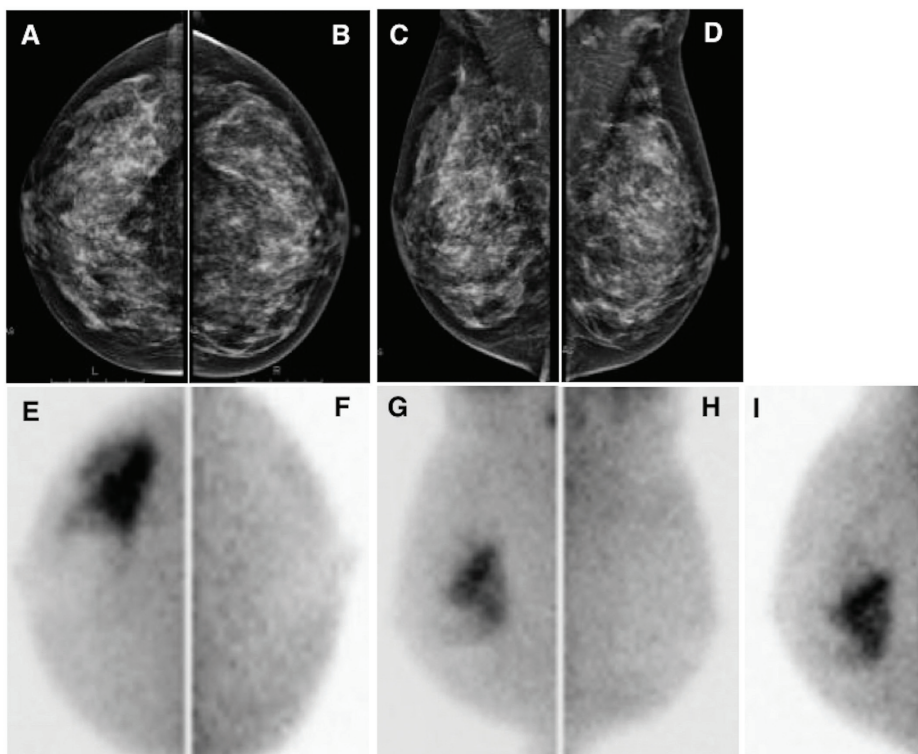
Figure 1. Mammography and MBI in a 47-year-old female with dense breasts. Mammography showed no abnormalities (BI-RADS I) in right (A) and left (B) craniocaudal views and in right (C) and left (D) mediolateral oblique images. MBI showed suspicious uptake (BI-RADS V) in right craniocaudal (E), lateral-oblique (G) and additional lateral views (I). Histopathological examination revealed invasive adenocarcinoma.

radiological BI-RADS lexicon terminology, as well as on the proposed BI-RADS-type lexicon for positron emission mammography (PEM).

^{99M}TC-SESTAMIBI MBI-GUIDED BIOPSY PROCEDURE

MBI-guided biopsy procedure is based on both preoperative imaging and intraoperative excision using ^{99m}Tc-sestamibi as radiotracer for target tissue localisation, according to the radioguided surgery concept. [23] To date, methodological aspects of PEM-guided biopsy using ^{18}F-fluorodeoxyglucose (^{18}F-FDG) have been described, [24] whereas no article has yet been reported the steps in MBI-guided breast biopsy using ^{99m}Tc-sestamibi. For this latter modality, slant-hole

Table 2. BI-RADS classification and MBI interpretation criteria according to the guidelines of the Society of Nuclear Medicine[12]

BI-RADS	MBI-interpretation
1 - Negative	Homogeneous uptake
2 - Benign	Patchy or diffusely increased uptake, often bilateral and correlating with MG anatomy
3 - Probably Benign	Multiple patchy areas of uptake, mild to moderate intensity
4 - Suspicious for malignancy	
4a - Low	
4b - Intermediate	Small focal areas of increased uptake
4c - Moderate	
5 - Highly suggestive of malignancy	Moderate to intense focal uptake with well-delineated contours

BI-RADS Breast Imaging-Reporting and Data System, **MBI** molecular breast imaging, **MG** mammography.

collimator technology (GammaLoc® MBI localisation system, Dilon Technologies, Newport News, Virginia, US) is used to calculate the lesion depth using a single-head system. [13] Biopsy is performed with the patient in seated position. The breast is placed between the detector and the paddle (CorreLocator™, Dilon Technologies, US) with light compression to reduce patient motion. A fiducial source using Cerium-139 (^{139}Ce) is imbedded into the compression paddle as spatial reference point for determining the position of the lesion. The patient is administered with approximately 600 MBq of ^{99m}Tc-sestamibi into an arm vein contralateral to the breast lesion. Approximately 5 min after the injection, a scout image is performed using a parallel-hole collimator for positioning of the lesion. The breast lesion is in the exact position when it is assumed to be visible in the FOV of both the left and right stereotactic views. Subsequently, left and right stereotactic images are performed using a sliding slant-hole collimator (StereoView™, Dilon Technologies, US) for determining the grid localisation (x, y) and the depth (z) of the lesion. Using this slant-hole collimator, 20 degree angle stereo views are required from both the left and right side (**Figure 3**, Step 1). The location and the depth are clearly identified at the point where the angles intersect. Subsequently, the software (GammaLoc®, Dilon Technologies, US) calculates
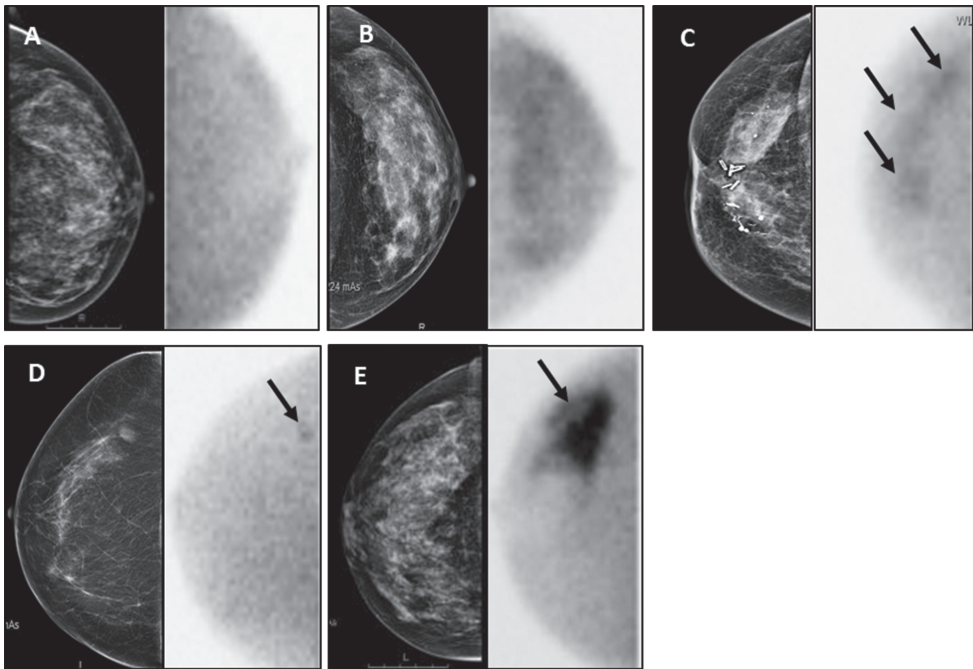
Figure 2. Examples of MBI images according to BI-RADS classification. [12] Left craniocaudal view showing homogeneous uptake (BI-RADS I) (A); left craniocaudal view showing diffusely increased uptake (BI-RADS II) (B); right craniocaudal view showing multiple patchy areas of uptake (BI-RADS III) pointed by arrows (C); right craniocaudal view showing small focal area of increased uptake (BI-RADS IV, arrow) (D); right craniocaudal view showing intense uptake (BI-RADS V, arrow) (E).

the x, y, z coordinates indicating the x and y coordinates in the grid and the depth of the trocar needle in the guidance block (**Figure 3**, Step 2). After injection of local anaesthetic, the guidance block is placed in the paddle in the correct position. After the trocar needle is introduced into the sheath and the depth marker is set in the right position, the trocar needle is placed into the breast (**Figure 3**, Step 3). Subsequently, a first image (pre-verification) is acquired in the energy window of ^{99m}Tc with the needle in place. Afterwards, the trocar needle is removed and replaced by a radioactive ^{139}Ce source followed by a second image (post-verification) using the energy window of ^{139}Ce. Both pre and post-verification images are acquired using both slant-hole collimators located under the lesion to verify the correct position of the needle (**Figure 3**, Step 4). After this verification step, the actual biopsy is performed using a vacuum-assisted device (VAD). The VAD

is composed of a large bore needle with an internal cutting trocar that rotates 360 degree around the axis of the needle cutting 6 specimens from the target lesion, which is vacuum aspirated into the sampling chamber. A radiological marker is left behind at the biopsy site to enable further lesion excision or follow-up. Tissue sample activity is measured ex vivo using the parallel-hole collimator, followed by histopathological analysis. Finally, MG is performed to verify the correct marker position (**Figure 3**, Step 5).

99MTC - SESTAMIBI MBI - GUIDED BIOPSY IN COMPARISON WITH MG -, US - AND MRI - GUIDED BIOPSY

In recent years, percutaneous image-guided breast biopsy has gained importance as an alternative to surgical biopsy, mainly using sonographic, stereotactic, or MRI guidance. US-guided biopsy is the first technique of choice for sampling breast lesions. The sampling probe is placed behind the lesion to be biopsied and the verification of the correct needle placement is real-time. The main advantages of US-guided biopsy are its wide availability, lack of ionizing radiation and low costs. [25] Stereotactic biopsy is usually performed for sampling microcalcifications and distortions not detected on US. [26] The patient is in upright or prone position and in both situations with compression of the breast. [27, 28] The prone position results in higher comfort for the patient, decreased likelihood of patient motion and less vasovagal reactions. [29] MRI-guided biopsy is principally performed when the breast lesion is occult both on US and MG. [30] The patient is in prone position with the breast located in a dedicated biopsy coil with compression in the mediolateral direction. The procedure time for MRI-guided biopsy is approximately 30–70 min. [31, 32] MRI-guided biopsy poses several challenges, such as the necessity to remove the patient from the magnet to perform the biopsy and the transient nature of the contrast enhancement. Furthermore, the access to the medial and posterior breast tissue is limited. An important limitation concerns the inability to verify the successful sampling of the target lesion, since tissue samples do not enhance ex vivo. [33, 34] As mentioned earlier, MBI is increasingly being used as adjunct modality to MG and US for detecting BC. In contrast to MG, MBI is a functional imaging technique that is not influenced by breast density and architectural distortion, regularly leading to the discovery of MG occult breast malignancies. [18, 35] For patients with occult or unclear breast lesions on MG and US but suspicious MBI, the possibility to use MBI-guided biopsy appears to be an excellent alternative to acquire representative tissue samples for histopathological analysis. To

Step 1

A scout image (*1a*) is performed using a parallel-hole collimator, showing an elongated lesion (red *arrow*) in the field of view.

Then, left (*1b*) and right (*1c*) stereotactic images are acquired, showing the lesion (*embedded circle*) and the fiducial reference point (*cross*).

Both stereotactic images are obtained using a sliding slant-hole collimator at +20 and -20 degrees (*1d*) for left and right views.

Step 2

The software calculates the X- and Y-coordinates (*green square in grid and green circle in guidance block*) together with the depth (Z) of the target lesion.

Step 3

The guidance block (*3a*) is positioned in the grid (location D3) and the trocar needle (*3b*) is introduced into the sheath (*3c*) with the depth marker (*red arrow*) in correct position (59 mm), followed by the breast incision (*3d*).

Figure 3. Procedure steps of 99mTc-Sestamibi MBI-guided biopsy using a stereotactic localisation system (GammaLoc®).

Step 4

A pre-verification image using the ^{99m}Tc energy window is performed (*4a*) with both slant-hole collimators under the lesion (*4b*).

Then, the trocar needle is replaced by a radioactive ^{139}Ce source (*4c*) followed by a post-verification image using the ^{139}Ce energy window.

Both pre- and post-verification images are overlaid (*4d*) to verify the correct position of the incision.

Step 5

Biopsy samples are acquired using the VAD (*5a*) and a radiological marker is left at the biopsy site (*5b*).

The tissue radioactivity is measured ex vivo (*5c*) using a parallel collimator and a mammography (*5d*) is performed to verify the position of the radiological marker (yellow arrow).

Figure 3. (continued)

date, several MBI-guided biopsy methods have been described in the literature. In 2004, Coover *et al.* reported on a method to localise the lesion using a dedicated breast camera with an open biopsy paddle. The site of the lesion was identified using Cobalt-57 (^{57}Co) point source on the breast and the camera monitor in the persistent mode. Subsequently, two localisation needles were placed into the site of the lesion followed by an open biopsy of the area where the two needles intersected. The authors reported a suspicious finding in 5 of 37 patients (13.7%) with dense breasts and at high-risk of breast cancer; biopsy revealed carcinoma in 3 out of 5 of these patients. [36] In 2006, Welch *et al.* reported on the development of a compact dedicated breast camera-guided stereotactic breast biopsy system. A fiducial marker containing 0.925 MBq of ^{57}Co was mounted inside the top of the breast compression paddle as spatial reference point. An algorithm for determining the spatial location of the breast lesion was implemented in the software of the dedicated breast camera. [37] More recently, Weinmann *et al.* developed a conical slant-hole (CSH) collimator for MBI-guided biopsy with dual-head CZT, improving the accuracy of lesion depth determination. [38] To our knowledge, no full studies have yet been reported on clinical validation of MBI-guided biopsy procedures. Based on our own clinical experience, the stereotactic biopsy method using the slant-hole collimator localisation system as described here shows good patient acceptability. The procedure time is approximately 75 min, which is longer than the MG- and US-guided methods. The difference is mainly explained by the prolonged image acquisition which is necessary to accurately display lesion uptake of ^{99m}Tc-sestamibi for subsequent stereotactic localisation and biopsy (**Figure 4**).

However, procedure time is comparable to MRI-guided biopsy. Complications are similar to those in other radiological biopsy methods such as syncope, hematoma formation and marker migration. **Table 3** describes the clinical indications for MBI-guided biopsy. This biopsy method

Table 3. Indications for MBI-guided biopsy in clinical practice

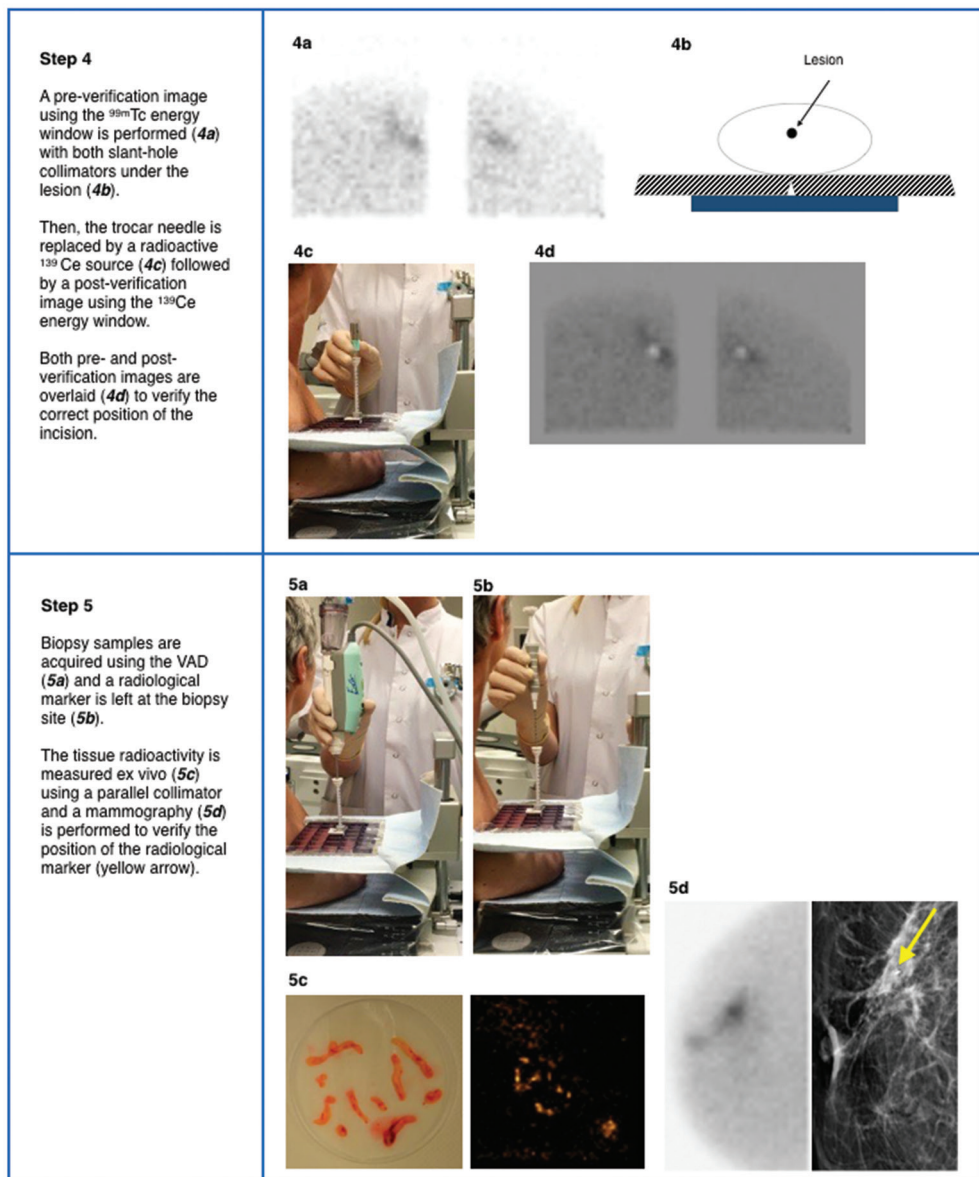| Indication for MBI-guided biopsy |
| --- |
| Occult lesions on MG/US but MBI-suspicious[a] and occult after second-look US |
| Unclear lesions on MG/US but MBI-suspicious[a] |
| Failure of earlier radiological biopsy |
| Future: targeted biopsy of large heterogeneous tumours in patients with locally advanced breast cancer |

[a] BI-RADS criteria 4 and 5. **MBI** molecular breast imaging, **MG** mammography, **US** ultrasound.
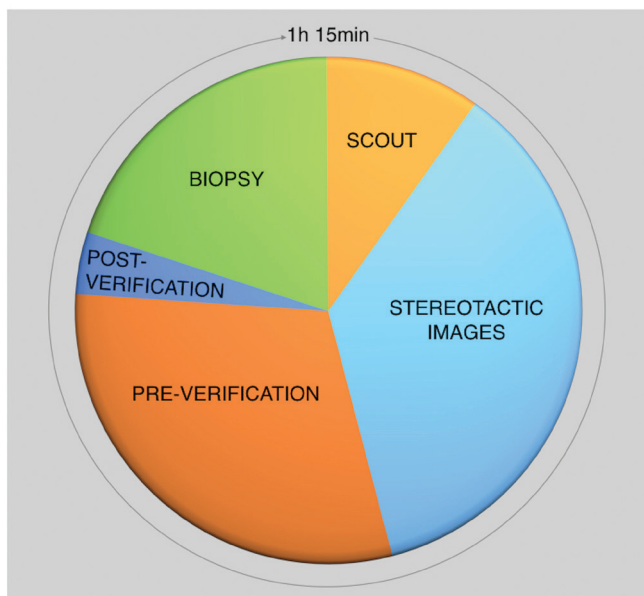
Figure 4. Procedure time of the different steps in ^{99m}Tc-sestamibi MBI-guided biopsy

using ^{99m}Tc-sestamibi is considered a complementary modality to MG-, US-guided biopsy and an alternative to MRI-guided biopsy. It is principally indicated in patients with occult lesions on MG/US but suspicious on MBI (BI-RADS criteria 4 or 5) and occult after second-look US. Other possible indications include: **i)** unclear lesions on MG/US but suspicious on MBI (BI-RADS criteria 4–5) and **ii)** failure of other biopsy methods.

A potential future indication concerns optimisation of primary tumour tissue sampling in patients with locally advanced breast cancer (LABC) by means of ^{99m}Tc-sestamibi-guided targeted biopsy. In the literature non-correspondence between the core biopsy location and the area with highest metabolic activity in the tumour has been described for stage II/III breast cancer patients scheduled for neoadjuvant chemotherapy. [39] Since early and increased concentration of ^{99m}Tc-sestamibi in breast carcinomas is associated with high proliferation rate, indicating more aggressive tumour behaviour, [40] the sampling of the most proliferative parts of the tumour that correspond with highest uptake of ^{99m}Tc-sestamibi in large heterogeneous tumours could result in more optimal therapy planning in patients with LABC. The advantages and disadvantages of the different

Table 4. Comparison of image-guided biopsy modalities

Biopsy method	Compression	Patient position	Advantages	Limitations
US-guided	No	Supine	Real time verification of needle position, fast, no ionizing radiation, low costs	Not useful for MC/distortions
Stereotactic	Yes	Upright/Prone	Useful for MC/distortions, sample verification ex vivo possible (MC)	Ionizing radiation
MRI-guided	Yes	Prone	Useful for US and MG occult lesions, no ionizing radiation	High costs, long procedure time, limitation in claustrophobia, obesity and renal insufficiently, sample verification ex vivo not possible
MBI-guided	Yes (mild)	Upright	Useful for indeterminate/unclear lesions on MG/US, sample verification ex vivo possible	Lesions close to the pectoral muscle, ionizing radiation, long procedure time

MBI molecular breast imaging, **MC** microcalcifications, **MG** mammography, **MRI** magnetic resonance imaging, **US** ultrasound.

biopsy methods are summarised in **Table 4**. The main advantage of MBI-guided biopsy compared to MRI-guided biopsy is the possibility to measure radioactivity of the tissue samples ex vivo, in this way verifying that the target lesion has been sampled successfully. However, biopsy may be difficult in lesions close to the pectoral muscle because they may not be completely visualised due to the vertical position of the patient in relation to the FOV of the camera.

In conclusion, MBI-guided biopsy represents an adjuvant tool to MG-, US-guided biopsy and a promising alternative to MRI-guided biopsy. The principal application of this new biopsy method is in patients with occult or unclear lesions on MG and US that are suspicious on MBI (BI-RADS criteria 4 and 5). The future indication is in targeted biopsies in patients with large heterogeneous tumours. Further studies are needed to define the accuracy of this biopsy procedure.

REFERENCES

1. Siegel RL, Miller KD, Jemal A. Cancer statistics, 2016. CA Cancer J Clin. 2016;66(1):7-30.
2. Tabár L, Fagerberg CJ, Gad A, Baldetorp L, Holmberg LH, Gröntoft O, *et al.* Reduction in mortality from breast cancer after mass screening with mammography. Randomised trial from the Breast Cancer Screening Working Group of the Swedish National Board of Health and Welfare. Lancet. 1985;1(8433):829-32.
3. Kolb TM, Lichy J, Newhouse JH. Comparison of the performance of screening mammography, physical examination, and breast US and evaluation of factors that influence them: an analysis of 27,825 patient evaluations. Radiology. 2002;225(1):165-75.
4. Berg WA, Blume JD, Cormack JB, Mendelson EB, Lehrer D, Böhm-Vélez M, *et al.* Combined screening with ultrasound and mammography vs mammography alone in women at elevated risk of breast cancer. JAMA. 2008;299(18):2151-63.
5. Brem RF, Lenihan MJ, Lieberman J, Torrente J. Screening breast ultrasound:past, present, and future. AJR Am J Roentgenol. 2015;204(2):234-40.
6. Saslow D, Boetes C, Burke W, Harms S, Leach MO, Lehman CD, *et al.* American Cancer Society guidelines for breast screening with MRI as an adjunct to mammography. CA Cancer J Clin. 2007;57(2):75-89.
7. Kriege M, Brekelmans CT, Boetes C, Besnard PE, Zonderland HM, Obdeijn IM, *et al.* Efficacy of MRI and mammography for breast-cancer screening in women with a familial or genetic predisposition. N Engl J Med. 2004;351(5):427-37.
8. Weinstein SP, Localio AR, Conant EF, Rosen M, Thomas KM, Schnall MD. Multimodality screening of high-risk women: a prospective cohort study. J Clin Oncol. 2009;27(36):6124-8.
9. Raikhlin A, Curpen B, Warner E, Betel C, Wright B, Jong R. Breast MRI as an adjunct to mammography for breast cancer screening in high-risk patients: retrospective review. AJR Am J Roentgenol. 2015;204(4):889-97.
10. Berg WA, Blume JD, Adams AM, Jong RA, Barr RG, Lehrer DE, *et al.* Reasons women at elevated risk of breast cancer refuse breast MR imaging screening: ACRIN 6666. Radiology. 2010;254(1):79-87.
11. Johnson N, Sorenson L, Bennetts L, Winter K, Bryn S, Johnson W, *et al.* Breast-specific gamma imaging is a cost effective and efficacious imaging modality when compared with MRI. Am J Surg. 2014;207(5):698-701.
12. Goldsmith SJ, Parsons W, Guiberteau MJ, Stern LH, Lanzkowsky L, Weigert J, *et al.* SNM practice guideline for breast scintigraphy with breast-specific gamma-cameras 1.0. J Nucl Med Technol. 2010;38(4):219-24.
13. Moadel RM. Breast cancer imaging devices. Semin Nucl Med. 2011;41(3):229-41.
14. Delmon-Moingeon LI, Piwnica-Worms D, Van den Abbeele AD, Holman BL, Davison A, Jones AG. Uptake of the cation hexakis(2-methoxyisobutylisonitrile)-technetium-99m by human carcinoma cell lines in vitro. Cancer Res. 1990;50(7):2198-202.
15. Mankoff DA, Dunnwald LK, Gralow JR, Ellis GK, Schubert EK, Charlop AW, *et al.* [Tc-99m]-sestamibi uptake and washout in locally advanced breast cancer are correlated with tumor blood flow. Nucl Med Biol. 2002;29(7):719-27.
16. Moretti JL, Hauet N, Caglar M, Rebillard O, Burak Z. To use MIBI or not to use MIBI? That is the question when assessing tumour cells. Eur J Nucl Med Mol Imaging. 2005;32(7):836-42.
17. Brem RF, Schoonjans JM, Kieper DA, Majewski S, Goodman S, Civelek C. High-resolution scintimammography: a pilot study. J Nucl Med. 2002;43(7):909-15.
18. Sun Y, Wei W, Yang HW, Liu JL. Clinical usefulness of breast-specific gamma imaging as an adjunct modality to mammography for diagnosis of breast cancer: a systemic review and meta-analysis. Eur J Nucl Med Mol Imaging. 2013;40(3):450-63.
19. Rhodes DJ, Hruska CB, Phillips SW, Whaley DH, O'Connor MK. Dedicated dual-head gamma imaging for breast cancer screening in women with mammographically dense breasts. Radiology. 2011;258(1):106-18.
20. Rhodes DJ, Hruska CB, Conners AL, Tortorelli CL, Maxwell RW, Jones KN, *et al.* Journal club: molecular breast imaging at reduced radiation dose for supplemental screening in mammographically dense breasts. AJR Am J Roentgenol. 2015;204(2):241-51.
21. Hruska CB, O'Connor MK. Nuclear imaging of the breast: translating achievements in instrumentation into clinical use. Med Phys. 2013;40(5):050901.

22. Conners AL, Hruska CB, Tortorelli CL, Maxwell RW, Rhodes DJ, Boughey JC, *et al*. Lexicon for standardized interpretation of gamma camera molecular breast imaging: observer agreement and diagnostic accuracy. Eur J Nucl Med Mol Imaging. 2012;39(6):971-82.

23. Zaknun JJ, Giammarile F, Olmos RA, Vidal-Sicart S, Mariani G. Changing paradigms in radioguided surgery and intraoperative imaging: the GOSTT concept. Eur J Nucl Med Mol Imaging. 2012;39(1):1-3.

24. Kalinyak JE, Schilling K, Berg WA, Narayanan D, Mayberry JP, Rai R, *et al*. PET-guided breast biopsy. Breast J. 2011;17(2):143-51.

25. Liberman L, Feng TL, Dershaw DD, Morris EA, Abramson AF. US-guided core breast biopsy: use and cost-effectiveness. Radiology. 1998;208(3):717-23.

26. Liberman L. Percutaneous image-guided core breast biopsy. Radiol Clin North Am. 2002;40(3):483-500.

27. Georgian-Smith D, D'Orsi C, Morris E, Clark CF Jr, Liberty E, Lehman CD. Stereotactic biopsy of the breast using an upright unit, a vacuum-suction needle,and a lateral arm-support system. AJR Am J Roentgenol. 2002;178(4):1017-24.

28. Jackman RJ, Marzoni FA Jr. Stereotactic histologic biopsy with patients prone: technical feasibility in 98% of mammographically detected lesions. AJR Am J Roentgenol. 2003;180(3):785-94.

29. Wunderbaldinger P, Wolf G, Turetschek K, Helbich TH. Comparison of sitting versus prone position for stereotactic large-core breast biopsy in surgically proven lesions. AJR Am J Roentgenol. 2002;178(5):1221-5.

30. Perlet C, Heinig A, Prat X, Casselman J, Baath L, Sittek H, *et al*. Multicenter study for the evaluation of a dedicated biopsy device for MR-guided vacuum biopsy of the breast. Eur Radiol. 2002;12(6):1463-70.

31. Morris EA, Liberman L, Dershaw DD, Kaplan JB, LaTrenta LR, Abramson AF, *et al*. Preoperative MR imaging-guided needle localization of breast lesions. AJR Am J Roentgenol. 2002;178(5):1211-20.

32. Daniel BL, Birdwell RL, Ikeda DM, Jeffrey SS, Black JW, Block WF, *et al*. Breast lesion localization: a freehand, interactive MR imaging-guided technique. Radiology. 1998;207(2):455-63.

33. Schnall MD, Orel SG, Connick TJ. MR guided biopsy of the breast. Magn Reson Imaging Clin N Am. 1994;2(4):585-9.

34. Liberman L. Centennial dissertation. Percutaneous imaging-guided core breast biopsy: state of the art at the millennium. AJR Am J Roentgenol. 2000;174(5):1191-9.

35. Brem RF, Ruda RC, Yang JL, Coffey CM, Rapelyea JA. Breast-specific γ-imaging for the detection of mammographically occult breast cancer in women at increased Risk. J Nucl Med. 2016;57(5):678-84.

36. Coover LR, Caravaglia G, Kuhn P. Scintimammography with dedicated breast camera detects and localizes occult carcinoma. J Nucl Med. 2004;45(4):553-8.

37. Welch BL, Brem R, Black R, Majewski S. Quality assurance procedure for a gamma guided stereotactic breast biopsy system. Phys Med. 2006;21(1):102-5.

38. Weinmann AL, Hruska CB, Conners AL, O'Connor MK. Collimator design for a dedicated molecular breast imaging-guided biopsy system: proof-of-concept. Med Phys. 2013;40(1):012503.

39. Koolen BB, Elshof LE, Loo CE, Wesseling J, Vrancken Peeters MJ, Vogel WV, *et al*. Does the pretreatment tumor sampling location correspond with metabolic activity on 18F-FDG PET/CT in breast cancer patients scheduled for neoadjuvant chemotherapy? Eur J Radiol. 2013;82(12):2353-8.

40. Del Vecchio S, Zannetti A, Fonti R *et al*. 99mTc-MIBI in the evaluation of breast cancer biology. In: Bomdardieri E, Bonadonna G, Gianni L (eds) Breast Cancer Nuclear Medicine in Diagnosis and therapeutic options. Berlin: Springer, 2008. p. 7

FIRST CLINICAL EXPERIENCE USING STEREOTACTIC BREAST BIOPSY GUIDED BY 99MTC-SESTAMIBI

adapted from:

A Collarino
RA Valdés Olmos
PA Neijenhuis
WC den Hartog
F Smit
LF de Geus-Oei
LM Pereira Arias-Bouda

CHAPTER 6

ABSTRACT

PURPOSE The purpose of this study is to evaluate a new device using molecular breast imaging (MBI) for ^{99m}Tc-sestamibi–guided stereotactic lesion localisation as a complementary biopsy tool.

METHODS From December 2012 to May 2016, a total of 38 consecutive women (mean age, 59 y; range, 41–77 y) underwent ^{99m}Tc-sestamibi–guided biopsy using a new MBI-based device and were retrospectively reviewed. The biopsy modality used five steps: stereotactic localisation of the ^{99m}Tc-sestamibi–avid lesion, calculation of coordinates of the lesion location using dedicated software, placement of the needle, verification of the correct needle position, and tissue sampling with a vacuum-assisted device followed by placement of a radiologic marker at the biopsy site and ex vivo measurement of the biopsy specimens.

RESULTS The procedure was technically successful in all 38 lesions. In all cases, biopsy samples were radioactive and adequate for histopathologic analysis. Nineteen lesions (50%) were found to be malignant, and the remaining lesions were found to be benign. The mean procedure time was 71 min (range, 44–112 min). The radiologic marker was successfully deployed in 37 lesions (97%). Two hematomas and three vasovagal reactions were observed.

CONCLUSION Technetium-99m sestamibi–guided biopsy performed using a dedicated MBI-based device is technically feasible and represents a valuable complementary biopsy tool in breast lesion diagnosis.

PART 2 | CHAPTER 6

INTRODUCTION

Since 1994, technetium-99m–labelled sestamibi has been used as a tumour-seeking radiotracer to detect breast cancer. [1, 2] Uptake of ^{99m}Tc-sestamibi occurs within the mitochondria of tumour cells and is related to regional blood flow, angiogenesis, mitochondrial density, and activity. [3–5] Currently, ^{99m}Tc-sestamibi is the radiotracer of choice for molecular breast imaging (MBI). This modality, also called breast-specific gamma-imaging, consists of a single- or dual-head small FOV gamma-camera designed for breast imaging. [6–10]

To date, MRI is the most commonly used imaging modality for breast cancer, after mammography and ultrasound (US). However, because of the limitations of MRI, such as high costs, limited use for patients with claustrophobia, obesity, or renal failure, [11] and a high rate of unnecessary biopsies, [12] MBI is evolving as a valuable complementary tool in the diagnostic workup of breast cancer. [12, 13]

According to the Society of Nuclear Medicine and Medical Imaging, MBI is indicated as an adjunct imaging tool to mammography and US for the following patients: patients with newly diagnosed breast cancer for whom MBI is used to assess multifocal, multicentric, or contralateral disease; patients at high-risk for breast cancer; those with indeterminate breast lesions and remaining diagnostic concerns; and those with technically difficult breast imaging. [14]

For patients with occult lesions on mammography and US that are ^{99m}Tc-sestamibi avid on MBI and are classified as BI-RADS category 4 or 5, [14, 15] second-look US is mandatory. If a sonographic substrate is found on second-look US, US-guided biopsy is performed during the clinical workup. However, for patients with suspicious MBI-detected lesions (BI-RADS category 4 or 5) that remain occult after second-look US or for patients with unclear lesions on mammography and US for whom mammography- or US-guided biopsy is considered technically impossible or has failed, other methods for accurate tissue sampling are necessary. Recently, a device for performing ^{99m}Tc-sestamibi–guided breast biopsy with the use of dedicated MBI was developed. This tool is based on stereotactic localisation of ^{99m}Tc-sestamibi–avid lesions with the use of a slant-hole collimator system and vacuum-assisted device. [16, 17]

The purpose of the current study is to evaluate the potential of this device as a complementary biopsy tool.

MATERIALS AND METHODS

PATIENTS

From December 2012 to May 2016, a total of 38 consecutive patients (mean age, 59 y; range, 41–77 y) underwent ^{99m}Tc-sestamibi–guided biopsy using a dedicated MBI device. Before the procedure, two nuclear medicine physicians in consensus evaluated the MBI images and assessed the feasibility of performing MBI-guided biopsy. Clinical data were retrospectively reviewed. All patients gave written informed consent for retrospective analysis of the data, and the study was approved by Institutional Review Board. All biopsied lesions were ^{99m}Tc-sestamibi avid on MBI (BI-RADS category 4 or 5) and were occult after second-look US or unclear on mammography and US without the possibility for mammography- and US-guided biopsy.

^{99m}TC-SESTAMIBI-GUIDED BIOPSY PROCEDURE

All biopsies were performed using ^{99m}Tc–sestamibi for radioguidance. A dedicated MBI device equipped with a stereotactic localisation system (GammaLoc®, Dilon Technologies, US), cleared by the U.S. Food and Drug Administration in 2009, was used to localise the target lesion (**Figure 1**). The methodologic aspects of this MBI-based biopsy device have been described elsewhere. [18] All patients received analgesics for pain relief on the day of the procedure. After fixation of the breast between the detector and the compression paddle while the patient was in a seated position, a

Figure 1. Molecular breast imaging–guided biopsy device equipped with compact stereotactic localisation system containing fiducial source (arrowhead), grid paddle (thin black arrow), slant-hole collimators (thick black arrow), and detector (white arrows). Monitor displays breast images from two angles for calculation of x, y, and z coordinates of lesion and for determination of corresponding grid hole to insert needle.

dose of 600 MBq of [99mTc]-sestamibi was IV administered.

The biopsy procedure subsequently was performed in five steps. In step 1, a scout image was acquired, followed by acquisition of left and right stereotactic images to determine lesion location. In step 2, software for the dedicated MBI device equipped with a stereotactic localisation system calculated the x, y, and z coordinates of the [99mTc]-sestamibi–avid lesion location. In step 3, local anaesthetic was injected and the needle was placed, and in step 4, verification of the correct needle position was performed using a Cerium-139 ([139Ce]) source, as previously described and illustrated in detail elsewhere. [18] Biopsy subsequently was performed using a vacuum-assisted device. As a rule, six specimens were obtained. Immediately thereafter, a radiologic marker (clip) was placed at the biopsy site. After biopsy, the breast was removed from the detector. In step 5, the radioactivity of the tissue samples was measured ex vivo with use of the MBI gamma-camera to confirm the representativeness of the biopsy specimens.

The biopsy samples were subsequently sent for histopathologic analysis. Breast mammography was performed immediately after the biopsy procedure to verify the correct position of the clip in all patients. For individual patients, further diagnostic steps were discussed during a multidisciplinary meeting attended by a radiologist, a nuclear medicine physician, a breast surgeon, and a pathologist. Subsequent decision making depended on such factors as histopathologic diagnosis, pre-test likelihood for malignancy, activity of the acquired samples, and visibility of the index lesion on radiologic imaging.

If a patient with a malignant lesion was scheduled for breast-conserving surgery, the tumour was preoperatively localised using a wire or Iodine-125 ([125I]) seed, which was placed at the site of the clip using sonographic guidance. For patients with benign histopathologic findings, the individual plan may vary from follow-up with MBI or MRI performed after 3–6 months (including resampling when indicated) to follow-up with mammography and US after 6–12 months or a return to the screening program (if applicable).

DATA COLLECTION AND ANALYSIS

Collected data included patient age, characteristics of the lesions based on [99mTc]-sestamibi uptake according to the lexicon for MBI, [15] clip placement, complications, and histopathologic findings after vacuum-assisted biopsy and surgical excision. The procedure time was determined by calculating the interval between initiation of acquisition of the scout image and placement of the clip at the biopsy site. The histopathologic findings from biopsy and excision were classified

as follows: malignant lesions (invasive ductal carcinoma), invasive lobular carcinoma, ductal carcinoma in situ (DCIS), or a combination of these types of lesions; high-risk lesions such as atypical ductal hyperplasia (ADH) and lobular carcinoma in situ;[19] and benign lesions. Data were entered into a computerized spreadsheet (Excel, Microsoft 2010) for analysis. Categoric variables were summarised as counts and percentages in each class. Quantitative variables, such as mean values and SDs, median values, and minimum and maximum values, were calculated.

RESULTS

The results of this study are summarised in **Table 1**. MBI-based biopsy was technically successful for all 38 patients (38 lesions). For all patients, samples were radioactive and adequate for histopathologic analysis. The procedure was well tolerated by all patients. The mean procedure time was 71 min (range, 44–112 min). For three patients, the mean procedure time was longer than 89 min (SD, 1) because of low ^{99m}Tc-sestamibi avidity (patient 10), a patchy uptake pattern (patient 3) making localisation more difficult, and incorrect switching of the slant-hole collimators (patient 8). The median size of the lesions was 14.5 mm (range, 5–60 mm). Of the 38 lesions, nine (24%) were located in the posterior third of the breast and therefore were close to the chest wall.

Histopathologic analysis of the biopsy specimens revealed that 19 lesions (50%) were malignant, with nine of these lesions identified as invasive ductal carcinoma, two as both invasive ductal carcinoma and DCIS, one as invasive lobular carcinoma, one as mucinous carcinoma, and six as DCIS (**Figures 2-3**). On MBI, these 19 malignant lesions had a median size of 12 mm (range, 5–45 mm). Five patients underwent mastectomy. The remaining 14 patients underwent breast-conserving surgery, with wire localisation used for 12 patients and ^{125}I seed localisation used for two patients. Of these 14 patients, 13 (93%) had negative surgical margins, with a median margin of 4.5 mm (range, 2–12 mm). In one patient (patient 15), the surgical margins were positive because of an extension of extralesional DCIS. For 18 of 19 malignant lesions, subsequent surgical excision confirmed the diagnosis of cancer. For one patient (patient 11) who had DCIS diagnosed after vacuum-assisted biopsy, no in situ carcinoma or invasive carcinoma was found after surgical excision. The small area of DCIS (11 mm) probably had been completely excised during ^{99m}Tc-sestamibi–guided biopsy. No high-risk lesions were found on histopathologic analysis of the biopsy specimens.
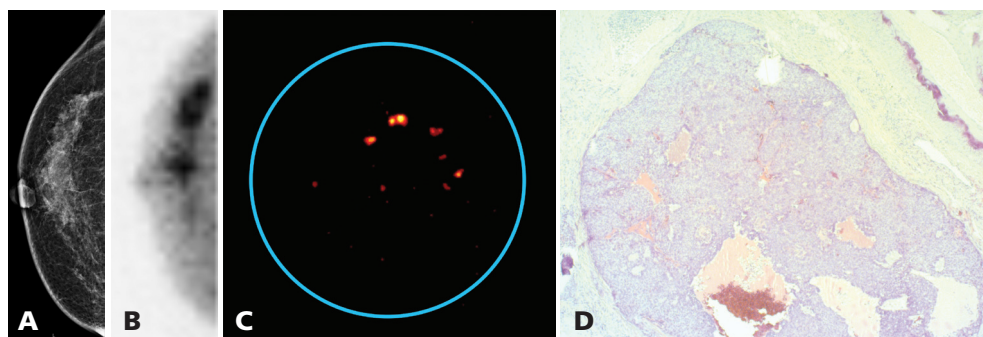
Figure 2. 68-year-old woman (patient 4) with ductal carcinoma in situ. Right craniocaudal mammographic view shows no suspicious breast mass (A); Right craniocaudal molecular breast imaging view shows two suspicious areas with focal ^{99m}Tc-sestamibi uptake in the upper outer quadrant of a small breast (B); Image of biopsy samples measured ex vivo shows radioactive specimens (C); composite photomicrograph (H and E x25) shows cancerization of a lobule by an intraluminal proliferation of atypical epithelial cells (ductal carcinoma in situ) (D).

Nineteen lesions (50%) were diagnosed benign: mastopathy in 11, adenosis in 4 and both mastopathy and adenosis in 4 (**Figure 4**). On MBI, the median size of these benign lesions was 15 mm (range, 7–60 mm). Placement of a localising clip was successful in 37 of 38 lesions (97%). In one patient (patient 7), the marker-needle dragged out the clip from the biopsy site when it was removed from the breast. Post-biopsy mammography showed correct position of the clip at the biopsy site in 33 of 37 patients (89%) and migration of the clip from the biopsy cavity in the remaining four patients. Complications were encountered in five patients (13%). In two patients, a hematoma developed but was resolved with compression. In another three patients, a vasovagal reaction occurred immediately after introduction of the trocar needle, but it was not necessary to abort the procedure.

Table 1. Summary of results

Patient	Age	Lesion size (mm)	Uptake pattern	Uptake score	Breast	Quadrant
		Sestamibi characteristics				
1	52	12	Focal	3	L	UIQ
2	62	10	Focal	3	R	UIQ
3	63	60	Patchy	2	R	UOQ
4	68	40	Focal	3	R	UOQ
5	56	7	Focal	2	L	LOQ
6	77	5	Focal	3	R	UIQ
7	69	15	Focal	3	R	LOQ
8	55	25	Patchy	2	R	UOQ
9	57	20	Focal	2	R	LOQ
10	53	30	Patchy	1	R	UOQ
11	72	11	Focal	2	R	UIQ
12	56	11	Focal	1	L	UIQ
13	75	10	Focal	3	R	UOQ
14	75	11	Focal	3	L	UOQ
15	67	25	Patchy	2	R	C
16	56	9	Focal	2	R	LIQ
17	51	15	Patchy	2	L	LIQ
18	69	30	Focal	3	L	UOQ
19	51	20	Patchy	2	R	C
20	41	20	Patchy	2	R	UOQ
21	61	14	Focal	2	L	C
22	50	20	Focal	2	R	UOQ
23	56	7	Focal	1	L	UOQ
24	67	45	Focal	3	R	UOQ
25	73	8	Focal	2	L	C
26	57	20	Focal	2	L	C
27	50	30	Patchy	3	R	UOQ
28	66	11	Focal	3	R	LIQ
29	67	20	Patchy	2	R	UOQ
30	51	9	Focal	2	L	UOQ
31	48	7	Focal	1	L	UOQ
32	50	15	Focal	3	L	UOQ
33	71	11	Focal	1	R	UOQ
34	46	45	Patchy	2	L	UOQ
35	51	12	Focal	1	L	UOQ
36	48	11	Focal	2	L	LIQ
37	47	11	Focal	3	L	UOQ
38	54	35	Patchy	1	R	C

Lesion depth	Clip failure	Complications	Histopathologic finding	
			From biopsy	**From excision**
C	-	-	IDC and DCIS	IDC and DCIS
P	-	Hematoma	DCIS	DCIS
C	Migration	-	Mastopathy	
C	Migration	-	DCIS	DCIS
C	-	-	Mastopathy	
C	-	-	IDC	IDC and DCIS
P	Failed	-	Mastopathy	
C	-	-	Mastopathy and adenosis	
P	-	-	IDC	IDC
C	-	-	Mastopathy	
C	-	-	DCIS	No malignant focus
C	-	-	ILC	ILC
C	-	-	DCIS	DCIS
P	-	Hematoma	IDC	IDC and DCIS
C	-	-	DCIS	IDC and DCIS
C	-	-	Mastopathy	
P	-	-	DCIS	DCIS
C	-	-	IDC	IDC
C	-	Vasovagal	Mastopathy	
P	-	-	IDC	IDC
A	-	-	Mastopathy	
C	-	-	Adenosis	
C	-	-	Mastopathy and adenosis	
C	-	-	IDC and DCIS	IDC and DCIS
C	-	-	IDC	IDC and DCIS
C	Migration	-	Adenosis	
P	-	Vasovagal	Mucinous carcinoma	Mucinous carcinoma
C	Migration	-	IDC	IDC and DCIS
A	-	-	Mastopathy	
C	-	Vasovagal	Mastopathy	
C	-	-	Adenosis	
A	-	-	Mastopathy	
C	-	-	Adenoma and mastopathy	
C	-	-	Adenosis	
C	-	-	IDC	IDC and LCIS
P	-	-	Mastopathy	
P	-	-	IDC	IDC
A	-	-	Mastopathy and adenosis	

Dash denotes no clip failure or no complication, L left, UIQ upper inner quadrant, C central, IDC invasive ductal carcinoma, DCIS ductal carcinoma in situ, R right, P posterior, UOQ upper outer quadrant, LOQ lower outer quadrant, ILC invasive lobular carcinoma, LIQ lower inner quadrant, A anterior, LCIS lobular carcinoma in situ. score 1 mild uptake, score 2 moderate uptake, score 3 marked uptake. [12]
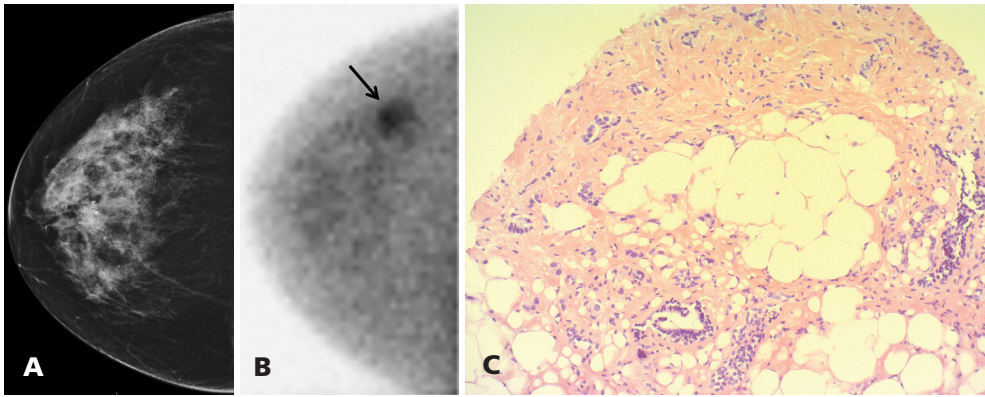
Figure 3. A 57-year-old woman (patient 9) with invasive ductal carcinoma. Right craniocaudal mammographic view, shows no suspicious breast mass (A); right craniocaudal molecular breast imaging view shows one suspicious area with focal ^{99m}Tc-sestamibi uptake in the lower outer quadrant of breast (arrow) (B); composite photomicrograph (H and E x100) shows normal ductolobular units, surrounded by irregular invasive glands and strands of atypical epithelial cells in stroma with desmoplastic changes and microcalcifications (invasive ductal carcinoma of no special type) (C).
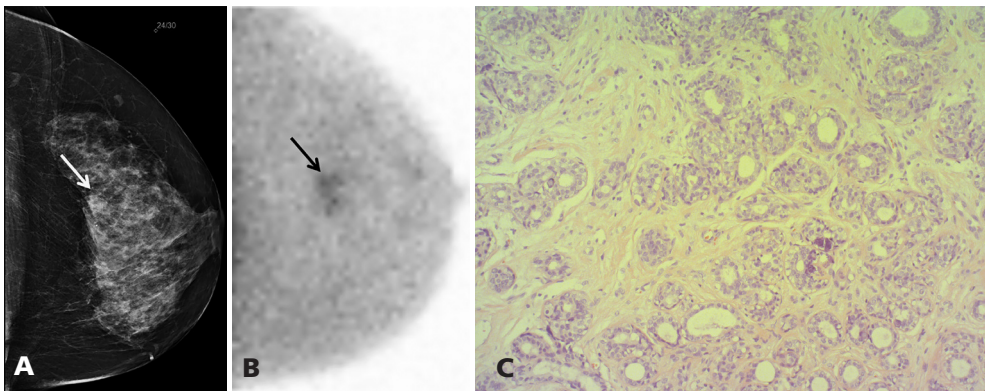
Figure 4. A 57-year-old woman (patient 26) with adenosis. Left craniocaudal mammographic view shows focally dense tissue (arrow) at the central dorsal site of the breast, which was considered to denote overprojection of normal fibroglandular tissue (probably benign, BI-RADS category 3) (A); left craniocaudal molecular breast imaging view shows suspicious focal uptake of ^{99m}Tc-sestamibi (arrow) in the centre of the breast, which is same area as BI-RADS 3 lesion shown on mammographic view in A (B); composite photomicrograph (H and E x100) shows a lobulocentric proliferation of mammary glands, lined with two epithelial layers with glandular compression, distortion caused by stromal proliferation and microcalcifications in lumina (adenosis) (C).

DISCUSSION

In this first clinical experience with this new MBI-based device, ^{99m}Tc-sestamibi–guided biopsy was successful for all 38 consecutive patients. According to our results, this new biopsy tool appears to be technically feasible and may enable dedicated breast cancer imaging specialists to obtain radioactive samples from ^{99m}Tc-sestamibi–avid lesions on MBI. Furthermore, our results show that this device allows one to verify the success of the procedure by measuring ex vivo radioactivity in the biopsy specimens and to separate radioactive from inactive specimens, thereby enabling the pathologist to give special attention to the radioactive specimens (vital tissue), avoiding re-biopsy and delay in diagnosis. According to our results, this biopsy procedure permits acquisition of adequate samples for histopathologic analysis because of the use of a vacuum-assisted device that obtains larger specimen volumes than does automated core needle biopsy. [20, 21] We have shown that ^{99m}Tc-sestamibi is useful in guiding the localisation and excision of ^{99m}Tc-sestamibi–avid breast lesions. This potentially may facilitate the selection of the most ^{99m}Tc-sestamibi–avid areas that reflect the part of tumour with high cellular proliferation, [22] leading to a more accurate genomic profile analysis [23] and avoiding sampling of stroma and fatty tissue, necrotic tissue, or both types of tissue, especially from large heterogeneous lesions. In our series, this new device allows successful sampling of subcentimetre lesions as well as lesions located in the posterior third of the breast and thus close to the chest wall. However, some posterior lesions may not be captured within the biopsy grid if they are in close proximity to the pectoral muscle, because they are not included in the FOV of the device. [18]

Placement of a clip at the biopsy site to facilitate subsequent excision, if needed, was successful in 97% of patients, a finding that is in concordance with findings from MRI-guided biopsies. [24, 25] In our series, the correct clip position was verified using mammography, which was performed immediately after biopsy, revealing a success rate of 89%, which is similar to data reported by Liberman *et al.* [24] for MRI-guided biopsy. Migration of the clip was encountered in four patients and was probably caused by the well-known accordion effect. [26] The time required for this new biopsy procedure appears to be comparable to that needed for MRI-guided biopsy. [24, 27] In the present study, time was principally spent acquiring the initial images necessary to localise the target lesion. The complications that were encountered are comparable to those reported in association with biopsy performed with MRI and a vacuum-assisted device. [24, 25] Hematoma can be controlled by post-procedural breast compression. Administration of anti-anxiolytic medication before the procedure could possibly reduce the amount of vasovagal responses. This new biopsy device appears to be well tolerated by patients, is easy to perform, and may cause less discomfort in patients with claustrophobia. In addition, it is

not contraindicated in patients who are overweight or patients who have implanted devices or renal insufficiency. The relatively high percentage of malignancies found in our series emphasises the value of this new biopsy tool at breast centres where MBI is implemented in the diagnostic pathway. Although half of the lesions biopsied because of MBI findings were found to be benign, this percentage is lower than the percentage of false-positive cases reported for MRI-guided biopsy. [24] MBI cases with false-positive results are the result of uptake of ^{99m}Tc-sestamibi in benign conditions such as adenosis and mastopathy. The present study has limitations. First, the study is retrospective. Second, the population is relatively small, with a low enrolment rate; however, only patients with occult or unclear lesions for which the possibility of mammography- and US-guided biopsy was excluded were eligible. Third, the possible limitations of this modality are related to difficult localisation of the lesion because of low or patchy uptake of ^{99m}Tc-sestamibi or localisation of the lesion in close proximity to the thoracic wall. Furthermore, as with any other biopsy procedure, the possibility of sampling error should be considered in case of discordance between imaging features and histologic results. In this regard, an advantage of MBI-based biopsy over MRI-guided biopsy is the possibility of verifying ex vivo whether lesion sampling is successful by measuring the radioactivity in the samples. For discordant cases, further management will be accorded by the institutional multidisciplinary oncology committee and will depend on the initial level of suspicion on MBI, the radioactivity of the obtained biopsy samples, and visibility of or suspicion for the index lesion on mammography, second-look US, or both. If follow-up is requested, short-term (3-month) follow-up with MBI may be performed or follow-up with MRI may be done after 6 months to avoid imaging of post-biopsy tissue changes. Another important aspect concerns the clip placed after biopsy. The fact that the clip is not visible on MBI may theoretically hinder verification of the correct position of the clip. In our experience, comparison of craniocaudal and lateromedial views from MBI with the corresponding views from post-biopsy mammography helps to solve this limitation because clip position can be adequately judged visually. In the future, co-registration in the acquisition of MBI and mammography images, followed by fusion of images, might help improve the procedure. Clip migration, however, may hamper preoperative lesion localisation when the lesion is found to be malignant and is radiologically occult.

Finally, this procedure involves IV injection of a radioactive tracer and, thus, the use of ionizing radiation. Although the mean glandular dose to the breast is lower with MBI than with digital mammography, the estimated whole-body effective dose is 5 mSv with MBI (using 600 MBq of ^{99m}Tc-sestamibi), compared with 0.5 mSv with digital mammography and 1.2 mSv with mammography combined with digital breast tomosynthesis. [28] A single MBI study with 740–1110 MBq of ^{99m}Tc-sestamibi is associated with a

lifetime attributable risk of fatal cancer that is 20–30 times greater than that of digital mammography in women aged 40 years. [29] One should notice that doses from both mammography and MBI are way lower than doses at which consideration of risks from radiation are warranted. [30] In addition, innovations in MBI technology allow a reduction in administered activity to 150 MBq of [99mTc]-sestamibi, leading to significant reductions in the absorbed dose to the breast (0.25 mGy) and the effective dose (1.1 mSv). [28] The fact remains, however, that one should strive to follow the as low as reasonably achievable (ALARA) principle for minimizing radiation exposure for each individual patient. In this context, the decision to perform MBI in the follow-up of patients with discordant pathologic findings or mistargeting during MBI-guided biopsy needs to outweigh the pros and cons based on patient characteristics, local options, and expertise. The introduction of modern MBI devices, working with lower administered radioactivity and reduced effective whole-body doses comparable to those delivered by digital mammography, may help to solve this limitation in the future.

In conclusion, [99mTc]-sestamibi–guided biopsy using a dedicated MBI device is technically feasible and seems to represent a reliable complementary biopsy tool. Further studies with larger series of patients are needed to establish the definitive clinical relevance of this device.

REFERENCES

1. Khalkhali I, Mena I, Jouanne E, Diggles L, Venegas R, Block J, *et al*. Prone scintimammography in patients with suspicion of carcinoma of the breast. J Am Coll Surg. 1994;178(5):491-7.

2. Kao CH, Wang SJ, Liu TJ. The use of technetium-99m methoxyisobutylisonitrile breast scintigraphy to evaluate palpable breast masses. Eur J Nucl Med. 1994;21(5):432-6.

3. Mankoff DA, Dunnwald LK, Gralow JR, Ellis GK, Schubert EK, Charlop AW, *et al*. [Tc-99m]-sestamibi uptake and washout in locally advanced breast cancer are correlated with tumor blood flow. Nucl Med Biol. 2002;29(7):719-27.

4. Scopinaro F, Schillaci O, Scarpini M, Mingazzini PL, Di Macio L, Banci M, *et al*. Technetium-99m sestamibi: an indicator of breast cancer invasiveness. Eur J Nucl Med. 1994;21(9):984-7.

5. Delmon-Moingeon LI, Piwnica-Worms D, Van den Abbeele AD, Holman BL, Davison A, Jones AG. Uptake of the cation hexakis(2-methoxyisobutylisonitrile)-technetium-99m by human carcinoma cell lines in vitro. Cancer Res. 1990;50(7):2198-202.

6. Brem RF, Schoonjans JM, Kieper DA, Majewski S, Goodman S, Civelek C. High-resolution scintimammography: a pilot study. J Nucl Med. 2002;43(7):909-15.

7. Rhodes DJ, O'Connor MK, Phillips SW, Smith RL, Collins DA. Molecular breast imaging: a new technique using technetium Tc 99m scintimammography to detect small tumors of the breast. Mayo Clin Proc. 2005;80(1):24-30.

8. Jones EA, Phan TD, Blanchard DA, Miley A. Breast-specific gamma-imaging: molecular imaging of the breast using 99mTc-sestamibi and a small-field-of-view gamma-camera. J Nucl Med Technol. 2009;37(4):201-5.

9. Weinmann AL, Hruska CB, O'Connor MK. Design of optimal collimation for dedicated molecular breast imaging systems. Med Phys. 2009;36(3):845-56.

10. Hruska CB, Weinmann AL, Tello Skjerseth CM, Wagenaar EM, Conners AL,Tortorelli CL, *et al*. Proof of concept for low-dose molecular breast imaging with a dual-head CZT gamma camera. Part II. Evaluation in patients. Med Phys. 2012;39(6):3476-83.

11. Berg WA, Blume JD, Adams AM, Jong RA, Barr RG, Lehrer DE, *et al*. Reasons women at elevated risk of breast cancer refuse breast MR imaging screening: ACRIN 6666. Radiology. 2010;254(1):79-87.

12. Johnson N, Sorenson L, Bennetts L, Winter K, Bryn S, Johnson W, *et al*. Breast-specific gamma imaging is a cost effective and efficacious imaging modality when compared with MRI. Am J Surg. 2014;207(5):698-701.

13. Sun Y, Wei W, Yang HW, Liu JL. Clinical usefulness of breast-specific gamma imaging as an adjunct modality to mammography for diagnosis of breast cancer: a systemic review and meta-analysis. Eur J Nucl Med Mol Imaging. 2013;40(3):450-63.

14. Goldsmith SJ, Parsons W, Guiberteau MJ, Stern LH, Lanzkowsky L, Weigert J, *et al*. SNM practice guideline for breast scintigraphy with breast-specific gamma-cameras 1.0. J Nucl Med Technol. 2010;38(4):219-24.

15. Conners AL, Hruska CB, Tortorelli CL, Maxwell RW, Rhodes DJ, Boughey JC, *et al*. Lexicon for standardized interpretation of gamma camera molecular breast imaging: observer agreement and diagnostic accuracy. Eur J Nucl Med Mol Imaging. 2012;39(6):971-82.

16. Moadel RM. Breast cancer imaging devices. Semin Nucl Med. 2011;41(3):229-41.

17. Weinmann AL, Hruska CB, Conners AL, O'Connor MK. Collimator design for a dedicated molecular breast imaging-guided biopsy system: proof-of-concept. Med Phys. 2013;40(1):012503.

18. Collarino A, Valdés Olmos RA, van der Hoeven AF, Pereira Arias-Bouda LM. Methodological aspects of (99m)Tc-sestamibi guided biopsy in breast cancer. Clin Transl Imaging. 2016;4(5):367-76.

19. Sewell CW. Pathology of high-risk breast lesions and ductal carcinoma in situ. Radiol Clin North Am. 2004;42(5):821-30.

20. Liberman L. Centennial dissertation. Percutaneous imaging-guided core breast biopsy: state of the art at the millennium. AJR Am J Roentgenol. 2000;174(5):1191-9.

21. Berg WA, Krebs TL, Campassi C, Magder LS, Sun CC. Evaluation of 14- and 11-gauge directional, vacuum-assisted biopsy probes and 14-gauge biopsy guns in a breast parenchymal model. Radiology. 1997;205(1):203-8.

22. Del Vecchio S, Salvatore M. 99mTc-MIBI in the evaluation of breast cancer biology. Eur J Nucl Med Mol Imaging. 2004;31(1):S88-96.

23. de Snoo F, Bender R, Glas A, Rutgers E. Gene expression profiling: decoding breast cancer. Surg Oncol. 2009;18(4):366-78.

24. Liberman L, Morris EA, Dershaw DD, Thornton CM, Van Zee KJ, Tan LK. Fast MRI-guided vacuum-assisted breast biopsy: initial experience. AJR Am J Roentgenol. 2003;181(5):1283-93.

25. Liberman L, Bracero N, Morris E, Thornton C, Dershaw DD. MRI-guided 9-gauge vacuum-assisted breast biopsy: initial clinical experience. AJR Am J Roentgenol. 2005;185(1):183-93.

26. Esserman LE, Cura MA, DaCosta D. Recognizing pitfalls in early and late migration of clip markers after imaging-guided directional vacuum-assisted biopsy. Radiographics. 2004;24(1):147-56.

27. Perlet C, Heinig A, Prat X, Casselman J, Baath L, Sittek H, *et al.* Multicenter study for the evaluation of a dedicated biopsy device for MR-guided vacuum biopsy of the breast. Eur Radiol. 2002;12(6):1463-70.

28. O'Connor MK. Molecular breast imaging: an emerging modality for breast cancer screening. Breast Cancer Manag. 2015;4(1):33-40.

29. Hendrick RE. Radiation doses and cancer risks from breast imaging studies. Radiology. 2010;257(1):246-53.

30. Hruska CB. Molecular Breast Imaging for Screening in Dense Breasts: State of the Art and Future Directions. AJR Am J Roentgenol. 2017;208(2):275-83.

RADIOGUIDED INTERVENTIONS IN OTHER FEMALE CANCERS

THE SENTINEL NODE APPROACH IN GYNAECOLOGICAL MALIGNANCIES

adapted from:

A Collarino
S Vidal-Sicart
G Perotti
RA Valdés Olmos

CHAPTER 7

ABSTRACT

This review discusses the state-of-the-art of sentinel lymph node mapping in gynaecological malignancies, including cervical cancer, endometrial cancer, and vulvar cancer, with an emphasis on new technological advances. For this objective, PubMed/MEDLINE was searched for relevant studies about the sentinel lymph node procedure in gynaecology. In particular, the use of preoperative lymphatic mapping with lymphoscintigraphy and single photon emission computed tomography/computed tomography (SPECT/CT) was identified in 18 studies. Other recent advances as hybrid tracers (e.g. ICG-^{99m}Tc-nanocolloid) and intraoperative tools (portable gamma-camera and 3D navigation devices) appear to also represent a useful guide for the surgeon during the operation. Concerning vulvar and cervical cancers, the sentinel lymph node procedure has been incorporated to the current guidelines in Europe and North America, whereas for endometrial cancer it is considered investigative.

GENERAL INTRODUCTION

In gynaecological tumours, the sentinel lymph node (SLN) procedure is principally performed in vulvar cancer (VC), cervical cancer (CC), and endometrial cancer (EC). Although both preoperative lymphatic mapping and intraoperative SLN detection are common parts of SLN procedure in gynaecological tumours, the type of injection and lymphatic drainage is different for each one of these malignancies (**Figure 1**). In vulvar tumour, the lymphatic drainage is predominantly superficial, and the first-draining lymph nodes are usually located in the groin. Instead, the lymphatic drainage of cervical and endometrial tumours is deep, and SLNs are located along the iliac vessels as well as in other areas with complex anatomy.

Therefore, the use of preoperative SPECT/CT appears to be mandatory in cervical and endometrial tumours; whereas in vulvar tumour, it is considered more optional. In addition, intraoperative imaging, such as portable gamma-camera and intraoperative 3D navigation SPECT/CT, represents complementary tools useful to guide the surgeon in patients with difficult SLN localisation, such as those close to the site of the injection or in complex anatomy areas. The new hybrid tracer using indocyanine green with ^{99m}Tc-nanocolloid (ICG-^{99m}Tc-nanocolloid) improves the intraoperative visualisation of SLN, resulting useful during the operation. All these particular aspects of SLN procedure in gynaecological malignancies will be discussed in this review. A research of the literature was performed on PubMed/MEDLINE using the following keywords (MeSH terms) to encounter the most relevant studies about the SLN procedure in gynaecology: "SLN biopsy", "lymphatic mapping", "lymphoscintigraphy", "SPECT/CT", "intraoperative SLN detection", "hybrid tracer", "vulvar cancer", "cervical cancer", and "endometrial cancer". The search has been restricted to the English language. The references of the retrieved articles were examined to identify additional articles. This review also includes meta-analyses published in the last five years.

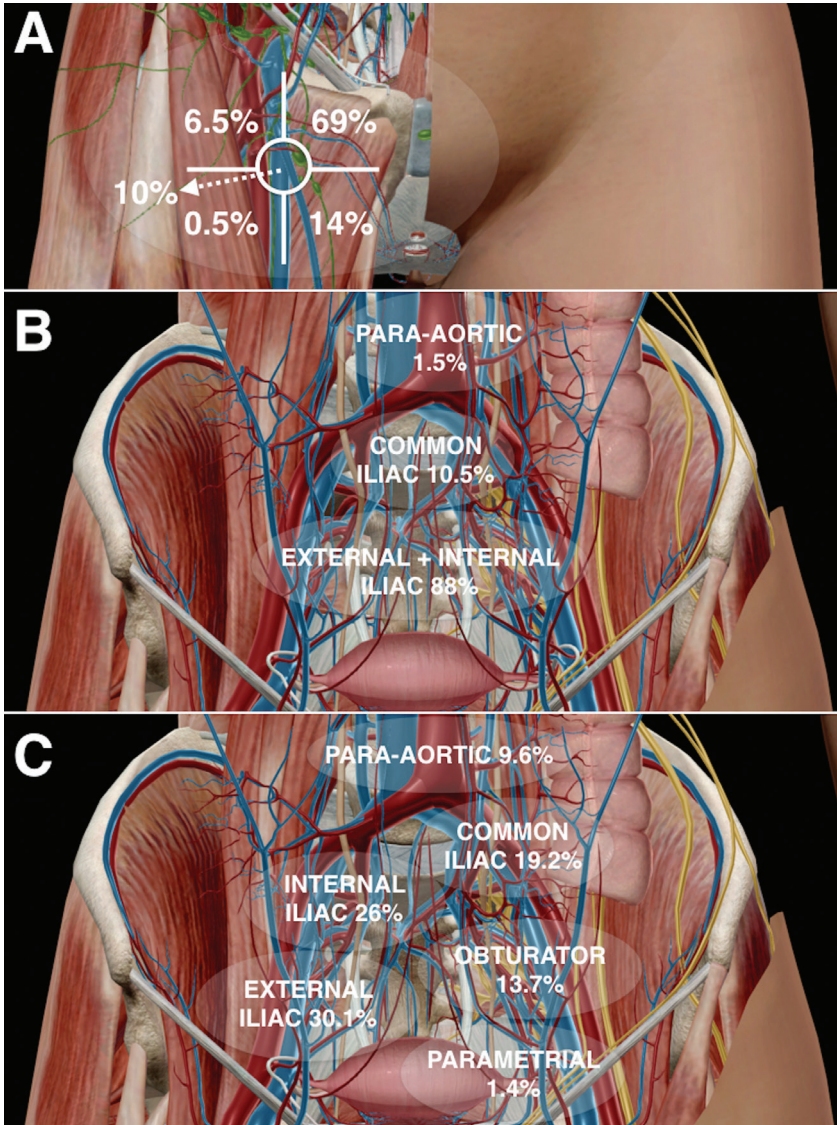**Figure 1.** Anatomical sentinel lymph node (SLN) distribution in gynaecological malignancies. In vulvar cancer, [48] SLNs are limited to the groin and are predominantly found in the superior, central, and medial inferior inguinal Daseler's zones (A); by contrast, in cervical cancer SLNs are mainly located along the iliac vessels (B), [15] whereas in endometrial cancer also para-aortic drainage is frequently observed (C).[17]

CERVICAL CANCER

INTRODUCTION

Cervical cancer is the third most common gynaecological cancer with an estimated of 12,990 new cases and 4,120 deaths in the United States, in 2016. [1] The pattern of dissemination of CC principally concerns the adjacent pelvic organs, but can also spread to locoregional lymph nodes (LN), while haematogenous spread to lung, liver, bone, and brain is rare. The most important prognostic factor is the presence of metastatic locoregional LN(s), including the pelvic and para-aortic lymph nodes. [2, 3] According to the current guidelines, the preferred treatment for early-stage disease (FIGO stages IA-2, IB-1, IIA-1) is radical hysterectomy and SLN mapping with or without bilateral pelvic lymphadenectomy. [4, 5] The SLN(s) are the lymph node(s) that receive direct drainage from the tumour; [6] thus, the tumour status of SLN(s) reflects the status of the entire lymph node field. The SLN status plays an important role, because when an SLN contains metastases at histopathology, the best treatment approach would be based on chemoradiotherapy. In addition, when SLNs are negative for metastases, the pelvic lymph node dissection can be safely avoided, [4] reducing concomitant surgical morbidity. The uterine cervix is a midline organ; thus, lymphatic drainage is almost always bilateral and principally to the pelvic region. The most frequent localisation of pelvic lymph node metastasis is the obturator followed by the external iliac basins. [7] In addition, the lymphatic drainage may spread to other areas, such as the common iliac and para-aortic basins.[8] Nevertheless, it is rare to find "skip metastasis" in the para-aortic basin without pelvic lymph node metastases. [9, 10] Therefore, the SLN mapping is useful for detection of lymphatic drainage patterns in particular to regions not routinely explored in conventional surgery, such as para-aortic chains.

The SLN mapping is performed by peritumoural/periorificial injection of radiocolloid (e.g. ^{99m}Tc-nanocolloid) in the four quadrants of the cervix using a 20 or 22-gauge spinal needle. In the case of previous conisation, the peri-cicatricial injection at the four quadrants is recommended. [5] The most frequently used tracer dose is approximately 110 MBq in a total volume of 2 mL. [11] The injection may be carried out the day before surgery or on the same day of surgery. The conventional planar images are acquired for 3–5 min in anterior and lateral views at 30 (early) and 60–120 (delayed) min after injection. [5] The early images are used to visualise lymphatic duct(s) and the first-draining lymph node(s). The delayed images are used to differentiate the SLN(s) from higher echelon nodes. [12] A higher echelon node is defined as an LN draining from the SLN(s). The preoperative planar lymphoscintigraphy does not give a precise anatomical localisation of

the SLN(s). [13] Therefore, SPECT in conjunction with low-dose CT (SPECT/CT) is recommended immediately after delayed imaging as a complementary modality, [5] providing not just better contrast and spatial resolution in comparison to planar imaging, but also accurate anatomical information (**Figure 2**).

ADVANTAGES OF PREOPERATIVE SPECT/CT IMAGING

SPECT/CT has higher SLN detection rate compared to the conventional planar images (98.6 vs. 85.3%), as reported in a recent meta-analysis, including eight studies. [14] In general, SPECT/CT provides an accurate anatomical SLN localisation. [15–18] In particular, SPECT/CT images are useful to detect SLN(s) close to injection sites, such as parametrial SLNs, as well as SLN(s) in uncommon locations, such as the para-aortic and presacral basins. [15, 17, 19] In addition, SPECT/CT leads to better detection of bilateral SLN(s) compared to planar imaging (**Table 1**). [20–22] Furthermore, Hoogendam *et al.* reported that SPECT/CT provides a valuable surgical roadmap, reducing the
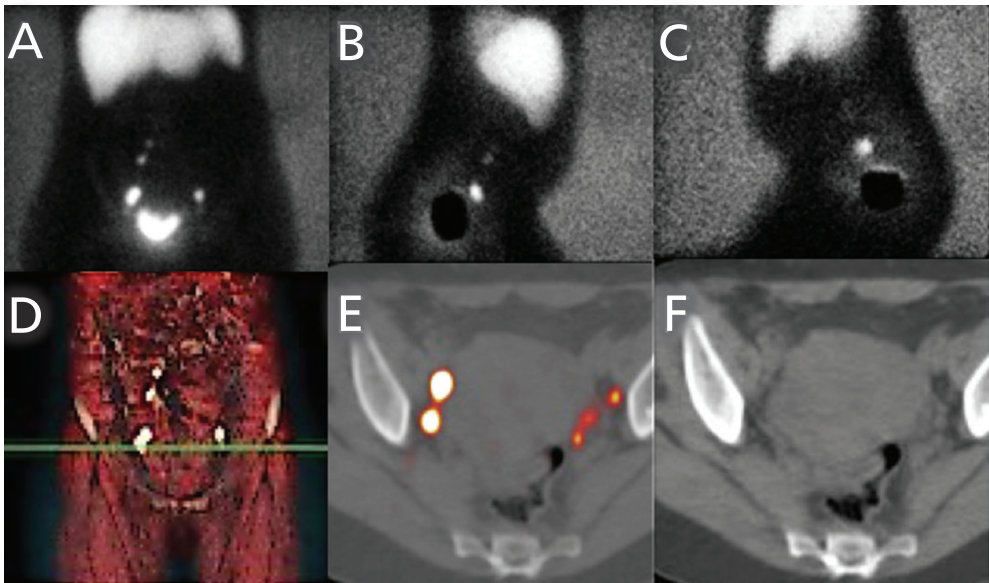
Figure 2. Cervical cancer. Planar images show a bilateral drainage in pelvic area (A-C). 3D volume-rendering image displays the level of sentinel nodes (D); SPECT/CT axial-fused images showing two separate nodes with high tracer uptake in right obturator fossa as well as three tiny nodes in left side (E); corresponding axial CT slice (F).

surgical time in cervical cancer in women undergoing robotic-assisted surgery. [22] Recently, ^{99m}Tc-SPECT/MRI-fused images have been used for SLN mapping in preoperative assessment of SLN metastases in the early-stage cervical cancer in women. The authors found a ^{99m}Tc-SPECT-MRI accuracy of 74.9% to non-invasively assess SLN metastases, including 136 SLNs of which 13 (9.6%) in 8/79 patients (10.7%) contained metastases. [23]

ENDOMETRIAL CANCER

INTRODUCTION

Endometrial cancer is the most common malignancy of gynaecological cancer with an estimated incidence of 60,050 new cases and 10,470 deaths in the United States, in 2016. [1] Lymph node status is a key prognostic factor in endometrial tumours. Indeed, the 5-y survival rate varies from 44% to 52% when pelvic or para-aortic node lymph nodes contained metastases. [24] Radical pelvic and para-aortic lymphadenectomies represent the standard treatment in high-risk group (grade 3, >50% myometrial invasion) or high-risk tumour histology (papillary serous, carcinosarcoma, and clear cell cancer). [25] The SLN technique may provide the surgical staging, avoiding the morbidity of complete lymphadenectomy in patients with negative SLN biopsy, but also ultra-staging assessment (micrometastases and isolated tumour cells) through extensive immunochemistry. Although there are several studies validating SLN mapping in EC, this technique is not yet the standard of care in the early-stage EC (Stage I-II high-risk). [5, 25] One of the most controversial aspects for SLN mapping is the modality of injection. Indeed, three different modalities of injection have been described in the currently literature: **i)** cervical injection; **ii)** endometrial peritumoural injection assisted by hysteroscopy; and **iii)** myometrial/subserosal intraoperative injection. The radiotracer can be injected on the day prior to surgery, providing lymphatic mapping with planar and SPECT/CT images. The most common and easiest approach is the cervical injection, which is performed peri-orificially into the four quadrants as well as for CC. The detection rate related to cervical injection is the highest of the three injection modalities used in endometrial cancer, ranging from 62% to 100%. [26] Endometrial radiotracer administration assisted by hysteroscopy allows direct injection around the tumour. This procedure is usually performed at the beginning of the surgery, without the possibility to obtain preoperative SLN mapping. The detection rate of this injection modality varies from 40% to 95% . [27–31] Finally, myometrial/subserosal injection is performed during the surgery and has been predominantly

Table 1. Detection of sentinel nodes in cervical cancer using planar lymphoscintigraphy and SPECT/CT

Authors	Year	Study type	Patients	Radiotracer (dosing)	Detection rate by LSG (%)	Detection rate by SPECT/CT (%)	SLNs detected by LSG	SLNs detected by SPECT/CT	Bilateral SLN detected by LSG (%)	Bilateral SLN detected by SPECT/CT (%)	False negative rate (%)
Martinez [15]	2010	Retrospective	41	99mTc-sulfur rhenium colloid (80 MBq)	-	95	-	86	-	49	0
Pandit [17]	2010	Prospective	10	99mTc-sulfur colloid (37-148 MBq)	70	100	26	51	-	-	0
Diaz [18]	2011	Prospective	22	99mTc-albumin nanocolloid (144 MBq)	100	100	35	40	-	-	0
Kraft [16]	2012	Retrospective	36	99mTc-nanocolloid (40 MBq)	89	97	-	-	-	-	-
Buda [39]	2012	Retrospective	10	99mTc-albumin nanocolloid (30-40 MBq)	80	100	-	-	-	-	0
Belhoncine [19]	2013	Prospective	7	99mTc-cysteine rhenium colloid (37 MBq)	86	100	15	23	-	-	0
Bournaud [21]	2013	Retrospective	42[a]	99mTc-sulfur rhenium colloid (60-120 MBq)	95	95	152	173	70	73	0
Hoogendam [22]	2013	Retrospective	62[b]	99mTc-nanocolloid (220-290 MBq)	85	93	71	58	76	79	5
Klapdor [20]	2014	Prospective	51	99mTc-nanocolloid (10 MBq)	84	92	-	-	57	64	0

LSG lymphoscintigraphy, SLNs sentinel lymph nodes, [a] no lymphoscintigraphy was performed in 3 of 42 patients, [b] 33patients underwent LSG and 29 patients SPECT/CT.

limited to the use of blue dye administered at a minimum of three locations. [32] This injection route is associated with a detection rate varying from 45% to 91%. [32–35] Robova *et al.* compared subserosal injection (using blue dye and radiotracer) with hysteroscopic injection (radiotracer only) in 67 and 24 patients, respectively; although the detection rate was 73% with subserosal injection and 50% with hysteroscopic injection; [36] the authors concluded that both injection routes provide insufficient SLN identification. An alternative modality for radiotracer administration has been recently introduced using myometrial/subserosal injection guided by transvaginal ultrasonography; with this technique, a high detection rate (88%) can be reached when a high-injected volume (8 mL) is achieved. [37]

ADDITIONAL VALUE OF PREOPERATIVE SPECT/CT IMAGING

The deep lymphatic drainage of the corpus uteri is a probable reason for the low correlation found between planar lymphoscintigraphy and surgical mapping. [38] This limiting factor may be solved when SPECT/CT is performed in addition to planar images (**Figure 3**).

This fused SPECT/CT is useful in areas of deep lymphatic drainage, such as the pelvis, providing correction for tissue attenuation with detection of additional SLN(s) in other basins accompanied by accurate anatomical localisation. Therefore, preoperative SPECT/CT plays an important role in the planning of surgery and may lead to a decrease of surgical time. Until now, there are few articles reporting the use of SPECT/CT in endometrial cancer. [16, 17, 39] Pandit-Taskar *et al.* have reported a series, including 40 patients, with endometrial tumour; the authors showed a higher detection rate using SPECT/CT (100%) compared to a planar lymphoscintigraphy (75%), a hand-held probe (93%), and blue dye alone (83%), and highlighted the ability of SPECT/CT to detect additional SLN(s) in the para-aortic basin. [17] More recently, Naaman *et al.* reported in 53 endometrial cancer patients that SPECT/CT contributed to increase SLN visualisation from 67%, when only planar lymphoscintigraphy was used, to 84% when SPECT/CT was included; in this series, anatomical accuracy of SPECT/CT was 91% (**Table 2**). [40]
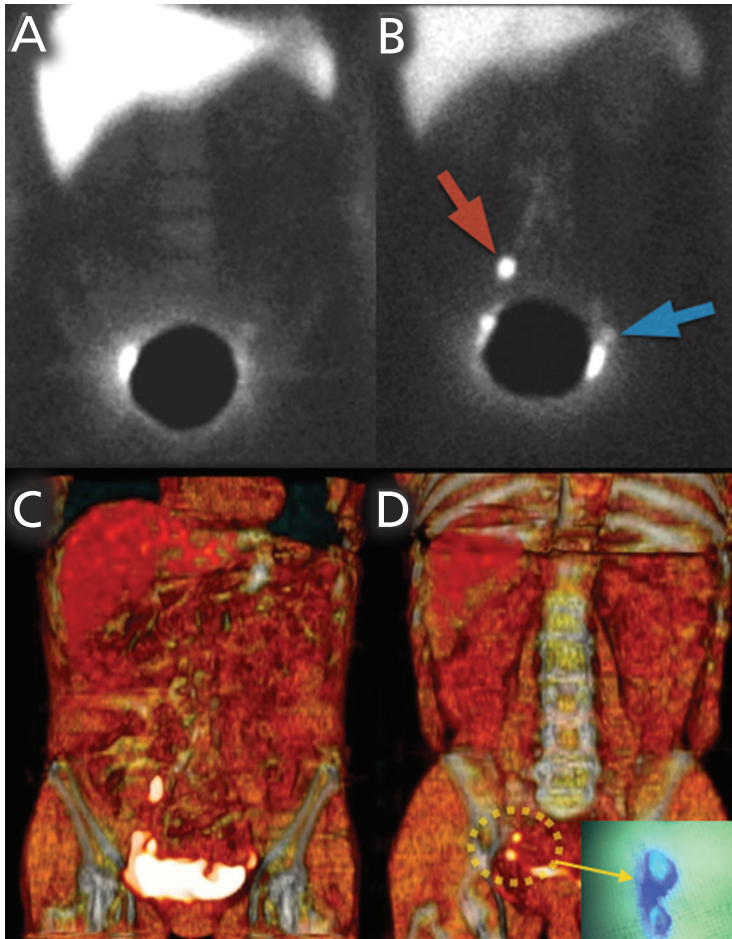
Figure 3. Endometrial cancer. Early planar image showed a very faint left node. A lead shield covered the injection area and high activity on the right side was supposed to be a partial zone of the injection area (A); delayed planar image displays a right sentinel node (red arrow) and the previously observed left sentinel node (blue arrow). 3D volume-rendering image shows the same node distribution like B (C); a more detailed analysis of SPECT/CT data and 3D reconstructed images showed two posterior and caudal nodes (dotted circle) previous to the marked as sentinel node in D corresponding to external iliac nodes during surgery (arrow).

Table 2. Detection of sentinel nodes in endometrial cancer using planar lymphoscintigraphy and SPECT/CT

Authors	Year	Study type	Patients	Injection site	Radiotracer (dosing)	Detection rate by LSG (%)	Detection rate by SPECT/CT (%)	SLNs detected by LSG	SLNs detected by SPECT/CT	Bilateral SLN detection by LSG (%)	Bilateral SLN detection by SPECT/CT (%)	False negative rate (%)
Pandit [17]	2010	Prospective	40	C	^{99m}Tc-sulfur colloid (37-148 MBq)	75	100	67	207	-	-	0
Kraft [16]	2012	Retrospective	21	C	^{99m}Tc-nanocolloid (40 MBq)	86	86	-	-	-	-	-
Buda [39]	2012	Prospective	25	C	^{99m}Tc-albumin nanocolloid (30-40 MBq)	40	88	-	-	-	-	0
Naaman [40]	2016	Retrospective	45[a]	C	^{99m}Tc-albumin nanocolloid (7.4-11.1 MBq)	67	84	-	-	29	49	0

C cervix, **LSG** lymphoscintigraphy, **SLNs** sentinel lymph nodes; [a] 37 of 45 patients underwent SPECT/CT.

VULVAR CANCER

INTRODUCTION

Vulvar cancer is a rare gynaecological malignancy with an estimated number of 5,950 new cases and 1,110 deaths in the United States, in 2016. [1] The pattern of dissemination is principally lymphogenic, with drainage first to the superficial inguinal nodes, then to the deep inguinal nodes and, finally, to the pelvic lymph nodes. Therefore, the presence of metastatic lymph node represents the most important prognostic factor. Indeed, the 5-y survival rate decreases from 94.7%, when the LNs are negative, to 62% when containing metastases. [41] The current standard treatment includes radical vulvectomy with SLN procedure and/or inguinofemoral lymphadenectomy.

In particular, the sentinel lymph node biopsy is recommended in the early squamous cell vulvar carcinoma (Stage FIGO 2009: Ib/II) with unifocal tumours less than 4 cm in size and clinically negative (cN0) lymph nodes in the groins. [5, 42, 43] The SLN mapping is performed through injection of radiocolloid (e.g. ^{99m}Tc-nanocolloid) in three or four intradermal/intramucosal around the primary lesion or excision scar a few minutes after the application of an anaesthetic lidocaine spray or crème. Simultaneous anterior and lateral dynamic lymphoscintigraphy is performed immediately after injection followed by early (15 min) and delayed (2 h) static planar imaging. Subsequently, SPECT/CT is recommended as complementary modality, providing anatomical and functional information facilitating more accurate virtual surgical planning. [5] The SLN detection rate using radiotracer injection has been found to be higher than 95%. [44, 45] In a recent meta-analysis, the SLN detection rate per groin using radiocolloid and blue dye was 87% (range, 82%–92%), the false-negative rate 6.4% (range, 4.4%–8.8%), and the recurrence rate 2.8% (range, 1.5%–4.4%). [42]

ADDITIONAL VALUE OF PREOPERATIVE SPECT/CT IMAGING

As reported in the current literature, SPECT/CT plays an important role to provide a better anatomical localisation of SLN(s) and to detect additional lymph nodes in the same region or in other regions with poor or even without visualisation at planar lymphoscintigraphy (**Figure 4**), as well as to reduce the false-positive rate possibly due to external contamination or presence of radioactivity in enlarged lymphatic vessels. [16, 19, 46, 47] Recently, Collarino *et al.* reported the use of SPECT/CT for anatomical mapping of lymphatic drainage in vulvar cancer. According to the five Daseler zones using the inguinal saphenofemoral junction as anatomical reference, the authors found that the

lymphatic drainage was principally to the medial inguinal region (83%), and the drainage to the lateral inferior groin was only incidental (0.5%) in 83 patients with cN0 vulvar cancer (**Figure 1**). Further drainage to higher echelon nodes was visualised in the groin (15%) and in the pelvis (85%). Therefore, SPECT/CT is able to personalise the lymphatic mapping, and has a potential role in limiting the extent of lymph node dissection to the lateral inferior zone in patients with positive SLN(s) (**Table 3**).[48]

ADVANCEMENTS IN INTRAOPERATIVE IMAGING AND INSTRUMENTATION

The indocyanine green (ICG) added to ^{99m}Tc-nanocolloid in one signature represents a new hybrid tracer for the detection of SLN. Recently, Mathéron *et al.* reported the use of a new hybrid tracer, in the SLN identification procedure in vulvar cancer. They showed that 98% of the SNs were radioactive at the time of excision, 96% were fluorescent, and only 65% were blue in 15 patients. The additional value of ICG is related to better intraoperative visualisation of SN to optimize the
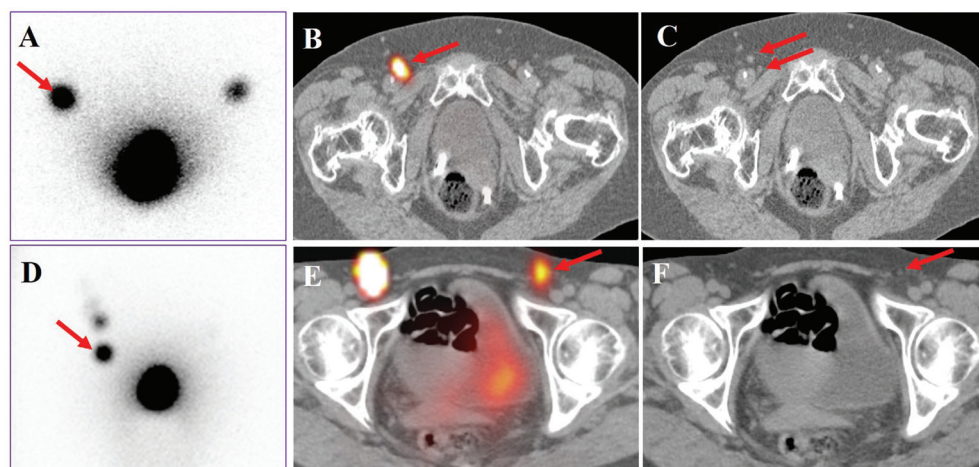
Figure 4. In a patient with vulvar cancer, delayed planar imaging (A) shows one SLN in the right groin (red arrow) corresponding with one allocated SLN uptake (red arrow) on transversal-fused SPECT/CT (B) and two not enlarged lymph nodes on transversal CT (C) (double arrows). In another patient, delayed planar image (D) shows unilateral lymphatic drainage with a single SLN in the right groin (red arrow), while transversal-fused SPECT/CT (E) shows bilateral drainage with also a contralateral SLN (red arrow) corresponding with a not enlarged lymph node in the left groin on CT (F).

Table 3. Detection of sentinel nodes in vulvar cancer using planar lymphoscintigraphy and SPECT/CT

Authors	Year	Study type	Patients	Radiotracer (dosing)	Detection rate by LSG (%)	Detection rate by SPECT/CT (%)	SLNs detected by LSG	SLNs detected by SPECT/CT	False negative rate (%)
Beneder [46]	2008	Prospective	10	99mTc-nanocolloid (60 MBq)	-	-	26	38	0
Kraft [16]	2012	Retrospective	7	99mTc-nanocolloid (40 MBq)	100	100	-	-	-
Belhoncine [19]	2013	Prospective	7	99mTc-cysteine rhenium colloid (37 MBq)	86	100	-	-	0
Mathéron [49]	2013	Prospective	14	ICG-99mTc-nanocolloid (87 MBq)	-	-	39	39	0
Collarino [48]	2015	Retrospective	83	99mTc-nanocolloid (81 MBq)	-	-	192	217	0

ICG indocyanine green, **LSG** lymphoscintigraphy, **SLNs** sentinel lymph nodes.

intraoperative SLN visualisation using the fluorescence component.[49] Nevertheless, there are no studies available on application of this hybrid tracer in cervical cancer and endometrial cancer. Indeed, a recently meta-analysis, including 67 studies in cervical cancer reported only the SLN detection rate using the combination of radiotracer with blue dye compared to the single use of radiotracer, blue dye, and florescence imaging (92.3% vs. 90.9% vs. 80.9% vs 76.5%). [50] In the future, the ICG-^{99m}Tc-nanocolloid may be used in the SLN(s) identification procedure during the robot-assisted laparoscopy. [51, 52] In addition, a portable gamma-camera might be a complementary tool during surgery in gynaecological cancer. With a portable gamma-camera an intraoperative real-time imaging is acquired before SLN resection. Subsequently, an additional image of the surgical field is performed to confirm the absence of any residual activity after excision. This device may improve the intraoperative detection rate in patients with difficult SLN localisation in parametrial and precaval lymph-node basins. Indeed, the hand-held gamma-probe has limitations to detect parametrial SLN(s) due to their location in the vicinity of the injection site, and in precaval SLN(s) because of the liver activity. Vidal-Sicart *et al.* reported the use of portable gamma-camera in gynaecological cancer, showing a higher detection (92%) when compared to just hand-held gamma-probe (77%) in the two cases of high-risk endometrial cancer, three cases of cervical cancer and one patients with vulvar cancer. [53] Furthermore, the incorporation of co-registered SPECT/CT to 3D navigation probe may be used during the operation offering a 3D roadmap to the surgeon and facilitating the anatomical localisation of SLN(s). In the current literature on radioguided surgery, this approach has been reported in penile cancer by Brower *et al.* [54]

CONCLUSION

In conclusion, the SLN procedure has widely been validated in vulvar cancer and cervical cancer. Its application in these malignancies is well standardised and has been incorporated to the current guidelines in Europe and North America. By contrast, in endometrial cancer, there are various controversial aspects (e.g. injection route) to be clarified and the use of the SLN procedure needs to be validated in larger clinical series. Beside these aspects, the present review showed that recent technological advances, such as preoperative and intraoperative use of SPECT/CT, the contribution of the hybrid tracer ICG-^{99m}Tc-nanocolloid, and technological advances like SLN robotic-guided procedure might play an increasing role to guide gynaecological cancer surgery in the future.

REFERENCES

1. Siegel RL, Miller KD, Jemal A. Cancer statistics, 2016. CA Cancer J Clin. 2016;66(1):7-30.

2. Stehman FB, Bundy BN, DiSaia PJ, Keys HM, Larson JE, Fowler WC. Carcinoma of the cervix treated with radiation therapy. I. A multi-variate analysis of prognostic variables in the Gynecologic Oncology Group. Cancer. 1991;67(11):2776-85.

3. Macdonald OK, Chen J, Dodson M, Lee CM, Gaffney DK. Prognostic significance of histology and positive lymph node involvement following radical hysterectomy in carcinoma of the cervix. Am J Clin Oncol. 2009;32(4):411-6.

4. Koh WJ, Greer BE, Abu-Rustum NR, Apte SM, Campos SM, Cho KR, *et al*. Cervical Cancer, Version 2.2015. J Natl Compr Canc Netw. 2015;13(4):395-404.

5. Giammarile F, Bozkurt MF, Cibula D, Pahisa J, Oyen WJ, Paredes P, *et al*. The EANM clinical and technical guidelines for lymphoscintigraphy and sentinel node localization in gynaecological cancers. Eur J Nucl Med Mol Imaging. 2014;41(7):1463-77.

6. Nieweg OE. The sentinel lymph node concept in oncology surgery. In: Mariani G, Manca G, Orsini P, Vidal-Sicar t S, Valdés Olmos R (eds) Atlas of lymphoscintigraphy and sentinel node mapping. Milan: Springer, 2012. p. 87–93.

7. Benedetti-Panici P, Maneschi F, Scambia G, Greggi S, Cutillo G, D'Andrea G, *et al*. Lymphatic spread of cervical cancer: an anatomical and pathological study based on 225 radical hysterectomies with systematic pelvic and aortic lymphadenectomy. Gynecol Oncol. 1996;62(1):19-24.

8. Sakuragi N, Satoh C, Takeda N, Hareyama H, Takeda M, Yamamoto R, *et al*. Incidence and distribution pattern of pelvic and paraaortic lymph node metastasis in patients with Stages IB, IIA, and IIB cervical carcinoma treated with radical hysterectomy. Cancer. 1999;85(7):1547-54.

9. Lea JS, Sheets EE, Duska LR, Miller DS, Schorge JO. Early-stage cervical adenocarcinoma treated by surgical intent: the role of para-aortic lymph node dissection. Gynecol Oncol. 2002;84(2):285-8.

10. Bader AA, Winter R, Haas J, Tamussino KF. Where to look for the sentinel lymph node in cervical cancer. Am J Obstet Gynecol. 2007;197(6):678. e1-7.

11. El-Ghobashy AE, Saidi SA. Sentinel lymph node sampling in gynaecological cancers: techniques and clinical applications. Eur J Surg Oncol. 2009;35(7):675-85.

12. Paredes P, Vidal-Sicart S. Preoperative and intraoperative lymphatic mapping for radioguided sentinel node biopsy in cancers of the female reproductive system. In: Mariani G, Manca G, Orsini P, Vidal-Sicart S, Valdés Olmos R, editors. Atlas of lymphoscintigraphy and sentinel node mapping. Milan: Springer; 2012. p. 249–68.

13. Vermeeren L, van der Ploeg IM, Olmos RA, Meinhardt W, Klop WM, Kroon BB, *et al*. SPECT/CT for preoperative sentinel node localization. J Surg Oncol. 2010;101(2):184-90.

14. Hoogendam JP, Veldhuis WB, Hobbelink MG, Verheijen RH, van den Bosch MA, Zweemer RP. 99mTc SPECT/CT versus planar lymphoscintigraphy for preoperative sentinel lymph node detection in cervical cancer: a systematic review and metaanalysis. J Nucl Med. 2015;56(5):675-80.

15. Martínez A, Zerdoud S, Mery E, Bouissou E, Ferron G, Querleu D. Hybrid imaging by SPECT/CT for sentinel lymph node detection in patients with cancer of the uterine cervix. Gynecol Oncol. 2010;119(3):431-5.

16. Kraft O, Havel M. Detection of Sentinel Lymph Nodes in Gynecologic Tumours by Planar Scintigraphy and SPECT/CT. Mol Imaging Radionucl Ther. 2012;21(2):47-55.

17. Pandit-Taskar N, Gemignani ML, Lyall A, Larson SM, Barakat RR, Abu Rustum NR. Single photon emission computed tomography SPECT-CT improves sentinel node detection and localization in cervical and uterine malignancy. Gynecol Oncol. 2010;117(1):59-64.

18. Díaz-Feijoo B, Pérez-Benavente MA, Cabrera-Diaz S, Gil-Moreno A, Roca I, Franco-Camps S, *et al*. Change in clinical management of sentinel lymph node location in early stage cervical cancer: the role of SPECT/CT. Gynecol Oncol. 2011;120(3):353-7.

19. Belhocine TZ, Prefontaine M, Lanvin D, Bertrand M, Rachinsky I, Ettler H, *et al*. Added-value of SPECT/CT to lymphatic mapping and sentinel lymphadenectomy in gynaecological cancers. Am J Nucl Med Mol Imaging. 2013;3(2):182-93.

20. Klapdor R, Mücke J, Schneider M, Länger F, Gratz KF, Hillemanns P, *et al*. Value and advantages of preoperative sentinel lymph node imaging with SPECT/CT in cervical cancer. Int J Gynecol Cancer. 2014;24(2):295-302.

21. Bournaud C, Le Bail-Carval K, Scheiber C, de Charry C, Mathevet P, Moreau-Triby C. Value of SPECT/CT in lymphatic mapping in cervix and endometrial cancer. Médecine Nucléaire 2013;37:387–96.

22. Hoogendam JP, Hobbelink MG, Veldhuis WB, Verheijen RH, van Diest PJ, Zweemer RP. Preoperative sentinel node mapping with (99m)Tc-nanocolloid SPECT-CT significantly reduces the intraoperative sentinel node retrieval time in robot assisted laparoscopic cervical cancer surgery. Gynecol Oncol. 2013;129(2):389-94.

23. Hoogendam JP, Zweemer RP, Hobbelink MG, van den Bosch MA, Verheijen RH, Veldhuis WB. 99mTc-nanocolloid SPECT/MRI fusion for the selective assessment of nonenlarged sentinel lymph nodes in patients with early-stage cervical cancer. J Nucl Med. 2016;57(4):551-6.

24. Partridge EE, Shingleton HM, Menck HR. The National Cancer Data Base report on endometrial cancer. J Surg Oncol. 1996;61(2):111-23.

25. National Comprehensive Cancer Network. Uterine Neoplasm, Version 2.2016. http://www.nccn.org/professionals/physician_gls/pdf/uterine.pdf

26. Cormier B, Rozenholc AT, Gotlieb W, Plante M, Giede C; Communities of Practice(CoP) Group of Society of Gynecologic Oncology of Canada (GOC). Sentinel lymph node procedure in endometrial cancer: A systematic review and proposal for standardization of future research. Gynecol Oncol. 2015;138(2):478-85.

27. Gien LT, Kwon JS, Carey MS. Sentinel node mapping with isosulfan blue dye in endometrial cancer. J Obstet Gynaecol Can. 2005;27(12):1107-12.

28. Maccauro M, Lucignani G, Aliberti G, Villano C, Castellani MR, Solima E, et al. Sentinel lymph node detection following the hysteroscopic peritumoural injection of 99mTc-labelled albumin nanocolloid in endometrial cancer. Eur J Nucl Med Mol Imaging. 2005;32(5):569-74.

29. Delaloye JF, Pampallona S, Chardonnens E, Fiche M, Lehr HA, De Grandi P, et al. Intraoperative lymphatic mapping and sentinel node biopsy using hysteroscopy in patients with endometrial cancer. Gynecol Oncol. 2007;106(1):89-93.

30. Clement D, Bats AS, Ghazzar-Pierquet N, Le Frere Belda MA, Larousserie F, Nos C, et al. Sentinel lymph nodes in endometrial cancer: is hysteroscopic injection valid? Eur J Gynaecol Oncol. 2008;29(3):239-41.

31. Solima E, Martinelli F, Ditto A, Maccauro M, Carcangiu M, Mariani L, et al. Diagnostic accuracy of sentinel node in endometrial cancer by using hysteroscopic injection of radiolabeled tracer. Gynecol Oncol. 2012;126(3):419-23.

32. Frumovitz M, Bodurka DC, Broaddus RR, Coleman RL, Sood AK, Gershenson DM, et al. Lymphatic mapping and sentinel node biopsy in women with high-risk endometrial cancer. Gynecol Oncol. 2007;104(1):100-3.

33. Altgassen C, Pagenstecher J, Hornung D, Diedrich K, Hornemann A. A new approach to label sentinel nodes in endometrial cancer. Gynecol Oncol. 2007;105(2):457-61.

34. Li B, Li XG, Wu LY, Zhang WH, Li SM, Min C, et al. A pilot study of sentinel lymph nodes identification in patients with endometrial cancer. Bull Cancer. 2007;94(1):E1-4.

35. Lopes LA, Nicolau SM, Baracat FF, Baracat EC, Gonçalves WJ, Santos HV, et al. Sentinel lymph node in endometrial cancer. Int J Gynecol Cancer. 2007;17(5):1113-7.

36. Robova H, Charvat M, Strnad P, Hrehorcak M, Taborska K, Skapa P, et al. Lymphatic mapping in endometrial cancer: comparison of hysteroscopic and subserosal injection and the distribution of sentinel lymph nodes. Int J Gynecol Cancer. 2009;19(3):391-4.

37. Torné A, Pahisa J, Vidal-Sicart S, Martínez-Roman S, Paredes P, Puerto B, et al. Transvaginal ultrasound-guided myometrial injection of radiotracer (TUMIR): a new method for sentinel lymph node detection in endometrial cancer. Gynecol Oncol. 2013;128(1):88-94.

38. Ballester M, Rouzier R, Coutant C, Kerrou K, Daraï E. Limits of lymphoscintigraphy for sentinel node biopsy in women with endometrial cancer. Gynecol Oncol. 2009;112(2):348-52.

39. Buda A, Elisei F, Arosio M, Dolci C, Signorelli M, Perego P, et al. Integration of hybrid single-photon emission computed tomography/computed tomography in the preoperative assessment of sentinel node in patients with cervical and endometrial cancer: our experience and literature review. Int J Gynecol Cancer. 2012;22(5):830-5.

40. Naaman Y, Pinkas L, Roitman S, Ikher S, Oustinov N, Vaisbuch E, et al. The added value of SPECT/CT in sentinel lymph nodes mapping for endometrial carcinoma. Ann Surg Oncol. 2016;23(2):450-5.

41. Burger MP, Hollema H, Emanuels AG, Krans M, Pras E, Bouma J. The importance of the groin node status for the survival of T1 and T2 vulval carcinoma patients. Gynecol Oncol. 1995;57(3):327-34.

42. Covens A, Vella ET, Kennedy EB, Reade CJ, Jimenez W, Le T. Sentinel lymph node biopsy in vulvar cancer: systematic review, meta-analysis and guideline recommendations. Gynecol Oncol. 2015;137(2):351-61.

43. National Comprehensive Cancer Network. Vulvar Cancer (Squamous Cell Carcinoma), Version 1.2016. http://www.nccn.org/professionals/physician_gls/pdf/vulvar.pdf

44. Hampl M, Hantschmann P, Michels W, Hillemanns P; German Multicenter Study Group. Validation of the accuracy of the sentinel lymph node procedure in patients with vulvar cancer: results of a multicenter study in Germany. Gynecol Oncol. 2008;111(2):282-8.

45. Vidal-Sicart S, Puig-Tintoré LM, Lejárcegui JA, Paredes P, Ortega ML, Muñoz A, *et al*. Validation and application of the sentinel lymph node concept in malignant vulvar tumours. Eur J Nucl Med Mol Imaging. 2007;34(3):384-91.

46. Beneder C, Fuechsel FG, Krause T, Kuhn A, Mueller MD. The role of 3D fusion imaging in sentinel lymphadenectomy for vulvar cancer. Gynecol Oncol. 2008;109(1):76-80.

47. Valdés Olmos RA, Rietbergen DD, Vidal-Sicart S, Manca G, Giammarile F, Mariani G. Contribution of SPECT/CT imaging to radioguided sentinel lymph node biopsy in breast cancer, melanoma, and other solid cancers: from "open and see" to "see and open". Q J Nucl Med Mol Imaging. 2014;58(2):127-39.

48. Collarino A, Donswijk ML, van Driel WJ, Stokkel MP, Valdés Olmos RA. The use of SPECT/CT for anatomical mapping of lymphatic drainage in vulvar cancer: possible implications for the extent of inguinal lymph node dissection. Eur J Nucl Med Mol Imaging. 2015;42(13):2064-71.

49. Mathéron HM, van den Berg NS, Brouwer OR, Kleinjan GH, van Driel WJ, Trum JW, *et al*. Multimodal surgical guidance towards the sentinel node in vulvar cancer. Gynecol Oncol. 2013;131(3):720-5.

50. Kadkhodayan S, Hasanzadeh M, Treglia G, Azad A, Yousefi Z, Zarifmahmoudi L, *et al*. Sentinel node biopsy for lymph nodal staging of uterine cervix cancer: a systematic review and meta-analysis of the pertinent literature. Eur J Surg Oncol. 2015;41(1):1-20.

51. KleinJan GH, van den Berg NS, Brouwer OR, de Jong J, Acar C, Wit EM, *et al*. Optimisation of fluorescence guidance during robot-assisted laparoscopic sentinel node biopsy for prostate cancer. Eur Urol. 2014;66(6):991-8.

52. KleinJan GH, van den Berg NS, de Jong J, Wit EM, Thygessen H, Vegt E, *et al*. Multimodal hybrid imaging agents for sentinel node mapping as a means to (re)connect nuclear medicine to advances made in robot-assisted surgery. Eur J Nucl Med Mol Imaging. 2016;43(7):1278-87.

53. Vidal-Sicart S, Paredes P, Zanón G, Pahisa J, Martinez-Román S, Caparrós X, *et al*. Added value of intraoperative real-time imaging in searches for difficult-to-locate sentinel nodes. J Nucl Med. 2010;51(8):1219-25.

54. Brouwer OR, van den Berg NS, Mathéron HM, Wendler T, van der Poel HG, Horenblas S, *et al*. Feasibility of intraoperative navigation to the sentinel node in the groin using preoperatively acquired single photon emission computerized tomography data: transferring functional imaging to the operating room. J Urol. 2014;192(6):1810-6.

THE USE OF SPECT/CT FOR ANATOMIC MAPPING OF LYMPHATIC DRAINAGE IN VULVAR CANCER: POSSIBLE IMPLICATIONS FOR THE EXTENT OF INGUINAL LYMPH NODE DISSECTION

adapted from:

A Collarino
ML Donswijk
WJ van Driel
MP Stokkel
RA Valdés Olmos

CHAPTER 8

ABSTRACT

PURPOSE To determine the lymphatic drainage pattern using SPECT/CT in clinically node-negative (cN0) patients with vulvar cancer, and to evaluate the possible implications for the extent of inguinal lymph node dissection.

METHODS A total of 83 patients with vulvar cancer scheduled for sentinel node (SN) biopsy were injected peritumorally with radioactive nanocolloid particles followed by lymphoscintigraphy and SPECT/CT for anatomical localisation. The SN and higher-echelon nodes on SPECT/CT were located in different zones in the groin and pelvic region. The groin was divided into five zones according to Daseler *et al.*: four zones obtained by drawing two perpendicular lines over the saphenofemoral junction and one zone directly overlying this junction. The lymph nodes in the pelvic region were classified into three zones: external iliac/obturator, the common iliac and the para-aortic zones.

RESULTS A total of 217 SNs and 202 higher-echelon nodes were localised on SPECT/CT. All SNs were located in the five zones according to Daseler *et al.*: 149 (69%) in the medial superior region, 31 (14%) in the medial inferior region, 22 (10%) in the central region, 14 (6.5%) in the lateral superior region and only 1 (0.5%) in the lateral inferior region. The higher-echelon nodes were located both in the groin (15%) and in the pelvic region (85%).

CONCLUSION In patients with cN0 vulvar cancer, lymphatic drainage occurs predominantly to the medial regions of the groin. Drainage to the lateral inferior region of the groin is only incidental and in SN-positive patients this zone might be spared in subsequent extended lymph node dissection. This may lead to a decrease in the morbidity associated with this procedure. SPECT/CT is able to personalise lymphatic mapping, providing detailed information about the number and anatomical location of SNs for adequate surgical planning in the groin.

INTRODUCTION

Vulvar cancer is a rare neoplasm, accounting for approximately 6–8% of gynaecological diseases with an incidence of 360 cases per year in The Netherlands.[1, 2] Squamous cell carcinoma (SCC) represents 80% of vulvar cancers, of which 60% is not associated with the human papilloma virus and occurs in elderly women. [1–3] In vulvar cancer, lymph node status is a key prognostic factor. Indeed, the 5-y survival rate decreases from 94.7% when the lymph nodes are negative to 62% when they contain metastases. [4] The standard treatment for vulvar cancer includes radical vulvectomy and unilateral or bilateral inguinal lymphadenectomy, depending on tumour location. [5] However, inguinofemoral lymphadenectomy is associated with short-term morbidity (wound breakdown, cellulitis) and long-term morbidity (lymphedema), resulting in a worse quality of life for these patients. [6] Regarding this, it is important either to obtain a map of lymphatic drainage from the tumour or to know whether lymphatic drainage is unilateral or bilateral. [7] In 1994 Levenback *et al.* reported the first study of the sentinel node (SN) biopsy procedure in patients with vulvar cancer. [8] Since then SN mapping in vulvar cancer has been validated in several studies. [9] Conventional lymph node mapping is performed by injection of a radiocolloid (e.g. ^{99m}Tc-nanocolloid) around the primary tumour followed by sequential lymphoscintigraphy to determine the number and location of lymph node(s) directly draining from the injection site, the SNs. [10] SPECT in conjunction with low-dose CT, e.g. SPECT/CT, imaging is used to accurately localise the anatomical region of the identified SN(s) and higher echelon nodes as well as to adjust surgical planning. [7] Recently, a hybrid tracer (ICG-^{99m}Tc-nanocolloid), combining radioactivity and fluorescence in one signature, was incorporated in the SN identification procedure in vulvar cancer, in order to optimise the intraoperative SN visualisation using the fluorescence component.[11]

The aim of the present study was to prospectively analyse SPECT/CT images to determine the anatomical location of the draining lymph nodes in patients with vulvar cancer and to evaluate the possible implications for the extent of the inguinal lymph node dissection.

MATERIALS AND METHODS

Between January 2007 and September 2014, 83 patients with vulvar cancer were referred to the Department of Nuclear Medicine after giving consent for a SN procedure. The patients' characteristics are presented in **Table 1**. Of the 83 patients, 80 had early-stage squamous cell carcinoma (Ib/II FIGO 2009), 2 had melanoma and 1 had adenocarcinoma of the vulva. The mean age of the patients was 67.8 y (range, 25–93 y). The BMI of the patients was 26.9 kg/m^2 (range, 15.4 – 43.7 kg/m^2). The tumour was located in the midline in 47 patients, on the right side in 16 patients and on the left in 20 patients. All patients were clinically node negative (cN0) as assessed by preoperative ultrasonography of the groin and if lymph node metastasis was suspected followed by fine needle aspiration cytology. All patients underwent resection of the primary tumour (or re-excision of the scar after irradical primary tumour excision), or excision of the melanoma, followed by SN biopsy. [12] Lymphoscintigraphy and SPECT/CT were performed in all patients. A SN was considered as any lymph node with visualised lymphatic drainage directly from the primary tumour. [10] A higher-echelon node was defined as a lymph node draining from the SN.

LYMPHATIC DRAINAGE, SNs AND HIGHER-ECHELON NODES FROM VULVAR CANCER

The expected areas for lymphatic drainage from vulvar cancer are the inguinal lymph node stations and subsequently the pelvic lymph node basins. The inguinal zone was divided into five anatomical regions following Daseler *et al.*: four quadrants are obtained by drawing a horizontal line and a vertical line over the saphenofemoral junction and a fifth zone directly overlying this junction. [13] Further, we divided the pelvic region into three lymph node zones: the external iliac/obturator, common iliac and para-aortic zones (**Figure 1**). Fused SPECT/CT images were analysed together with the CT slices using orthogonal re-slicing to facilitate localisation of the SN in the five zones of Daseler *et al.* and to correctly differentiate between the SN and higher-echelon nodes (**Figure 2**).

Three dimensional multiplanar reconstruction (MPR) and volume rendering were also used to confirm the anatomical localisation of the draining lymph nodes. All planar and SPECT/CT images were analysed by an experienced and dedicated nuclear medicine physician to determine the number and exact location of SNs and higher-echelon nodes.

Table 1. Patient characteristics

Characteristic	Value
No. of patients	83
Mean age (y)	67.8 (range, 25-93)
Mean BMI (kg/m^2)	26.9 (range, 15.4-43.7)
Mean administered activity (MBq)	81 (range, 52.9-132)
Mean tumour size (cm)	2.2 (range, 0.2-5.3)
Tumour location, *n*	
Central	47 (4[a])
Right	16 (2[a])
Left	20 (1[a])
Histology, *n*	
SCC	80
Melanoma	2
Adenocarcinoma	1
SCC grade, *n*	
1	31
2	35
3	14
Stage, [n]	
SCC[b]	
IB	51
II	9
IIIA-B	18
IVA	2
Melanoma	
IB	1
IIIA	1
Adenocarcinoma I	1
FNAC	
No. of patients	36
No. of groins	47

BMI body mass index, FNAC fine needle aspiration cytology, SCC squamous cell carcinoma, [a] These patients came for a re-excision of the tumour scar, [b] FIGO 2009.
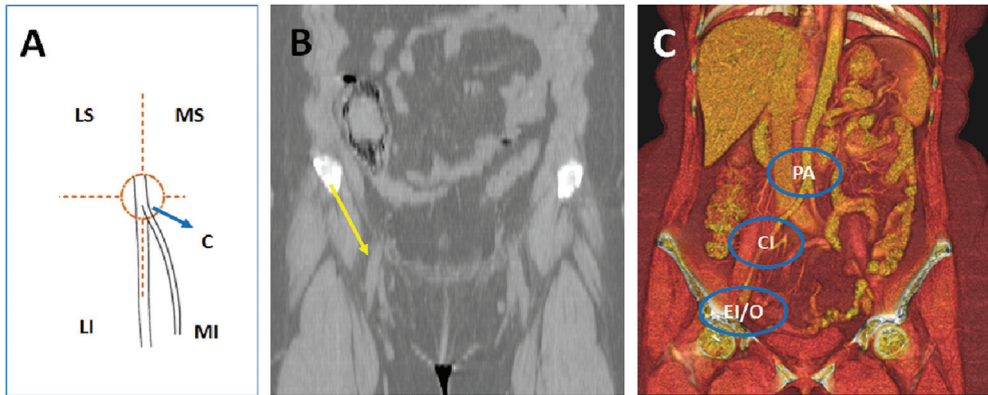
Figure 1. Schematic division of the superficial groin according to Daseler *et al.* into five zones using the saphenofemoral junction as intersection (LS lateral superior zone, MS medial superior zone, LI lateral inferior zone, MI medial inferior zone, C central zone) (A). Coronal CT image shows the saphenofemoral junction (yellow arrow) (B). Coronal CT image with 3D volume rendering shows the pelvic region with the three zones delineated (PA para-aortic zone, CI common iliac zone, EI/O external iliac/obturator zone) (C).
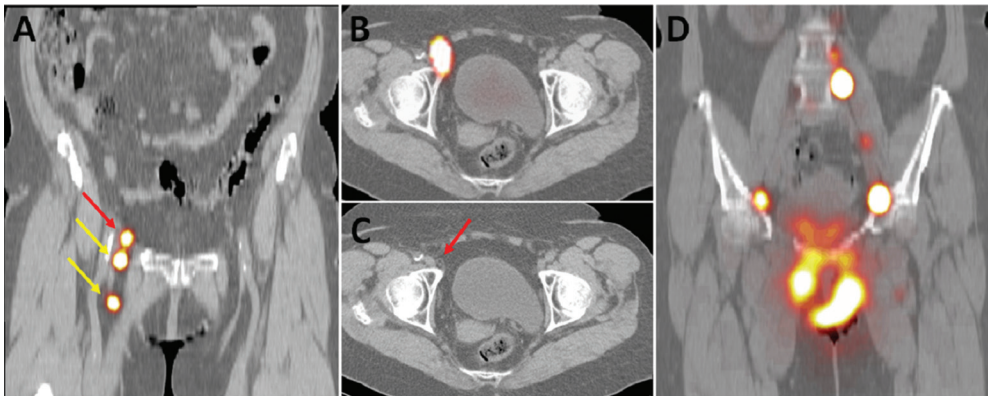
Figure 2. Coronal fused SPECT/CT image shows the sentinel lymph nodes (yellow arrows), one located in the medial superior inguinal zone and one in the medial inferior inguinal zone. The remaining node (red arrow) is a higher-echelon node in the iliac zone (A). Transverse fused SPECT/CT image (B) and CT image (C) also show the higher-echelon node. Coronal fused SPECT/CT image shows higher-echelon nodes along the trajectory of the iliac vessels and the aorta (D).

PREOPERATIVE PROCEDURE

After application of lidocaine spray for local anaesthesia, a mean of 81 MBq (range, 52.9–132 MBq) radiocolloid (^{99m}Tc-nanocolloid or ICG-^{99m}Tc-nanocolloid) was injected intradermally in three or four deposits around the lesion (total volume 0.4 mL). ^{99m}Tc-nanocolloid (Nanocoll®; GE Healthcare, Eindhoven, The Netherlands) was used in 68 patients, and ICG-^{99m}Tc-nanocolloid in 15 patients. An additional dose of radiopharmaceutical was given in three patients with midline tumour in whom initially no bilateral drainage was observed. Simultaneous anterior and lateral dynamic lymphoscintigraphy was performed immediately after injection followed by early (15 min) and delayed (2 h) static planar imaging (128 × 128 matrix, 30 frames, 20 s/frames, zoom 1). The early images were acquired to visualise lymphatic duct(s) and the first-draining lymph node(s). The delayed images were used to differentiate the SN(s) from higher-echelon nodes. Subsequently, SPECT/CT (Symbia T, Siemens, Erlangen, Germany) images were obtained using a 128 × 128 matrix, 60 frames, and 25 s/frame with angular steps of 6° to provide better anatomical localisation and to detect additional lymph nodes in other regions. The CT images (130 kV, 40 mAs, B30s kernel) were obtained using axial 2 mm slices. After correction for tissue attenuation and scattering, the SPECT and CT images were fused using an Osirix Dicom viewer.

The fused SPECT/CT images were viewed using MPR and volume rendering. For image interpretation, the first draining lymph node(s) appearing with or without an afferent lymphatic vessel from the primary lesion were considered as SNs. Lymph nodes appearing later in the same regions were considered to be higher-echelon nodes. [7] Additional hot spots depicted later and closer to the injection area were also considered to be SNs. The location of the SNs was marked on the skin with indelible ink before surgery. All radioactive SNs and higher-echelon nodes seen on SPECT/CT were correlated with CT in order to anatomically localise the corresponding lymph nodes.

INTRAOPERATIVE PROCEDURE

All patients underwent excision of the SN(s) and subsequent removal of the primary lesion or re-excision of the scar. Surgery was started between 4 and 24 h after radiocolloid administration. Shortly before the operation, 1.0 mL of patent blue dye (Laboratoire Guerbert, Aulnay-Sous-Bois, France) was injected intradermally around the tumour in three or four deposits. SNs were identified intraoperatively with patent blue dye and using a gamma-ray detection probe (Neoprobe; Johnson & Johnson Medical). When ICG-^{99m}Tc-nanocolloid was administered a portable gamma-camera (Sentinella; Oncovision, Valencia, Spain) in combination with a fluorescence camera

(Photodynamic Eye; Hamamatsu) were also used for real-time visualisation and confirmation of SN localisation during surgery. Excised lymph nodes were postoperatively confirmed to be SNs with the gamma-ray detection probe. Higher-echelon lymph nodes, defined by preoperative lymphoscintigraphy and SPECT/CT, were left in situ.

HISTOPATHOLOGICAL EXAMINATION

All harvested SNs were fixed in formalin, bisected, embedded in paraffin, and cut at a minimum of six levels at intervals of 50–150 µM. Tissue sections were evaluated for the presence of (micro) metastases with haematoxylin and eosin (H&E) and a keratin AE13 staining.

STATISTICAL METHODS

The chi-squared test was used to correlate results of planar lymphoscintigraphy and SPECT/CT. The chi-squared test with Fisher's correction was used to analyse the correlation between the results of metastatic SNs and the zones of Daseler *et al*. A *p* value of < 0.05 was considered statistically significant.
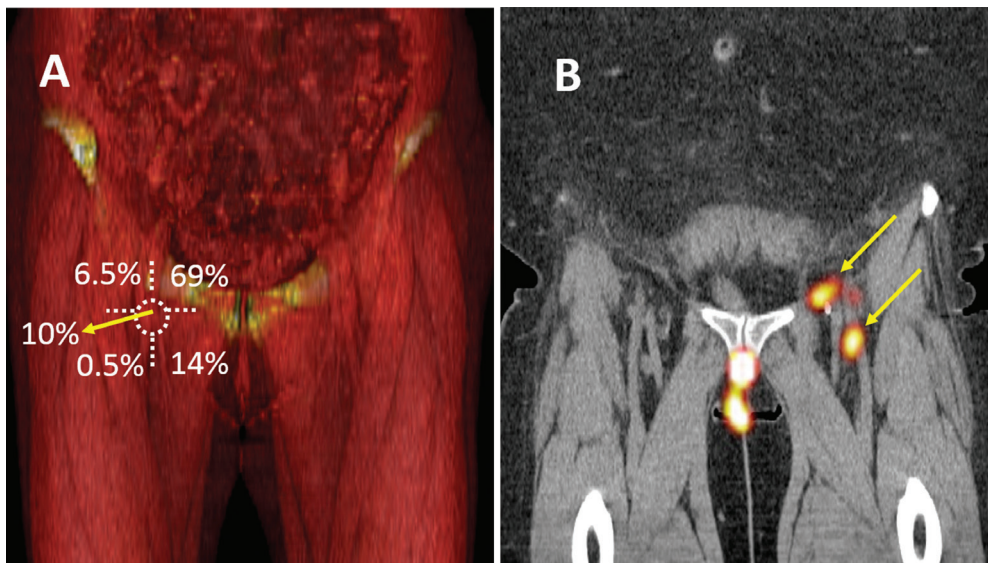
Figure 3. The five inguinal zones of drainage in vulvar cancer according to Daseler *et al*. (A). Coronal fused SPECT/CT image shows one node located in the medial superior inguinal zone and one node in the lateral inferior inguinal zone (yellow arrows) (B).

RESULTS

A total of 83 patients were included in this study. The SNs were identified on preoperative images in 80 of the 83 patients with a detection rate of 96.3%. The planar lymphoscintigraphy images showed 192 SNs in 141 groins whereas SPECT/CT images showed 217 SNs in 146 groins. This difference in detection of SNs between planar and SPECT/CT images was not statistically significant (p = 0.5, **Table 2**).

All SNs were visualised in the inguinal zone, and no direct drainage was identified to the pelvic lymph nodes. Of the 217 SNs identified preoperatively, 149 (69%) were found in the medial superior region, 31 (14%) in the medial inferior region, 22 (10%) in the central region, 14 (6.5%) in the lateral superior region and only 1 (0.5%) in the lateral inferior region (**Figure 3**).

A total of 137 SNs were identified preoperatively in 47 patients with midline tumour and of these 49.6% (68) drained to the right groin and 50.4% (69) to the left groin. The location of SNs according to the zones of Daseler *et al.* was 94 (69%) in the medial superior zone, 19 (14%) in the medial inferior zone, 14 (10%) in the central zone and 10 (7%) in the lateral superior zone; no lymphatic drainage was seen in the lateral inferior zone. A total of 31 SNs were identified preoperatively in 16 patients with tumour on the right side of the vulva and of these 74% (23) drained to the right groin and 26% (8) to the left groin. The location of SNs according to the zones of Daseler *et al.* was 23 (74%) in the medial superior zone, 2 (6.5%) in the medial inferior zone, 4 (13%) in the central zone and 2 (6.5%) in the lateral superior zone; no lymphatic drainage was seen in the lateral inferior zone. Finally, a total of 49 SNs were identified preoperatively in 20 patients with tumour on the left side of the vulva and of these 65 % (32) drained to the left groin and 35% (17) to the right groin. The location of SNs according to the zones of Daseler *et*

Table 2. Location of sentinel nodes on planar lymphoscintigraphy and SPECT/CT

	Planar lymphoscintigraphy	**SPECT/CT**	***p* value**
No. of sentinel nodes			
Right	89	108	0.55
Left	103	109	
Total	192	217	
No. of groins	141	146	

al. was 32 (65%) in the medial superior zone, 10 (21%) in the medial inferior zone, 4 (8%) in the central zone, 2 (4%) in the lateral superior zone and 1 (2 %) in the lateral inferior zone (**Table 3**).

A total of 252 SNs were excised from 144 groins with a median of 1.6 SNs (range, 1–3) per groin. Pathological examination of the excised SNs showed a total of 26 metastases (diameter 0.1–12 mm) in 19 patients (22.8%, 21 groins). In particular, 15 metastatic SNs were located in the medial superior zone, 1 in the medial inferior zone, 2 in the central zone and 1 in the lateral superior zone. The difference in localisation of 19 metastatic SNs according to the zones of Daseler *et al.* was statistically significant ($p < 0.0001$). For the remaining 7 metastatic SNs there were no available data concerning

Table 3. Location of sentinel nodes following Daseler's zones in relation to the tumour location

	Drainage zone	Tumour side			
		Right	Midline	Left	Total
No. of patients		16	47	20	83
No. of sentinel nodes					
Right	Medial superior	18	47	13	78
	Medial inferior	2	12	2	16
	Central	2	4	0	6
	Lateral superior	1	5	2	8
	Lateral inferior	0	0	0	0
	Total	23 (74%)	68 (49.6%)	17 (35%)	108
Left	Medial superior	5	47	19	71
	Medial inferior	0	7	8	15
	Central	2	10	4	16
	Lateral superior	1	5	0	6
	Lateral inferior	0	0	1	1
	Total	8 (26%)	69 (50.4%)	32 (65%)	109
Total		**31**	**137**	**49**	**217**

surgical localisation; however, these SNs were not located in lateral inferior zone.

Of the 19 patients with a tumour-positive SN, 13 underwent radiotherapy and 6 underwent radical inguinal lymph node dissection on the affected side. In 4 of the 19 patients with tumour-positive SN, additional nodal metastases were found in the inguinal lymph node dissection specimen, with 6 of 75 nodes being positive. SPECT/CT identified a total of 202 higher-echelon nodes both in the groin and in the pelvic region (**Table 4**) of which 153 (75.7%) were located in the external iliac/ obturator zone (**Figure 4**). No higher-echelon nodes were found in the inferior lateral zone of the groin. In 8 patients, there was disagreement between the number of groins with drainage of SNs identified by preoperative images and the number of groins eventually excised by the surgeon. In 5 of these patients a total of 5 SNs located in 5 groins were visualised on the preoperative image but not found during surgery. Subsequently, 2 of these patients underwent radiotherapy, 1 patient received an inguinofemoral lymphadenectomy and 2 patients were followed up. In contrast, in 3 patients a total of 3 SNs located in 3 groins were not seen on the preoperative images but were removed by the surgeon: 2 SNs showed blue dye only and 1 SN was only radioactive.

DISCUSSION

The inguinal lymph node basins are the expected areas of lymphatic drainage in vulvar cancer. In the present study, all SNs were visualised in the inguinal zone, and no direct drainage was identified to the pelvic lymph basins. However, clitoral tumour can drain directly to pelvic lymph nodes but there is no evidence in literature of the presence of pelvic lymph node metastases without simultaneous involvement of inguinofemoral lymph nodes. [6] The principal objective of the present study was to analyse the lymphatic drainage pattern and distribution of SNs in patients with vulvar cancer using SPECT/CT imaging. According to the zones of Daseler *et al.*, SNs were found predominantly in the medial superior zone (69%) and the medial inferior zone (14%), and in only one patient in the lateral inferior zone (0.5%). By comparison, in penile cancer, Leijte *et al.* found no drainage to the medial and lateral inferior zones of Daseler *et al.* [14] There are two important differences between the findings of Rob *et al.* [15] and those of the present study. First, we found 14 SNs in the lateral superior zone and 1 SN in the lateral inferior zone, while Rob *et al.* found no SNs in these zones. Second, Rob *et al.* found 16.1% of SNs in the deep femoral zone, while using SPECT/CT we found no SNs in the deep femoral zone. In our study, all patients with a

Table 4. Location of sentinel nodes and higher-echelon nodes

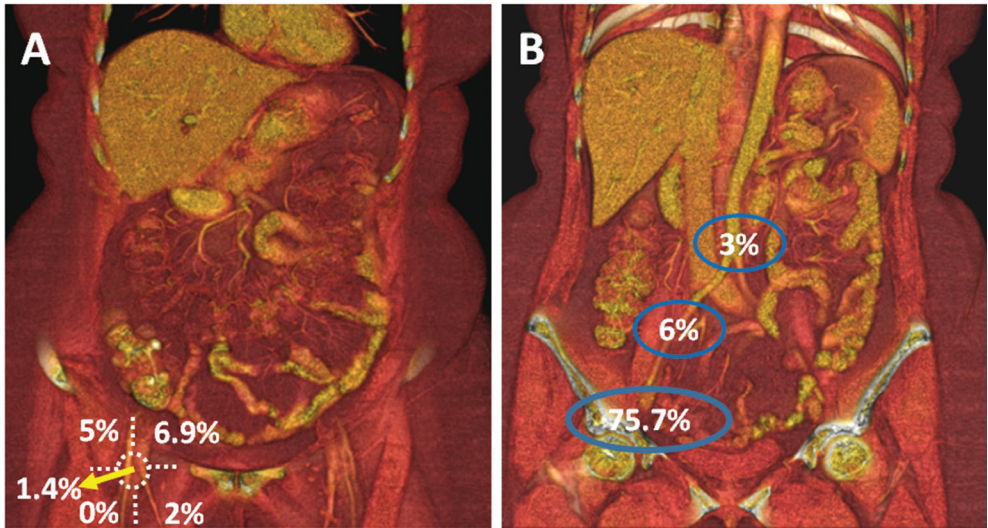| Nodes	Drainage region							
	Medial superior	Medial inferior	Centre	Lateral superior	Lateral inferior	External iliac / obturator	Common iliac	Para-aortic
Sentinel (217)	149 (69%)	31 (14%)	22 (10%)	14 (6.5%)	1 (0.5%)	0	0	0
Higher-echelon (202)	14 (6.9%)	4 (2%)	3 (1.4%)	10 (5%)	0	153 (75.7%)	12 (6%)	6 (3%)

Figure 4. CT images with 3D volume rendering showing the percentages of higher-echelon nodes in the groin (A) and in the pelvic region (B).

midline tumour had bilateral drainage, and of patients with well-lateralised tumour (right or left), approximately 30% had bilateral drainage, probably those with a short distance between the tumour and the midline. [7, 16] The use of 3D SPECT/CT improved the anatomical localisation of the SNs compared with the planar imaging, facilitating more accurate virtual surgical planning. This may also be useful to guide further regional lymph node dissection when a positive SN is found in other malignancies such as melanoma of the leg [17] and penile cancer. [14] In the present series, only one SN was located in the lateral inferior zone, which suggests that this zone could be excluded from complete dissection in the SN-positive patients. In theory, the tumour spreads through the lymphatic system in a step-wise fashion, and the next higher-echelon node is probably the next lymph node to be involved in SN-positive patients. [18, 19] In the present study, the majority of higher-echelon nodes were located in the external iliac/obturator zone as shown by SPECT/CT imaging. In tumour-positive SN patients, these results might suggest the need to include these higher echelon nodes in the subsequent lymph node dissection. SPECT/CT provided better preoperative prediction of the number of SNs. We visualised a higher number of SNs on SPECT/CT images than on planar lymphoscintigraphy images, which is in agreement with current literature. [20–22] A recent review of the literature showed the usefulness of SPECT/CT as a complementary modality to planar imaging, allowing anatomical localisation of SNs already visualised on planar images and detection of additional SNs, especially in areas of deep lymphatic drainage such as the pelvis. [23] A higher number of SNs were removed during surgery than the number visualised on preoperative images. We believe that the main explanation for this was the presence of clustered lymph nodes at the SN site that were not always visualised separately on preoperative images, not even on SPECT/CT, although SPECT/CT is a great improvement over planar imaging as stated above. This was one of the reasons for introducing the use of a portable gamma-camera in our hospital to confirm excision of all SNs. The additional use of a portable gamma-camera might lead to a higher intraoperative detection rate as reported by Vidal-Sicart *et al.* in six patients with gynaecological cancer. [24]

In our study in five patients a total of five SNs visualised on the preoperative images were not removed during surgery. The most plausible explanations were a weak radioactive signal in the node localised in anatomical areas with difficult access or a prolonged time between radiotracer injection and the operative SN procedure. On the contrary, in three patients a total of three SNs not visualised on the preoperative images were found during surgery. In one of these patients the SN was found using a gamma-probe. In this patient the SPECT/CT images were acquired too

early (1.5 h after injection, which was not according to standard protocol), possibly leading to the missed visualisation of late drainage to the SN. The guidelines of the European Association of Nuclear Medicine recommend that SPECT/CT images are acquired 2 to 4 h after injection of the radiopharmaceutical in order to achieve the best accuracy in localising the SN. [12] Two SNs were found intraoperatively because they showed blue dye positivity without being radioactive.

A recent meta-analysis on the accuracy of SN biopsy with ^{99m}Tc and/or blue dye in 1779 patients with vulvar cancer showed a SN detection rates of 97.7% for ^{99m}Tc combined with blue dye compared with 94.0% for ^{99m}Tc alone and 68.7% for blue dye alone. [9] Recently a hybrid tracer (ICG-^{99m}Tc-nanocolloid) was developed for SN detection and was found to be superior to blue dye alone in vulvar cancer by Mathéron et al. [11] and in melanoma by van der Berg et al. [25] It was no possible to analyse separately SN detection including SPECT/CT, fluorescence and blue dye in all patients. However, as shown by Mathéron et al. in our previous study of 15 patients with vulvar cancer, 98% of the SNs were radioactive at the time of excision, 96% were fluorescent and only 65% were blue. In our study, no significant difference was found in terms of drainage pattern and number of SNs between ^{99m}Tc-nanocolloid and ICG-^{99m}Tc-nanocolloid. This is in agreement with previous reports from our group. In fact, as reported by several authors, the drainage pattern of ICG-^{99m}Tc-nanocolloid and ^{99m}Tc-nanocolloid is identical. The additional value of ICG is better intraoperative visualisation of SN. [26, 27] In our series, 64 patients (77.1%) had SN negative for metastases and for this reason these patients did not undergo inguinofemoral lymphadenectomy, leading to a reduction in morbidity. Van der Zee et al. found that the short-term morbidity of SN biopsy was 11.7%, in contrast to 34% for inguinofemoral lymphadenectomy, and the long-term morbidity was 0.4% in contrast to 16.2%, respectively. [6] In addition, a SN procedure is associated with a shorter surgical time than groin node dissection. [28] Recently, Robinson et al. reported a low inguinal recurrence rate (5.2%) with decreased complications (17.5%) in patients who underwent isolated SN biopsy alone with a median follow-up of 58.3 months. [29] However, non-SN metastases occur more often as the size of SN metastasis increases, as found in the GROINSSV study. Therefore, all patients require additional groin treatment when SN is metastatic. [30]

Our study had some limitations. It was a retrospective study and for this reason, it was difficult to establish the exact location of excised SN and excised non-SN according to the five zones of Daseler et al. In addition, the role of blockage of lymphatic drainage due to involved metastatic lymph nodes was limited in our study, because all patients underwent preoperative ultrasonography in rder to identify lymph nodes with macrometastases in the groin.

CONCLUSION

In patients with cN0 vulvar cancer, lymphatic drainage predominantly occurs to the medial regions of the groin, and to a lesser extent to other inguinal areas. Drainage to the lateral inferior region of the groin is only incidental and in SN positive patients this zone might be spared in subsequent extended lymph node dissection; this may lead to a decrease in morbidity associated with this procedure. SPECT/CT is able to personalise lymphatic mapping, providing detailed information about the number and anatomical location of SNs for adequate surgical planning in the groin. Investigation of the correlation between SPECT/CT and surgical and histopathologic findings in future studies is highly recommended.

REFERENCES

1. Schuurman MS, van den Einden LC, Massuger LF, Kiemeney LA, van der Aa MA, de Hullu JA. Trends in incidence and survival of Dutch women with vulvar squamous cell carcinoma. Eur J Cancer. 2013;49(18):3872-80.
2. Netherlands Cancer Registry. http://www.cijfersoverkanker.nl
3. van der Avoort IA, Shirango H, Hoevenaars BM, Grefte JM, de Hullu JA, de Wilde PC, *et al*. Vulvar squamous cell carcinoma is a multifactorial disease following two separate and independent pathways. Int J Gynecol Pathol. 2006;25(1):22-9.
4. Burger MP, Hollema H, Emanuels AG, Krans M, Pras E, Bouma J. The importance of the groin node status for the survival of T1 and T2 vulval carcinoma patients. Gynecol Oncol. 1995;57(3):327-34.
5. Saito T, Kato K. Management of lymph nodes in the treatment of vulvar cancer. Int J Clin Oncol. 2007;12(3):187-91.
6. Van der Zee AG, Oonk MH, De Hullu JA, Ansink AC, Vergote I, Verheijen RH, *et al*. Sentinel node dissection is safe in the treatment of early-stage vulvar cancer. J Clin Oncol. 2008;26(6):884-9.
7. Paredes P, Vidal-Sicart S. Preoperative and intraoperative lymphatic mapping for radioguided sentinel node biopsy in cancers of the female reproductive system. In: Mariani G, Manca G, Orsini P, Vidal-Sicart S, Valdés Olmos R, editors. Atlas of lymphoscintigraphy and sentinel node mapping. Milan: Springer; 2012. p. 249–68.
8. Levenback C, Burke TW, Gershenson DM, Morris M, Malpica A, Ross MI. Intraoperative lymphatic mapping for vulvar cancer. Obstet Gynecol. 1994;84(2):163-7.
9. Meads C, Sutton AJ, Rosenthal AN, Małysiak S, Kowalska M, Zapalska A, *et al*. Sentinel lymph node biopsy in vulval cancer: systematic review and meta-analysis. Br J Cancer. 2014;110(12):2837-46.
10. Nieweg OE, Tanis PJ, Kroon BB. The definition of a sentinel node. Ann Surg Oncol. 2001;8(6):538-41.
11. Mathéron HM, van den Berg NS, Brouwer OR, Kleinjan GH, van Driel WJ, Trum JW, *et al*. Multimodal surgical guidance towards the sentinel node in vulvar cancer. Gynecol Oncol. 2013;131(3):720-5.
12. Giammarile F, Bozkurt MF, Cibula D, Pahisa J, Oyen WJ, Paredes P, *et al*. The EANM clinical and technical guidelines for lymphoscintigraphy and sentinel node localization in gynaecological cancers. Eur J Nucl Med Mol Imaging. 2014;41(7):1463-77.
13. Daseler EH, Anson BJ, Reimann AF. Radical excision of the inguinal and iliac lymph glands; a study based upon 450 anatomical dissections and upon supportive clinical observations. Surg Gynecol Obstet. 1948;87(6):679-94.
14. Leijte JA, Valdés Olmos RA, Nieweg OE, Horenblas S. Anatomical mapping of lymphatic drainage in penile carcinoma with SPECT-CT: implications for the extent of inguinal lymph node dissection. Eur Urol. 2008;54(4):885-90.
15. Rob L, Robova H, Pluta M, Strnad P, Kacirek J, Skapa P, *et al*. Further data on sentinel lymph node mapping in vulvar cancer by blue dye and radiocolloid Tc99. Int J Gynecol Cancer. 2007;17(1):147-53.
16. Coleman RL, Ali S, Levenback CF, Gold MA, Fowler JM, Judson PL, *et al*. Is bilateral lymphadenectomy for midline squamous carcinoma of the vulva always necessary? An analysis from Gynecologic Oncology Group (GOG) 173. Gynecol Oncol. 2013;128(2):155-9.
17. van der Ploeg IM, Kroon BB, Valdés Olmos RA, Nieweg OE. Evaluation of lymphatic drainage patterns to the groin and implications for the extent of groin dissection in melanoma patients. Ann Surg Oncol. 2009;16(11):2994-9.
18. Kapteijn BA, Nieweg OE, Petersen JL, Rutgers EJ, Hart AA, van Dongen JA, *et al*. Identification and biopsy of the sentinel lymph node in breast cancer. Eur J Surg Oncol. 1998;24(5):427-30.
19. Reintgen D, Cruse CW, Wells K, Berman C, Fenske N, Glass F, *et al*. The orderly progression of melanoma nodal metastases. Ann Surg. 1994;220(6):759-67.
20. Beneder C, Fuechsel FG, Krause T, Kuhn A, Mueller MD. The role of 3D fusion imaging in sentinel lymphadenectomy for vulvar cancer. Gynecol Oncol. 2008;109(1):76-80.
21. Belhocine TZ, Prefontaine M, Lanvin D, Bertrand M, Rachinsky I, Ettler H, *et al*. Added-value of SPECT/CT to lymphatic mapping and sentinel lymphadenectomy in gynaecological cancers. Am J Nucl Med Mol Imaging. 2013;3(2):182-93.
22. Kraft O, Havel M. Detection of sentinel lymph nodes in gynecologic tumours by planar scintigraphy and SPECT/CT. Mol Imaging Radionucl Ther. 2012;21(2):47-55.

23. Valdés Olmos RA, Rietbergen DD, Vidal-Sicart S, Manca G, Giammarile F, Mariani G. Contribution of SPECT/CT imaging to radioguided sentinel lymph node biopsy in breast cancer, melanoma, and other solid cancers: from "open and see" to "see and open". Q J Nucl Med Mol Imaging. 2014;58(2):127-39.

24. Vidal-Sicart S, Paredes P, Zanón G, Pahisa J, Martinez-Román S, Caparrós X, et al. Added value of intraoperative real-time imaging in searches for difficult-to-locate sentinel nodes. J Nucl Med. 2010;51(8):1219-25.

25. van den Berg NS, Brouwer OR, Schaafsma BE, Mathéron HM, Klop WM, Balm AJ, et al. Multimodal surgical guidance during sentinel node biopsy for melanoma: combined gamma tracing and fluorescence imaging of the sentinel node through use of the hybrid tracer indocyanine green-(99m)Tc-nanocolloid. Radiology. 2015;275(2):521-9.

26. Brouwer OR, Buckle T, Vermeeren L, Klop WM, Balm AJ, van der Poel HG, et al. Comparing the hybrid fluorescent-radioactive tracer indocyanine green-99mTc-nanocolloid with 99mTc-nanocolloid for sentinel node identification: a validation study using lymphoscintigraphy and SPECT/CT. J Nucl Med. 2012;53(7):1034-40.

27. Frontado LM, Brouwer OR, van den Berg NS, Mathéron HM, Vidal-Sicart S, van Leeuwen FW, et al. Added value of the hybrid tracer indocyanine green-99mTc-nanocolloid for sentinel node biopsy in a series of patients with different lymphatic drainage patterns. Rev Esp Med Nucl Imagen Mol. 2013;32(4):227-33.

28. Hefler LA, Grimm C, Six L, Seebacher V, Polterauer S, Joura E, et al. Inguinal sentinel lymph node dissection vs. complete inguinal lymph node dissection in patients with vulvar cancer. Anticancer Res. 2008;28(1):515-7.

29. Robison K, Roque D, McCourt C, Stuckey A, DiSilvestro PA, Sung CJ, et al. Long-term follow-up of vulvar cancer patients evaluated with sentinel lymph node biopsy alone. Gynecol Oncol. 2014;133(3):416-20.

30. Oonk MH, van Hemel BM, Hollema H, de Hullu JA, Ansink AC, Vergote I, et al. Size of sentinel-node metastasis and chances of non-sentinel-node involvement and survival in early stage vulvar cancer: results from GROINSS-V, a multicenter observational study. Lancet Oncol. 2010;11(7):646-52.

EVALUATION OF DUAL TIME POINT IMAGING ^{18}F-FDG PET/CT FOR LYMPH NODE STAGING IN VULVAR CANCER

adapted from:

A Collarino and G Garganese
RA Valdés Olmos
A Stefanelli
G Perotti
P Mirk
SM Fragomeni
FP Ieria
G Scambia
A Giordano
V Rufini

CHAPTER 9

ABSTRACT

PURPOSE This study aimed to assess the value of dual-time-point ^{18}F-FDG PET/CT in the prediction of lymph node (LN) status in patients with invasive vulvar cancer (VC) scheduled for inguinofemoral LN dissection.

METHODS From April 2013 to July 2015, all consecutive patients with VC scheduled for inguinofemoral LN dissection were prospectively enrolled. All patients underwent a preoperative whole-body ^{18}F-FDG PET/CT scan at 1 h (standard examination) and an additional scan from T11 to the groins at 3 h (delayed examination) after ^{18}F-FDG injection. On both scans, each groin was visually scored 0 or 1 concerning ^{18}F-FDG LN uptake relative to background. Semi-quantitative analysis included SUV_{max} and the corresponding retention index of SUV_{max}, measured on both scans. The optimal cut-off value of these parameters was defined using a receiver operating characteristic analysis. Histopathology was the standard of reference.

RESULTS Thirty-three patients were included, with a total of 57 groins dissected and histologically evaluated. At histopathology, 21 of 57 (37%) groins contained metastatic LNs. Concerning visual score, sensitivity, specificity, negative predictive value, positive predictive value, and accuracy were 95.2%, 75%, 96.4%, 69%, and 82.5% on standard scanning and 95.2%, 77.8%, 96.6%, 71.4%, and 84.2% on delayed scanning, respectively. At receiver-operating-characteristic analysis, sensitivity and specificity were 95.2% and 77.8% on standard and delayed ^{18}F-FDG PET/CT for an SUV_{max} cut-off of greater than 1.32 and 1.88, respectively, and 95.2% and 80% for a retention index of SUV_{max} cut-off of greater than 0.

CONCLUSION Standard ^{18}F-FDG PET/CT is an effective preoperative imaging method for the prediction of LN status in VC, allowing the prediction of pathologically negative groins and thus the selection of patients suitable for minimally invasive surgery. Delayed ^{18}F-FDG PET/CT did not improve the specificity and the positive predictive value in our series. Larger studies are needed for a further validation.

INTRODUCTION

Invasive vulvar carcinoma (VC) is an uncommon gynaecologic tumour, with an incidence of 2,4 new cases/100,000 women per year. [1] The pattern of dissemination of VC is mainly lymphatic, with prevalent involvement of the groins, whereas haematogenous spread is rare. [2] Thus, the most important prognostic factor is the presence of metastatic lymph nodes (LNs) in the groins. [3] In fact, the 5-y survival rate decreases from 94.7% when locoregional LNs are negative to 62% when they contain metastases. [4] Therefore, accurate preoperative LN staging is critical to customise the extent of groin surgery and to select patients suitable for minimally invasive procedures, thus avoiding unnecessary inguinofemoral lymph node dissection (IFLD), which is associated with a high morbidity and worse quality of life. In recent years, PET/CT using the glucose analogue ^{18}F-FDG has been used increasingly for the evaluation of LN status in gynaecologic malignancies, [5] but only recently it has been recommended in VC. [6] However, because of the low incidence of VC there are few studies in small series on the diagnostic accuracy of ^{18}F-FDG PET/CT in the detection of metastatic LNs in VC; the reported sensitivity ranges from 67% to 92% and the specificity from 91% to 95% per groin. [7, 8] Recently, dual-time-point (DTP) or dual-phase ^{18}F-FDG PET/CT has been suggested as a means for detecting metastatic LN in several gynaecologic cancers, [9] but its usefulness in VC has not yet been evaluated. In particular, DTP ^{18}F-FDG PET/CT requires 2 acquisitions after a single injection of the radiotracer, that is, standard images (1 h after injection) followed by delayed images (3 h after injection) of the body region under assessment. The rationale is that malignant cells, compared with benign cells, usually show increased ^{18}F-FDG uptake retention on delayed-time point imaging because of the high glycolysis activity. [10]

The aim of this prospective study was to investigate the value of DTP ^{18}F-FDG PET/CT for the assessment of LN status in patients with VC scheduled for IFLD.

MATERIALS AND METHODS

PATIENTS AND STUDY DESIGN

The Institutional Review Board approved this longitudinal prospective monocentric study, and all patients signed a written informed consent form. Between April 2013 and July 2015, all consecutive patients with primary histologically proven invasive VC (i.e., depth of stromal invasion > 1 mm) referred to the Division of Gynaecologic Oncology at A. Gemelli Hospital were evaluated with clinical examination and conventional imaging. [6] The surgical plan was traced on the base of the disease site and extent, according to international recommendations. [6, 11] All patients scheduled for IFLD were considered eligible for the study and underwent preoperative ^{18}F-FDG PET/CT scanning with DTP acquisition. Patients with the following characteristics were excluded: prior inguinal surgery dissection; previous chemotherapy or locoregional radiotherapy within the last 5 y; contraindication to the surgery due to age or comorbidities; pregnancy or breast-feeding; blood glucose greater than 200 mg/dL; and surgery performed more than 20 d after ^{18}F-FDG PET/CT. Pathologic results were used as the standard of reference to assess the presence of LN metastases.

^{18}F-FDG PET/CT ACQUISITION

^{18}F-FDG PET/CT scans were obtained according to the standard procedure of our centre. [12] All patients fasted for at least 6 h, and the glucose blood levels were less than 190 mg/dL before the ^{18}F-FDG injection. According to body weight, 118–303 MBq of ^{18}F-FDG were intravenously administrated. Before ^{18}F-FDG PET/CT acquisition, patients were hydrated with 500 mL of saline solution by IV administration. No oral or intravenous contrast agents were used. All ^{18}F-FDG PET/CT scans were acquired using the same PET scanner (Gemini GXL [Philips] or Biograph mCT [Siemens Medical Solutions US, Inc.]) for each patient at 2 time points: 60 ± 10 min (standard ^{18}F-FDG PET/CT scanning) and 180 ± 10 min (delayed ^{18}F-FDG PET/CT scanning) after ^{18}F-FDG injection. Standard ^{18}F-FDG PET/CT scans were acquired from the skull base to mid-thigh. Delayed ^{18}F-FDG PET/CT scans were obtained from the 11th vertebra (T11) to the inguinal region. Before the ^{18}F-FDG PET/CT acquisition, low-dose CT images (using a voltage of 110–120 kVp and tube current of 20–40 mAs, with the patient breathing normally) were acquired for anatomic reference and attenuation correction. PET images were then acquired in 3-dimensional mode, with 7–8 acquisition beds (of 2.5 min each) on standard scans and 1–2 acquisition beds (of 4 min each) on delayed scans. Matched CT and PET images were reconstructed with a field-of-view of 50 cm. The line-of-response row-action maximum likelihood algorithm was used for reconstruction

with 144 x 144 or 256 x 256 matrix. Attenuation-corrected PET images were reviewed in transverse, sagittal, and coronal planes. PET data were also displayed in a rotating maximum-intensity projection images. To evaluate the images, PET and CT datasets were transferred to an independent computer workstation by DICOM transfer.

¹⁸F-FDG PET/CT IMAGE ANALYSIS

All ¹⁸F-FDG PET/CT images were interpreted and visually scored by two nuclear medicine physicians in consensus.

QUALITATIVE ANALYSIS

Qualitative analysis was performed both on standard and on delayed ¹⁸F-FDG PET/CT, and the degree of ¹⁸F-FDG uptake in the LNs was classified as follows: normal, uptake lower than or equal to background (score 0); and abnormal, uptake higher than background (score 1). The gluteus muscle tissue was used to estimate background activity. The size of the largest LN per groin (short axis) was detected on transaxial CT images of PET/CT.

SEMIQUANTITATIVE ANALYSIS

A spherical volume of interest was placed over the inguinal LN with the highest glucose uptake on the transaxial PET images, for each groin, using an isocontour threshold of 40% method (Syngo. via, MM oncology VA30; Siemens Medical Solution) based on the SUV. [13, 14] SUV normalization to body weight and to injected dose was automatically assessed using the following equation:

$$SUV = \frac{\text{Tissue radioactivity concentration (MBq/mL)}}{\text{Injected dose (MBq)/Body weight (g)}}$$

The SUV_{max} within the volume of interest was measured on standard (SUV_{max} standard) and delayed (SUV_{max} delayed) PET images. Volumes of interest were carefully placed in exactly the same anatomic site, both on standard and on delayed PET/CT scans. When several hypermetabolic LNs per groin were seen on PET/CT images, the highest SUV_{max} was considered the representative value of that groin. When inguinal LNs did not show a significant ¹⁸F-FDG uptake, an arbitrary value of 1 for SUV_{max} was adopted.

Furthermore, we calculated the retention index of SUV_{max} (RI_{max}) using the following formula:

$$RI_{max} = (SUV_{max}\ delayed - SUV_{max}\ standard) \times 100\ /\ SUV_{max}\ standard$$

The ^{18}F-FDG PET/CT findings and histopathological results for the inguinal LNs were compared on a groin-by-groin analysis.

STATISTICAL ANALYSIS

Sensitivity, specificity, negative predictive value (NPV), positive predictive value (PPV), and accuracy of standard and delayed PET/CT were calculated considering qualitative analysis. The receiver-operating-characteristic analysis was used to determine the optimal cut-off values of SUV_{max} standard, SUV_{max} delayed, and RI_{max}, for differentiating benign and malignant inguinal LNs. Differences in sensitivity, specificity, and accuracy between standard and delayed ^{18}F-FDG PET/CT were determined using the Chi-square or Fisher test. A p value of less than 0.05 was considered statistically significant. Statistical analysis was performed using MedCalc Statistical Software (version 15.11.4).

60 patients with primary VC
referred to the Division of Gynaecologic Oncology

11 patients
scheduled for SLNB

49 patients scheduled for IFLD
and underwent DTP PET/CT scan

16 patients with >20 days
between PET/CT scan
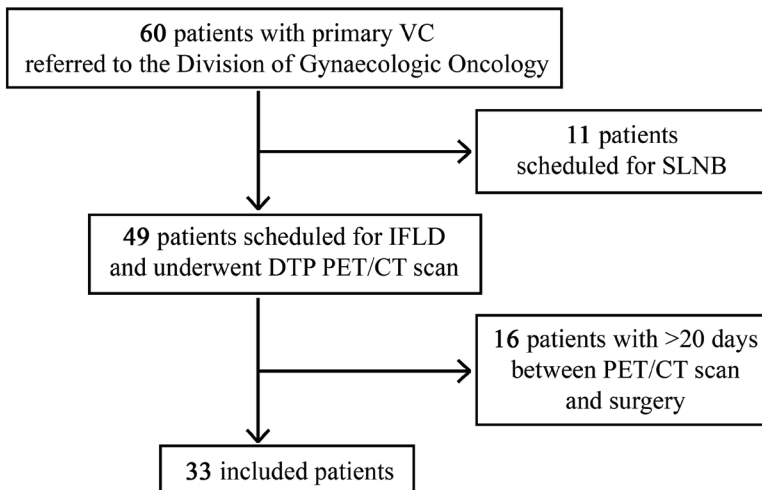and surgery

33 included patients

Figure 1. Flowchart of patients' selection

VC vulvar cancer, **SLNB** sentinel lymph node biopsy, **IFLD** inguinofemoral lymph node dissection, **DTP** dual-time-point, **PET/CT** positron emission tomography/computed tomography.

RESULTS

A total of 60 patients with primary VC were referred to the Division of Gynaecologic Oncology during the study period. Among these, 33 patients fulfilled the inclusion criteria (**Figure 1**). Patients' characteristics are reported in **Table 1**. All patients had a squamous cell carcinoma of the vulva. The time interval between the ^{18}F-FDG injection and PET/CT acquisition was 60 ± 11 min for standard PET/CT and 162 ± 24 min for delayed PET/CT. Most PET/CT studies (22/33 patients, 67%) were

Table 1. Patients' characteristics

Characteristic	Number	Percentage
No. of patients	33	
Mean age ± SD	69 ± 13.4	
Mean body mass index (Kg/m^2)	24 (range, 21-42)	
Tumour site		
Central	16	48%
Monolateral	11	34%
Multifocal	6	18%
Vulvar surgical procedure		
Partial vulvectomy	11	33%
Radical vulvectomy	22	67%
IFLD		
Monolateral dissection	9	27%
Bilateral dissection	24	73%
Tumour size		
< 4 cm	25	76%
≥ 4 cm	8	24%
Grading		
G1	4	12%
G2	24	73%
G3	5	15%
Figo Stage [a]		
Ib	15	45.5%
II	3	9%
III	15	45.5%

SD standard deviation, **IFLD** inguinofemoral lymph node dissection,
[a] 2009 revised FIGO staging system.

acquired using the GXL scanner. The time interval between ^{18}F-FDG PET/CT study and surgery was 18 ± 1 d. Fifty-seven groins (24 bilateral, 9 unilateral) in 33 patients were dissected. At pathologic examination, 21 groins contained metastatic LNs and 36 groins were negative for metastases.

The mean size of all measured LNs was 9.4 ± 3.6 mm (median, 8 mm; range, 5-21 mm). The mean size of metastatic LNs was 11.8 ± 4.6 mm (median, 10 mm; range, 6-21 mm), whereas the mean size of non-metastatic LNs was 8.1 ± 1.7 mm (median, 8 mm; range, 5-12 mm). Significant difference was found between the size of metastatic and non-metastatic LNs measured on low-dose CT ($p < 0.002$).

QUALITATIVE ANALYSIS

Standard ^{18}F-FDG PET/CT was positive in 29 of 57 groins and negative in 28 of 57 groins. Visual score results are reported in **Table 2**. Of the 21 groins with metastatic LNs at pathological examination, standard ^{18}F-FDG-PET/CT showed ^{18}F-FDG uptake above the background (score 1) in 20 groins and under background (score 0) in 1 groin. Of the 36 groins with no metastatic LNs at pathological examination, standard ^{18}F-FDG PET/CT was negative in 27 groins and positive in 9 groins. On a groin-by-groin basis, standard ^{18}F-FDG PET/CT yielded a sensitivity of 95.2% (95% confidence interval [CI], 85.2%-99.8%), specificity of 75% (95% CI, 61.5%-85.1%), NPV of 96.4% (95% CI, 86.7%-99.4%), PPV of 69% (95% CI, 55.2%-80.2%), and accuracy of 82.5% (95 % CI, 72.7%-92.3%) (**Table 3**).

Table 2. Qualitative (visual score) results of standard ^{18}F-FDG PET/CT and delayed ^{18}F-FDG PET/CT

PET/CT	Visual score	Pathological evaluation		
		LN metastasis	No LN metastasis	Total
Standard	0	1	27	28
	1	20	9	29
	Total	21	36	57
Delayed	0	1	28	29
	1	20	8	28
	Total	21	36	57

Score 0 uptake ≤ than background, **score 1** uptake > than background, **LN** lymph node.

Table 3. Qualitative analysis

PET/CT	PET/CT results	Pathological evaluation			Sensitivity (%)	Specificity (%)	Accuracy (%)	PPV (%)	NPV (%)
		LN metastasis	No LN metastasis	Total					
Standard									
per groin	Positive	20	9	**29**	95.2	75	82.5	69	96.4
	Negative	1	27	**28**	(85.2-99.8)	(61.5-85.1)	(72.7-92.3)	(55.2-80.2)	(86.7-99.4)
	Total	**21**	**36**	**57**					
Delayed									
per groin	Positive	20	8	**28**	95.2	77.8	84.2	71.4	96.6
	Negative	1	28	**29**	(85.2-99.8)	(64.5-87.3)	(74.8-93.6)	(57.7-82.2)	(86.9-99.4)
	Total	**21**	**36**	**57**					

LN lymph node, **PPV** positive predictive value, **NPV** negative predictive value. Data in parentheses are 95% CIs.
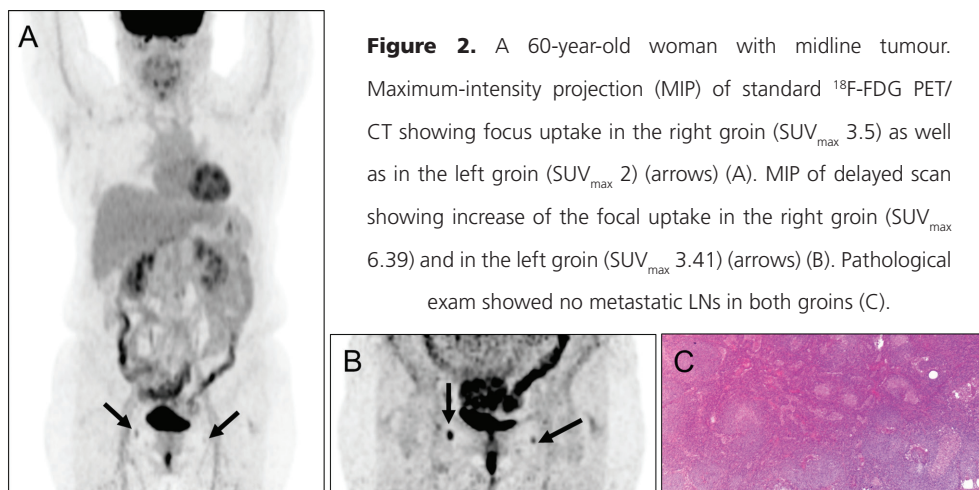
Figure 2. A 60-year-old woman with midline tumour. Maximum-intensity projection (MIP) of standard ^{18}F-FDG PET/CT showing focus uptake in the right groin (SUV_{max} 3.5) as well as in the left groin (SUV_{max} 2) (arrows) (A). MIP of delayed scan showing increase of the focal uptake in the right groin (SUV_{max} 6.39) and in the left groin (SUV_{max} 3.41) (arrows) (B). Pathological exam showed no metastatic LNs in both groins (C).

Delayed ^{18}F-FDG PET/CT was positive in 28 of 57 groins and negative in 29 of 57 groins (**Table 2**). Of the 21 groins with metastatic LNs at pathological examination, delayed ^{18}F-FDG PET/CT showed abnormal ^{18}F-FDG uptake in 20 groins, with a false-negative (FN) result occurring in 1 groin (same groin that was FN at standard imaging). Of the 36 groins with no metastatic LNs at pathological examination, delayed ^{18}F-FDG PET/CT was true negative in 28 groins and false positive (FP) (**Figure 2**) in 8 groins. On a groin-by-groin basis, delayed ^{18}F-FDG PET/CT yielded a sensitivity of 95.2% (95% CI, 85.2%-98.8%), specificity of 77.8% (95% CI, 64.5%-87.3%), NPV of 96.6%, (95% CI, 86.9%-99.4%), PPV of 71.4% (95% CI, 57.7%-82.2%), and accuracy of 84.2% (95% CI, 74.8%-93.6%) (**Table 3**). No significant differences in sensitivity, specificity and accuracy between standard and delayed PET/CT were found.

SEMIQUANTITATIVE ANALYSIS

Mean and median values of SUV_{max} standard, SUV_{max} delayed and RI_{max} for metastatic groins (group 1) and non-metastatic groins (group 0) are shown in **Table 4**. SUV_{max} standard, SUV_{max} delayed and RI_{max} were significantly higher for group 1 than for group 0 ($p < 0.0001$) (**Figure 3**). The area under the curve was larger in SUV_{max} standard, which was 0.919 ($p < 0.0001$; 95% CI, 81.5%-97.5%) compared with 0.899 in SUV_{max} delayed ($p < 0.0001$; 95% CI, 79%-96.3%) and 0.833 in RI_{max} ($p < 0.0001$; 95% CI, 71%-92%). There was no significant difference between the areas under the curve in SUV_{max} standard and SUV_{max} delayed ($p = 0.10$) nor between

Table 4. Mean and Median of SUV$_{max}$ value on standard scan, on delayed scan and RI for metastatic and non-metastatic groups

Lymph node (LN)	SUV$_{max}$ standard	p	SUV$_{max}$ delayed	RI (%)
Metastatic LNs (group 1)				
Mean ± SD	5.43 ± 3	0.11	7.17 ± 3.9	31.42 ± 15.61
Median	5.51 (range, 1-12.62)		6.88 (range, 1-15.82)	34.39 (range, 0-56.49)
Non-metastatic LNs (group 0)				
Mean ± SD	1.56 ± 1.2	0.3	1.94 ± 1.9	12.21 ± 25.75
Median	1 (range, 1-5.64)		1 (range, 1-6.98)	0 (range, -1.79-82.57)
p	< 0.0001		< 0.0001	0.003

SUV$_{max}$ maximum standardised uptake value, **RI** retention index, **SD** standard deviation.
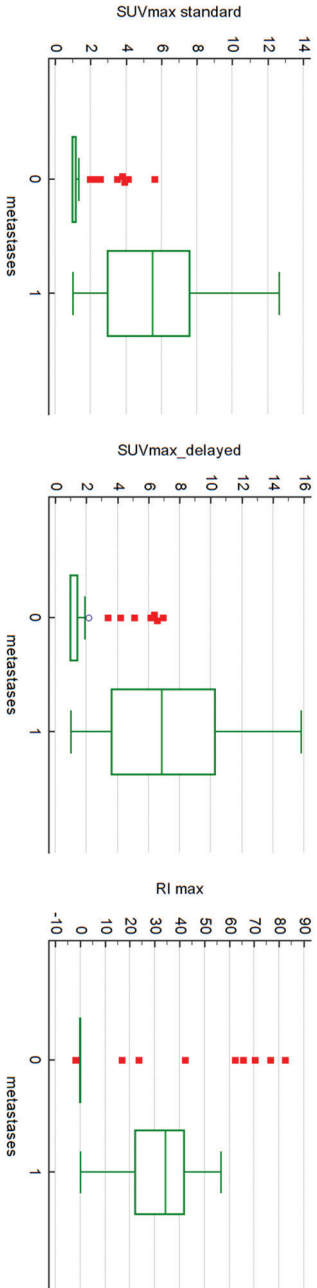
Figure 3. Box plots showing distribution of SUV_{max} standard, SUV_{max} delayed and RI_{max} for metastatic and non-metastatic groins. **0** absence of metastases, **1** presence of metastases.
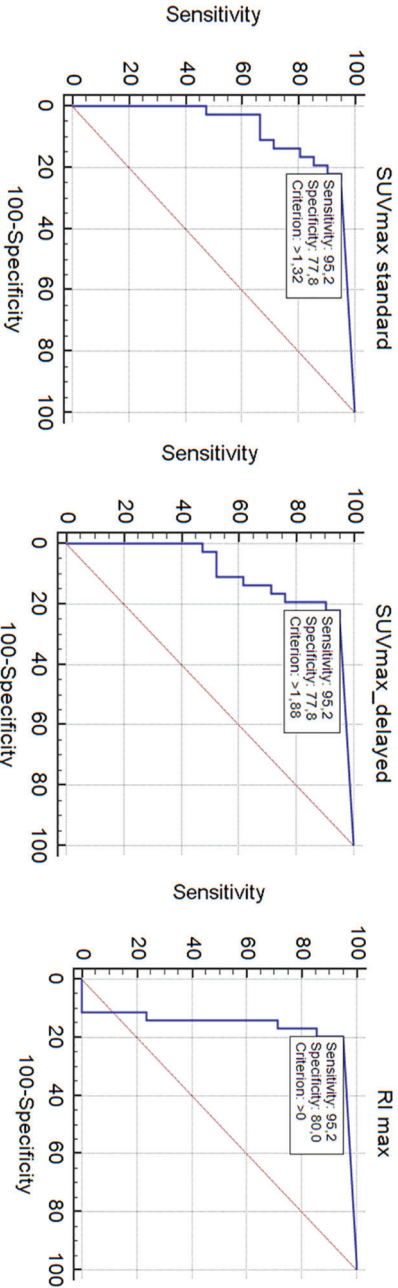

Figure 4. The receiver-operating-characteristic curves of SUV_{max} on standard scan and delayed scan and RI.

SUV$_{max}$ delayed and RI$_{max}$ ($p = 0.055$), whereas a significant difference was found between SUV$_{max}$ standard and RI$_{max}$ ($p = 0.04$). At receiver-operating-characteristic analysis, the optimal cut-off values of SUV$_{max}$ standard, SUV$_{max}$ delayed and RI$_{max}$ were > 1.32, > 1.88 and > 0, respectively. With these cut-off values, the sensitivity and specificity, respectively, were 95.2% and 77.8%, for both SUV$_{max}$ standard and SUV$_{max}$ delayed and 95.2% and 80% for RI$_{max}$, (**Figure 4**).

DISCUSSION

In this prospective study, we evaluated the value of DTP ^{18}F-FDG PET/CT for LN staging. We chose to include only patients candidates for lymphadenectomy, excluding those addressed to the sentinel node biopsy, to ensure that the reference standard (histopathologic results), could include all the inguinal LNs examined preoperatively by ^{18}F-FDG PET/CT. Moreover, given the rapid progression of VC, we decided to include only those patients for whom a maximum 3-week interval between the preoperative study and surgery was compiled. On the basis of criteria that considered metastatic LNs if they have ^{18}F-FDG uptake higher than background, standard ^{18}F-FDG PET/CT showed high sensitivity (95.2%) and relatively low specificity (75%) in detecting metastatic groins. In particular, we found 9 FP groins and 1 FN groin, the latter due to a metastatic LN of 8 mm in diameter. In 9 FP groins, pathological examination revealed no LN metastases in 7 groins and inflammatory LNs in 2 groins. Concerning the FP results, it is widely known in the literature that inflammatory cells and activated macrophages represent a common cause of increased ^{18}F-FDG uptake, as occurring in inguinal reactive LNs after vulvar biopsy or shaving. [15] Conversely, FN results are most likely be associated to PET-undetected micrometastatic foci in not enlarged nodes as well as with extensive necrosis within metastatic LNs with subsequent loss of ^{18}F-FDG uptake. [7] Previous PET or PET/CT studies in the literature showed a range of sensitivity (from 50% to 100%) and specificity (from 91% to 100%) for detecting metastatic involvement of inguinofemoral LNs in VC patients. [7, 8, 16, 17] In those studies, no cut-off values of SUV$_{max}$ were determined for metastatic LNs. In our study, a SUV$_{max}$ value of greater than 1.32 was found to be the optimal cut-off point on standard PET/CT to provide a sensitivity similar to the one obtained from visual analysis (95.2%) but accompanied by a slightly better (77.8% vs 75%) although not statistically significant ($p = 0.81$) specificity, in detecting metastatic groins. As already mentioned, increased ^{18}F-FDG uptake is not specific for neoplastic involvement, because it may

also be reactive to inflammation or infection. [18] On the basis of our data, standard ^{18}F-FDG PET/CT showed a high NPV (96.4%) together with a low PPV (69%) in detecting metastatic groins. Therefore, a negative ^{18}F-FDG PET/CT scan is highly predictive in excluding groin metastases and could potentially be used to select patient candidate for a minimal groin surgery. In contrast, a positive ^{18}F-FDG PET/CT scan finding is not highly predictive for groin metastases and needs to be interpreted with caution. On the basis of our data, significant difference was found between the size of metastatic and non-metastatic LNs measured on low-dose CT. However, further studies are needed to investigate whether the combination of PET and CT criteria can better differentiate between metastatic and non-metastatic LNs.

The rationale of DTP ^{18}F-FDG PET/CT is that ^{18}F-FDG uptake usually increases in malignant lesions for several hours after intravenous injection, whereas benign lesions and inflammatory cells show stable or decreasing ^{18}F-FDG uptake over time. [19, 20] Such different behaviour on delayed PET/CT is believed to be due to increased cell proliferation rate, enhanced expression of hexokinase type-II and glucose transporter-1 in malignant lesions, and continued clearance of background activity, thus resulting in images with improved contrast to noise ratio. [10] Up until now, no studies have yet been performed using qualitative and semi-quantitative parameters on both standard and delayed ^{18}F-FDG PET/CT to assess LN status in VC. To our knowledge, only Lin *et al.* performed delayed PET scanning in VC staging, showing that it did not modify the qualitative analysis of a standard scan. However, they did not apply semi-quantitative evaluation and the sample size in their study was limited (11 patients). [8] According to our qualitative analysis, delayed ^{18}F-FDG PET/CT showed similar sensitivity and NPV (95.2% and 96.5%) as standard scan with relatively higher specificity (77.8% vs 75%) and PPV (71.4% vs 69%) not reaching statistical significance (p = 0.9) in detecting metastatic groins. In particular, in the patient with FN groin no ^{18}F-FDG uptake, even on the delayed scan was seen, most likely due to the limited extent of the metastatic involvement (with micrometastases on histopathology). Moreover, on delayed PET/CT we found 8 FP groins compared with 9 FP groins on standard PET/CT. This finding suggests that the behaviour of inflammatory lesions as concerning ^{18}F-FDG uptake is not always predictable, and that delayed PET/CT appears to not reduce the rate of FP results. According to other studies, inflammatory lesions as well as infection may induce higher ^{18}F-FDG uptake on delayed scan mimicking malignant lesions. [21-24] In the literature, the use of DTP ^{18}F-FDG PET/CT in gynaecological malignancies is still a subject of discussion and in our study, the delayed ^{18}F-FDG PET/CT also was not superior to standard images in detecting LN disease. This is in accordance with the results reported in a recent meta-analysis by Shen *et al.*, [21] which concluded that DTP ^{18}F-FDG PET/CT had higher sensitivity, but

lower specificity in detecting LNs metastases on a per-patient analysis, and performed only slightly better than standard PET/CT on a per-lesion basis. On the contrary, in a retrospective study on cervical, endometrial, and ovarian cancer patients, Nogami *et al.* reported that DTP ^{18}F-FDG PET/CT only significantly improved the specificity for detection of LN metastases, but also concluded that DTP scanning had an unsatisfactory impact on the overall diagnostic efficacy for LN metastasis. [9] Regarding the semi-quantitative analysis, a SUV_{max} value greater than 1.88 was considered the optimal cut-off point on delayed PET/CT providing a same sensitivity and specificity as standard [8]F-FDG PET/CT images. Concerning the RI, prior studies reported that the RI might improve the accuracy of DTP ^{18}F-FDG PET/CT in gynaecological cancer for detecting LN metastases. [9, 25] In the present study, we found that a RI of greater than 0% was the optimal cut-off point for nodal evaluation because it improved the specificity (80% for RI on delayed exam compared to 77.8% for SUV_{max} on standard PET/CT $p = 0.8$) but did not improve the sensitivity (95.2% in both cases). Our study suffered some limitations. First, the population was relatively small, but in accordance with the incidence of VC (2.4/100000 inhabitants per year). [1] Second, the patients were scanned on two different scanners in our department and this could have minimally affected the SUV homogeneity; [26, 27] however, only 11 patients were scanned on a different scanner. Third, the cut-off value of SUV_{max} and RI in this study was based on the data collected at our institute alone, and the absolute value of SUV_{max} might vary somewhat according to different imaging systems used at other institutions. However, this study has yet several strengths. First, it is, to our knowledge, the first prospective study to evaluate the comparison between standard and delayed scan using qualitative and semi-quantitative analysis. Second, it evaluates only patients who underwent surgery shortly after PET/CT, in order to compare PET/CT results with histopathologic findings.

CONCLUSION

In the light of our results, standard ^{18}F-FDG PET/CT has high sensitivity and NPV in detecting groin lymph node metastases in VC patients. This confirms that standard ^{18}F-FDG PET/CT represents an effective preoperative imaging method for LN staging in VC, allowing better planning of groin surgical procedures and selection of patients potentially suitable for minimally invasive surgery. However, delayed PET/CT has not significantly been able to improve the specificity and the PPV in our study. Larger studies are needed to further validate our results.

REFERENCES

1. Howlader N, Noone AM, Krapcho M, *et al.* SEER Cancer Statistics Review, 1975-2013, National Cancer Institute. Bethesda, MD. http://seer.cancer.gov/csr/1975_2013/ Update April 2016.

2. Hacker NF. Vulvar cancer. In: Berek JS, Hacker NF, eds. Practical gynecologic oncology. 4th ed. Philadelphia: Williams &Wilkins; 2005. p. 585–602.

3. Homesley HD, Bundy BN, Sedlis A, Yordan E, Berek JS, Jahshan A, *et al.* Assessment of current international federation of gynecology and obstetrics staging of vulvar carcinoma relative to prognostic factors for survival (a gynecologic oncology group study). Am J Obstet Gynecol. 1991;164(4):997-1003.

4. Burger MP, Hollema H, Emanuels AG, Krans M, Pras E, Bouma J. The importance of the groin node status for the survival of T1 and T2 vulval carcinoma patients. Gynecol Oncol. 1995;57(3):327-34.

5. Lai CH, Lin G, Yen TC, Liu FY. Molecular imaging in the management of gynecologic malignancies. Gynecol Oncol. 2014;135(1):156-62.

6. Koh WJ, Greer BE, Abu-Rustum NR, Campos SM, Cho KR, Chon HS, *et al.* Vulvar Cancer, Version 1.2017, NCCN Clinical Practice Guidelines in Oncology. J Natl Compr Canc Netw. 2017;15(1):92-120.

7. Cohn DE, Dehdashti F, Gibb RK, Mutch DG, Rader JS, Siegel BA, *et al.* Prospective evaluation of positron emission tomography for the detection of groin node metastases from vulvar cancer. Gynecol Oncol. 2002;85(1):179-84.

8. Lin G, Chen CY, Liu FY, Yang LY, Huang HJ, Huang YT, *et al.* Computed tomography, magnetic resonance imaging and FDG positron emission tomography in the management of vulvar malignancies. Eur Radiol. 2015;25(5):1267-78.

9. Nogami Y, Banno K, Irie H, Iida M, Masugi Y, Murakami K, *et al.* Efficacy of 18-FDG PET-CT dual-phase scanning for detection of lymph node metastasis in gynecological cancer. Anticancer Res. 2015;35(4):2247-53.

10. Cheng G, Torigian DA, Zhuang H, Alavi A. When should we recommend use of dual time-point and delayed time-point imaging techniques in FDG PET? Eur J Nucl Med Mol Imaging. 2013;40(5):779-87.

11. Giammarile F, Bozkurt MF, Cibula D, Pahisa J, Oyen WJ, Paredes P, *et al.* The EANM clinical and technical guidelines for lymphoscintigraphy and sentinel node localization in gynaecological cancers. Eur J Nucl Med Mol Imaging. 2014;41(7):1463-77.

12. Treglia G, Calcagni ML, Rufini V, Leccisotti L, Meduri GM, Spitilli MG, *et al.* Clinical significance of incidental focal colorectal (18)F-fluorodeoxyglucose uptake: our experience and a review of the literature. Colorectal Dis. 2012;14(2):174-80.

13. Miller TR, Grigsby PW. Measurement of tumor volume by PET to evaluate prognosis in patients with advanced cervical cancer. Int J Radiat Oncol Biol Phys. 2002;53(2):353-9.

14. Kitajima K, Suenaga Y, Ueno Y, Maeda T, Ebina Y, Yamada H, *et al.* Preoperative risk stratification using metabolic parameters of (18)F-FDG PET/CT in patients with endometrial cancer. Eur J Nucl Med Mol Imaging. 2015;42(8):1268-75.

15. Perry LJ, Guralp O, Al-Niaimi A, Zucker NA, Kushner DM. False positive PET-CT scan and clinical examination in a patient with locally advanced vulvar cancer. Gynecol Oncol Case Rep. 2013;4:29-31.

16. Kamran MW, O'Toole F, Meghen K, Wahab AN, Saadeh FA, Gleeson N. Whole-body [18F]fluoro-2-deoxyglucose positron emission tomography scan as combined PET-CT staging prior to planned radical vulvectomy and inguinofemoral lymphadenectomy for squamous vulvar cancer: a correlation with groin node metastasis. Eur J Gynaecol Oncol. 2014;35(3):230-35.

17. Dolanbay M, Ozcelik B, Abdulrezzak U, Serin IS, Kutuk MS, Uludag S. F-18 fluoro-D-glucose (FDG)-positron emission tomography (PET)/computed tomography (CT) in planning of surgery and sentinel lymph node screening in vulvar cancers. Arch Gynecol Obstet. 2016;293(6):1319-24.

18. Kubota R, Kubota K, Yamada S, Tada M, Ido T, Tamahashi N. Microautoradiographic study for the differentiation of intratumoral macrophages, granulation tissues and cancer cells by the dynamics of fluorine-18-fluorodeoxyglucose uptake. J Nucl Med. 1994;35(1):104-12.

19. Zhuang H, Pourdehnad M, Lambright ES, Yamamoto AJ, Lanuti M, Li P, *et al.* Dual time point 18F-FDG PET imaging for differentiating malignant from inflammatory processes. J Nucl Med. 2001;42(9):1412-7.

20. Hamberg LM, Hunter GJ, Alpert NM, Choi NC, Babich JW, Fischman AJ. The dose uptake ratio as an index of glucose metabolism: useful parameter or oversimplification? J Nucl Med. 1994;35(8):1308-12.

21. Shen G, Deng H, Hu S, Jia Z. Potential performance of dual-time-point 18F-FDG PET/CT compared with single-time-point imaging for differential diagnosis of metastatic lymph nodes: a meta-analysis. Nucl Med Commun. 2014;35(10):1003-10.

22. Yen RF, Chen KC, Lee JM, Chang YC, Wang J, Cheng MF, *et al.* 18F-FDG PET for the lymph node staging of non-small cell lung cancer in a tuberculosis-endemic country: is dual time point imaging worth the effort? Eur J Nucl Med Mol Imaging. 2008;35(7):1305-15.

23. Umeda Y, Demura Y, Morikawa M, Ameshima S, Tsuchida T, Fujibayashi Y, *et al.* Prognostic value of dual-time-point 18F-fluorodeoxyglucose positron emission tomography in patients with pulmonary sarcoidosis. Respirology. 2011;16(4):713-20.

24. Cloran FJ, Banks KP, Song WS, Kim Y, Bradley YC. Limitations of dual time point PET in the assessment of lung nodules with low FDG avidity. Lung Cancer. 2010;68(1):66-71.

25. Ma SY, See LC, Lai CH, Chou HH, Tsai CS, Ng KK, *et al.* Delayed (18)F-FDG PET for detection of paraaortic lymph node metastases in cervical cancer patients. J Nucl Med. 2003;44(11):1775-83.

26. Boellaard R, Delgado-Bolton R, Oyen WJ, Giammarile F, Tatsch K, Eschner W, *et al.* FDG PET/CT: EANM procedure guidelines for tumour imaging: version 2.0. Eur J Nucl Med Mol Imaging. 2015;42(2):328-54.

27. Boellaard R. Standards for PET image acquisition and quantitative data analysis. J Nucl Med. 2009;50(1):11S-20S.

PART IV

DISCUSSION
AND
FUTURE PERSPECTIVES

NOVEL FRONTIERS OF DEDICATED MOLECULAR IMAGING IN BREAST CANCER DIAGNOSIS

adapted from:

A Collarino
V Fuoco
LM Pereira Arias-Bouda
AM Sánchez
LF de Geus-Oei
R Masetti
RA Valdés Olmos

CHAPTER 10

ABSTRACT

Breast cancer (BC) is the most common cancer in women worldwide. In the last years, the contribution of nuclear medicine has grown, based on the use of dedicated molecular breast devices for diagnosis and biopsy. Recent technical improvements have been achieved in order to increase the detection of smaller breast lesions using lower doses of radiotracers as well as to facilitate accurate biopsy sampling. Furthermore, new prototypes have been developed combining anatomic and functional imaging. Although the gamma-emitting ^{99m}Tc-sestamibi (^{99m}Tc-MIBI) and the positron-emitting ^{18}F-fluorodeoxyglucose (^{18}F-FDG) are the most widely used radiotracers, several new and more specific tracers for BC proliferation, angiogenesis and tumour receptor status have been investigated. Dedicated molecular breast devices have been introduced as an adjunct imaging tool to mammography and ultrasound in the clinical workup for BC. Additionally, due to the increased interest in molecular tumour subtype analysis and ribonucleic acid (RNA)-based gene expression profiling tests in the routine clinical practice, a possible new clinical application of dedicated molecular breast imaging concerns locally advanced breast cancer, principally in order to visualise intra-tumoural metabolic heterogeneity enabling selection of areas with highest tracer uptake (vital tissue) for core needle biopsy. Hence, it will be possible to more adequately tailor the individual treatment, also enabling therapy response monitoring. This review evaluates the current and future perspectives as well as the shortcomings of molecular breast imaging using dedicated nuclear medicine devices.

GENERAL INTRODUCTION

Breast cancer (BC) is the most common tumour in women worldwide, with an estimated 252,710 cases and 40,610 deaths in the United States, in 2017. [1] Currently, mammography (MG) is the primary screening test for BC. [2] However, MG has a limited ability to detect breast lesions in women with dense breasts. [3] Since the detection of BC in an early stage is associated with better prognosis, [4] other imaging modalities have been introduced as complementary tools to MG. [2] Indeed, magnetic resonance imaging (MRI) is recommended for BC screening in high-risk women. [5-7] However, this procedure is limited in patients with obesity, claustrophobia, presence of implanted devices and renal insufficiency. [8] In the last years, there has been an increasing interest towards nuclear medicine imaging techniques that enable the visualisation of malignant functional changes in the breast tissue. Several dedicated molecular imaging devices, including both single-photon and positron emission-based systems, are nowadays used as adjunct modalities to improve the detection of breast malignancies. [9] Until now the main approach using dedicated molecular breast imaging (MBI) has been oriented to the complementary aspects provided by this modality for assessing extent of primary disease in patients with newly diagnosed BC and for problem solving, especially in patients with very dense breasts. [10] However, a new area of interest has recently been delineated on the basis of the potential visualisation of heterogeneity in locally advanced breast cancer (LABC). In this respect, and thanks to a better resolution, dedicated molecular breast imaging devices appear to be more suitable than conventional tomographic imaging (PET/CT, SPECT/CT) opening a new diagnostic window for tumour characterization and biopsy. [11] In this review we discuss these advances in dedicated breast imaging with an emphasis on recently introduced dedicated devices and radiotracers.

DEDICATED NUCLEAR MEDICINE BREAST IMAGING

In **Table 1** the characteristics of some commercially available dedicated breast imaging devices are summarised.

MOLECULAR BREAST IMAGING

The terminology MBI is habitually used to refer to dedicated breast devices based on the use of single-photon emitting radiotracers like ^{99m}Tc-sestamibi (^{99m}Tc-MIBI). [12]

One of the first devices using MBI technology was a single detector system known as breast-specific gamma-imaging (BSGI) developed by Dilon Technologies (Newport News, Virginia, US). [13] More recently, dual-head detector MBI systems like Discovery NM750b and LumaGem 3200s were introduced by GE Healthcare (Milwaukee, Wisconsin, US) and by Gamma Medica, Inc. (Northridge, California, US), respectively. [14] All these devices are generically included in the MBI modality using a positioning similar to that of MG. In particular, the breast is placed between a compression paddle and the detector for BSGI or between two detectors when using the MBI device. The advantages of single-head configuration (BSGI) are lower costs and the possibility to perform a biopsy using an available complementary tool. [15, 16] The advantages of dual-head configuration (MBI) are higher spatial resolution and therefore a potentially higher detection rate of small breast tumours and the possibility to use lower injected doses of ^{99m}Tc-MIBI. [17, 18] The clinical protocol consists of an IV administration of the radiotracer (740–1.100 MBq ^{99m}Tc-MIBI for single-head or 150-300 MBq for dual-head systems) into the arm contralateral to the breast lesion. Image acquisition starts 5–10 min after injection of the radiotracer and includes acquisitions of 8-10 min in both craniocaudal (CC) and mediolateral oblique (MLO) projections of each breast (**Figure 1**), with a duration of approximately 40 min in total per study. [19] Since for MBI positioning is analogous to that of MG, nuclear medicine technologists need to receive an additional training in mammographic positioning. MBI images are interpreted according to a functional BI-RADS classification lexicon. [19, 20] Sun *et al.* reported a meta-analysis including a total of 19 studies on clinical usefulness of MBI for diagnosis of BC. The authors showed pooled sensitivity of 95% (95% confidence interval [CI], 93%-96%) and pooled specificity of 80% (95% CI, 78%-82%) for detecting BC, including eight studies and 2183 lesions. [21] MBI examinations are well tolerated by patients, no preparation (e.g. fasting) is required and the acquisition is performed in a comfortable upright position of the patient. Nevertheless, MBI examinations require ionizing radiation. Newest MBI devices allow a reduced administered dose of 150–300 MBq ^{99m}Tc-MIBI [18] resulting in an effective whole body dose of 1.2–2.4 mSv. [22]

Table 1. Summary of characteristics of some commercially available dedicated breast imaging devices

Device	Design	Detector type	FOV (cm)	3D	Modality used for image correlation	Patient positioning	Breast compression	Biopsy possibility
Dilon 6800 (Dilon Technologies)	Single flat panel	NaI	20 x 15	No	MG	Seated	Yes	FDA-approved
Dilon 6800 Acella (Dilon Technologies)	Single flat panel	CsI	25 x 20	No	MG	Seated	Yes	FDA-approved
Discovery NM750b (GE Healthcare)	Dual flat panels	CZT	24 x16	No	MG	Seated	Yes	FDA-approved
LumaGEM 3200s (Gamma Medica)	Dual flat panels	CZT	20 x 16	No	MG	Seated	Yes	Not FDA cleared
PEM Flex Solo II (CMR Naviscan Corporation)	Dual flat panels	LYSO	24 x 16.4	Yes	MG	Seated	Yes	FDA-approved
Clear-PEM (Crystal Clear Collaboration)	Dual flat panels rotating	LYSO	16.2 x 14.1	Yes	MRI	Prone	Yes	Not known
O-scanner (Shimadzu Medical Systems)	Three full rings	LGSO	18 [d], 15.5 [a]	Yes	MRI	Prone	No	Not known
C-scanner (Shimadzu Medical Systems)	Two partial rings	LGSO	17.9 [d], 10.5 [a]	Yes	MRI	Semi-prone	No	Not known
MAMMI-PET (Oncovision)	Single full ring	LYSO	17 [d], 4 [a]	Yes	MRI	Prone	No	Prototype
MAMMI-PET (Oncovision)	Double full rings	LYSO	17 [d], 9.4 [a]	Yes	MRI	Prone	No	Prototype

FOV field-of-view, 3D three dimensional, BI-RADS Breast Imaging Reporting and Data System, NaI sodium iodide, MG mammography, FDA Food and Drug Administration, CsI cesium iodide, CZT cadmium zinc telluride, LYSO lutetium-yttrium oxyorthosilicate, MRI magnetic resonance imaging, LGSO lutetium gadolinium oxyorthosilicate, [d] diameter, [a] axial FOV length.

POSITRON EMISSION MAMMOGRAPHY

Positron emission mammography (PEM) is a dedicated breast imaging device, commercially introduced by CMR-Naviscan Corporation (Carlsbad, California, US), based on the use of positron-emitting radiopharmaceuticals like ^{18}F-fluorodeoxyglucose (^{18}F-FDG). PEM uses two flat detectors with mild compression of the breast and the patient in seated position. The PEM images are comparable to CC and MLO projections of MG. [23] Unlike whole body positron emission tomography combined with computed tomography (PET/CT), PEM allows the detection of small breast lesions using lower ^{18}F-FDG doses with shorter acquisition times. [24] The clinical PEM imaging protocol includes an IV injected dose of ^{18}F-FDG (approximately 370 MBq) into an antecubital vein contralateral to the breast lesion. Prior to ^{18}F-FDG injection, all patients have to fast for at least 4-6 hours and the blood glucose level has to be below 200 mg/dL. Images are acquired 60–120 min after radiotracer injection and require approximately 20 min per breast (10 min per CC and 10 min per MLO views). [25] PEM images are interpreted according to a functional BI-RADS classification. [26] The sensitivity of PEM has been found to be 93% for known index lesions as small as 3 mm. Although this sensitivity is comparable to MRI, specificity of PEM is higher than MRI
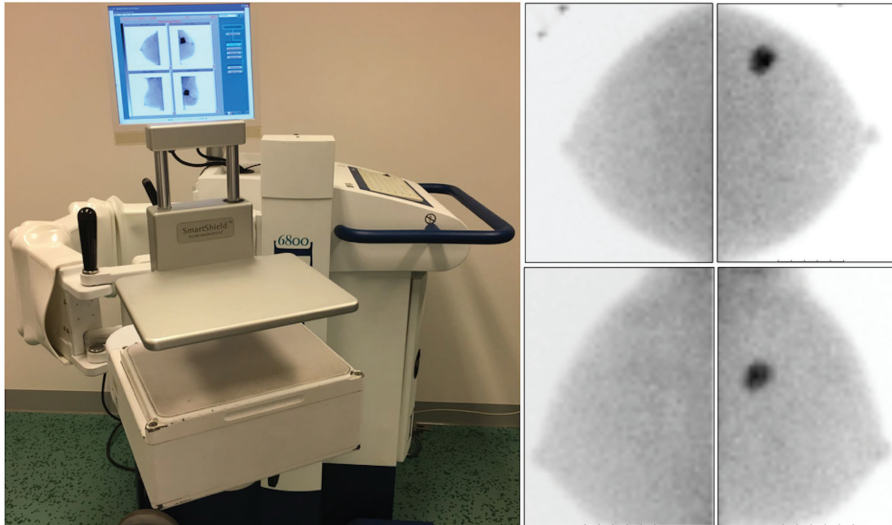
Figure 1. Breast-specific gamma-imaging (BSGI) device with in foreground the gamma-camera detector and a compression paddle to immobilise the breast during image acquisition (on the left). BSGI craniocaudal (top) and latero-oblique (bottom) images of both breasts in a 49-year-old woman showing an invasive ductal carcinoma (diameter of 18 mm) in the left breast (on the right).

(74% vs 48%) for the identification of lesions. [27] A meta-analysis evaluating 8 studies and 873 patients showed pooled sensitivity and specificity for PEM of 85% (95% CI, 83%-88%) and 79% (95% CI, 74%-83%), respectively. [28] Advantages of PEM in comparison to PET/CT are in depicting small lesions as well as the possibility to perform breast biopsies using a special module. [29] Despite the radiation exposure, PEM is considered an alternative tool in case of contraindications for MRI like obesity, claustrophobia, presence of implanted devices and renal insufficiency.

DEDICATED BREAST PET DEVICES

MAMmography with Molecular Imaging (MAMMI)-PET is a new breast dedicated PET system. MAMMI-PET is manufactured by Oncovison (Valencia, Spain) with a single or double full ring of detectors for tomographic image reconstruction with high resolution (1.6 mm). MAMMI-PET does not require compression of the breast; actually the patient is positioned in prone position with hanging breast [30, 31] as illustrated in **Figure 2**.

Although there are few studies on MAMMI-PET, this device enables the visualisation of small tumours as well as tumours with heterogeneous ^{18}F-FDG uptake. [11, 32] In an extensive evaluation including 234 index lesions of at least 5 mm size in BC patients, MAMMI-PET was found to be

Figure 2. MAMMI-PET device for breast imaging with patient in prone position (on the left) with hanging breast configuration thanks to the special bed and ring camera (middle). On the right, internal view of the scanner showing a version with a single (top) and a double (bottom) full ring of detectors.

more sensitive than standard PET/CT for lesions within the field-of-view (FOV). [33] Similar to other dedicated breast imaging devices, [23] proper positioning of the breast is essential for MAMMI-PET examinations and some difficulties of the device to visualise breast lesions located close to the pectoralis muscle have been reported causing the need of a technical optimisation of the bed for prone patient positioning. [33] The MAMMI-PET protocol provides an IV administration of the radiotracer (180-240 MBq of ^{18}F-FDG) according to the body mass index. Images are obtained 60–120 min after the radiotracer injection with an acquisition time of approximately 5–15 min per breast depending on the breast size and type of device used (single or double ring). [11] The use of standardised terminology to report MAMMI-PET images has not been defined yet. One of the advantages of MAMMI-PET is the ability to perform semi-quantitative analysis by measuring the standardised uptake value (SUV). Compared to the whole body PET/CT, MAMMI-PET offers lower doses as well as shorter acquisition times. Recently, another dedicated breast PET (dbPET) device, known as O-scanner (Shimadzu, Kyoto, Japan) has been developed. [34] This device consists of 36 detector modules arranged in three contiguous full rings with an estimated spatial resolution of 1.5 mm at the centre of FOV. Working protocols using O-scanner are comparable to the MAMMI-PET but acquisition times are shorter due to a transaxial effective FOV of 180 mm. Nishimatsu *et al.* have evaluated the diagnostic performance of O-scanner compared to whole body PET/CT including 179 index BC lesions in 150 patients. Based on pathological findings, the authors did not find a significant difference between both devices in terms of sensitivity per patient nor per lesion (95% and 92% for O-scanner vs 95% and 88% for PET/CT, respectively). However, tumour-to-background ratios were significantly higher for O-scanner increasing levels of confidence in the diagnosis by observers thanks to higher tumour conspicuousness.

The same group of investigators also evaluated a dbPET with an open end through which the patient's arms can be placed. This device known as C-scanner, consists of 24 detector blocks arranged in two contiguous rings. Its evaluation in 159 women showed a lesion-based sensitivity of 81.1% increasing to 93% when lesions outside the FOV of the system were excluded. [35]

CURRENT INDICATIONS

Currently, dedicated nuclear breast imaging is considered an imaging tool complementary to MG and ultrasound (US) in patients with the following conditions: **a)** with newly diagnosed BC to exclude multicentric, multifocal or contralateral disease and to assess response to neoadjuvant chemotherapy; **b)** with suspected recurrence, especially when previous malignancy is occult on MG and US; **c)** with indeterminate breast lesions and remaining diagnostic concerns; **d)** with technically difficult breast imaging like dense breast tissue, prosthesis; **e)** with contraindication for MRI like obesity, claustrophobia, presence of implanted devices, renal insufficiency. [19]

DEDICATED BREAST DEVICES FOR RADIOGUIDED BIOPSY

In addition to dedicated breast imaging various complementary tools using radioguidance for lesion localisation and vacuum-assisted biopsy have recently been developed.

MBI-GUIDED BIOPSY

MBI-guided biopsy is a tool based on the use of ^{99m}Tc-MIBI as guiding radiotracer. One of the first developed devices (GammaLoc®, Dilon Technologies, Newport News, US) has been validated and approved by the U.S. Food and Drug Administration (FDA) in 2009 for complementary use with the BSGI camera. The tool is equipped with a small, single-head detector with a slant-hole collimator for dedicated stereotactic localisation (**Figure 3**). The patient is in seated position and the breast is mildly compressed between the grid paddle and the detector. The biopsy protocol is based on a 5-step procedure: **a)** scout image and two stereotactic images (± 20 degree angle) are obtained to determine the positioning of the lesion; **b)** the software measures the index lesion coordinates; **c)** the trocar needle is placed into the breast; **d)** subsequently, the verification of the correct needle placement is performed using Cerium-139 (^{139}Ce) as source; **e)** this is followed by the biopsy using vacuum-assisted device (VAD), a clip marker is placed at the biopsy site, a post-biopsy specimen scan is performed to confirm adequate biopsy specimens and post-biopsy MG is acquired to evaluate the placing of clip.[16] Recently, the first clinical study has been performed including 38 patients (38 lesions). This biopsy tool was technically successful in all ^{99m}Tc-MIBI avid lesions. Indeed, all biopsy samples were radioactive and proved adequate for histopathology analysis. The mean procedure time was 71 min (range, 44-112 min). All biopsy procedures were well-tolerated by patients with
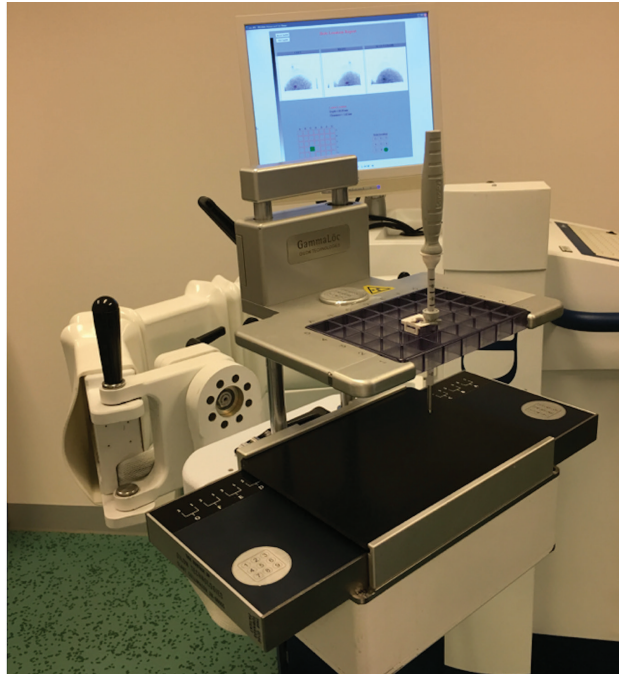
Figure 3. Biopsy device for complementary use with the BSGI device now equipped with a grid paddle for both breast immobilization and vacuum-assisted biopsy. For calculation of the depth of the primary breast lesion two stereotactic images are acquired using a slant-hole collimator placed oppositely to the biopsy device.

merely two hematomas and three vasovagal reactions. Based on these results, this new biopsy tool appears to be technically feasible to obtain accurate radioactive samples.[36] However, further studies are needed to investigate the role of this device in the clinical workup.

PEM-GUIDED BIOPSY

PEM-guided biopsy is a biopsy device using principally ^{18}F-FDG as radiotracer. This device has been validated in 2001 and has been approved by FDA in 2008. [37] PEM-guided biopsy is a portable and compact device comprising two plate PET detectors and stereotactic technology (Stereo Navigator™ Naviscan, Carlsbad, California, US) to calculate the coordinates of the breast lesion. The patient is in seated position and the breast is placed between both PET detectors with mild compression. The biopsy procedure involves five steps as follows: **a)** initial biopsy scan to identify and target the lesion; **b)** alignment scan to verify the correct position of the needle using Germanium-68 (^{68}Ge) as line source; **c)** pre-biopsy scan to confirm the correct positioning with biopsy needle in the breast; **d)**

post-biopsy scan to ensure appropriate lesion is removed and **e)** specimen scan to confirm adequate biopsy specimens. Post-biopsy MG is performed to ensure that clip placement corresponds with the biopsy site. [29] To date, one multicentre study has been performed including 19 patients (24 lesions) showing that this biopsy device proved technically successful in all cases and was well-tolerated by patients. The authors reported a median procedure time of 32 min (range, 19-119 min), and 14 of 24 (58%) biopsied lesions were smaller than 10 mm. [29] Based on these results, PEM-guided biopsy appears to be a promising biopsy tool for ^{18}F-FDG-avid breast lesions. In particular, this device allows re-imaging of the biopsied breast and biopsy sampling to ensure adequate biopsy without injection of an additional radiotracer. Recently, Argus *et al.* evaluated the feasibility of performing diagnostic PEM and PEM-guided biopsy on the same day, including 20 patients (27 lesions). The authors showed that it is possible for most patients (24 of 27 lesions) reducing radiation dose for both patient and medical staff. [38]

MAMMI-GUIDED BIOPSY

Recently, a semi-robotized system for MAMMI-guided biopsy tool was developed in the context of the European Union FP7-SME-2013-606017 MAMMOcare project and has technically been validated in 2017. [39] This biopsy tool comprises a dedicated dual-ring PET-detector with automated lesion localisation software together with a vacuum-assisted biopsy needle attached to a robot-controlled arm (**Figure 4**).

The patient is in prone position and the breast is placed in the opening of the device without compression (hanging freely). The biopsy procedure requires five steps. **a)** First, acquisition of the whole hanging breast with closed PET-ring is acquired to determine the index lesion coordinates, afterward the system automatically calculates the shortest needle trajectory and subsequently positions the biopsy needle in that trajectory. **b)** Second, scanning with the closed PET-ring and mild compression is obtained including only the part of breast with the index lesion. This step aims to adjust the new index lesion coordinates due to breast compression. **c)** Third step involves placing a biopsy needle into the index lesion, with the affected breast in compression and opened PET-ring. **d)** A new acquisition is performed with needle in place to verify the correct needle position in the index lesion. **e)** Finally, biopsy is performed manually using VAD. Based on phantom experiment, the estimated time per lesion is approximately 30 min. [39] Until now, only a technical evaluation has been performed showing an accuracy of 0.5, 0.6 and 0.4 mm for the x/y/z-axes. The system has been developed to optimize both conventional histopathology and ribonucleic acid (RNA)-based molecular diagnostics but no clinical study has yet been reported in the current literature.
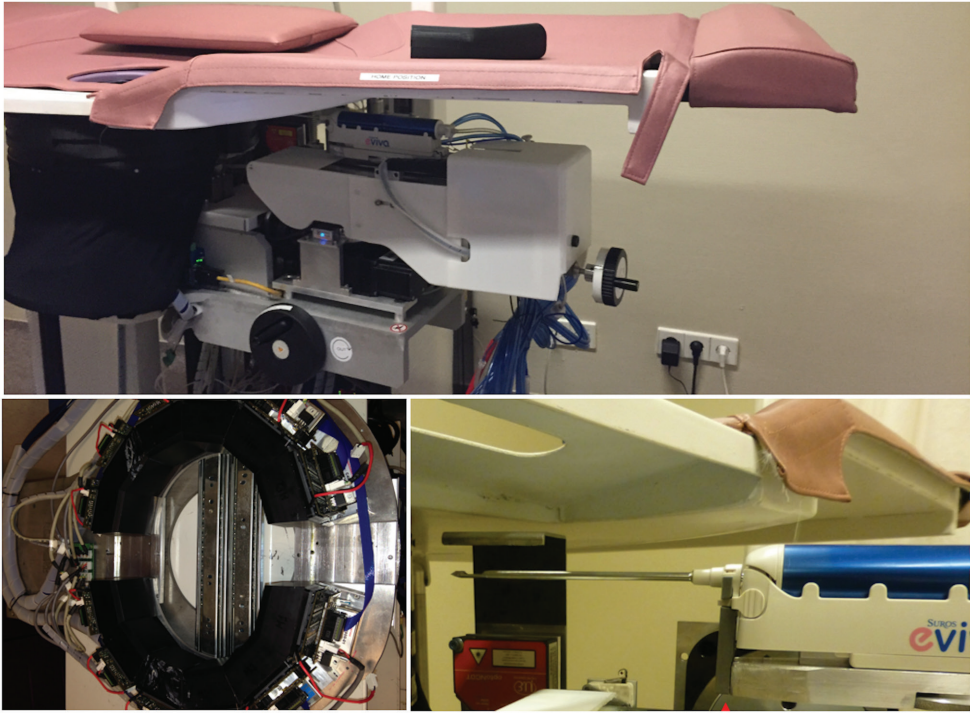
Figure 4. Prototype of the MAMMOcare device composed of a special bed for prone position of the patient, a PET-ring detector for image acquisition and a semi-robotized arm for vacuum-assisted biopsy (top). For biopsy, the PET-ring moves from a closing stand to an opening one (bottom on the left) facilitating introduction of the needle (bottom on the right).

FUTURE APPLICATIONS

TARGET BIOPSY AND PRECISION BREAST CANCER MEDICINE

In the last years, the interest toward molecular analysis in routine practice has increased, incorporating assessments of various genetic alterations and tumour gene expression profiles. Several specific molecular tests have been developed for breast tumours. [40, 41] Among them, MAMMAPrint (Agendia, Amsterdam, The Netherlands) test measures the expression of 70 genes through microarray analysis [42] for predicting the risk tumour for recurrence and for better selecting patients for adjuvant chemotherapy. [43] Therefore, the goal of breast biopsy is to obtain an adequate sampling not only for increasing likelihood of finding tumour tissue, but also for

assessing the tumour subtype and genetic expression profile. This will facilitate stratifying patients and planning target-specific therapies in the context of a recently introduced concept of precision medicine in breast cancer. [44] Buyse *et al.* reported that only 81% of the tumour samples obtained with US-guided biopsy contained sufficient RNA for genetic analysis. [45] Radioguided biopsy offers the possibility to obtain radioactive tumour samples that correspond with vital tumour areas clear of both necrotic and stromal tissue. Therefore, radioguided biopsy may be able to obtain sufficient RNA in the sampling useful for genetic expression profiles based on the principle of radiotracer uptake that associates areas with higher ^{18}F-FDG uptake with those parts of the tumour with increased glycolysis, representing the most proliferative parts of the tumour. As reported in the literature, high ^{18}F-FDG uptake of the primary tumour is associated with poor prognostic features such as grade 3 and triple negative BC. [46, 47] A similar working model is assumable using ^{99m}Tc-MIBI which also shows a positive association between the level of tracer uptake in breast tumours and the amount of viable tumour tissue. Hence, the possibility for biopsy of the most proliferative part of the tumour may increase the accuracy of tumour sampling for genetic analysis, and consequently lead to better individual treatment planning with possible improvement of patient outcome.

This new clinical possibility for targeted biopsy using radioguidance was the rationale behind the design of the precision biopsy device described in the above mentioned MAMMOcare project. This may be of interest in locally advanced breast cancer, principally in tumours with heterogeneous uptake (**Figure 5**) enabling selection of those areas with highest tracer uptake, avoiding sampling of necrotic or fat tissues. Indeed, Koolen *et al.* reported non-correspondence of ≥ 2 cm between the core biopsy location indicated with a marker and the tumour area with highest ^{18}F-FDG uptake in 28 (14%) of 203 tumours in stage II and III BC. [48] Further studies are needed to evaluate the feasibility of this potential application.

USE OF NEW RADIOTRACERS FOR MBI, PEM, MAMMI

^{99m}Tc-MIBI and ^{99m}Tc-tetrofosmin are currently used as gamma-emitting radiotracers to detect BC. ^{99m}Tc-MIBI is the preferred radiotracer for MBI due to its uptake inside mitochondria, [49] thus reflecting mitochondrial activity and electric transmembrane potential of breast cancer cells. [50, 51] ^{99m}Tc-tetrofosmin is similar to ^{99m}Tc-MIBI with localisation mostly within cytosol. [49, 52, 53] Another potential gamma-emitting radiotracer is ^{99m}Tc-maraciclatide, also known as ^{99m}Tc-NC100692,

which is an angiogenesis marker. Indeed, ^{99m}Tc-maraciclatide binds to receptors of integrins, such as αvβ3, which are significantly upregulated in endothelial cells during angiogenesis. [54] In a series evaluating 39 patients ^{99m}Tc-maraciclatide showed comparable lesion uptake to ^{99m}Tc-MIBI in both malignant and benign breast lesions. [55] Furthermore, as shown in **Table 2**, there are new radiotracers like ^{99m}Tc-annexin V for apoptosis, [56] ^{99m}Tc-bombesine for gastrin-releasing peptide receptor [57] and ^{123}I-labeled estrogen receptor ligand.[58]

Regarding the positron-emission radiotracers, ^{18}F-FDG is the most used in BC. ^{18}F-FDG is a glucose analogue, and so it is used for assessing the metabolism of breast tumour cells. In the last years, several new radiotracers (as shown in **Table 2**) have been developed: **a)** ^{18}F-fluoromisonidazole (^{18}F-FMISO) as a marker of tumour hypoxia, **b)** ^{18}F-fluorothymidine (^{18}F-FLT) reflecting cell proliferation, **c)** ^{18}F-galacto-recognizing arginine-glycine-aspartatic acid (^{18}F-Galacto-RGS) as an angiogenesis tracer, **d)** ^{18}F-annexin as an apoptosis radiotracer, **e)** radiopharmaceuticals with receptor affinity like ^{18}F-fluoroestradiol (^{18}F-FES) for tumour estrogen receptor (ER), ^{18}F-fluoro furanyl norprogesterone (^{18}F-FFNP) for progesterone receptor (PR), and [89]Zr-trastuzumab for human epidermal growth factor receptor 2 (HER2). [59]
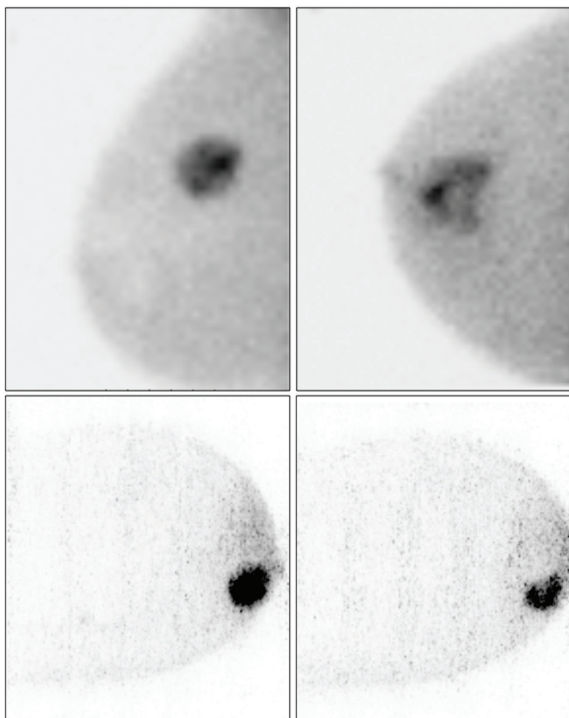
Figure 5. Above, heterogeneous uptake of ^{99m}Tc-MIBI in invasive ductal breast carcinoma with a 3 cm lesion (on the left) and a 5 cm lesion (on the right) as shown using breast-specific gamma-imaging. Below, in another patient uptake heterogeneity of ^{18}F-FDG is seen after the first cycle of neoadjuvant chemotherapy in the superior part of the lesion (on the right), which was homogenous at baseline acquisition (on the left) with a dedicated hanging breast PET scanner.

Table 2. Some existing and potential radiotracers for dedicated molecular breast imaging

Radiotracer	Type of emission	Functional information (uptake mechanism)
^{99m}Tc-MIBI	Single-photon	Mitochondrial uptake
[99m]Tc-maraciclatide	Single-photon	Angiogenesis
[99m]Tc-annexin V	Single-photon	Apoptosis
[99m]Tc-bombesine	Single-photon	Binding to BN receptor
[123]I-labeled Z-MIVE	Single-photon	Binding to ER
^{18}F-FDG	Positron	Glucose metabolism
^{18}F-FMISO	Positron	Hypoxia
^{18}F-FLT	Positron	Proliferation
[18]F-Galasco-RGS	Positron	Angiogenesis
[18]F-annexin	Positron	Apoptosis
^{18}F-FES	Positron	Binding to ER
^{18}F-FFNP	Positron	Binding to PR
[89]Zr-trastuzumab	Positron	Binding to HER2

[99m]**Tc-MIBI** Technetium 99m- methoxyisobutylisonitrile, **BN** growth factor bombesin, [123]**I-labeled Z-MIVE** Iodine 123 labelled *cis*-11β-methoxy-17α-iodovinyl oestradiol, **ER** estrogen receptor, [18]**F-FDG** ^{18}F-fluorodeoxyglucose, [18]**F-FMISO** ^{18}F-fluoromisonidazole, [18]**F-FLT** ^{18}F-fluorothymidine, [18]**F-Galacto-RGS** ^{18}F-galacto-recognizing arginine-glycine-aspartatic acid, [18]**F-FES** ^{18}F-fluoroestradiol, [18]**F-FFNP** ^{18}F-fluoro furanyl norprogesterone, **HER2** human epidermal growth factor receptor 2.

DEDICATED HYBRID SYSTEM

Another important advance in breast cancer imaging is the development of dedicated hybrid devices combining anatomic and functional imaging. Various prototypes concerning these hybrid systems have been introduced in recent years.

DUAL-MODALITY BREAST TOMOSYNTHESIS

One of the new hybrid scanners is dual-modality breast tomosynthesis (DMT), which involves the digital x-ray detector and an MBI detector. Both detectors rotate around a common axis with mild breast compression. [60] DMT provides co-registered anatomic and functional breast images in three dimensions (3D). Although the results of the pilot studies are encouraging, further clinical studies are necessary to optimise patient positioning and the acquisition protocol as well as to assess the additional value of this device relative to its separate modalities. [60]

DEDICATED BREAST SPECT/CT

Recently, a new dedicated hybrid system was developed using single photon emission computed tomography combined with low-dose CT technology (breast SPECT/CT). [61] Compared to planar devices, dedicated breast SPECT/CT enables 3-dimentional (3D) imaging, functional and anatomic fused images, no necessity for breast compression, making it more comfortable for the patients and with possibility to perform in vivo quantification of ^{99m}Tc-sestamibi uptake.

MBI/US SYSTEM

An integrated MBI/US prototype composed of an upper US mesh panel and a lower MBI detector was first introduced by O'Connor *et al.* in 2017. [62] An optical tracking system provides the real-time position of the US probe relative to the breast lesion. A software application enables projection of the US FOV onto the MBI images. Therefore, this prototype system allows integration of the anatomical US images with the functional MBI images. Hence, MBI/US may resolve positive findings on MBI that are occult on MG, as well as obtain a better lesion correlation between US and MBI. [62]

CONCLUDING REMARKS

The increasing use of dedicated devices for molecular imaging in breast cancer goes hand in hand with an evolution concerning their clinical applications. Based on the initial experience with these devices in detection of small breast lesions, there is a growing interest in studying the metabolic heterogeneity of locally advanced breast cancer, opening a future window for tumour characterization and selection of areas for biopsy. In the context of precision medicine, the contribution of dedicated breast cancer imaging using different radiotracers may become important not only to personalise therapeutic approaches on an individual basis, but also to monitor primary tumour response. Finally, the incorporation of allied technologies tends to gradually transform the current generation of dedicated nuclear medicine devices into hybrid systems with the ability to simultaneously evaluate the functional and morphological characteristics of breast cancer.

REFERENCES

1. Siegel RL, Miller KD, Jemal A. Cancer statistics, 2017. CA Cancer J Clin. 2017;67(1):7-30.
2. Gradishar WJ, Anderson BO, Balassanian R, et al. NCCN Clinical practice guidelines in oncology: breast cancer, version 2.2017. https://www.nccn.org/professionals/physician_gls/pdf/breast.pdf
3. Jackson VP, Hendrick RE, Feig SA, Kopans DB. Imaging of the radiographically dense breast. Radiology. 1993;188(2):297-301.
4. Chavez-MacGregor M, Mittendorf EA, Clarke CA, Lichtensztajn DY, Hunt KK, Giordano SH. Incorporating tumor characteristics to the American Joint Committee on cancer breast cancer staging system. Oncologist. 2017; In press.
5. Saslow D, Boetes C, Burke W, Harms S, Leach MO, Lehman CD et al. American Cancer Society guidelines for breast screening with MRI as an adjunct to mammography. CA Cancer J Clin. 2007;57(2):75-89.
6. Bevers TB, Anderson BO, Bonaccio E, Buys S, Daly MB, Dempsey PJ, et al. NCCN clinical practice guidelines in oncology: breast cancer screening and diagnosis. J Natl Compr Canc Netw. 2009;7(10):1060-96.
7. Sardanelli F, Boetes C, Borisch B, Decker T, Federico M, Gilbert FJ, et al. Magnetic resonance imaging of the breast: recommendations from the EUSOMA working group. Eur J Cancer. 2010;46(8):1296-316.
8. Berg WA, Blume JD, Adams AM, Jong RA, Barr RG, Lehrer DE, et al. Reasons women at elevated risk of breast cancer refuse breast MR imaging screening: ACRIN 6666.Radiology. 2010;254(1):79-87.
9. Hsu DF, Freese DL, Levin CS. Breast-dedicated radionuclide imaging systems. J Nucl Med. 2016;57(1): 40S-5S.
10. Berg WA. Nuclear breast imaging: clinical results and future directions. J Nucl Med. 2016;57(1):46S-52S.
11. Koolen BB, Vidal-Sicart S, Benlloch Baviera JM, Valdés Olmos RA. Evaluating heterogeneity of primary tumor (18)F-FDG uptake in breast cancer with a dedicated breast PET (MAMMI): a feasibility study based on correlation with PET/CT. Nucl Med Commun. 2014;35(5):446-52.
12. Hruska CB. Molecular breast imaging for screening in dense breasts: state of the art and future directions. AJR Am J Roentgenol. 2017;208(2):275-83.
13. Brem RF, Schoonjans JM, Kieper DA, Majewski S, Goodman S, Civelek C. High-resolution scintimammography: a pilot study. J Nucl Med. 2002;43(7):909-15.
14. Hruska CB, Phillips SW, Whaley DH, Rhodes DJ, O'Connor MK. Molecular breast imaging: use of a dual-head dedicated gamma camera to detect small breast tumors. AJR Am J Roentgenol. 2008;191(6):1805-15.
15. Kieper DA, Welch BL, Fairchild LH, inventors; Dilon Technologies, Inc., assignee. Gamma guided stereotactic localization system. US Patent US8249693. August 21, 2012.
16. Collarino A, Valdés Olmos RA, van der Hoeven AF, Pereira Arias-Bouda LM. Methodological aspects of (99m)Tc-sestamibi guided biopsy in breast cancer. Clin Transl Imaging. 2016;4(5):367-76.
17. Hruska CB, Weinmann AL, Tello Skjerseth CM, Wagenaar EM, Conners AL, Tortorelli CL, et al. Proof of concept for low-dose molecular breast imaging with a dual-head CZT gamma camera. Part II. Evaluation in patients. Med Phys. 2012;39(6):3476-83.
18. Long Z, Conners AL, Hunt KN, Hruska CB, O'Connor MK. Performance characteristics of dedicated molecular breast imaging systems at low doses. Med Phys. 2016;43(6):3062-70.
19. Goldsmith SJ, Parsons W, Guiberteau MJ, Stern LH, Lanzkowsky L, Weigert J, et al. SNM practice guideline for breast scintigraphy with breast-specific gamma-cameras 1.0. J Nucl Med Technol. 2010;38(4):219-24.
20. Conners AL, Hruska CB, Tortorelli CL, Maxwell RW, Rhodes DJ, Boughey JC, et al. Lexicon for standardized interpretation of gamma camera molecular breast imaging: observer agreement and diagnostic accuracy. Eur J Nucl Med Mol Imaging. 2012;39(6):971-82.
21. Sun Y, Wei W, Yang HW, Liu JL. Clinical usefulness of breast-specific gamma imaging as an adjunct modality to mammography for diagnosis of breast cancer: a systemic review and meta-analysis. Eur J Nucl Med Mol Imaging. 2013;40(3):450-63.
22. O'Connor MK. Molecular breast imaging: an emerging modality for breast cancer screening. Breast Cancer Manag. 2015;4(1):33-40.

23. Kalles V, Zografos GC, Provatopoulou X, Koulocheri D, Gounaris A. The current status of positron emission mammography in breast cancer diagnosis. Breast Cancer. 2013;20(2):123-30.

24. Glass SB, Shah ZA. Clinical utility of positron emission mammography. Proc (Bayl Univ Med Cent). 2013;26(3):314-9.

25. Fowler AM. A molecular approach to breast imaging. J Nucl Med. 2014;55(2):177-80.

26. Narayanan D, Madsen KS, Kalinyak JE, Berg WA. Interpretation of positron emission mammography: feature analysis and rates of malignancy. AJR Am J Roentgenol. 2011;196(4):956-70.

27. Schilling K, Narayanan D, Kalinyak JE, The J, Velasquez MV, Kahn S, et al. Positron emission mammography in breast cancer presurgical planning: comparisons with magnetic resonance imaging. Eur J Nucl Med Mol Imaging. 2011;38(1):23-36.

28. Caldarella C, Treglia G, Giordano A. Diagnostic performance of dedicated positron emission mammography using fluorine-18-fluorodeoxyglucose in women with suspicious breast lesions: a meta-analysis. Clin Breast Cancer. 2014;14(4):241-8.

29. Kalinyak JE, Schilling K, Berg WA, Narayanan D, Mayberry JP, Rai R, et al. PET-guided breast biopsy. Breast J. 2011;17(2):143-51.

30. Moliner L, Gonzalez AJ, Soriano A, Sanchez F, Correcher C, Orero A, et al. Design and evaluation of the MAMMI dedicated breast PET. Med Phys. 2012;39(9):5393-404.

31. García Hernández T, Vicedo González A, Ferrer Rebolleda J, Sánchez Jurado R, Roselló Ferrando J, Brualla González L, et al. Performance evaluation of a high resolution dedicated breast PET scanner. Med Phys. 2016;43(5):2261.

32. Koolen BB, Aukema TS, González Martínez AJ, Vogel WV, Caballero Ontanaya L, Vrancken Peeters MJ, et al. First clinical experience with a dedicated PET for hanging breast molecular imaging. Q J Nucl Med Mol Imaging. 2013;57(1):92-100.

33. Teixeira SC, Rebolleda JF, Koolen BB, Wesseling J, Jurado RS, Stokkel MP, et al. Evaluation of a hanging-breast PET system for primary tumor visualization in patients with stage I-III breast cancer: comparison with standard PET/CT. AJR Am J Roentgenol. 2016;206(6):1307-14.

34. Nishimatsu K, Nakamoto Y, Miyake KK, Ishimori T, Kanao S, Toi M, et al. Higher breast cancer conspicuity on dbPET compared to WB-PET/CT. Eur J Radiol. 2017;90:138-45.

35. Nakamoto R, Nakamoto Y, Ishimori T, Nishimatsu K, Miyake KK, Kanao S, et al. Diagnostic performance of a novel dedicated breast PET scanner with C-shaped ring detectors. Nucl Med Commun. 2017;38(5):388-95.

36. Collarino A, Valdés Olmos RA, Neijenhuis PA, et al. First Clinical Experience Using Stereotactic Breast Biopsy Guided by 99mTc-Sestamibi. AJR Am J Roentgenol. 2017; In press.

37. Raylman RR, Majewski S, Weisenberger AG, Popov V, Wojcik R, Kross B, et al. Positron emission mammography-guided breast biopsy. J Nucl Med.2001;42(6):960-6.

38. Argus A, Mahoney MC. Positron emission mammography: diagnostic imaging and biopsy on the same day. AJR Am J Roentgenol. 2014;202(1):216-22.

39. Hellingman D, Teixeira SC, Donswijk ML, Rijkhorst EJ, Moliner L, Alamo J, et al. A novel semi-robotized device for high-precision (18)F-FDG-guided breast cancer biopsy. Rev Esp Med Nucl Imagen Mol. 2017;36(3):158-65.

40. Hagemann IS. Molecular testing in breast cancer: a guide to current practices. Arch Pathol Lab Med. 2016;140(8):815-24.

41. Scope A, Essat M, Pandor A, Rafia R, Ward SE, Wyld L, et al. Gene expression profiling and expanded immunohistochemistry tests to guide selection of chemotherapy regimens in breast cancer management: a systematic review. Int J Technol Assess Health Care. 2017;33(1):32-45.

42. van 't Veer LJ, Dai H, van de Vijver MJ, He YD, Hart AA, Mao M, et al. Gene expression profiling predicts clinical outcome of breast cancer. Nature. 2002;415(6871):530-6.

43. Cardoso F, van't Veer LJ, Bogaerts J, Slaets L, Viale G, Delaloge S, et al. 70-Gene Signature as an Aid to Treatment Decisions in Early-Stage Breast Cancer. N Engl J Med. 2016;375(8):717-29.

44. Carels N, Spinassé LB, Tilli TM, Tuszynski JA. Toward precision medicine of breast cancer. Theor Biol Med Model. 2016;13:7.

45. Buyse M, Loi S, van't Veer L, Viale G, Delorenzi M, Glas AM, *et al.* Validation and clinical utility of a 70-gene prognostic signature for women with node-negative breast cancer. J Natl Cancer Inst. 2006;98(17):1183-92.

46. Groheux D, Giacchetti S, Moretti JL, Porcher R, Espié M, Lehmann-Che J, *et al.* Correlation of high 18F-FDG uptake to clinical, pathological and biological prognostic factors in breast cancer. Eur J Nucl Med Mol Imaging. 2011;38(3):426-35.

47. Koolen BB, Vrancken Peeters MJ, Wesseling J, Lips EH, Vogel WV, Aukema TS, *et al.* Association of primary tumour FDG uptake with clinical, histopathological and molecular characteristics in breast cancer patients scheduled for neoadjuvant chemotherapy. Eur J Nucl Med Mol Imaging. 2012;39(12):1830-8.

48. Koolen BB, Elshof LE, Loo CE, Wesseling J, Vrancken Peeters MJ, Vogel WV, *et al.* Does the pretreatment tumor sampling location correspond with metabolic activity on 18F-FDG PET/CT in breast cancer patients scheduled for neoadjuvant chemotherapy? Eur J Radiol. 2013;82(12):2353-8.

49. Arbab AS, Koizumi K, Toyama K, Araki T. Uptake of technetium-99m-tetrofosmin, technetium-99m-MIBI and thallium-201 in tumor cell lines. J Nucl Med. 1996;37(9):1551-6.

50. Maublant JC, Zhang Z, Rapp M, Ollier M, Michelot J, Veyre A. In vitro uptake of technetium-99m-teboroxime in carcinoma cell lines and normal cells: comparison with technetium-99m-sestamibi and thallium-201. J Nucl Med. 1993;34(11):1949-52.

51. Scopinaro F, Schillaci O, Scarpini M, Mingazzini PL, Di Macio L, Banci M, *et al.* Technetium-99m sestamibi: an indicator of breast cancer invasiveness. Eur J Nucl Med. 1994;21(9):984-7.

52. Schillaci O, Spanu A, Danieli R, Madeddu G. Molecular breast imaging with gamma emitters. Q J Nucl Med Mol Imaging. 2013;57(4):340-51.

53. Spanu A, Sanna D, Chessa F, Cottu P, Manca A, Madeddu G. Breast scintigraphy with breast-specific -camera in the detection of ductal carcinoma in situ: a correlation with mammography and histologic subtype. J Nucl Med. 2012;53(10):1528-33.

54. Bach-Gansmo T, Bogsrud TV, Skretting A. Integrin scintimammography using a dedicated breast imaging, solid-state gamma-camera and (99m)Tc-labelled NC100692. Clin Physiol Funct Imaging. 2008;28(4):235-9.

55. O'Connor MK, Morrow MMB, Hunt KN, Boughey JC, Wahner-Roedler DL, Conners AL, *et al.* Comparison of Tc-99m maraciclatide and Tc-99m sestamibi molecular breast imaging in patients with suspected breast cancer. EJNMMI Res. 2017;7(1):5.

56. Kurihara H, Yang DJ, Cristofanilli M, Erwin WD, Yu DF, Kohanim S, *et al.* Imaging and dosimetry of 99mTc EC annexin V: preliminary clinical study targeting apoptosis in breast tumors. Appl Radiat Isot. 2008;66(9):1175-82.

57. Scopinaro F, Varvarigou A, Ussof W, De Vincentis G, Archimandritis S, Evangelatos G, *et al.* Breast cancer takes up 99mTc bombesin. A preliminary report. Tumori. 2002;88(3):S25-8.

58. Bennink RJ, Rijks LJ, van Tienhoven G, Noorduyn LA, Janssen AG, Sloof GW. Estrogen receptor status in primary breast cancer: iodine 123-labeled cis-11beta-methoxy-17alpha-iodovinyl estradiol scintigraphy. Radiology. 2001;220(3):774-9.

59. Peñuelas I, Domínguez-Prado I, García-Velloso MJ, Martí-Climent JM, Rodríguez-Fraile M, Caicedo C, *et al.* PET tracers for clinical imaging of breast cancer. J Oncol. 2012;2012:710561.

60. Williams MB, Judy PG, Gunn S, Majewski S. Dual-modality breast tomosynthesis. Radiology. 2010;255(1):191-8.

61. Mann SD, Perez KL, McCracken EK, Shah JP, Wong TZ, Tornai MP. Initial In Vivo Quantification of Tc-99m Sestamibi uptake as a function of tissue type in healthy breasts using dedicated breast SPECT-CT. J Oncol. 2012;2012:146943.

62. O'Connor MK, Morrow MM, Tran T, Hruska CB, Conners AL, Hunt KN. Technical Note: Development of a combined molecular breast imaging/ultrasound system for diagnostic evaluation of MBI-detected lesions. Med Phys. 2017;44(2):451-9.

FUTURE PERSPECTIVES IN VULVAR CANCER AND OTHER GYNAECOLOGICAL MALIGNANCIES

The interest of nuclear medicine in the field of female cancer is growing. As described in this thesis the contribution of nuclear medicine in breast cancer has become clinically relevant for staging of both early and advanced disease. In gynaecological malignancies the contribution of nuclear medicine techniques has been more heterogeneous. In this context the following question arises: beyond breast cancer imaging, what can be expected from nuclear medicine in other female cancers?

In this thesis, amongst others, the role of nuclear medicine in gynaecological malignancies is being discussed in relation to the use of sentinel lymph node (SLN) procedures for early cancer stages and ^{18}F-FDG PET/CT to assess dissemination in lymph nodes. In the previous chapter, future perspectives for molecular imaging and intervention in breast cancer were discussed. In the current chapter we will outline some recent advances for gynaecological malignancies and vulvar cancer in particular.

GYNAECOLOGICAL MALIGNANCIES

The three most common gynaecological cancers in Europe are the carcinoma of uterine corpus, ovary and cervix uteri with respectively 98,900, 65,500 and 58,300 new cases per 100,000 women per year in 2012. [1] However, breast cancer is the most common tumour in women with an estimated incidence of 464,000 new cases per year in Europe. [1] In contrast, vulvar cancer is rare with an incidence of 1-2 new cases per 100,000 women per year in Europe. [2] Within Europe, women in Eastern and Northern countries are at highest risk, whereas in Western and Southern countries the risk is the lowest. When vulvar cancer is diagnosed in an early stage, 5-year survival is 80%. In advanced disease however, 5-year survival significantly decreases to 55% in patients with regional dissemination and to 16% in case of distant metastases. [3] In gynaecological cancers, nuclear medicine can contribute in the sentinel procedure and in the detection of distant disease using ^{18}F-FDG PET/CT.

SENTINEL NODE PROCEDURE

As extensively reviewed in chapter 7 of this thesis, in gynaecological cancers the SLN biopsy allows for greater accuracy in staging early disease and the possibility to improve patient stratification for personalised treatment. New technologies are also increasingly applied to refine the localisation

procedure of SLN before and during surgery. This trend is characterised by the synergistic use of radioguidance with allied technologies like fluorescence and navigation tools in the operation room. Some specific technological advances are the following:

a) Incorporation of SPECT/CT for anatomical localisation of SLNs. In general, the role of SPECT/CT proportionally increases as the degree of complexity of lymphatic drainage. This is based not only on the detection of additional SLNs but also surgical management changes. [4] Although the SLN procedure has been incorporated into the current guidelines for vulvar cancer and cervical cancer in Europe [5] and North America [6, 7], until now the use of SPECT/CT has not been properly standardised in spite of specific validations in this field. There is a growing necessity to incorporate this modality in consensus meetings, elaborating good practice recommendations for the future.

b) Improvement of the intraoperative localisation using navigation tools and hybrid tracers. The navigation tools based on mixed reality protocols may be utilised for the localisation of pelvic SLNs during laparoscopic surgery or robot-assisted surgery. Preoperatively acquired SPECT/CT images can be used during surgical procedure. This approach is helpful for the localisation of deep SLNs, near to the primary lesion, with weak radioactive signal or in complex anatomic areas. Using a tracked freehand SPECT gamma-probe, suitable for 3D image generation, real time depth information can continuously be displayed, enabling surgeons to navigate towards SLNs. The same freehand SPECT probe is also able to generate new virtual elements to be added to the anatomy of the patient in an augmented-reality approach. [8] Another tool facilitating the search of sentinel nodes is based on the use of a hybrid tracer combining radioactivity and fluorescence in one signature. This approach enables nuclear physicians to perform preoperative lymphatic mapping, including SPECT/CT and subsequently enables surgeons in the operating room to combine portable gamma detection with fluorescence NIR-camera imaging. [9]

c) Development of novel accessory devices, such as drop-in gamma-probes for insertion and application inside the pelvis and abdominal cavity, enabling robot-assisted gripping for radioguided lymphadenectomy. [10] This drop-in gamma-probe, which makes identification of sentinel nodes during laparoscopic surgery more flexible by improving accessibility and geometric angles of detection, has recently been tracked to generate robotic SPECT enabling augmented-reality image guidance. [11]

FUTURE USE OF ¹⁸F – FDG PET/CT

Currently, ¹⁸F-FDG PET/CT is widely used in staging, response evaluation and detection of recurrence of gynaecological malignancies like ovarian, cervical and endometrial cancer. [12] The recent PET/MRI may potentially be used in gynaecological malignancies instead of PET/CT. PET/ MRI is useful for staging of cervical and endometrial cancer, planning of radiation therapy in cervical cancer, and assessing response to chemotherapy in ovarian cancer. [13] Recently, various quantitative PET parameters have been investigated for prediction of prognosis in gynaecological malignancies. [14-17] In epithelial ovarian cancer, for instance, metabolic tumour volume and total lesion glycolysis are prognostic factors for a progression-free interval.[14] Tumours with high intratumoural heterogeneity have poorer prognoses, potentially reflecting intrinsically aggressive tumour biology or treatment resistance. Texture analysis is a recent non-invasive method to assess ¹⁸F-FDG uptake heterogeneity within tumour in PET/CT imaging. [18, 19] To date, few studies have been investigated texture analysis in gynaecological malignancies, principally in cervical cancer. [20-22] A possible future application is to evaluate texture analysis in vulvar cancer (**Figure 1**).

Finally, PET/CT and PET/MRI, in analogy with SPECT/CT for sentinel node detection, are increasingly being used in interventional imaging approaches. Both modalities can provide simultaneous 3D anatomical roadmaps to reduce sampling errors by allowing targeted biopsies in heterogeneous tumours and to guide resection in case of recurrent disease.
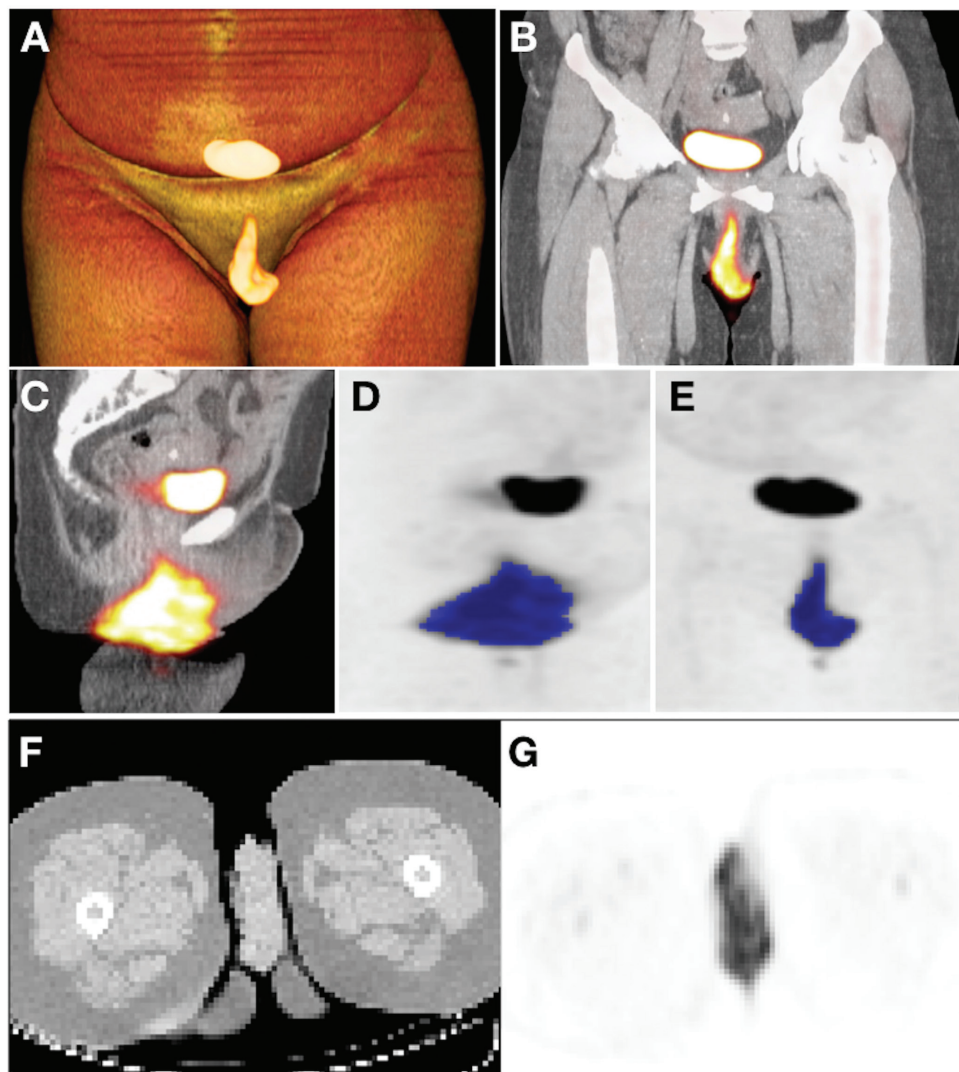
Figure 1. Fused PET/CT showing an 18F-FDG avid of a large vulvar carcinoma (diameter of 9 cm) on volume rendering (A), coronal (B) and sagittal (C) images. These sagittal (D) and coronal (E) PET slices illustrate the delineation of the tumour. Additionally, on axial CT projection (F) corresponding axial PET (G) shows heterogeneous voxel 18F-FDG distribution within tumour.

REFERENCES

1. Ferlay J, Steliarova-Foucher E, Lortet-Tieulent J, Rosso S, Coebergh JW, Comber H, at al. Cancer incidence and mortality patterns in Europe: estimates for 40 countries in 2012. Eur J Cancer. 2013;49(6):1374-403.

2. European Society of Gynaecological Oncology. Gynaecological cancer in Europe, facts and figures in 2015. ESGO, September 2015. www.esgo.org

3. Howlader N, Noone A, Krapcho M *et al*. SEER Cancer Statistics Review, 1975-2012. 2015. http://seer.cancer.gov/statfacts/

4. Jimenez-Heffernan A, Ellmann A, Sado H, Huić D, Bal C, Parameswaran R, *et al*. Results of a Prospective Multicenter International Atomic Energy Agency Sentinel Node Trial on the Value of SPECT/CT Over Planar Imaging in Various Malignancies. J Nucl Med. 2015;56(9):1338-44.

5. Giammarile F, Bozkurt MF, Cibula D, Pahisa J, Oyen WJ, Paredes P, *et al*. The EANM clinical and technical guidelines for lymphoscintigraphy and sentinel node localization in gynaecological cancers. Eur J Nucl Med Mol Imaging. 2014;41(7):1463-77.

6. National Comprehensive Cancer Network, 2016. Vulvar Cancer (Squamous Cell Carcinoma), Version 1.2016. http://www.nccn.org/professionals/physician_gls/pdf/vulvar.pdf

7. Koh WJ, Greer BE, Abu-Rustum NR, Apte SM, Campos SM, Cho KR, *et al*. Cervical Cancer, Version 2.2015. J Natl Compr Canc Netw. 2015;13(4):395-404.

8. Bowles H, Sánchez N, Tapias A, Paredes P, Campos F, Bluemel C, *et al.* Radioguided surgery and the GOSTT concept: From pre-operative image and intraoperative navigation to image-assisted excision. Rev Esp Med Nucl Imagen Mol. 2017;36(3):175-84.

9. Van Den Berg NS, Buckle T, Kleinjan GI, Klop WM, Horenblas S, Van Der Poel HG, *et al*. Hybrid tracers for sentinel node biopsy. Q J Nucl Med Mol Imaging. 2014;58(2):193-206.

10. van Oosterom MN, Simon H, Mengus L, Welling MM, van der Poel HG, van den Berg NS, *et al.* Revolutionizing (robot-assisted) laparoscopic gamma tracing using a drop-in gamma probe technology. Am J Nucl Med Mol Imaging. 2016;6(1):1-17.

11. Fuerst B, Sprung J, Pinto F, Frisch B, Wendler T, Simon H, *et al*. First robotic SPECT for minimally invasive sentinel lymph node mapping. IEEE Trans Med Imaging. 2016;35(3):830-8.

12. Oldan JD, Patel PS. Positron emission tomography/computed tomography for gynecologic malignancies. Obstet Gynecol Surv. 2016;71(9):545-56.

13. Oldan JD, Shah SN, Rose TL. Applications of PET/MR imaging in urogynecologic and genitourinary Cancers. Magn Reson Imaging Clin N Am. 2017;25(2):335-50.

14. Lee JW, Heo EJ, Moon SH, Lee H, Cheon GJ, Lee M, *et al*. Prognostic value of total lesion glycolysis on preoperative (18)F-FDG PET/CT in patients with uterine carcinosarcoma. Eur Radiol. 2016;26(11):4148-54.

15. Kim CY, Jeong SY, Chong GO, Son SH, Jung JH, Kim DH, *et al*. Quantitative metabolic parameters measured on F-18 FDG PET/CT predict survival after relapse in patients with relapsed epithelial ovarian cancer. Gynecol Oncol. 2015;136(3):498-504.

16. Miccò M, Vargas HA, Burger IA, Kollmeier MA, Goldman DA, Park KJ, *et al*. Combined pre-treatment MRI and 18F-FDG PET/CT parameters as prognostic biomarkers in patients with cervical cancer. Eur J Radiol. 2014;83(7):1169-76.

17. Chung HH, Kwon HW, Kang KW, Park NH, Song YS, Chung JK, *et al*. Prognostic value of preoperative metabolic tumor volume and total lesion glycolysis in patients with epithelial ovarian cancer. Ann Surg Oncol. 2012;19(6):1966-72.

18. Chicklore S, Goh V, Siddique M, Roy A, Marsden PK, Cook GJ. Quantifying tumour heterogeneity in 18F-FDG PET/CT imaging by texture analysis. Eur J Nucl Med Mol Imaging. 2013;40(1):133-40.

19. Davnall F, Yip CS, Ljungqvist G, Selmi M, Ng F, Sanghera B, *et al*. Assessment of tumor heterogeneity: an emerging imaging tool for clinical practice? Insights Imaging. 2012;3(6):573-89.

20. Ho KC, Fang YH, Chung HW, Yen TC, Ho TY, Chou HH, *et al*. A preliminary investigation into textural features of intratumoral metabolic heterogeneity in (18)F-FDG PET for overall survival prognosis in patients with bulky cervical cancer treated with definitive concurrent chemoradiotherapy. Am J Nucl Med Mol Imaging. 2016;6(3):166-75.

21. Tsujikawa T, Rahman T, Yamamoto M, Yamada S, Tsuyoshi H, Kiyono Y, *et al.* (18)F-FDG PET radiomics approaches: comparing and clustering features in cervical cancer. Ann Nucl Med. 2017 Aug 16. In press.

22. Shen WC, Chen SW, Liang JA, Hsieh TC, Yen KY, Kao CH. [18]Fluorodeoxyglucose positron emission tomography for the textural features of cervical cancer associated with lymph node metastasis and histological type. Eur J Nucl Med Mol Imaging. 2017;44(10):1721-31.

SUMMARY

The work described in this thesis shows new possibilities for molecular imaging in breast and vulvar cancer and demonstrates how to simultaneously encompass all current and future applications of nuclear medicine in female cancers. General introduction and outline of this thesis are reported in **Chapter 1**. In part one of this thesis the reader is introduced to molecular imaging using ^{99m}Tc-sestamibi in breast cancer. Part two of this thesis describes the methodological aspects and clinical evaluation of ^{99m}Tc-sestamibi-guided biopsy. Part three presents the radioguided intervention in gynaecological malignancies. Discussion and future perspectives are reported in the fourth part of this thesis.

PART I

Chapter 2 provides a systematic review and meta-analysis on ^{99m}Tc-sestamibi imaging in the prediction of pathological nonresponse to neoadjuvant chemotherapy in primary locally advanced breast cancer. Up till now, only planar ^{99m}Tc-sestamibi imaging has been investigated, showing low sensitivity to predict pathologic nonresponse. ^{99m}Tc-sestamibi uptake during neoadjuvant chemotherapy seems highly sensitive, but the experience is limited to a few studies. The introduction of quantitative SPECT/CT imaging for early nonresponse monitoring could provide a new horizon. **Chapter 3** presents the experimental validation of SPECT/CT quantification for response monitoring in breast cancer. Our results show that quantification using SPECT/CT is feasible when a 42% isocontour is used for delineation for tumour of at least 17 mm diameter. However, with tumour shrinkage, response evaluation should be handled with care, especially when using $SUV_{max.}$ In **chapter 4**, the clinical use of MBI is evaluated in 287 patients with newly diagnosed breast cancer scheduled for lumpectomy. In this setting, MBI revealed more accurately the disease extent and presence of additional tumour foci, adjusting surgical management in 9% of the patients. Hence, incorporation of this modality in the clinical workup could improve the selection of patients for lumpectomy.

The general conclusion from **part I** is that technological advances in dedicated devices and SPECT/CT have the potential to lead to improvements in the detection and therapy monitoring in patients with breast cancer, and can also lead to relevant changes in patient management.

PART II

Part II of this thesis focuses on ^{99m}Tc-sestamibi guided biopsy in breast cancer. **Chapter 5** addresses the methodological aspects of ^{99m}Tc-sestamibi MBI-guided biopsy. All procedure steps of this new biopsy modality are described and its advantages and limitations are discussed in comparison with radiology-guided modalities. Finally, future clinical applications, such as targeted biopsies in large and heterogeneous tumours, are discussed. In **chapter 6**, the first clinical experience using stereotactic biopsy guided by ^{99m}Tc-sestamibi is evaluated in 38 women. This biopsy procedure proved to be successful, acquiring representative samples in all patients. All samples were adequate for histopathological analysis. The procedure was well tolerated in all patients.

The general conclusion from **part II** of this thesis is that ^{99m}Tc-sestamibi MBI-guided biopsy is a valid tool for biopsy of breast lesions, complementary to radiology-assisted biopsy modalities. Moreover, the results of the above-described study show that this new biopsy tool is technically feasible and reliable. These promising results encourage a further validation in large (multicentre) studies.

PART III

Part III of this thesis discusses the issue of radioguided interventions in other female cancers. **Chapter 7** provides an overview of the state-of-the-art of sentinel lymph node mapping in gynaecological malignancies, including vulvar cancer, cervical cancer and endometrial cancer. Currently, the sentinel node biopsy is a standard procedure in early stage vulvar- and cervical cancer, while it is considered investigational in endometrial cancer. This chapter also describes the methodological advances in preoperative and intraoperative imaging. In **chapter 8**, the lymphatic drainage pattern, using SPECT/CT, is evaluated in 83 patients with vulvar cancer scheduled for the sentinel lymph node procedure. Lymphatic drainage occurred mainly to the medial regions of the groin with only incidental drainage to the lateral inferior region. Therefore, in patients with metastatic sentinel node(s), scheduled for inguinal lymph node dissection, the lateral inferior region of the groin might be spared. In **Chapter 9**, we investigate the value of dual-time-point ^{18}F-FDG PET/CT in the prediction of lymph node status in 33 patients with invasive vulvar cancer, scheduled for inguinofemoral lymph node dissection. The results underline that standard PET/

CT (at 1 hour after ^{18}F-FDG injection) is highly predictive of pathological negative groins and thus valuable for selecting patients suitable for minimal invasive surgery. Delayed PET/CT (at 3 hours after ^{18}F-FDG injection) did not improve the specificity and positive predictive value of the modality.

From **part III** it can be concluded that preoperative SPECT/CT is a valid roadmap for surgeons and that PET/CT enables identification of patients for minimal invasive surgery.

PART IV

Part IV of this thesis presents the future perspective of nuclear medicine imaging in female tumours. **Chapter 10** discusses the novel frontiers of dedicated molecular imaging in breast cancer diagnosis. In particular, targeted biopsy and precision breast cancer medicine will be the future application of dedicated breast devices. Additionally, new and specific radiotracers as well as the introduction of novel hybrid devices will facilitate cancer detection and therapy monitoring. **Chapter 11** highlights some recent advances for gynaecological malignancies particularly in vulvar cancer. The combined use of radiotracer and fluorescence as well as the incorporation of new technological tools will improve the localisation of sentinel lymph nodes before and during the surgical procedure. A novel technique in quantitative PET/CT is texture analysis to evaluate intra-tumoural heterogeneity. This technique may be of particular interest in the characterization and prediction of prognosis of locally advanced vulvar cancer and other gynaecological malignancies.

CURRICULUM VITAE

Angela Collarino

Angela Collarino was born on May 11th 1984 in Lagonegro, Potenza, Italy. She graduated with full marks in 2001 at scientific high school "Carlo Levi" in Sant'Arcangelo, Potenza, Italy. In 2009, she obtained her master degree (_cum laude_) in Medicine and Surgery (Università Cattolica del Sacro Cuore, Rome, Italy). Afterwards, she started her nuclear medicine training as resident physician at the Department of Nuclear Medicine of Università Cattolica del Sacro Cuore (UCSC) in Rome. During her specialisation she explored the field of molecular imaging in the context of the European Radioguided Surgery Network with the first internship (September-December 2014) at the Department of Nuclear Medicine of the Netherlands Cancer Institute in Amsterdam and a second research period (March-April 2015) at the Department of Radiology, section of Nuclear Medicine at Leiden University Medical Centre (LUMC). In 2015 she received the title of nuclear medicine physician (_cum laude_) after which she started her PhD at the Department of Radiology, Nuclear Medicine Section of the LUMC in cooperation with the Biomedical Photon Imaging group of MIRA Institute for Biomedical Technology and Technical Medicine of the University of Twente (Enschede, The Netherlands). In addition to her PhD research she also coordinates a multicentric study (_Texture analysis in vulvar cancer study, Study Code: 1633_) in close collaboration between LUMC and UCSC. She is a member of the Italian Radioguided Surgery Group and is currently responsible for the elaboration of the Italian clinical and technical guidelines for lymphoscintigraphy and sentinel node localisation in gynaecological cancers.

PUBLICATION LIST, AWARDS AND NOMINATIONS

PUBLICATIONS

* = shared first authorship

1.   Testa AC, Moro F, Pasciuto T, Moruzzi MC, Di Legge A, Fuoco G, Autorino R, **Collarino A**, Gui B, Zannoni GF, Gambacorta A, Miccò M, Rufini V, Scambia G, Ferrandina G. Prospective multimodal imaging assessment of locally advanced cervical cancer patients administered by chemoradiation followed by radical surgery. The PRICE (PRospective Imaging of CErvical cancer and neoadjuvant treatment) study 2: the role of ultrasound after chemoradiation to assess residual tumor. Ultrasound Obstet Gynecol. 2017; In press.

2.   **Collarino A,** Fuoco V, Pereira Arias-Bauda LM, Sánchez AM, de Geus-Oei LF, Masetti R, Valdés Olmos RA. Novel frontiers of dedicated molecular imaging in breast cancer diagnosis. Transl Cancer Res 2017; In press.

3.   **Collarino A**, Valdés Olmos RA, Neijenhuis PA, den Hartog WC, Smit F, de Geus-Oei LF, Pereira Arias-Bauda LM. First clinical experience using stereotactic breast biopsy guided by 99mTc-sestamibi. AJR Am J Roentgenol. 2017; In press.

4.   Garganese G*, **Collarino A***, Fragomeni SM, Rufini V, Perotti G, Gentileschi S, Evangelista MT, Ieria FP, Zagaria L, Bove S, Giordano A, Scambia G. Groin sentinel node biopsy and (18)F-FDG PET/CT-supported preoperative lymph node assessment in cN0 patients with vulvar cancer currently unfit for minimally invasive inguinal surgery: The GroSNaPET study. Eur J Surg Oncol. 2017;43(9):1776-83.

5.   **Collarino A**, de Koster EJ, Valdés Olmos RA, de Geus-Oei LF, Pereira Arias-Bouda LM. Is technetium-99m sestamibi imaging able to predict pathologic nonresponse to neoadjuvant chemotherapy in breast Cancer? A meta-analysis evaluating current use and shortcomings. Clin Breast Cancer. 2017; In press.

6.   Testa AC, Ferrandina G, Moro F, Pasciuto T, Moruzzi MC, De Blasis I, Mascilini F, Foti E, Autorino R, **Collarino A**, Gui B, Zannoni GF, Gambacorta MA, Valentini AL, Rufini V, Scambia G. Prospective multimodal imaging assessment of locally advanced cervical cancer patients administered by chemoradiation followed by radical surgery. The PRICE (PRospective Imaging of CErvical cancer and neoadjuvant treatment) study: the role of ultrasound. Ultrasound Obstet Gynecol. 2017; In Press.

7.   **Collarino A***, Garganese G*, Valdés Olmos RA, Stefanelli A, Perotti G, Mirk P, Fragomeni SM, Ieria FP, Scambia G, Giordano A, Rufini V. Evaluation of dual time point imaging (18)F-FDG PET/CT for lymph node staging in vulvar cancer. J Nucl Med. 2017; In press.

8.   **Collarino A**, Vidal-Sicart S, Perotti G, Valdés Olmos RA. The sentinel node approach in gynaecological malignancies. Clin Transl Imaging. 2016;4(5):411-20.

9.   **Collarino A**, Valdés Olmos RA, van der Hoeven AF, Pereira Arias-Bouda LM. Methodological aspects of (99m)Tc-sestamibi guided biopsy in breast cancer. Clin Transl Imaging. 2016;4(5):367-76.

10. **Collarino A**, Donswijk ML, van Driel WJ, Stokkel MP, Valdés Olmos RA. The use of SPECT/CT for anatomical mapping of lymphatic drainage in vulvar cancer: possible implications for the extent of inguinal lymph node dissection. Eur J Nucl Med Mol Imaging. 2015;42(13):2064-71.

11. **Collarino A**, del Ciello A, Perotti G, Rufini V. Intrapancreatic accessory spleen detected by 68Ga DOTANOC PET/CT and 99mTc-colloid SPECT/CT scintigraphy. Clin Nucl Med. 2015;40(5):415-8.

12. Testa AC, Di Legge A, De Blasis I, Moruzzi MC, Bonatti M, **Collarino A**, Rufini V, Manfredi R. Imaging techniques for the evaluation of cervical cancer. Best Pract Res Clin Obstet Gynaecol. 2014;28(5):741-68.

13. Treglia G, **Collarino A**, Lago M, Rindi G, Giordano A. Nodular nongranulomatous vasculitis of the lung detected by 18F-FDG PET/CT. Clin Nucl Med. 2013;38(3):148e-51e.

14. Caldarella C, Leccisotti L, Bruno I, **Collarino A**, Maggi F, Giordano A. Myocardial perfusion single-photon emission tomography (SPET) and positron emission tomography-computed tomography (PET-CT) imaging for congenitally corrected transposition of great arteries. Pediatr Cardiol. 2012;33(8):1435-9.

BOOK CHAPTERS

Collarino A, Perotti G, Giordano A. Pitfall detected by SPECT/CT in vulvar cancer sentinel lymph node mapping. Case Reports In: Herrmann K, Nieweg O E, Povoski SP Stephen P, editors. Radioguided current applications and innovative directions in clinical practice. Springer 2016. p 483-94.

AWARDS AND NOMINATIONS

1.   Best scientific poster award at the XIII National Congress of AIMN (Italian Association of Nuclear Medicine and Molecular Imaging) in 2017. Poster title: ^{99m}Tc-sestamibi guided biopsy for occult or unclear breast lesions on mammography and ultrasound.

2.   Nomination Marie Curie Award at the XXX European Congress of EANM (European Association of Nuclear Medicine) in 2017. Oral presentation title: Experimental validation of absolute SPECT/CT quantification for response monitoring in breast cancer.

ACKNOWLEDGEMENTS

ACKNOWLEDGEMENTS

This PhD trajectory has been an important life experience for me. I have enjoyed the opportunity to grow as a researcher, to participate in international conferences and share ideas and ambitions with young researchers as well as with senior experts. I have also had the benefit of living in a foreign country and learning a different culture. The Netherlands have taught me their straightforward and sustainable work mentality, which I have adopted as my own.

Supervisor & co-supervisors

Dear professor **Lioe-Fee** de Geus-Oei, thank you for giving me the opportunity to work in your group as a PhD candidate. You educated me as a researcher and as a person.

Dear dr. **Renato** A. Valdés Olmos, your enthusiasm for research is contagious and very encouraging for young researchers such as myself. You are an inspiration to me. I hope be able to transfer this stimulating effect to students, residents and PhD students in my future work.

Dear dr. **Lenka** Pereira Arias-Bouda, your continuous attention to the clinical and practical aspects of our research projects has been of great teaching. It is a pleasure to be your first PhD. Thank you.

Graduation committee

I want to thank all members of the doctoral thesis committee for their time and effort spent in reading and judging this dissertation.

Colleagues & Friends

Dear Elizabeth J. de Koster, dear **Lis**, you are the first PhD candidate I met in Leiden, and now my best friend. You are unique. I am lucky to know you. Thank you for being there for me.

Dear **Floris** H.P. van Velden, you are my favourite physicist. You taught me so much and I enjoyed the time spent together. Thank you.

Dear **Willem** Grootjans, you will be a great professor. Thank you for your help in this adventure.

Dear **Lis**, **Floris** and **Willem**, we will continue to cooperate in the future and surely have a lot of fun as well. I will miss you a lot.

Dear **Marianne** Valdés Olmos, thank you for reviewing and editing all my manuscripts.

Dear Athanasios Adamopoulos, dear **Nassos**, my Greek friend, thank you for sharing this adventure and giving me suggestions.

I want to thank all **researchers**, **doctors**, **technicians**, and **secretaries** that I have met during my PhD trajectory. Last but not least I would like to thank the **patients**, without whom my research would not be possible.

Family

Cara **mamma** e **papà**, grazie mille per avermi supportata in questo percorso. Le grinta e la determinazione che mi avete insegnato sono racchiuse in questa tesi. Vi voglio bene.

Dear **brother**, you are my computer engineer. We not only share a passion for travelling, but also the determination in our professional career. Thank you for your support.

Dear **Antonio**, you were the first person to encourage me to follow this dream. This thesis is also yours. I love you.

I am extremely grateful to all of you.